UNIVERSITE DE NEUCHATEL FACULTE DES SCIENCES

Cluster Chemistry with Sulfur-Containing Ligands: Reactivity of Ru_3 and Ru_6 Diphenylthioureato Clusters and Reactions of M_3-Carbonyl Clusters with Trithiane (M = Fe, Ru, Os).

Thèse présentée à la Faculté des Sciences par

Lisa Hoferkamp

B.Sc., University of Idaho - Moscow, Idaho USA,
M.Sc., Florida State University - Tallahassee, Florida USA

pour l'obtention du grade
de Docteur ès Sciences

Institut de Chimie de
l'Université de Neuchâtel

July 1995

IMPRIMATUR POUR LA THÈSE

Cluster Chemistry with Sulfur-Containing Ligands: Reactivity of Ru_3 and Ru_6 Diphenylthioureato Clusters and Reactions of M_3 Carbonyl Clusters with Trithiane ($M = Fe, Ru, Os$)

de Mme Lisa Hoferkamp

UNIVERSITÉ DE NEUCHÂTEL

FACULTÉ DES SCIENCES

La Faculté des sciences de l'Université de Neuchâtel sur le rapport des membres du jury,

M. G. Süss-Fink, Mme H. Stoeckli-Evans, M. R. Roulet (Lausanne)

autorise l'impression de la présente thèse.

Neuchâtel, le 11 octobre 1995

Le doyen:

H.-H. Nägeli

The experimental work for this investigation was carried out under the direction of Prof. Dr. Georg Süss-Fink between August 1991 and January 1995 at the Institut de Chimie, Université de Neuchâtel, Neuchâtel Switzerland.

I would like to express my gratitude to

Professor Dr. Georg Süss-Fink

my thesis advisor, for his enthusiasm, suggestions and direction as well as for providing me the opportunity to work with his group.

I am grateful to Professor Helen Stoeckli-Evans for guidance with the analyses of the X-ray structural data and for the time spent collecting those data. I would also like to thank Dr. Gerd Rheinwald for the collection of X-ray structural data, Dr. S. Claude for the collection of the standard pressure NMR data, Professor Raymond Roulet and Dr. Gabor Laurenczy of the Institut de Minerale et Chimie de l'Université de Lausanne for the high pressure NMR data and Professor Dr. T.A. Jenny of the Université de Fribourg for the mass spectral data.

My thanks to the members of my thesis committee, Professor Helen Stoeckli-Evans and Professor Raymond Roulet of the Université de Lausanne, for their time and for the useful suggestions they have offered.

I wish to thank the Stipendienfonds der Baseler Chemischen Industrie zur Unterstützung von Doktoranden and the Canton de Neuchâtel for their financial support.

Finally, thanks to the special people for all kinds of support.

Table of Contents

I Introduction

Compounds containing metal-metal bonds are by no means recent additions to inorganic chemistry. For instance calomel was known to alchemists of the middle ages. However it is the formation of extensive metal-metal bonds (i.e. M-M ≥ 3) which comprises the relatively modern field known as cluster chemistry. The term "metal cluster" was first proposed by F.A. Cotton, and his definition included several types of metal clusters, among which are the metal carbonyl clusters.[1] The carbonyl group is particularly suited as a ligand for metal clusters given its ability to draw electron density from the metal centers. The characteristics of metal carbonyls were not truly explored until after the fortuitous discovery of $Ni(CO)_4$ by L. Mond in the last part of the nineteenth century.[2] Through a productive research career, which started some 20 years after the death of Mond, it was W. Hieber who earned the title "father of metal carbonyl chemistry". Hieber developed preparative routines for many mono- and multi-nuclear carbonyl compounds and went on to explore their reactivity patterns.[3] Surprisingly, most of these early advances in organometallic chemistry were made without the benefit of modern instrumentation, i.e. X-ray crystallography, high resolution NMR and Fourier Transform Infrared spectroscopy. Nowadays, these methods represent the principal tools in the structural elucidation of cluster complexes. At about the same time Hieber was exploring metal carbonyls, many of those compounds were finding use as catalysts for organic reactions of industrial importance.[4]

Many of the catalytic applications of transition metal clusters stem from their ability to reversibly coordinate small organic molecules thus rendering these substrates susceptible to further reaction. This process is similar in nature to the adsorption of atoms or molecules onto the surface of catalytically active metals, for instance the adsorption of CO and NO on a Rh surface to yield CO_2 and N_2.[5] This resemblance ultimately led to the proposal of a cluster-surface analogy by Muetterties *et al.*.[6] However, even though this analogy can be used in explanations of catalysis by metal clusters, often the drastically different conditions used to study metal surfaces as compared to those present in typical commercial catalysis limit the number of conclusions to be drawn. A case in which this analogy has found particular application is that of hydrudesulfurization (HDS) reactions at metal surfaces.[7] Low-energy routes to these reactions take on increasing importance as light petroleum reserves dwindle and the shift to heavier crude oils, of which sulfur-containing species comprise a major

contaminant, becomes inevitable. Discrete metal clusters with sulfur-containing molecules at different binding sites have been used to model certain stages of the HDS process. Although the original HDS models involved Mo-Ni or Mo-Co based clusters, several reviews of the subject point out that clusters of Fe, Ru and Os are also proving effective to this end.[8] These clusters have proven useful not only as models in the heterogeneous catalytic processes occurring at metal surfaces, but have often shown activity as homogeneous catalysts themselves.[9]

The ability of sulfur to donate up to six electrons to metal clusters makes its ligands capable of multiple bonding modes. In fact polynuclear binding of sulfur in metal clusters provides the most likely starting point in modelling the desulfurization processes mentioned above.[7] Bonding of sulfur to multiple metals has also been implicated in another surface process. Specifically, the group of sulfur-containing molecules known as thioureas have been extensively investigated with respect to their corrosion inhibiting properties.[10] Here metal clusters have proven particularly adequate as models.[11] In addition, desulfurization of thiourea has been shown to occur in reactions with $Fe_2(CO)_9$.[12] These properties of thiourea led to an extensive investigation of its reactions with $Ru_3(CO)_{12}$ carried out previously in this laboratory[13]. Among the many products isolated was a trinuclear cluster containing a substituted thiourea bound to the metal framework in a μ_3,η^2 fashion [$(\mu_2$-H)$Ru_3(CO)_9(\mu_3,\eta^2$-SCNHPhNPh)].[14] This particular compound could be isolated in high yield and was relatively air stable. When one considers that many questions concerning intermediates as well as products in catalytic cycles have been answered through reactivity studies of model compounds, it seems logical that such a study on the cluster above might provide some very interesting results.

A major problem associated with use of metal clusters as homogeneous catalysts is their tendency to undergo cluster fragmentation under the forcing conditions required in most catalytic processes.[15] One approach to this problem is the use of ligands which serve as clamps, essentially holding the metal skeleton together. This approach has been pursued previously but primarily with potentially tripodal phoshine type ligands.[16] The limited success of these endeavors was most likely due to the tendency of phosphine ligands to occupy equatorial coordination sites in metal complexes. In light of the capacity of sulfur to serve in multiple bonding modes as well as its relative indifference to coordination site, it is a likely

candidate for this role. While the thiourea cited above represents one prospect, an attractive possibility also exists in the group of sulfur-containing species known as cyclic thioethers. Notably, the cyclic thioether trithiacyclohexane holds a geometry appropriate for coordination to the triangular face of M_3 clusters. Information acquired from a study of thioether coordination to transition metal clusters could also be applied to the process of desulfurization, considering a major sulfur contaminant of crude oil is the cyclic thioether, thiophene.

Of course for both thioureas and thioethers biological activity is relevant. The biological toxicity of thioureas is documented.[17] The possibility of a thiourea scavenger should not be ignored. In contrast thioethers play a vital role in the human body. The unusual properties displayed by the blue copper proteins has been shown to result from an interaction between Cu and the essential amino acid methionine, itself a thioether.[18] The interactions of iron with sulfur containing compounds also merits interest. The non-heme proteins ferredoxin and rubredoxin contain iron bonded to the sulfur of cysteine.[19]

Although a fascinating topic in its own right, the biological significance of thioureas and thioethers is outside the range of this study. Instead, the coordination chemistry of the above-mentioned thioether (trithiacyclohexane) towards group VIII metal clusters will be presented followed by the results obtained from a reactivity study on tri- and hexanuclear clusters containing diphenylthioureato ligands. The major issue to be addressed in this second portion is the influence of the thiourea ligand on other sites of the cluster.

References

[1] Cotton F.A., *Quart. Rev.*, 1966, *20*, 389.

[2] Mond L., Langer C., Quincke F., *J. Chem. Soc.*, 1890, 749.

[3] Hieber O., *Adv. Organomet. Chem.*, 1970, *8*, 1.

[4] Herrmann W.A., *J. Organomet. Chem.*, 1990, *383*, 21.

[5] Fisher G.B., Oh S.H., Carpenter J.E., DiMaggio C.L., Schmieg S.J., Goodman D.W., Root T.W., Schwartz S.B., Schmidt L.K., *Stud. Surf. Sci. Catal.*, 1987, *30* (Catal. Automot. Pollut. Control), 215.

[6] Muetterties E.L., Rhodin T.N., Band E., Brucker C.F., Pretzer W.R., *Chem. Rev.*, 1979, *79(2)*, 91.

[7] Wiegand B.C., Friend C.M., *Chem. Rev.*, 1992, *92(4)*, 491.

[8] a. Delmon B., *Catal. Lett.*, 1993, *22*, 1.

b. Brenner J.R., Carvill B.T., Thompson L.T. Jr., *Appl. Organomet. Chem.*, 1992, *6*, 463.

c. Carvill B.T., Thompson L.T., *Appl. Catal.*, 1991, *75*, 249.

d. Reynolds J.G., *Chem. Indust.*, 1991, *16*, 570.

e. Riaz U., Curnow O., Curtis D.M., *J. Amer. Chem. Soc.*, 1991, *113*, 1416.

f. Angelici R.J., *Acc. Chem. Res.*, 1988, *21(11)*, 387.

[9] Süss-Fink G., Meister G., *Adv. Inorg. Chem.*, 1993, *35*, 41.

[10] a. Agrawal R., Namboodhiri T.K.G., *Corr. Sci.*, 1990, *30*, 37.

b. Oza R.M., Badher P.C., Patel A.B., Vora J.C., *J. Electrochem. Soc., India*, 1985, *34(2)*, 143.

[11] Jeannin S., Jeannin Y., Lavigne G., *Inorg. Chem.*, 1978, *17(8)*, 2103.

[12] Petz W., *J. Organomet. Chem.*, 1979, *172*, 415.

[13] Bodensieck U., *Doctoral Thesis*, Université de Neuchâtel, 1992.

[14] Bodensieck U., Stoeckli-Evans H., Süss-Fink G., *Chem. Ber.*, 1990, *123*, 1603.

[15] Mingos D.M.P., Wales D.J. in "Introduction to Cluster Chemistry"; Grimes R.N., Ed.; Prentice Hall International Editions: Inc. New Jersey, 1990, *chap. 1*.

[16] a. Mague J.T., Lloyd C.L., *Organomet.*, 1992, *11* 26.

b. Harding M.J., Nicholls B.S., Smith A.K., *J. Organomet. Chem.*, 1982, *226*, C17.

c. DeBoer J.J., VanDoorn J.A., Masters C., *J. Chem. Soc., Chem. Commun.*, 1978, 1005.

[17] Schroeder D.C., *Chem. Rev.*, 1955, *55*, 181.

[18] Bernert H., *Coord. Chem. Rev.*, **1980**, *33*, 55.

[19] Bezdorovainy A., "Biochemistry of Nonheme Iron", Plenum Press, New York, **1980**, *chap. 8.*

II Group VIII Metal Clusters with the Cyclic Thioether 1,3,5-Trithiacyclohexane

2.1 *Thioethers in Coordination Chemistry*

Polythia macrocycles are the sulfur analogues of crown ethers and are therefore often referred to as crown thioethers. A general representation of the crown thioether is a cycle composed of alternating sulfur atoms linked by alkyl groups of varying length. Citation of the number of sulfur atoms in the ring in conjunction with the total ring size leads to the nomenclature used here in referring to the thioether in question. Most often the sulfur of a coordinated thioether will act as a two-electron donor, forming σ-bonds to the metals in coordination complexes. However thioethers are weak σ-donors and thus lack significant charge neutralization capabilities. Since these ligands act as weak donors, often the metal ion of thioether complexes retains coordinated anions.[20] In addition, a degree of π-acidity, intermediate between that of amines and phosphines has been established in these ligands.[21] Increases in IR stretching frequencies of the CO ligand trans to a thioether in substituted metal carbonyl complexes suggests a degree of π-backbonding competition.[22] Delocalization of t_{2g} electron density from the metal into thioether ligand orbitals, resulting in decreased electron-electron repulsion, also explains the predominance of low-spin state metal-thioether complexes. This same delocalization has also been used to explain the inert behavior to thermal decomposition of some metal complexes of crown thioethers.[23] These two characteristics of thioethers, lack of charge neutralization and π-acidity, are primarily responsible for their tendency to coordinate to metals of low oxidation state. Considering the chemistry of low-valent transition metals has found extensive applications in homogeneous catalysis, the potential of these ligands is considerable. Thioether complexes of Ru have shown activity towards catalytic desulfurization of heavier crude oils.[24] Iron complexes of thioethers have also shown promise in this area.[25]

Crown thioethers form mononuclear complexes with a large number of transition metals.[26] These complexes could easily provide a more robust series of catalysts considering the additional stability which could be provided by the cyclic thioether (the macrocyclic effect). Typical examples of these coordination complexes are the mononuclear complexes of trithiacyclononane. Trithiacyclononane is particularly well-studied due to the ease with which it forms chelate complexes with metal ions. This nine-membered cycle is the exception to the

typical *exo* orientation of the sulfur atoms exhibited by other crown thioethers. Here the sulfur atoms are arranged in an *endo* fashion. That is to say, the sulfur atoms point into the macrocyclic cavity of the crown thioether and are thus preorganized for facial coordination to metal ions.[27]

Two molecules of this nine-membered crown thioether were observed to bind to a trigonal face of Fe(II) in a chelate fashion via the six sulfur atoms.[28] Cooper *et coll.* were among the first to synthesize the Ru(II) complexes of trithiacyclononane.[29] Here as well, two molecules of the thioether bind through each of the six S atoms to form an octahedral complex. Reactions of chloride salts of Os(II) with trithiacyclononane also gave homoleptic thioether complexes.[26c] Each of these complexes showed reversible one-electron oxidations ($E_{1/2}$=+0.98V[28], $E_{1/2}$=+1.40V[29b], $E_{1/2}$=+1.16V[26c] resp. vs Fc^+/Fc) all assigned to the M(II)/M(III) couple. The anodic potential of these couples is attributed to the π-acidity of the ligand. X-ray structural data obtained for the Fe complexes shows longer Fe-S bonds in the Fe(III) species as compared to those of the Fe(II), further implying significant π-backbonding between the metal center and the thioether ligand in the +2 oxidation state.[30]

Extending the stability of crown thioether complexes to the industrially useful platinum metals is the driving force behind the majority of research into those mononuclear complexes of Ru.[31] With this goal in mind, attempts to combine the useful properties of thioethers and other ligands have been pursued. Hill *et al.* have investigated the properties of several Ru(II) complexes containing phosphine and cyclic thioether ligands.[32] A particularly interesting dinuclear Ru(II) complex of a fourteen membered crown thioether contains an unsupported hydride bridging the two mononuclear units.[33]

2.2 1,3,5-Trithiacyclohexane and its Derivative *cis* 2,4,6-Tribenzyl-1,3,5-Trithiacyclohexane

Trithiacyclohexane is the thioether analogue of cyclohexane. It occurs as an odorless, colorless solid and is commercially available. In the crystalline form the melting point is 219-220 °C. Electron diffraction studies in the vapor phase[34] and X-ray diffraction in the solid state[35] have shown the molecule to adopt the chair conformation in both phases further accentuating the cyclohexane analogy. A graphical representation of trithiacyclohexane (herein

referred to as ttch) is displayed in Figure 1. Bond lengths and bond angles taken from reference 35 are provided in the figure caption. The molecule crystallizes as an orthorhombic unit cell in the space group $Pmn2_1$. Given the sp^3 hybridization of the sulfur orbitals in such a configuration, two lone pairs of electrons remain available for bonding to one or more metal centers. Metal bonding could occur in either equatorial or axial directions with respect to the sulfur atoms.

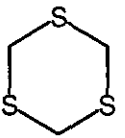

Figure 1: 1,3,5-trithiacyclohexane (ttch), C-S 1.82 Å; ∠CSC, 100.7°; ∠SCS, 115.3°.

Coordination of the intact ttch ligand is quickly verified with routine spectroscopy. A relatively intense band occurs at 727 cm^{-1} in infrared spectra of KBr pellets of ttch. This band has been assigned to the CSC ring stretch.[36] Results obtained here show only slight shifts of this band upon coordination of ttch to metal clusters. ^1H NMR spectra of ttch in $CDCl_3$ show a single broad peak at 4.14 ppm. The single signal for ttch is attributed to a fluxional process in solution which results in interconversion of the axial and equatorial protons rendering them indistinguishable on the NMR timescale.[37]

Substitution of one of each of the methylene protons of ttch with alkyl groups makes the heterocycle more soluble in common organic solvents. Judicious choice of the substituting group may also provide additional sites for coordination to metal centers. Recently the tribenzyl-substituted trithiane was prepared and characterized crystallographically by Edema *et al.*.[38] A graphical representation of this heterocycle and some relevant bond lengths and angles are presented in Figure 2. The substituted ttch crystallizes in the trigonal crystal system and belongs to the space group R3.

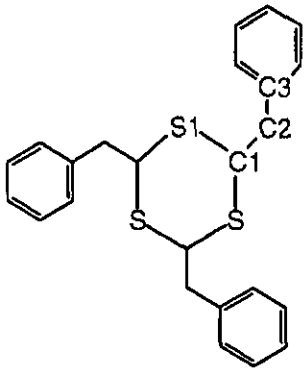

Figure 2: *cis* 2,4,6-tribenzyl-1,3,5-trithiacyclohexane, C1-S1; 1.811(1)Å, C1-C2; 1.536(2)Å, C2-C3; 1.512(2)Å, ∠C1S1C1b; 99.97°, ∠S1C1S1a; 114.35°.

Following the same synthetic procedure as Edema, the tribenzyl-substituted species was prepared here for use in reactions with metal carbonyl clusters. The reaction involves abstraction of a methylene proton with n-BuLi to produce the trithiane anion. This anion then undergoes addition at the acidic benzylic proton with subsequent elimination of bromide. Alkylations are carried out at the two remaining CH_2 groups by successive treatment with n-BuLi. The *cis* isomer is formed preferentially. This stereospecificity presumably results from the greater stability of the equatorial anion formed upon abstraction of a proton from the parent ttch by n-BuLi.[39] ^{1}H NMR and IR spectra of the sample prepared agreed completely with the values reported for the *cis* conformation, indicating the presence of a single isomer.

2.3 1,3,5-Trithiacyclohexane in Cluster Compounds

The extension of crown thioether chemistry to cluster complexes is apparent given their ability to stabilize low oxidation states. Furthermore ttch has a geometry particularly well-suited for coordination to the triangular face of a metal cluster, a bonding situation leading to increased cluster stability. Reactions with transition metal clusters show a marked tendency towards a face-capping mode via the three sulfur atoms of ttch with formation of bridging carbonyl groups at the cluster. The X-ray structures of clusters in which ttch is bound to the face of tetrahedral Ir_4[40] and Rh_4[41] metal frameworks reveal this somewhat

ubiquitous structural feature as does a series of tetrahedral clusters with ruthenium-cobalt metal frameworks and tteh ligands.[42] Bridging carbonyl groups are better π-acids and more effectively reduce the electron density at the metal centers resulting from the coordination of the primarily σ-donor tteh. As will be shown later, this structural feature can be used to advantage in studies of the fluxionality between bridging and terminal carbonyls. The Rh cluster above (ref. 41) provided an especially interesting fluxionality study. Upon bonding to the tteh, a metal-metal bond is broken, forming a butterfly-type skeleton with a μ_2-CO between the non-bonded wing-tip Rh atoms. This carbonyl group was shown to commute between each of the three basal Rh atoms by opening and reforming that end of the Rh-C bond while the Rh-C bond to the apical metal atom remained intact.

As yet no published reports of Os clusters containing tteh ligands are available. However other crown thioethers as well as sulfur-containing heterocycles have found application in osmium cluster chemistry. Adams *et al.*[43] have found that coordination of four-membered cyclic thioethers ($SCH_2CR_2CH_2$, R=H, Me, Ph) to trinuclear Os clusters leads to ring-opening oligomerizations, a preliminary step in the synthesis of trithia macrocycles. The authors suggest the μ_2-bridging mode of the sulfur results in Lewis acid behavior on the part of the bridged Os centers thus activating the ligated thioether toward nucleophilic attack by a free thietane molecule. Anticipating the same type of C-S bond cleavage, that group carried out reactions with the six-membered cyclic thioether, thiacyclohexane.[44] However, under similar conditions no oligomerization occurred. This work will be further discussed in connection with the reactions involving $Os_3(CO)_{12}$ and tteh presented here. Some trinuclear Os clusters of the crown thioether trithiacyclododecane, where the sulfur bonds to the cluster through either a simple σ bond or a μ_2-bridge have been prepared but as of yet, neither oligomerization nor C-H activation in those reactions has been reported.[45]

2.4 Reaction of $Fe_3(CO)_{12}$ with 1,3,5-Trithiacyclohexane

Refluxing a solution of $Fe_3(CO)_{12}$ and 1,3,5-trithiacyclohexane in benzene resulted in cluster fragmentation and C-S bond cleavage at the tteh to produce the dinuclear cluster $Fe_2(CO)_6(S_3C_3H_6)$ (**1**) as the major product (12.9%). This type of bond activation is not uncommon in reactions of Fe clusters.[46] As apparent from the deposition of an iron mirror on the tube walls, decomposition of the starting $Fe_3(CO)_{12}$ occurred to a significant degree also.

Filtration of the yellow reaction solution followed by standard TLC resulted in isolation of a yellow-orange solid which was shown by mass spectra to be **1**. In an alternative approach, starting from the mononuclear iron carbonyl, the same compound was isolated and characterized by Raubenheimer *et al.*.[47] There it was shown that reactions of $Fe(CO)_5$ with ttch under UV irradiation produced **1** in yields between 10 and 15%. This dinuclear cluster is represented graphically in Figure 3.

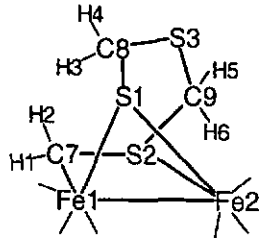

Figure 3: Graphical illustration of $Fe_2(CO)_6(\mu_2,\eta^3\text{-}SCH_2SCH_2SCH)$ (**1**)

Table **1** lists our IR and ^1H NMR data. Mass spectra (FAB) of **1** showed a well-defined M^+ peak at 418 mass units.

Table 1: IR and NMR data of $Fe_2(CO)_6(\mu_2,\eta^3\text{-}SCH_2SCH_2SCH_2)$ **1**

IR(c-hex,298K)	{$\nu_{CO}(cm^{-1})$}:	2071m	2030vs	2003s
		1993s	1981w	1970w
IR(KBr)	{$\nu_{CS}(cm^{-1})$}:	727w		
^1H NMR ($CDCl_3$, 298K)[a]	{δ(ppm)}:	4.24 (d(d),1H,J=14.2(2.1) Hz)		
		3.36 (d,1H,J=14.2 Hz)		
		3.28 (d, 1H,J=13.6 Hz)		
		3.23(d(d),1H,J=13.6(2.1)Hz)		
		2.22 (d,1H,J=10.7 Hz)		
		1.42 (d,1H,J=10.7 Hz)		

[a] 400 MHz

As shown in Table 1, solution IR spectra of **1** in non-polar solvents display six lines all falling within the frequency range of terminal carbonyl ligands. Taking account of slight shifts due to the different solvent, this spectrum compares well with that reported by Raubenheimer.

^{1}H NMR spectra obtained on a 400 MHz spectrometer however indicated a fine structure not reported in reference 47. There three doublets and one broad line were reported. In fact, room temperature spectra obtained for this work revealed six doublets two of which were further split into doublets. This spectrum is reproduced in Figure 4 and the peaks assigned according to the arguments which follow.

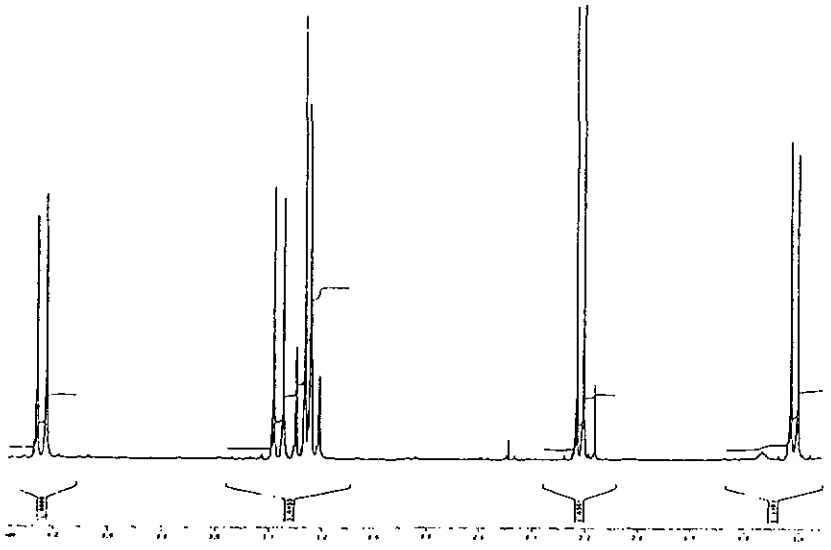

Figure 4: ^{1}H NMR ($CDCl_3$, 400 MHz) spectra of $Fe_2(CO)_6(\mu_2,\eta^3\text{-}SCH_2SCH_2SCH)$ **1**.

Homonuclear spin decoupling experiments revealed complex coupling between the protons of the ttch ligand of **1**. Decoupling at either of the upfield doublets (1.42 or 2.22 ppm) resulted in a singlet for the other signal. No effect was observed at any other part of the spectrum. The two upfield doublets thus represent two types of protons, one coupled to the other but distinct from one another and from other protons in the ligand. There remains four groups of signals (see Fig. 4). If the spectrum is obtained with irradiation at the frequency of the downfield doublet of doublets (4.24 ppm), a singlet is observed at 3.36 ppm, while the 3.23 ppm signal displays a simple doublet (fine splitting is no longer observed at 3.23 ppm). Decoupling at the 3.36 ppm signal resulted in a simple doublet at 4.24 ppm displaying the smaller coupling constant of 1.99Hz. It is implied that the larger coupling constant observed at

the 4.24 ppm signal (J=14.2Hz) results from interaction with the proton generating the doublet at 3.36 ppm (J=14.2Hz) analogous to the situation for the upfield signals (see above), however a secondary interaction occurs resulting in the fine splitting of the signal at 4.24 ppm (J=2.1Hz). The coupling constant of the doublet remaining at 4.24 ppm, after irradiation at the 3.36 signal, corresponds to the fine splitting at the 3.23 ppm signal (2.1Hz). Therefore the proton generating the 3.23 ppm signal produces the fine splitting at 4.24 ppm. The larger splitting observed at the 3.23 signal (J=13.6Hz) is a result of coupling to the protons at 3.28 ppm (J=13.6Hz).

In accordance with the structure of **1**, these features of the ^{1}H NMR spectrum suggest the inherent asymmetry of **1**. Restricted movement of the ttch upon coordination to a multinuclear metal framework resulting in distinguishable axial and equatorial protons, has been observed among other clusters presented in this work. Dynamic NMR studies of dinuclear ttch complexes of platinum also indicate chemically inequivalent axial and equatorial protons.[48] Increased activation energy for pyramidal sulfur inversion and ring reversal upon coordination of ttch to a metal center was cited as responsible for this feature. In the free ligand, it is these processes which render all the protons equivalent.

For compound **1** each proton of the fixed CH_2 groups produces a unique signal which is then split into a doublet by its geminal counterpart. Furthermore each distinct CH_2 group generates a pair of these doublets thus producing the main features of the spectrum; three pairs of doublets, integrating as 1:1:1. One CH_2 group is isolated from the others and shows no interaction with them (the two upfield doublets). These signals are assigned to H1 and H2 (see Fig. 3). The upfield shift is presumably due to proximity to the metal center. The CH_2 group located between the σ-bonded S atom (S2) and the S atom showing no bonds to the metal centers (S3) generates the doublets at 3.23 and 3.28 ppm (H5 and H6). The remaining two doublets (3.36 ppm and 4.24 ppm) are assigned to protons H3 and H4 located on C8 of the ttch derived ligand. The two CH_2 groups corresponding to the four downfield doublets are situated in a manner which allows an interaction between their equatorial protons. This interaction occurs for the two protons labeled H3 and H6 (Fig. 3) which in conjunction with S3, form a "w", or zigzag system. Coupling in a system of this type is documented and the reported coupling constant of 3-4 Hz[49] agrees within reason for that found here (1.99 Hz).

Reactions of triirondodecacarbonyl with σ-donor ligands have been shown to result in cluster fragmentation.[50] It was noted that elevated temperatures produced a greater degree of cluster breakup. Given that thermal activation was used to initiate reaction between $Fe_3(CO)_{12}$ and ttch, products of lower nuclearity were unavoidable. Moreover, the formation of metallic iron indicates that the major reaction occurring was thermal decomposition of the carbonyl. Compound **1** was most likely the result of reaction between the transitory "$Fe_2(CO)_7$"[51] and ttch. In contrast to these results, Raubenheimer *et al.*[47,52] have shown the formation of metal-metal bonds in reactions of $Fe(CO)_5$ with thioethers to produce several di- and trinuclear clusters. Both cluster build-up and cluster fragmentation seem to favor the dinuclear species. However, the significance of C-S bond breaking in this reaction cannot be ignored. The ability of $Fe_2(CO)_9$ to completely remove sulfur from thiophene has already been noted.[53]

2.5 Reaction of $Ru_3(CO)_{12}$ with 1,3,5-Trithiacyclohexane[54]

Refluxing a THF solution of $Ru_3(CO)_{12}$ and 1,3,5-trithiacyclohexane yielded the trinuclear cluster $Ru_3(\mu_2\text{-}CO)_3(CO)_6(\mu_3,\eta^3\text{-}S_3C_3H_6)$ (**2**) as the primary product. Compound **2** was soluble only in very polar solvents such as THF and acetone. Thin-layer chromatography was used to isolate the reaction products, however a very polar solvent mixture was necessary to elute a broad yellow band which could only be isolated from the Al_2O_3 support by rinsing with alternating portions of THF and methanol to give **2** (71%). Yellow block crystals of this compound were easily obtained from slow evaporation of a concentrated THF solution.

IR spectra of **2** showed four terminal carbonyl absorptions and one very intense band in the bridging carbonyl region (Table 2). The four bands in the terminal carbonyl region appear to be a typical indication of three axially disposed and three equatorially disposed CO groups[55]. The ^1H NMR spectrum shows two doublets of equal intensity in the alkyl region of the δ-scale (Table 2). These absorptions are assigned to the CH_2 groups of the ttch ligand. In contrast to the unligated ttch where unrestrained movement produces equivalent protons, the presence of two separate peaks for **2** in addition to their multiplicity reinforces the idea of restrained movement of the ligand. The NMR spectra imply that the protons of each CH_2 group are fixed rigidly in axial and equatorial positions so as to render them chemically inequivalent, a phenomenon of the thioether ligand already also noted in the Fe compound.

Table 2: IR and NMR data for $Ru_3(\mu_2\text{-}CO)_3(CO)_6(\mu_3,\eta^3\text{-}S_3C_3H_6)$ (2)

IR(THF, 298K)	{$\nu_{CO}(cm^{-1})$}:	2052m	2004s	1972w
		1950m	1810s	
IR (KBr)	{$\nu_{CS}(cm^{-1})$}:	731w		
^{1}H NMR ([D_8]THF, 298K)[a]	{δ(ppm)}:		4.16 (d, 3H,J=14.6 Hz)	
			2.38 (d, 3H,J=14.7 Hz)	

[a] 200 MHz

The molecular structure of **2** was determined through X-ray structural analysis of a single crystal and is illustrated in Figure 5. Bond distances and angles are given in Table 3. Cluster **2** was found to crystallize in the orthorhombic crystal system, in the space group P $na2_1$. In an independent study Pakkanen *et col.* also isolated and structurally characterized compound **2**.[56]

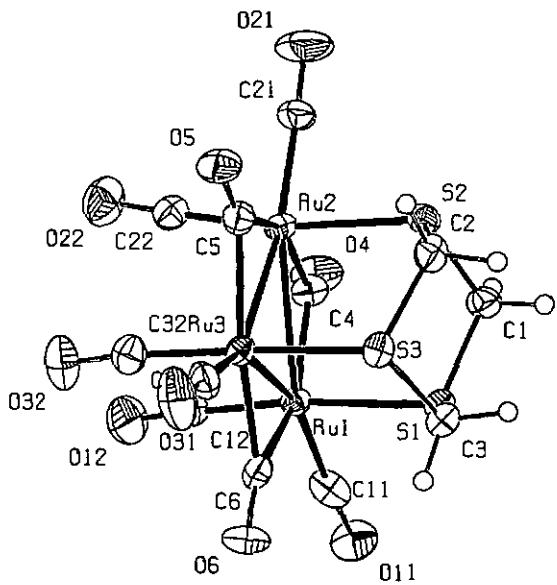

Figure 5: Molecular structure of $Ru_3(\mu_2\text{-}CO)_3(CO)_6(\mu_3,\eta^3\text{-}S_3C_3H_6)$ (2).

Table 3: Bond lengths (Å) and bond angles (°) for non-hydrogen atoms of $Ru_3(\mu_2\text{-}CO)_3(CO)_6(\mu_3,\eta^3\text{-}S_3C_3H_6)$ (2).

Ru(1)-Ru(2)	2.8687(8)	Ru(1)-Ru(3)	2.8378(9)	Ru(1)-S(1)	2.4315(17)
Ru(1)-C(4)	2.155(8)	Ru(1)-C(6)	2.124(8)	Ru(1)-C(11)	1.911(8)
Ru(1)-C(12)	1.884(8)	Ru(2)-Ru(3)	2.8306(13)	Ru(2)-S(2)	2.4276(18)
Ru(2)-C(4)	2.150(8)	Ru(2)-C(5)	2.143(9)	Ru(2)-C(21)	1.887(8)
Ru(2)-C(22)	1.865(8)	Ru(3)-S(3)	2.4248(18)	Ru(3)-C(5)	2.117(8)
Ru(3)-C(6)	2.158(8)	Ru(3)-C(31)	1.894(10)	Ru(3)-C(32)	1.882(7)
S(1)-C(1)	1.798(7)	S(1)-C(3)	1.805(7)	S(2)-C(1)	1.823(7)
S(2)-C(2)	1.788(9)	S(3)-C(2)	1.798(9)	S(3)-C(3)	1.809(7)
C(4)-O(4)	1.141(11)	C(5)-O(5)	1.150(9)	C(6)-O(6)	1.150(10)
Ru(2)-Ru(1)-Ru(3)	59.47(3)	Ru(2)-Ru(1)-S(1)	92.02(4)	Ru(2)-Ru(1)-C(4)	48.1(2)
Ru(2)-Ru(1)-C(6)	108.5(2)	Ru(2)-Ru(1)-C(11)	150.7(2)	Ru(2)-Ru(1)-C(12)	95.6(2)
Ru(3)-Ru(1)-S(1)	92.51(4)	Ru(3)-Ru(1)-C(4)	107.4(2)	Ru(3)-Ru(1)-C(6)	49.0(2)
S(1)-Ru(1)-C(4)	94.2(2)	S(1)-Ru(1)-C(11)	83.1(2)	S(1)-Ru(1)-C(12)	170.9(2)
C(4)-Ru(1)-C(6)	155.9(3)	Ru(1)-Ru(2)-Ru(3)	59.72(2)	Ru(1)-Ru(2)-S(2)	92.00(5)
Ru(1)-Ru(2)-C(4)	48.3(2)	Ru(1)-Ru(2)-C(5)	107.7(2)	Ru(3)-Ru(2)-S(2)	93.30(5)
Ru(3)-Ru(2)-C(4)	107.8(2)	Ru(3)-Ru(2)-C(5)	48.0(2)	S(2)-Ru(2)-C(4)	93.4(2)
C(4)-Ru(2)-C(5)	155.6(3)	Ru(1)-Ru(3)-Ru(2)	60.81(2)	Ru(1)-Ru(3)-S(3)	92.58(5)
Ru(1)-Ru(3)-C(5)	109.6(2)	Ru(1)-Ru(3)-C(6)	48.0(2)	Ru(2)-Ru(3)-S(3)	92.10(6)
Ru(2)-Ru(3)-C(5)	48.8(2)	Ru(2)-Ru(3)-C(6)	108.8(2)	S(3)-Ru(3)-C(6)	92.1(2)
C(5)-Ru(3)-C(6)	157.5(3)	Ru(1)-S(1)-C(1)	110.6(3)	Ru(1)-S(1)-C(3)	108.7(2)
C(1)-S(1)-C(3)	100.9(3)	Ru(2)-S(2)-C(1)	110.7(2)	Ru(2)-S(2)-C(2)	109.0(2)
C(1)-S(2)-C(2)	98.0(3)	Ru(3)-S(3)-C(2)	110.5(2)	Ru(3)-S(3)-C(3)	108.9(2)
C(2)-S(3)-C(3)	98.0(3)	S(1)-C(1)-S(2)	114.1(4)	S(2)-C(2)-S(3)	117.1(4)
S(1)-C(3)-S(3)	115.3(4)	Ru(1)-C(4)-Ru(2)	83.6(3)	Ru(1)-C(4)-O(4)	137.5(6)
Ru(2)-C(5)-Ru(3)	83.3(3)	Ru(2)-C(5)-O(5)	137.8(7)	Ru(1)-C(6)-Ru(3)	83.0(3)
Ru(1)-C(6)-O(6)	138.8(7)	S(3)-Ru(3)-C(5)	89.6(2)		

The metal framework of 2 is a triangular array of three Ru-atoms. Two terminal CO groups are bonded to each Ru-atom, one of which takes an axial position and the other an equatorial position. The three metal-metal bonds are spanned by μ_2-CO ligands. In a plane above and parallel to the plane of the Ru triangle lies the three S-atoms of the ttch ligand, each σ-bonded to the Ru-atom directly beneath it and acting as a 2-electron donor. The CH_2 groups of the ttch ligand occupy regular positions above the plane of the S-atoms. H atoms were placed at calculated positions. Overall the ttch ligand assumes a chair-like conformation.

Two sides of the Ru triangle are slightly shorter than the third (Ru1-Ru2, 2.8687(8) Å; Ru2-Ru3, 2.8306(13)Å vs. Ru1-Ru3, 2.8378(9)Å). These metal-metal distances are little changed from those in $Ru_3(CO)_{12}$[57] in spite of the presence of the μ_2-CO ligands. All μ_2-C(O)-

M distances are nearly equivalent resulting in symmetrically bridging carbonyl ligands. The Ru triangle and the bridging CO groups occupy a plane in which atom C4 shows the maximum deviation from that plane (C4-M_3, 0.153(9)Å) while C5 and C6 remain essentially in the M_3 plane (C5-M_3, 0.018(9)Å; C6-M_3, 0.042(8)Å). The planarity of the cluster can be alternatively illustrated by defining an M_3 plane and three M-{μ_2-C(O)}-M planes and citing the dihedral angle between them. For compound **2** those angles vary from 0.6° to 5.50°.

Within the tripodal ligand C-S bonds are uniform and contribute little to distortions in the symmetry of the molecule. The dihedral angle between the plane formed by the three S-atoms and that formed by the metal base is calculated at 0.14(6)Å. A nearly perfect C_3 axis extends through the center of the molecule and contains three vertical mirror planes resulting in C_{3v} symmetry for the entire molecule. The somewhat analogous structures cited earlier and involving tetrahedral metal frameworks in which the ttch ligand is bonded to the triangular metal base (M = Ir[40]; M = Rh[41]; M = Ru[42]) show similar trends in terms of M-M, M-S, and S-C bonds. A species of C_{3v} symmetry occurs as one isomer of the Ir_4 cluster.

Inspection of the packing arrangement of **2** in the crystalline state reveals extensive intermolecular hydrogen bonding. Calculations show the distances between the methylene protons of the ttch ligand on one molecule of **2** and the carbonyl groups of a second molecule, approach one another at distances significantly below the sums of their Van der Waals radii. These interactions are outlined in Table 4. Here it is clear that while all the carbonyl groups are involved, the bridging carbonyl groups undergo the majority of these interactions. In one case (CO5), the μ_2-CO is seen to interact with two adjacent methylene protons of a neighboring ttch ligand. Braga *et al.* published a series of studies detailing these interactions in several organometallic crystal systems.[58] The most recent of these publications compares the tendencies of the three species $Ru_3(CO)_{12}$, $Ru_3(CO)_9(\mu_3,\eta^2,\eta^2,\eta^2\text{-}C_6H_6)$ and **2**[59] and their tendencies to form intermolecular hydrogen bonds. It was shown through a series of MO calculations, that more intermolecular hydrogen bonding occurs in **2** mostly as a result of the increased acidity of the ttch hydrogens as compared to those of the benzene ligand as well as the increased basicity of bridging versus terminal carbonyls.

Table 4: Hydrogen bonding interactions in **2**.

donor-H···acceptor	D···A (Å)	H···A (Å)*	D-H···A (°)*
C1-H1-O32	3.312(10)	2.548	127.39
C1-H1-O6	3.154(10)	2.334	131.82
C1-H1A-O5	3.297(10)	2.309	149.45
C3-H3-O4	3.338(10)	2.536	132.72
C3-H3A-O22	3.166(10)	2.596	111.09
C3-H3A-O5	3.244(9)	2.218	153.32

**Since the methylene hydrogens were placed in calculated positions, no error is available for interactions involving these atoms.*

2.6 A Monosubstituted Derivative of $Ru_3(\mu_2\text{-}CO)_3(CO)_6(\mu_3,\eta^3\text{-}S_3C_3H_6)$.

Compound **2** was found to be very stable towards substitution of its carbonyl groups. Exposure to elevated temperatures and/or trimethylamine oxide in the presence of t-butylisocyanide showed no indication of reaction. In order to obtain a monosubstituted derivative of compound **2**, it was necessary to first prepare the monosubstituted t-butylisocyanide derivative of triruthenium dodecacarbonyl, $Ru_3(CO)_{11}\{(CH_3)_3CNC\}$, which was then refluxed with one equivalent of ttch in hexane for 8 hours. The yellow solid thus obtained was then purified by preparative TLC and characterized as $Ru_3(\mu_2\text{-}CO)_3(CO)_5\{(CH_3)_3CNC\}(\mu_3,\eta^3\text{-}S_3C_3H_6)$ (**3**) (Fig. 6).

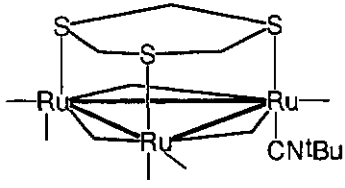

Figure 6: Graphical representation of $Ru_3(\mu_2\text{-}CO)_3(CO)_5(^tBuNC)(\mu_3,\eta^3\text{-}S_3C_3H_6)$ (**3**).

IR spectra of compound **3** were consistent with a monosubstituted derivative (Table 5). The band indicative of The NC group of the t-butylisonitrile was present at 2159 cm^{-1}, shifted little from the unligated species. As in IR spectra of the parent compound **2**, four bands in the region of terminal carbonyl groups and one strong band in the bridging carbonyl region

were found. Spectra exhibit approximately the same intensity pattern as in **2** but each band is shifted to 31-7 cm^{-1} lower energy. The better σ-donating abilities of the t-butylisonitrile ligand compared to the carbonyl ligands allows for more electron density at the metal atoms, resulting in an increased M→CO π*-acceptor backbonding interaction for both types of CO groups and a concomitant decrease in CO bond order, producing these frequency shifts in the IR spectra. This is a common effect of weak π-acceptor ligands located *trans* to CO groups.

Normal temperature and pressure ^1H NMR spectra of **3** (Table 5) show a broad singlet for the protons of the ttch ligand as well as a singlet for the methyl groups of the t-butylisonitrile. The presence of a broad singlet for the methylene protons of the ttch ligand implies the barrier to interconversion of axial and equatorial hydrogens has been lowered in the substituted cluster. Although no crystal structure of **3** was undertaken, one could assume a less tightly held ttch ligand due to the decreased electronic requirements of the cluster in the presence of the t-butylisonitrile ligand which in turn would allow more flexibility on the part of the CH_2 groups.

Table 5: IR and NMR data for $Ru_3(\mu_2\text{-}CO)_3(CO)_5(^tBuNC)(\mu_3,\eta^3\text{-}S_3C_3H_6)$ (**3**)

IR(THF,298K)	{$\nu_{NC}(cm^{-1})$}	2159m		
	{$\nu_{CO}(cm^{-1})$}:	2021s	1988vs	1956s
		1943vs	1794vs	
IR(KBr)	{$\nu_{CS}(cm^{-1})$}:	725w		
^1H NMR ([D_8]THF, 298K)[a]	{δ(ppm)}:	2.52 (s,br, 6H)	1.31 (s, 9H)	

[a] 200 MHz

Given the isotopic distribution of Ru, mass spectra of its cluster compounds appear complicated and are often difficult to decipher. However certain aspects of the mass spectra for compound **3** are discernible and can be interpreted. For instance, a group of peaks centered at 749 mass units can be considered as the M^+ peak of **3**. The loss of four CO groups is indicated by a group of peaks centered at 638. Successive loss of carbonyls continues down to 520 mass units at which point the t-BuNC group is lost.

2.7 NMR Study of the Carbonyl Fluxionality in $Ru_3(\mu_2\text{-}CO)_3(CO)_6(\mu_3,\eta^3\text{-}S_3C_3H_6)$ (2) and $Ru_3(\mu_2\text{-}CO)(CO)_5(t\text{-}BuNC)(\mu_3,\eta^3\text{-}S_3C_3H_6)$ (3)[60]

Changes in the ^{13}C NMR spectra with temperature, provided qualitative evidence that a dynamic process involving the carbonyl groups occurs for compound 2. Detailed variable temperature ^{13}C NMR experiments produced rate constants and activation parameters while variable pressure ^{13}C NMR results indicated the types of transition states employed in the exchange. The effect of a slight change in the ligand envelope is provided by substituting an axial carbonyl group in compound 2 with the σ-donor ligand t-butylisonitrile (compound 3) and carrying out the same experiments.

A fluxional molecule is one that possesses the ability to interconvert between two different configurations, both of which represent an energy minimum. The time-scale on which these interconversions occur falls within the range of nuclear magnetic resonance techniques (10^{-1}s to 10^{-9}s) thus NMR spectroscopy has proven extremely useful in analysis of these systems. Investigations of the fluxionality of the carbonyl ligands in trinuclear group VIII carbonyl clusters using ^{13}C NMR is an area that began to attract interest almost two decades ago [61],[62]but to this day, investigations continue concerning the mechanisms by which these interconversions take place.[63] The solid-state molecular structure of all $M_3(CO)_{12}$ species has been determined but only in the case of M = Os do room temperature ^{13}C NMR spectra agree with the X-ray crystal structure, that is to say separate signals corresponding to axial COs and to equatorial COs are found.[64] In contrast only a single resonance line for the carbonyl carbons is observed in room temperature ^{13}C NMR spectra of the Fe and Ru species. The Fe and Ru carbonyls' behavior exemplifies a fluxional process among the carbonyl ligands. Ligand fluxionality occurs for $Os_3(CO)_{12}$ also but only at elevated temperatures. The mechanism of ligand exchange in was proposed to occur via cycling of an intermediate with two bridging carbonyls on one edge of the metal triangle.[61a] The same exchange mechanism was postulated for the Ru and Os clusters, however Cotton *et al.* later suggested the possibility of an alternative process involving bridging carbonyls over all three metal edges.[65] As illustrated in scheme I this exchange mechanism can interconvert either axial carbonyls, as proposed for $Fe_3(CO)_{12}$,. The carousel-like exchange of equatorial CO groups has been termed the "merry-go-round" exchange process.

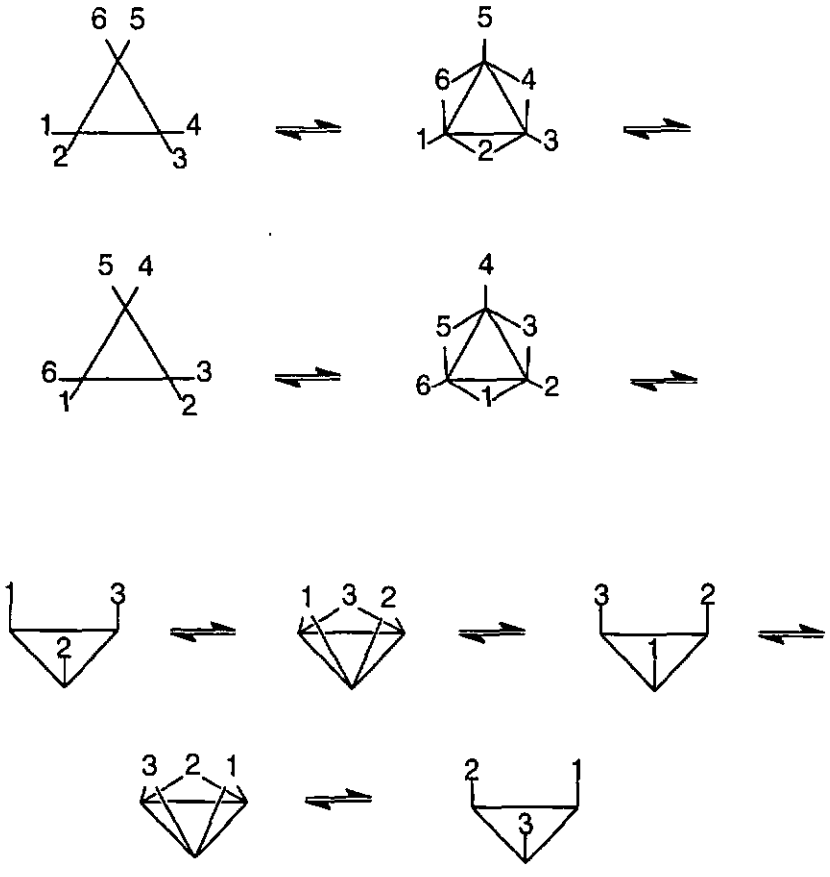

Scheme I: Exchange processes for equatorial and axial carbonyls in $M_3(CO)_{12}$ clusters.

Magnetic resonance studies of carbonyl fluxionality in tetrahedral carbonyl clusters adopting a molecular structure akin to the triply-bridged intermediate shown in scheme I indicate a merry-go-round process.[40,41] As per Figure 5, compound **2** possesses the structural traits associated with carbonyl cycling vis-à-vis the merry-go-round process. It is the tendency of the ttch ligand to encourage such structural characteristics that render it so useful in studies of the merry-go-round fluxional process.

The appearance of the ^{13}C NMR spectrum in the region of slow-exchange compared to fast-exchange, i.e. the number of peaks and their relative intensities is indicative of the type of exchange taking place. The population dependence of the chemical shift with respect to temperature can be estimated from a typical spectrum but complete line shape analysis is necessary to generate precise rate constants. The mean lifetime (τ_i) of a given species *i* is determined from the full width at half maximum height (FWHM) ($\Delta\nu_{1/2}$) in the region of signal coalescence:

$$1/\tau_i = \pi\Delta\nu/\sqrt{2} \qquad (1)$$

For a first-order reaction, as for an isomerization, the inverse of τ_i (τ_i^{-1}) yields the rate constant (k) for the isomerization in question:

$$k = 1/\tau_i \qquad (2)$$

The spectra obtained over the temperature range are simulated using a method involving *Kubo-Sak* matrices.[66]

The activation parameters ($\Delta H^{\ddagger}$ and $\Delta S^{\ddagger}$) are obtained by measuring the temperature dependence of the rate constant and fitting the results to the Eyring equation.

$$k = (k_B T/h)\exp\{(\Delta S^{\ddagger}/R) - (\Delta H^{\ddagger}/RT)\} \qquad (3)$$

where k_B is the Boltzmann constant and h is Planck's constant.

A number of publications exist describing the fundamental concepts involved in interpretation of high pressure NMR data.[67] Van Eldik derives the basic relationship from the pressure dependence of the chemical potential at constant temperature:[67a]

$$\left(\frac{\partial\mu}{\partial P}\right)_T \equiv \overline{V}i \qquad (4)$$

where $\overline{V}i$ is the partial molar volume of species i. This relationship holds true only when considering a pressure-independent concentration scale (i.e. mole fraction or molality) otherwise the compressibility of the solution must be taken into account. The definition of chemical potential with respect to concentration ($\mu_i = \mu^\circ + RT\ln(x_i)$) combined with the prerequisite that the chemical potential of a reaction at equilibrium is equal to zero, provides the relation between the change in equilibrium constant with respect to pressure at constant temperature and the reaction volume ($\Delta\overline{V}$).

$$-RT\left(\frac{\partial \ln K}{\partial P}\right)_T = \Delta\overline{V} \qquad (5)$$

A restatement of the basic pretext of the transition state theory follows and places a transition state $M^\ddagger$ in equilibrium with reactants A and B which then goes on to form the product(s). This theory can be applied to isomerization reactions and allows the rate constant k for the reaction to be expressed as a function of the equilibrium constant. Thus a relationship entirely analogous to (5) above between the rate constant's pressure dependence and the activation volume ($\Delta V^\ddagger$) is possible. The activation volume consists of two terms. The first considers volume changes due to electrostrictive forces ($\Delta V^\ddagger_{elec}$) and is the predominant factor in reactions involving charged species. The other represents volume changes due to intrinsic factors ($\Delta V^\ddagger_{int}$) and results from changes in internuclear distances within the reactants during the formation of the transition state. Often $\Delta V^\ddagger_{elec}$ can be so large as to change the sign of the observed activation volume. For isomerization reactions however, this term becomes negligible and the observed changes in rate constant accurately reflect the volume changes involved in the activation step of the reaction in question. Changes in rate constant with respect to pressure indicate the types of transition states employed in the isomerization. Dissociative mechanisms are characterized by positive activation volumes and decreasing rate constants with increasing pressure while associative mechanisms display increasing rate constants with increasing pressure i.e. negative activation volumes are observed. An activation volume of zero is observed for interchange mechanisms.

The ^{13}C NMR spectrum of a sample of $Ru_3(\mu_2\text{-}CO)_3(CO)_6(\mu_3,\eta^3\text{-}S_3C_3H_6)$ (**2**) enriched in ^{13}CO (*ca.* 30%) in [D_8]THF is blocked at 178 K and presents three signals of equal

intensities in the CO region (see Fig. 7). The resonances at 264.8, 200.8, and 199.1 ppm can be attributed to the bridging, axial, and equatorial carbonyl groups respectively.[68] This would imply that the C_{3v} geometry of 2 in the solid state is roughly maintained in solution. With increasing temperature, the signals at 264.8 and 199.1 ppm start to broaden, indicating an intramolecular exchange process between the bridging and equatorial carbonyls. The axial carbonyl ligands do not participate in this "merry-go-round" scrambling process. Figure 7 shows the measured (left) and calculated (right) spectra at five different temperatures. The rate constants of the merry-go-round were determined at different temperatures from the calculated spectra using a non-linear, least-squares fitting procedure.[69] The activation parameters were calculated from those rate constants via the Eyring equation[70] using a non-linear least squares program and are summarized in Table 6.

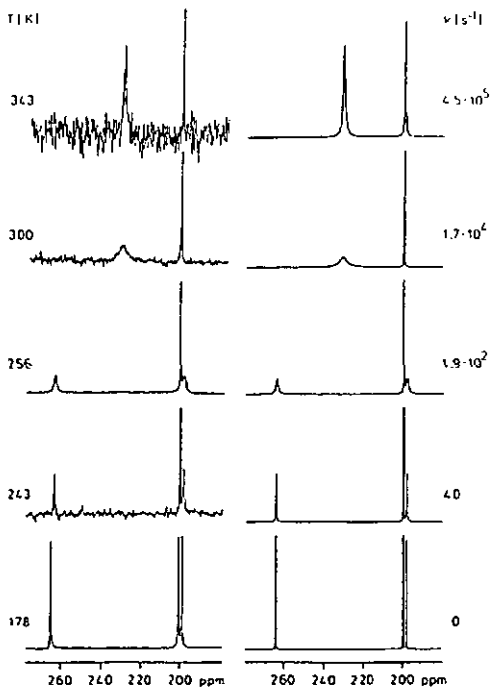

Figure 7: Experimental (left) and calculated (right) variable-temperature spectra of **2** in [D_8]THF.

Table 6: Kinetic Parameters for the Merry-go-Round Process in $Ru_3(\mu_2\text{-}CO)_3(CO)_6(\mu_3,\eta^3\text{-}S_3C_3H_6)$ (**2**) and $Ru_3(\mu_2\text{-}CO)_3(CO)_5(t\text{-}BuNC)(\mu_3,\eta^3\text{-}S_3C_3H_6)$ (**3**).

	$k_{298}[s^{-1}]$	$\Delta H^{\ddagger}$[kJ/mol]	$\Delta S^{\ddagger}$[J/mol]	$\Delta G^{\ddagger}$[kJ/mol]	$\Delta V^{\ddagger}[cm^3/mol]$
2	$(1.4\pm0.2)\cdot10^4$	62.7±3	+45.1±11	49.3±0.4	+13.3±1.2[a]
3	71±11	102.6±7	+153.9±26	56(.7±0.6	+14.1±1.8[b]

[a] *T = 253.1K;* [b] *T = 279.5K.*

The *C*, geometry of $Ru_3(\mu_2\text{-}CO)_3(CO)_5(t\text{-}BuNC)(\mu_3,\eta^3\text{-}S_3C_3H_6)$ (**3**) in solution is similar to that of **2** with the isocyanide ligand replacing an axial carbonyl group. Indeed, the ^{13}C NMR spectrum of a sample of **3** enriched in ^{13}CO (*ca.* 30%) in [D_8]THF is blocked at 263 K and shows two resonances in the region of bridging carbonyls with an intensity ratio 2:1 (a,b), two resonances with relative intensities 2:1 for equatorial carbonyls (c,d), and a single resonance for the axial carbonyls (e) (Figure 8 shows the ^{13}C NMR spectra along the top). The FWHM of the resonance assigned to the axial carbonyl groups is unaffected upon raising the temperature, while the former four resonances start to broaden indicating that an exchange process takes place in this cluster also. A ^{13}C EXSY spectrum of **3** in [D_8]THF at 263 K (Fig. 8) shows the following dynamic connectivities for the CO groups: a - b, b - c, a - d, which correspond to the merry-go-round of the bridged and equatorial carbonyls analogous to that of **2**. The simulation of the ^{13}C NMR spectra of **3** at different temperatures by the same procedure as that used for **2** led to the activation parameters reported in Table 6.

The pressure dependence of the rate constants of the merry-go-round were determined from spectra obtained at different pressures (1 - 2000 bar) using the same fitting procedure as that used in the variable-temperature work. Those rate constants were then fitted to equation (6) as shown in Figure 9.

$$\ln(k) = \ln(k_0) - \Delta V^{*} P/RT \qquad (6)$$

The intercept of that line gives the rate constant (k_0) at 0.1 MPa and the slope gives the activation volume. The values obtained are arranged in Table 6.

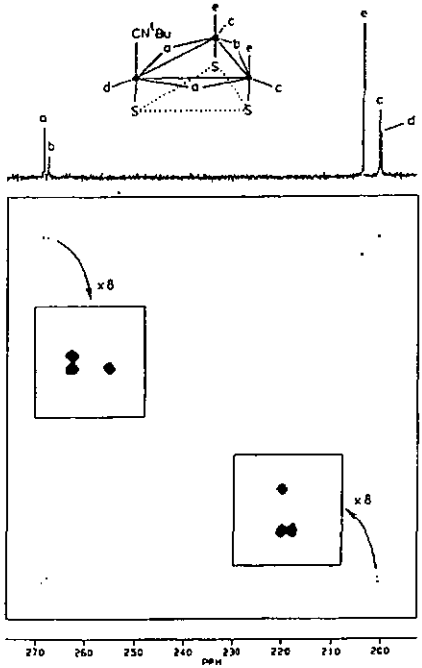

Figure 8: EXSY ^{13}C NMR spectrum of 3 in [D_8]THF at 263K. Mixing time: 100ms.

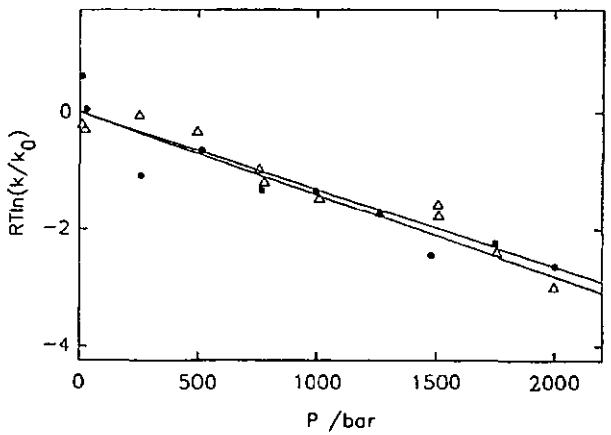

Figure 9: Pressure effect on the normalized natural logarithm of the rate constants for the CO scrambling in 2 at 253.1K (•) and in 3 at 279.5K (Δ).

Introducing the t-BuNC ligand in an axial position of **2** slows the CO scrambling process. The isocyanide ligand is a better σ-donor and weaker π-acceptor than CO and a μ_2-CO group is a better π-acceptor than a terminal one. Therefore the CO-bridged ground-state geometry of **3** is stabilized relative to that of **2**, and the observed increase in activation enthalpy is expected.

The activation volumes of the merry-go-round process in **2** and **3** are equal within experimental error. A similar study of the merry-go-round in $Ir_4(CO)_9(\mu_3,\eta^3\text{-}S_3C_3H_6)$ offers the only activation volume available for comparison (+8.3 cm^3 mol^{-1}).[71] In contrast to **2** and **3**, two isomers of the Ir_4 cluster were isolated one with three edge-bridging carbonyl groups, analogous to the geometry of **2**, and the other with all terminal carbonyl groups. This allowed for calculation of the difference in volume between the two isomers (+15.4 cm^3 mol^{-1}) which was attributed to the conversion of the three bridging carbonyls groups to the unbridged form. Since the activation volume (+8.3 cm^3 mol^{-1}) was approximately 50% the reaction volume (+15.4 cm^3 mol^{-1}), and since the isomerization involves the breaking of three Ir-CO bonds to form three additional terminal carbonyls, a transition state characterized by three semi-bridging carbonyls was proposed. An unbridged transition state would have required a change of volume of 5.1 cm^3 mol^{-1} per carbonyl ligand (15.4÷3 ~5.1). For clusters **2** and **3** the activation volume is greater than that of the Ir_4 cluster by ca. 6 cm^{-3} mol^{-1}. One can therefore propose a transition state of the merry-go-round for clusters **2** and **3** having a geometry which is closer to the limiting dissociative case (with six equatorial, terminal carbonyls) than the semi-bridging transition state proposed for the Ir cluster. These results are illustrated graphically in Figure 10.

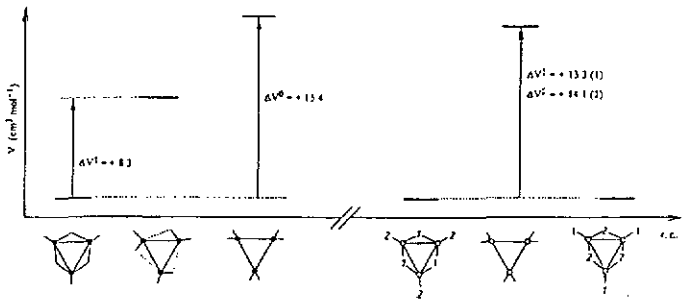

Figure 10: Volume profiles for the merry-go-round process a) in $Ir_4(CO)_9(\mu_3,\eta^3\text{-}S_3C_3H_6)$ (• = Ir) and b) in **2** and **3** (° = Ru). Only the basal face of the Ir cluster is shown; r.c. = reaction coordinate.

2.8 Reaction of $Ru_3(CO)_{12}$ with 1,3,5-Trithia-2,4,6-tribenzylcyclohexane

A refluxing THF solution of $Ru_3(CO)_{12}$ and the pre-prepared ligand 1,3,5-trithia-2,4,6-tribenzylcyclohexane produced the capped trinuclear Ru cluster $Ru_3(\mu_2\text{-}CO)_3(CO)_6\{\mu_3,\eta^3\text{-}S_3(CHCH_2Ph)_3\}$ (**4**). Compound **4** shows a wider solubility range than compound **2**, presumably due to the benzyl groups of the ligand. Preparative TLC in an acetonitrile/toluene mixture was found to most effectively elute a wide yellow band which was easily isolated with CH_2Cl_2 to produce **4** as a yellow solid. Rectangular block crystals of **4** were obtained from an acetone solution maintained at -18°C over a period of 5-7 days.

As for compounds **2** and **3**, five bands were found in the carbonyl region of IR spectra of **4** (Table 7). However in contrast to consistent ν_{CO} energy decreases caused by axial substitution at the metal framework by the better σ-donor t-butylisocyanide, for compound **4** slight energy increases of 5-9 cm^{-1} for the terminal CO bands and a decrease of 9 cm^{-1} for the bridging CO bands is observed. The frequency reductions at the bridging carbonyl bands can

be associated with the slightly better electron donating abilities of the thioether ligand brought about by substitution of a proton with the benzyl group (enabled through the stability of the benzyl cation). The enhanced π-acceptor abilities of bridging carbonyl groups relative to terminal groups allow them to compete more effectively for the slightly greater electron density at the metal centers. This populates the π* CO orbitals and produces a weaker μ_2-C-O bond.

A contrary effect most likely produces the frequency shifts observed for the terminal groups. Since terminal carbonyl groups interact with the metal through primarily σ-bonds, the slightly better donor properties of the substituted ttch could lead to an increased σ-bonding interaction. Valence bond theory can be used to describe this phenomenon. Given higher electron density at the metal, canonical form I is preferred over canonical form II:

$$\underset{\text{I}}{M\text{-}C{\equiv}O|^{\ominus\ \oplus}} \leftrightarrow \underset{\text{II}}{M{=}C{=}\ddot{O}^{\ddot{-}}}$$

The increased t-CO bond order produces an increase in $\nu_{t\text{-}CO}$.

The decreased electron density at the thioether portion of the ligand is evident in the ^{1}H NMR (Table 7) where a shift in the CH proton of ttch downfield to 5 ppm is observed.

Table 7: IR and NMR data for $Ru_3(\mu_2\text{-}CO)_3(CO)_6\{\mu_3,\eta^3\text{-}S_3(CHCH_2Ph)_3\}$ (4)

IR(c-hex, 298K)	{$\nu_{CO}(cm^{-1})$}:	2058vs	2014vs	1981m
		1959s,br	1802s,br	
IR(KBr)	{$\nu_{CS}(cm^{-1})$}:	700m		
^{1}H NMR ([D_6]acetone, 298K)[a]	{δ(ppm)}:		7.20-7.34 (m, 4H, Ph-*H*)	
			5.00 (t, 1H, J=8.2 Hz,C-*H*)	
			2.82 (d, 2H,J=8.2 Hz,C-H_2)	

[a] 200 MHz

Two different views of the molecular structure of **4** as determined by an X-ray structural analysis are illustrated in Figure 11. Bond distances and angles are reported in Table 8. Crystals of **4** are monoclinic and of the space group $P2_1$.

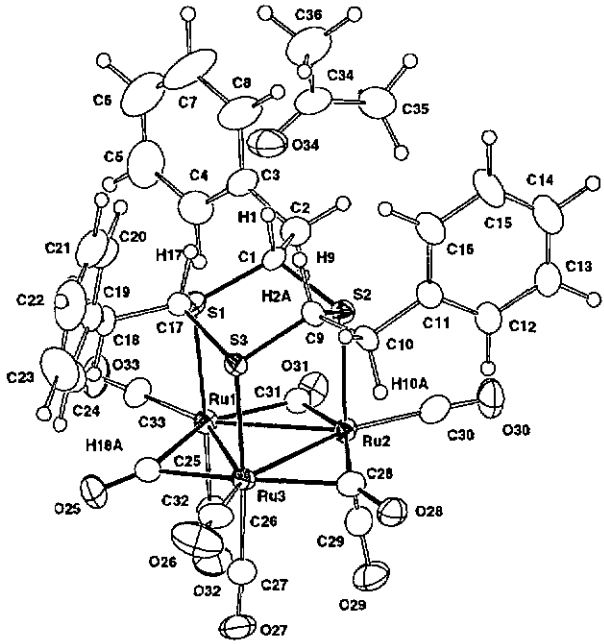

Figure 11a. Molecular structure of $Ru_3(\mu_2\text{-}CO)_3(CO)_6\{\mu_3,\eta^3\text{-}S_3(CHCH_2Ph)_3\}$ (**4**).

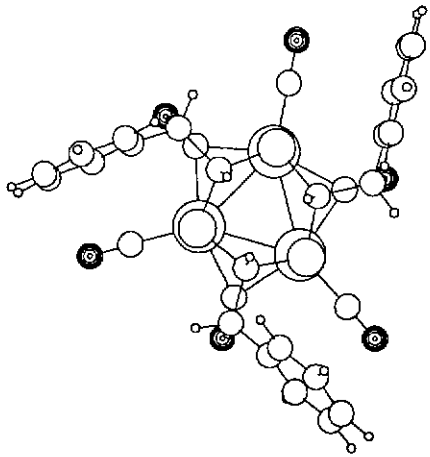

Figure 11b: View of $Ru_3(\mu_2\text{-}CO)_3(CO)_6\{\mu_3,\eta^3\text{-}S_3(CHCH_2Ph)_3\}$ (**4**) along C_3 axis.

Table 8: Selected bond lengths (Å) and bond angles (°) for non-hydrogen atoms of $Ru_3(\mu_2\text{-}CO)_3(CO)_6\{\mu_3,\eta^3\text{-}S_3(CHCH_2Ph)_3\}$ (**4**).

Ru(1)-Ru(2) 2.8500(8)	Ru(1)-Ru(3) 2.8359(8)	Ru(1)-S(1) 2.4388(16)
Ru(1)-C(25) 2.126(6)	Ru(1)-C(31) 2.157(6)	Ru(2)-Ru(3) 2.8453(10)
Ru(2)-S(2) 2.4489(16)	Ru(2)-C(28) 2.168(7)	Ru(2)-C(31) 2.118(7)
Ru(3)-S(3) 2.4431(16)	Ru(3)-C(25) 2.130(6)	Ru(3)-C(28) 2.124(7)
S(1)-C(1) 1.816(6)	S(1)-C(17) 1.824(6)	S(2)-C(1) 1.828(6)
S(2)-C(9) 1.832(5)	S(3)-C(9) 1.818(5)	S(3)-C(17) 1.823(6)
C(1)-C(2) 1.542(8)	C(2)-C(3) 1.514(9)	C(9)-C(10) 1.522(8)
C(10)-C(11) 1.496(8)	C(18)-C(19) 1.518(8)	O(34)-C(34) 1.206(10)
C(34)-C(35) 1.508(11)	C(34)-C(36) 1.473(11)	Ru(1)-Ru(2)-Ru(3) 59.73(2)
Ru(1)-Ru(2)-S(2) 91.95(4)	Ru(1)-Ru(3)-Ru(2) 60.22(2)	Ru(1)-Ru(3)-S(3) 92.96(4)
Ru(1)-Ru(3)-C(25) 48.2(2)	Ru(1)-S(1)-C(1) 110.9(2)	Ru(1)-S(1)-C(17) 113.0(2)
Ru(2)-Ru(1)-Ru(3) 60.05(2)	Ru(2)-Ru(3)-S(3) 92.41(4)	Ru(2)-Ru(1)-S(1) 92.67(4)
Ru(2)-Ru(1)-C(25) 108.2(2)	Ru(2)-Ru(1)-C(31) 47.6(2)	Ru(2)-S(2)-C(1) 111.3(2)
Ru(2)-Ru(3)-C(25) 108.2(2)	Ru(2)-Ru(3)-C(28) 49.1(2)	Ru(2)-S(2)-C(9) 111.4(2)
Ru(2)-C(28)-Ru(3) 83.0(2)	Ru(3)-Ru(2)-S(2) 92.03(4)	Ru(3)-Ru(2)-C(28) 47.8(2)
Ru(3)-Ru(1)-S(1) 91.78(4)	Ru(3)-Ru(1)-C(25) 48.28(2)	Ru(3)-Ru(1)-C(31) 107.4(2)
Ru(3)-Ru(2)-C(31) 108.3(2)	Ru(3)-S(3)-C(9) 111.9(2)	Ru(3)-S(3)-C(17) 111.5(2)
S(1)-Ru(1)-C(25) 93.5(2)	S(1)-Ru(1)-C(31) 95.97(15)	S(2)-Ru(2)-C(28) 94.5(2)
S(2)-Ru(2)-C(31) 95.0(1)	S(3)-Ru(3)-C(25) 95.0(2)	S(3)-Ru(3)-C(28) 94.0(2)
C(25)-Ru(1)-C(31) 154.3(2)		

A triangular metal framework defines the base of compound **4**. To each Ru atom two terminal CO groups are bonded. A bridging CO group spans each of the metal-metal bonds. The substituted ttch ligand sits over the trinuclear metal base and shows a chair conformation of the S_3C_3 ring. Each sulfur ligand is bonded to the Ru atom directly beneath it. The benzyl groups of the ligand extend laterally from the S_3C_3 ring with the phenyl rings adopting a propeller-like orientation. All protons were placed in calculated positions.

The range of bond distances among the Ru atoms of the triangular base of compound **4** is relatively small (Ru1-Ru2, 2.8500(8)Å; Ru1-Ru3, 2.8359(8)Å; Ru2-Ru3, 2.8453(10)Å) displaying slightly less variation than those bond lengths of compound **2**. All three Ru-S bonds are longer than those exhibited by compound **2** (**4**; avg. Ru-S distance; 2.444(7)Å) but vary little among themselves. The longer Ru-S bonds further verify the increased σ-donor nature of the substituted ttch.

The M-(μ-)CO bond lengths are uniform, thus categorizing the bridging carbonyls as symmetrical bridging groups. All the μ_2-CO groups are shown to fall below the M_3 plane. The

distances to the M_3 plane from the carbon atoms of the μ_2-CO groups falls between 0.141(7)Å and 0.171(7)Å. The dihedral angles between the M_3 plane and the three different M-{μ_2-C(O)}-M planes varies from 5.1(2)° to 6.1(2)°. Figure 11b shows the bridging carbonyl groups to eclipse the HC-CH_2 bonds of the substituted ligand, and suggests that one factor in the bending away of the μ_2-CO groups may be the increased steric requirements of the substituted tch ligand

The S-C and C-C bond distances within the ligand deviate little among themselves and compare with the bond lengths reported for the unbound ligand. The benzyl groups of the ligand are oriented in a regular fashion about the exterior of the S_3C_3 ring however their presence lowers the C_{3v} symmetry displayed by the parent compound to C_3 for this derivative. One molecule of acetone was found to co-crystallize with cluster **4**.

This cluster exhibits an interesting sort of intramolecular hydrogen bonding. In Table 9 where all observed hydrogen bonding is summarized, a noticeably short distance is seen between the benzylic protons which are perpendicular to the S_3C_3 plane and the bridging carbonyls directly beneath them (these interactions are marked with a †). Figure 11b accentuates the orientation of the benzylic protons of the ligand and in itself predicts this interaction This hydrogen bonding interaction would compete with the steric interaction mentioned above causing the molecule to orient the bridging carbonyls in a manner which would compensate both effects.

Similar to cluster **2**, intermolecular hydrogen bonding was also observed in **4**. The distances between the relevant atoms are summarized in Table 9. The basic nature of the bridging carbonyl groups is apparent here as it was for cluster **2**. That is to say an intermolecular interaction is observed, however the donor groups in **4** are comprised of phenyl carbons of the benzyl groups and their hydrogens (C15-H15···O25, C20-H20···O28) similar to that observed in $Ru_3(CO)_9(\mu_3,\eta^2,\eta^2,\eta^2\text{-}C_6H_6)$.[59] This most likely reflects the unavailability of the methylene protons of the tch ligand to another molecule of **4** due to steric crowding. The phenyl hydrogens are simply more accessible.

The solvent molecule found to crystallize with **4** also takes a role in these van der Waals interactions. The hydrogens of its methyl groups are shown to interact with the

equatorial carbonyls of a molecule of **4**. Yet at the other end of this solvent molecule, the ketonic oxygen is found to approach very closely, the methylene protons of the ttch ligand of a second molecule of **4**. Figure 11a shows this interaction clearly. The oxygen atom is oriented so as to point down into the recess formed by the chair conformation of the S_3C_3 ring. The distances between the flagpole hydrogens of the ligand and the oxygen of the solvent are all considerably less than the sum of their van der Waals radii (H1-O34; 2.096Å, H9-O34; 2.357Å, H17-O34; 2.587Å). These distances also show the interaction to be significantly biased toward H1. Thus, while a C-H···O network among molecules of **4** is clearly responsible for the formation of a Van der Waals solid by **4**, it appears that the solvent molecule also plays a large role in crystal cohesion.

Table 9: Hydrogen bonding interactions in **4**.

donor-H···acceptor	D···A (Å)	H···A (Å)*	D-H···A (°)*
C1-H1···O34	3.159(9)	2.096	167.54
C2-H2A···O31†	3.508(9)	2.443	168.90
C9-H9···O34	3.378(9)	2.357	157.10
C10-H10A···O28†	3.528(8)	2.465	167.71
C15-H15···O25	3.335(11)	2.500	133.33
C16-H16···O33	3.560(9)	2.592	148.70
C17-H17···O34	3.581(8)	2.587	152.75
C18-H18A···O25†	3.510(8)	2.450	166.68
C20-H20···O28	3.324(9)	2.499	132.37
C36-H36A···O30	3.305(12)	2.565	125.02

**Since the methylene and solvent hydrogens were placed in calculated positions, no error is available for interactions involving these atoms.*

†These are intramolecular interactions.

2.9 Reaction of $Os_3(CO)_{12}$ with trithiacyclohexane

Several compounds containing tripodal ligands capping an Os_3 triangle have been reported.[72] Given the existence of these capped clusters, it was reasonable to believe that the osmium analogue of **2** could be easily prepared. However a series of reactions each under different conditions consistently produced the monosubstituted compound, $Os_3(CO)_{11}(S_3C_3H_6)$ (**5**) as the principal product. For instance, initiation of the reaction between $Os_3(CO)_{12}$ and ttch by the radical anion Ph_2CO^- as well as reaction of $Os_3(CO)_{10}(NCMe)_2$ with ttch, gave at least 15 different products, of which the only significant product was **5** (5-7%). It was found that room temperature reactions of the unsubstituted osmium carbonyl and ttch, carried out

either with or without trimethylamineoxide gave **5** in good yields. In the former case two secondary products were isolated, the known $Os_3(CO)_{10}(\mu_2\text{-}OH)$[73] (*6*) as well as ($\mu_2$-H)$Os_3(CO)_9(\mu_3,\eta^2\text{-}SCHS_2C_2H_4)$ (**7**). Chromatographic work-up of the reaction of $Os_3(CO)_{12}$ with ttch in THF in the presence of trimethylamineoxide produced compound **5** as a prominent yellow band which eluted to the center of the plates. Compounds **6** and **7** were found as fainter yellow bands between the band of compound **5** and the residue. Yellow block crystals of **5** and **6** were obtained from THF solutions allowed to stand at room temperature.

The spectroscopic data of compounds **5-7** are summarized in Table 10.

Table 10: IR and NMR data for compounds 5-7

IR(c-hex, 298K)	{ν_{OH}(cm^{-1})}:	**6:**	3598m-s		
	{ν_{CO}(cm^{-1})}:	**5:**	2110m-w	2057s	2037s
			2022vs	1993m	1976m
		6:	2071s	2060m	2021vs
			2000m,br		
		7:	2099m	2057s	2021vs
			2014s	2007s	1979s,br
			1947m,br		
	{ν_{CS}(cm^{-1})}:	**5:**	730m		
		7:	721w,br		
^{1}H NMR ($CDCl_3$, 298K)[a]	{δ(ppm)}:	**5:**		4.13 (s,br, C-H_2)	
		6:		0.26 (s, O-*H*)	
				-12.60 (s, Os_2-*H*)	
		7:		4.58 (s,br, C-H_2)	
				4.12 (s,br, C-*H*)	
				-11.73 (s, Os_2-*H*)	

[a] 200 MHz

Compound **5** was always the major product in this reaction. Single-crystal X-ray diffraction measurements of **5** revealed the structure shown in Figure 12. Selected bond distances and angles are compiled in Table 11. The yellow block crystals of **5** are monoclinic; space group P $2_1/a$. An analogous product, in which sulfur-bound trithiacyclododecane replaces one CO group in $Os_3(CO)_{12}$, was reported by Lewis *et al.*[74] but no crystal structure was included. Several other trinuclear Os clusters in which a single CO ligand has been replaced in a σ-bond to the sulfur of a thioether have been isolated.[43] Of those trinuclear Os clusters, only $Os_3(CO)_{11}(SCH_2CH_2CH_2)$ has been characterized crystallographically.[75]

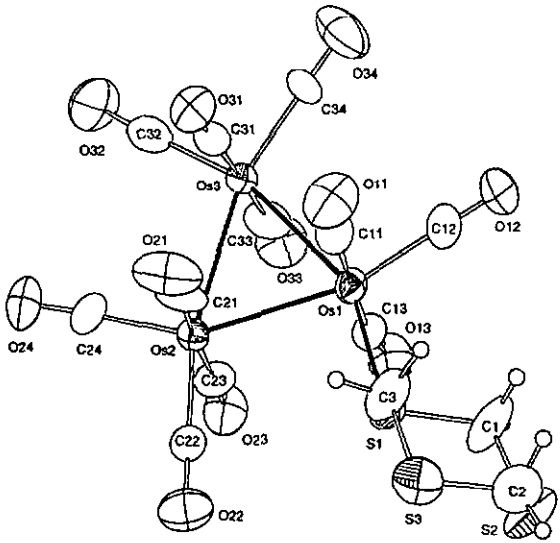

Figure 12: Molecular structure of $Os_3(CO)_{11}(S_3C_3H_6)$ (5).

Table 11: Bond lengths (Å) and bond angles (°) for non-hydrogen atoms of $Os_3(CO)_{11}(S_3C_3H_6)$ (5).

Os(1)-C(13)	1.90(2)	Os(1)-C(12)	1.90(2)	Os(1)-C(11)	1.91(2)
Os(1)-S(1)	2.389(5)	Os(1)-Os(3)	2.855(2)	Os(1)-Os(2)	2.893(2)
Os(2)-C(24)	1.87(2)	Os(2)-C(22)	1.89(2)	Os(2)-C(23)	1.91(2)
Os(2)-C(21)	1.93(2)	Os(2)-Os(3)	2.882(2)	Os(3)-C(32)	1.89(2)
Os(3)-C(34)	1.91(2)	Os(3)-C(33)	1.93(2)	Os(3)-C(31)	1.96(2)
S(1)-C(1)	1.80(2)	S(1)-C(3)	1.80(2)	S(2)-C(1)	1.77(2)
S(2)-C(2)	1.81(3)	S(3)-C(2)	1.78(3)	S(3)-C(3)	1.80(2)
C(11)-O(11)	1.16(2)	C(12)-O(12)	1.13(3)	C(13)-O(13)	1.18(2)
C(21)-O(21)	1.12(2)	C(22)-O(22)	1.15(2)	C(23)-O(23)	1.14(2)
C(24)-O(24)	1.14(2)	C(31)-O(31)	1.16(2)	C(32)-O(32)	1.18(2)
C(33)-O(33)	1.14(2)	C(34)-O(34)	1.13(2)		
C(13)-Os(1)-C(12)	90.5(9)	C(13)-Os(1)-C(11)	176.1(9)	C(12)-Os(1)-C(11)	86.5(9)
C(13)-Os(1)-S(1)	90.4(5)	C(12)-Os(1)-S(1)	104.8(7)	C(11)-Os(1)-S(1	92.8(7)
C(13)-Os(1)-Os(3)	90.1(5)	C(12)-Os(1)-Os(3)	102.7(7)	C(11)-Os(1)-Os(3)	88.1(6)
S(1)-Os(1)-Os(3)	152.5(1)	C(13)-Os(1)-Os(2)	88.4(5)	C(12)-Os(1)-Os(2)	162.8(7)
C(11)-Os(1)-Os(2)	93.8(6)	S(1)-Os(1)-Os(2)	92.4(1)	Os(3)-Os(1)-Os(2)	60.19(2)
C(24)-Os(2)-C(22)	101.6(8)	C(24)-Os(2)-C(23)	93.0(8)	C(22)-Os(2)-C(23)	86.6(8)
C(24)-Os(2)-C(21)	92.8(9)	C(22)-Os(2)-C(21)	89.9(7)	C(23)-Os(2)-C(21)	173.7(8)
C(24)-Os(2)-Os(3)	92.7(6)	C(22)-Os(2)-Os(3)	165.5(5)	C(23)-Os(2)-Os(3)	90.5(5)

Table 11: cont.

C(21)-Os(2)-Os(3)	91.6(5)	C(24)-Os(2)-Os(1)	151.8(6)	C(22)-Os(2)-Os(1)	106.6(6)
C(23)-Os(2)-Os(1)	90.1(6)	C(21)-Os(2)-Os(1)	85.9(7)	Os(3)-Os(2)-Os(1)	59.25(4)
C(32)-Os(3)-C(34)	98.0(8)	C(32)-Os(3)-C(33)	89.7(9)	C(34)-Os(3)-C(33)	93.1(8)
C(32)-Os(3)-C(31)	89.4(8)	C(34)-Os(3)-C(31)	89.0(7)	C(33)-Os(3)-C(31)	177.8(8)
C(32)-Os(3)-Os(1)	163.0(6)	C(34)-Os(3)-Os(1)	99.0(6)	C(33)-Os(3)-Os(1)	88.7(7)
C(31)-Os(3)-Os(1)	91.6(5)	C(32)-Os(3)-Os(2)	102.6(6)	C(34)-Os(3)-Os(2)	159.1(6)
C(33)-Os(3)-Os(2)	91.1(6)	C(31)-Os(3)-Os(2)	87.1(5)	Os(1)-Os(3)-Os(2)	60.56(4)
C(1)-S(1)-C(3)	97.2(10)	C(1)-S(1)-Os(1)	107.8(8)	C(3)-S(1)-Os(1)	108.3(7)
C(1)-S(2)-C(2)	98.9(11)	C(2)-S(3)-C(3)	100.5(11)	S(2)-C(1)-S(1)	115.6(14)
S(3)-C(2)-S(2)	114.3(14)	S(3)-C(3)-S(1)	115.4(11)	O(11)-C(11)-Os(1)	175(2)
O(12)-C(12)-Os(1)	176(2)	O(13)-C(13)-Os(1)	172(2)	O(21)-C(21)-Os(2)	174(2)
O(22)-C(22)-Os(2)	176(2)	O(23)-C(23)-Os(2)	176(2)	O(24)-C(24)-Os(2)	177(2)
O(31)-C(31)-Os(3)	175(2)	O(32)-C(32)-Os(3)	176(2)	O(33)-C(33)-Os(3)	177(2)
O(34)-C(34)-Os(3)	179(2)				

Analogous to $Os_3(CO)_{11}(SCH_2CH_2CH_2)$, the sulfur heterocycle of **5** is found to lie in an equatorial coordination site of the metal. In replacing a carbonyl group, the sulfur acts as a two-electron donor to the metal cluster, maintaining the overall 48-electron count typical of triangular cluster compounds. From the coordinated sulfur, the tteh adopts its standard chair conformation in the solid state. The protons of the tteh ligand were placed in calculated positions and not further refined. Room temperature ^1H NMR spectra of **5** show a single broad peak indicating a non-rigid state for the ligand. At elevated temperatures ^1H NMR solution spectra of the complexes $M(CO)_5(S_3C_3H_6)$ (M = Cr, W)[76] also show a single peak for the ligand protons. This behavior was attributed to a series of sulfur inversions and ring reversals at the tteh ligand rendering axial and equatorial protons equivalent. Individual CH_2 groups were imperceptible due to a series of 1,3-jumps of the metal center; a process also found in dinuclear Pt complexes of tteh.[77] A single peak in the ^1H NMR spectrum of **5** indicates not only that some proton scrambling process is occurring but also there is equilibration of the methylene groups. It is proposed that both, pyramidal sulfur inversion/ring reversal and migration of the metal center over each sulfur of tteh occurs for **5**.

In comparing the structure of **5** to that of the unsubstituted parent $Os_3(CO)_{12}$[78], distinct alterations in the metal framework upon coordination of the thioether are apparent. These changes manifest themselves primarily in a wider range of M-M bond lengths. Both the longer (Os1-Os2; 2.893(2)Å) and the shorter (Os1-Os3; 2.855(2)Å) M-M bonds of **5** involve the sulfur bonded Os (Os1). The single equatorial carbonyl ligand bonded to Os1 displays an

Os-C bond length little changed from that of $Os_3(CO)_{12}$ (Os1-C12; 1.90(2)Å for **5**). On the other hand, the M-C bonds of the axial carbonyl carbons are significantly shortened (for **5** Os1-$C_{axial,avg}$=1.90(2)Å; for $Os_3(CO)_{12}$ Os-$C_{axial,avg}$=1.95(1) Å) while the opposite trend is seen for their C-O bond lengths (for **5** avg. axial C-O=1.17( )Å; for $Os_3(CO)_{12}$ avg. axial C-O=1.13(1)Å). In replacing a carbonyl ligand with a weaker π-acceptor, ttch in this case, the carbonyl trans to the new group has available more electron density and responds with increased M→C backbonding. Intensified metal to carbonyl backbonding leads to stronger M-C bonds and weaker C-O bonds. The carbonyl ligands on the unsubstituted Os atoms show the same bond length trends as observed for $Os_3(CO)_{12}$.

The ttch ligand was found to bind reversibly to the Os cluster. If cluster **5** was dissolved in an appropriate solvent and stirred at room temperature under a moderate pressure of CO (2.5 b) the ttch ligand was replaced and $Os_3(CO)_{12}$ recovered in 65% yield.

Of the two lower yield products isolated from the reactions of $Os_3(CO)_{12}$ and ttch in the presence of trimethylamineoxide, the first (**6**), undoubtedly results from reaction of the activated complex $Os_3(CO)_{11}(NMe_3)^t$ with any residual water in the reaction environment to yield $Os_3(CO)_{10}(\mu_2\text{-}OH)$ (**6**). Attempts to minimize contact with water which included using freshly sublimed Me_3NO, thoroughly dried solvents and flame-dried glassware did not eliminate this product from the reaction mixture. An X-ray structural analysis of cluster **6** was performed and the results are presented in Figure 13. Selected bond distances and angles are found in Table 12. The X-ray structural determination of **6** indicated monoclinic crystals of the space group P $2_1/n$. At the time of this analysis no crystal structure of **6** had been published, but since then two separate reports have appeared.[79]

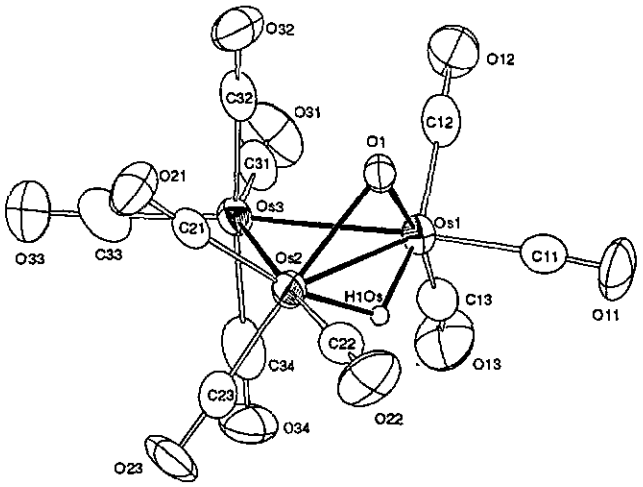

Figure 13: Molecular structure of $(\mu_2\text{-H})Os_3(CO)_{10}(\mu_2\text{-OH})$ (6).

Table 12: Bond lengths (Å) and angles (°) for $(\mu_2\text{-H})Os_3(CO)_{10}(\mu_2\text{-OH})$ (6).

Os(1)-Os(2)	2.8091(14)	Os(1)-Os(3)	2.8218(12)	Os(1)-C(13)	1.86(2)
Os(1)-C(12)	1.89(2)	Os(1)-C(11)	1.95(2)	Os(1)-O(1)	2.150(11)
Os(1)-H(1Os)	1.7(2)	Os(2)-Os(3)	2.8326(12)	Os(2)-C(23)	1.87(2)
Os(2)-C(22)	1.92(2)	Os(2)-C(21)	1.92(2)	Os(2)-O(1)	2.145(10)
Os(2)-H(1Os)	1.6(2)	Os(3)-C(31)	1.91(2)	Os(3)-C(33)	1.94(2)
Os(3)-C(32)	1.95(2)	Os(3)-C(34)	1.98(2)	C(11)-O(11)	1.14(2)
C(12)-O(12)	1.14(2)	C(13)-O(13)	1.16(2)	C(21)-O(21)	1.13(2)
C(22)-O(22)	1.14(2)	C(23)-O(23)	1.15(2)	C(31)-O(31)	1.14(2)
C(32)-O(32)	1.12(2)	C(33)-O(33)	1.13(2)	C(34)-O(34)	1.12(2)
Os(1)-Os(2)-Os(3)	60.02(3)	Os(1)-Os(2)-H(1Os)	33(7)	Os(1)-Os(3)-Os(2)	59.58(3)
Os(2)-Os(1)-Os(3)	60.40(3)	Os(2)-Os(1)-H(1Os)	31(7)	Os(2)-O(1)-Os(1)	81.7(4)
Os(3)-Os(1)-H(1Os)	82(7)	Os(3)-Os(2)-H(1Os)	83(7)	O(1)-Os(1)-Os(2)	49.1(3)
O(1)-Os(1)-Os(3)	84.2(3)	O(1)-Os(1)-H(1Os)	69(7)	O(1)-Os(2)-Os(1)	49.2(3)
O(1)-Os(2)-Os(3)	84.0(3)	O(1)-Os(2)-H(1Os)	70(7)	C(11)-Os(1)-Os(2)	114.8(5)
C(11)-Os(1)-Os(3)	174.9(5)	C(11)-Os(1)-O(1)	93.6(6)	C(11)-Os(1)-H(1Os)	93(7)
C(12)-Os(1)-Os(2)	133.0(5)	C(12)-Os(1)-Os(3)	89.3(6)	C(12)-Os(1)-O(1)	96.6(6)
C(12)-Os(1)-C(11)	95.5(7)	C(12)-Os(1)-H(1Os)	164(7)	C(13)-Os(1)-C(12)	90.1(8)
C(13)-Os(1)-C(11)	92.1(8)	C(13)-Os(1)-O(1)	170.7(6)	C(13)-Os(1)-Os(2)	121.7(5)
C(13)-Os(1)-Os(3)	89.5(6)	C(13)-Os(1)-H(1Os)	104(7)	C(23)-Os(2)-C(22)	90.4(8)
C(23)-Os(2)-C(21)	89.1(7)	C(22)-Os(2)-C(21)	96.7(8)	C(23)-Os(2)-O(1)	172.2(6)
C(22)-Os(2)-O(1)	93.1(6)	C(21)-Os(2)-O(1)	97.3(5)	C(23)-Os(2)-Os(1)	123.0(6)
C(22)-Os(2)-Os(1)	112.3(5)	C(21)-Os(2)-Os(1)	134.7(5)	C(23)-Os(2)-Os(3)	91.6(6)
C(22)-Os(2)-Os(3)	171.7(5)	C(21)-Os(2)-Os(3)	91.4(5)	C(23)-Os(2)-H(1Os)	103(7)
C(22)-Os(2)-H(1Os)	88(7)	C(21)-Os(2)-H(1Os)	167(7)	O(11)-C(11)-Os(1)	175(2)
O(12)-C(12)-Os(1)	179(2)	O(13)-C(13)-Os(1)	177(2)	O(21)-C(21)-Os(2)	176(2)
O(22)-C(22)-Os(2)	176(2)	O(23)-C(23)-Os(2)	177(2)		

Cluster **6** is a structural analogue to the previously characterized $(\mu\text{-H})Os_3(\mu\text{-OMe})(CO)_{10}$.[80] For **6** the main structural feature consists of a triangular metal framework of

which one edge is doubly bridged by a hydroxide group and a hydride. The hydroxide group forms a symmetrical bridge across Os1 and Os2. The hydride bridging Os1 and Os2 was located in a difference Fourier map and could be refined. In contrast the hydroxide hydrogen could not be located and was thus placed in a calculated position. Distances between adjacent Os atoms are consistently shorter than those found in $Os_3(CO)_{12}$[91] for both **6** and the methoxy derivative (avg. Os-Os in **6** = 2.8212(13)Å). No elongation of the hydride bridged Os-Os bond is observed, presumably due to the contrasting effect of the bridging hydroxide. As in the case of **5**, the trans effect is expressed through a shortening of the Os-C bonds of the axial carbonyl groups (Os1-C13; 1.86(2)Å, Os2-C23; 1.87(2)Å).

The second of these products (**7**) proved to be more elusive. It was never possible to obtain X-ray quality crystals of this product. Furthermore, obtaining a sufficiently pure sample in a large enough quantity to carry out detailed spectroscopic analysis was difficult. Therefore the characterization of **7** is based on comparison of its IR spectra with those of known compounds and analysis of ^{1}H NMR spectra obtained with relatively pure samples. Those results indicate a trinuclear cluster of the form shown in Figure 14.

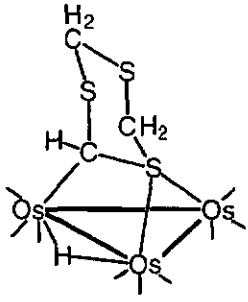

Figure 14: Proposed structure of compound **7**.

As per Figure 14, this cluster consists of a triangular Os_3 base onto which a ttch molecule has bonded in a μ_3,η^2-fashion via a sulfur and the adjacent carbon. In so doing, the ttch molecule has undergone CH activation, transferring a hydride to the cluster base. The presence of the hydride is based on the ^{1}H NMR signal at -11.73 ppm, a region typically assigned to hydride atoms bridging metal-metal bonds. This type of activation is not unfounded in reactions of the heterocyclic thioethers thiacyclohexane[44] and dithiacyclohexane[56]

with metal clusters. In the latter case, μ_3- coordination to $Ru_3(CO)_{12}$ was accomplished through the two sulfur atoms and the carbon atom between them. Similarly the C-H bond was activated and a hydride transferred to the metal core. The former case is the more relevant. Here thermal reactions of thiacyclohexane with $Os_3(CO)_{12}$ or thermolysis of $Os_3(CO)_{10}(SCH_2CH_2CH_2CH_2CH_2)_2$ resulted in a cluster entirely analogous to that observed here; $(\mu_2\text{-H})Os_3(CO)_9(\mu_3,\eta^2\text{-}SCH_2CH_2CH_2CH_2C)$. This cluster was fully characterized through X-ray structural analysis. The bridging hydride was located crystallographically and spans the non-sulfur bonded cluster edge. The IR spectra of this compound compares with that of **7**.

As shown in Table 10, ^1H NMR spectra of **7** show two broad peaks in the region 4-5 ppm. Given the poor sample quality, integration of these peaks was not reliable, as was the case for effective assignment of the peak from the single proton of the metal-bonded carbon. However a series of low temperature spectra produced results consistent with a cluster of the type suggested. Specifically, spectra obtained over the temperature range 25°C down to -50°C show the two broad peaks to collapse into one poorly defined peak at 0°C. By -30°C fine structure begins to appear and by -50°C a series of doublets (J=14.8-13.8 Hz) all falling in the range 5.55-3.74 ppm are clearly visible. The coupling constants for these doublets are similar in magnitude to those found for the methylene protons in clusters **1** and **2**. The single peak assigned to the bridging hydride was also shown to broaden at 0°C and by -50°C to sharpen to two singlet peaks at -11.64 and -12.18 ppm present in a ratio of 1.0/0.65. The large number of doublets observed in the methylene region at low temperature as well as the appearance of two hydride peaks of unequal intensity indicate the existence of at least two isomers in solutions of **7**. These isomers are most likely the result of reorientation of the ttch ligand with respect to the cluster skeleton. Although not elaborated on, the existence of two isomers in solutions of $(\mu_2\text{-H})Os_3(CO)_9(\mu_3,\eta^2\text{-}SCH_2CH_2CH_2CH_2C)$ was also suggested.

The ttch molecule acts as a 5-electron donor in this bonding mode. The hydride ligand and ttch fragment combined provide the cluster with its closed shell requirement of 48 electrons.

References

[20] Young I.R., Ochrymowycz L.A., Rorabacher D.B., *Inorg. Chem.*, **1986**, *25*, 2576.

[21] Murray S.G., Hartley F.R., *Chem. Rev.*, **1981**, *81*, 365.

[22] Ainscough E.W., Birch E.J. Brodie A.M., *Inorg, Chim. Acta*, **1976**, *20*, 187.

[23] Poon C.K., Kwong S.S., Che C.M., Kan Y.P., *J. Chem. Soc., Dalton Trans.*, **1982**, 1457.

[24] a. Arce A.J., Arrojo P., Deeming A.J., DeSanctis Y., *J. Chem. Soc., Dalton Trans.*, **1992**, 2423.

b. Moser W.R., Rosetti G.A. Jr., Gleaves J.T., Ebner J.R., *J. Catal.* **1991**, *127*, 190.

[25] Rauschfuss T.B., *Progr. Inorg. Chem.*, **1991**, *39*, 259.

[26] a. Cooper S.R., Rawle S.C., *Struct. Bond.*, **1990**, *72*, 1.

b. Cooper S.R., *Acc. Chem. Res.*, **1988**, *21*, 141.

c. Blake A.J., Schröder M., *Adv. Inorg. Chem.*, **1990**, *35*, 1.

d. Bell M.N., Blake A.J., Holder A.J., Hyde T.I., Schröder M., *J. Chem. Soc., Dalton Trans.*, **1990**, 3841.

[27] Burgen D., Dale J., Anet F.A.L., Krone J., *J. Chem. Soc., Chem. Commun.*, **1974**, 243.

[28] Küppers H.J., Wieghardt K., Nuber B., Weiss J., Bill E., Trautwein A.X., *Inorg. Chem.*, **1987**, *26*, 3762.

[29] a. Rawle S.C., Cooper S.R., *J. Chem. Soc., Chem. Commun.*, **1987**, 308.

b. Rawle S.C., Sewell T.J., Cooper S.R., *Inorg. Chem.*, **1987**, *26*, 3769.

[30] Blake A.J., Holder A.J., Hyde T.I., Schröder M., *J. Chem. Soc., Chem. Commun.*, **1989**, 1433.

[31] Blake A.J., Gould R.O., Holder J.J., Hyde T.I., Reid G., Schröder M., *J. Chem. Soc., Dalton Trans.*, **1990**, 1759, and references therein.

[32] a. Hill A.F., Alcock N.W., Cannadine J.C., Clark G.R., *J. Organomet. Chem.*, **1992**, *426(2)*, C40.

b. Cannadine J., Hector A., Hill A.F., *Organometallics*, **1992**, *11(7)*, 2323.

[33] Yoshida T., Adachi T., Tanaka T., Goto F., *J. Organomet. Chem.*, **1992**, *428*, C12.

[34] Hassal O., Viervoll H., *Acta Chem. Scand.*, **1947**, *1*, 149.

[35] Fleming J.L., Lynton H., *Can. J. Chem.*, **1967**, *45*, 353.

[36] Klaboe P., *Spectrochim. Acta*, **1969**, *25A*, 1437.

[37] Campaigne E., Chamberlain N.F., Edwards B.E., *J. Org. Chem.*, **1962**, *27*, 135.

[39] Edema J.J.H., Hoogenraad M., Schoonbeek F.S., Kellogg R.M., Kooijman H., Spek A.L., *Recl. Trav. Chim. Pays-Bas*, **1993**, *112*, 370.

[39] Eliel E., Hartmann A.A., Abatjoglou A.G., *J. Am. Chem. Soc.*, **1974**, *96*, 1807.

[40] Suardi G., Strawczynski A., Ros R., Roulet R., Grepioni F., Braga D., *Helv. Chim. Acta*, **1990**, *73*, 154.

[41] Crowte R.J., Evans J., Webster M., *J. Chem. Soc., Chem. Commun.*, **1984**, 1344.

[42] Rossi S., Pursiainen J., Pakkanen T.A., *J. Organamet. Chem.*, **1992**, *436*, 55.

[43] a. Adams R.D., Pompeo M.P., *Organometallics*, **1992**, *11*, 2281.
b. Adams R.D., Pompeo M.P., *Organametallics*, **1992**, *11*, 103.
c. Adams R.D., Pompeo M.P., *J. Am. Chem. Soc.*, **1991**, *113*, 1619.

[44] Adams R.D., Cortopassi J.E., Yamamoto J.H., Wengan Wu, *Organometallics*, **1993**, *12*, 4955.

[45] Edwards A.J., Johnson B.F.G., Khan F.K., Lewis J., Raithby P.R., *J. Organomet. Chem.*, **1992**, *426*, C44.

[46] Jeannin S., Jeannin Y., Robert F., Rosenberger C., *C.R. Acad. Sci. Paris*, **1992**, *314*, 1165.

[47] Raubenheimer H.G., Linford L., Van A. Lombard A., *Organometallics*, **1989**, *8*, 2062.

[48] Abel E.W., Boothe M., Orrell K.G., Pring G.M., Cameron T.S., *J. Chem. Soc., Chem. Commun.*, **1981**, 29.

[49] Friebolin G. in "*Basic One and Two Dimensional NMR Spectroscapy*", VCH Verlagsgesellschaft mbH, D-6940 Weinheim (Germany), **1991**, pg 84.

[50] Grant S.M., Manning A.R., *Inorg. Chim. Acta*, **1978**, *31*, 41.

[51] Johnson B.F.G., Forster A., *The Chemistry of Metal Clusters*; Shriver D.F., Kaesz G.D., Adams R.D., Eds.; VCH Publishers, Inc.: New York, **1990**, Chap. 2, pp 323.

[52] Kruger G.J., Linford L., Raubenheimer H.G., *J. Organomet. Chem.*, **1984**, *262*, 69.

[53] Cotton F.A., Troup J.M., *J. Am. Chem. Soc.*, **1974**, *96*, 5070.

[54] Hoferkamp L., Rheinwald G., Stoeckli-Evans H., Süss-Fink G., *Helv. Chim. Acta*, **1992**, *75*, 2227.

[55] Harding M.M., Nicholls B.S., Smith A.K., *J. Organomet. Chem.*, **1982**, *226*, C17.

[56] Rossi S., Kallinen K., Pursiainen J., Pakkanen T.T., Pakkanen T.A., *J. Organomet. Chem.*, **1992**, *440*, 367.

[57] Churchill M.R., Hallander F.J., Hutchinson J.P., *Inorg. Chem.*, **1977**, *16*, 2655.

[58] a. Braga D., Grepioni F., Sabatino P., Desiraju G.R., *Organometallics*, **1994**, *13*, 3532.

b. Braga D., Grepioni F., Biradha K., Pedireddi V.R., Desiraju G.R., *J. Amer. Chem. Soc.*, **1995**, *117*, 3156.

[59] Braga D., Grepioni F., Calhorda M.C., Veiros L.F., *Organometallics*, **1995**, *14*, 1992.

[60] Laurenczy G., Merbach A.E., Moullet B., Roulet R., Hoferkamp L., Süss-Fink G., *Helv. Chim. Acta*, **1993**, *76*, 2936.

[61] a. Forster A., Johnson B.F.G., Lewis J., Matheson T.W., Robinson B.H., Jackson G.W., *J. Chem. Soc., Chem. Commun.*, **1974**, 1042.

b. Aime S., Gambino O., Milone L., Sappa E., Rosenberg E., *Inorg. Chim. Acta*, **1975**, *15*, 53.

[62] a. Cotton F.A., Hunter D.L., *Inorg. Chim. Acta*, **1974**, *11*, L9.

b. Cotton F.A., Jamerson J.D., *J. Am. Chem. Soc.*, **1976**, *98*, 1273.

[63] Braga D., Grepioni F., *J. Chem. Soc., Dalton Trans.*, **1993**, 1223.

[64] M=Fe: Cotton F.A., Troup J.M., *J. Am. Chem. Soc.*, **1974**, *96*, 4155.

M=Ru: see reference 61b.

M=Os: see reference 61b.

[65] a. Cotton F.A., Jamerson J.D., *J. Am. Chem. Soc.*, **1976**, *98*, 5396.

b. Cotton F.A., Hanson B.E., Jamerson J.D., *J. Am. Chem. Soc.*, **1977**, *99*, 6588.

c. Cotton F.A., Hanson B.E., *Inorg. Chem.*, **1977**, *16(11)*, 2820.

[66] Johnson Jr. C.S., Morcland C.G., *J. Chem. Ed.*, **1973**, *50(7)*, 477.

[67] a. Van Eldik R. in "*Inorganic High Pressure Chemistry*" Elsevier, Amsterdam-Oxford-New York-Tokyo, **1986**.

b. Merbach A.E., *Pure & Appl. Chem.*, **1982**, *54(8)*, 1479.

c. Van Eldik R., Merbach A.E., *Comments Inorg. Chem.*, **1992**, *12(6)*, 341.

d. Jonas J., *Acc. Chem. Res.*, **1984**, *17*, 74.

[68] Aime S., Botta M., Gobetto R., Osella D., Milone L., *Inorg. Chim. Acta*, **1988**, *146*, 151.

[69] "EXCHANGE", program library, Computing Center, University of Lausanne.

[70] "EYRING", program library, Computing Center, University of Lausanne.

[71] Orlandi A., Frey Ul, Suardi G., Merbach A.E., Roulet R., *Inorg. Chem.*, **1992**, *31*, 1304.

[72] a. Constahle E.C., Johnson B.F.G., Khan F.K., Lewis J., Raithby P.R., Mikulcik P., *J. Organomet. Chem.*, **1991**, *403*, C15.

b. Green M.L.H., *J. Chem. Soc., Chem. Commun.*, **1985**, 355.

c. Pilar Gomez-Sal M., Johnson B.F.G., Lewis J., Raithby P.R., Wright A.H., *J. Chem. Soc., Chem. Commun.*, **1985**, 1682.

[73] Forster A., Johnson B.F.G., Lewis J., Matheson T.W., *J. Chem. Soc., Dalton Trans.*, **1978**, 196.

[74] Edwards A.J., Johnson B.F.G., Khan F.K., Lewis J., Raithby P.R., *J. Organomet. Chem.*, **1992**, *426*, C44.

[75] a. Adams R.D., Pompeo M.P., *Organomet.*, **1992**, *11*, 2281.

[76] Abel E.W., Bhargava S.K.,Orrell K.G., *Progr. Inorg. Chem.*, **1984**, *32*, 1.

[77] Abel E.W., Boothe M., Orrell K.G., Pring G.M., Cameron T.S., *J. Chem. Soc., Chem. Commun.*, **1981**, 29.

[78] Churchill M.W., DeBoer B.G., *Inorg. Chem.*, **1977**, *16(4)*, 878.

[79] a. Karpov M.G., Tunik S.P., Denisov V.R., Starova G.L., Nikolskii A.B., Dolgushin F.M., Yanovsky A.I., Struchkov Y.T., *J. Organomet. Chem.*, **1995**, *485*, 219.

b. Khoeppel D.W., Chung J.H., Shore S.G., *Acta Crystall.*, **1995**, *C51*, 42.

[80] Clauss A.D., Tachikawa M., Shapley J.R., Pierpoint C.G., *Inorg. Chem.*, **1981**, *20*, 1528.

3 *Reactivity Study of Tri- and Hexanuclear Ruthenium Clusters Containing the* Diphenylthiourento Ligand.

3.1 Coordination Chemistry of Thiourea and its Derivatives.

In classical coordination compounds, thiourea-based ligands coordinate primarily in a monodentate fashion through the S atom. For example six-coordinate complexes of the type $[Fe\{SC(NHMe)_2\}_6]^{2+}$ are formed.[81] For this complex the bond angles around the sulfur (∠ Fe-S-C = 113.2(7)°) suggest a bonding mode intermediate between that of a thione (sp^2) and a thiol (sp^3). Not surprisingly, the thiourea molecule has been shown to exhibit tautomerism between the thione and thiol form in the unligated state also.

Coordination complexes similar to the Fe species are also formed with Os as the central metal atom. OsO_4 reacts with thiourea in acidic solution resulting in partial oxidation of the thiourea but also producing $[Os\{SC(NH_2)_2\}_6]^{3+}$.[82] This reaction was later used in a study which suggested that the thiol form of thiourea could be stabilized by replacement of the amine hydrogen atoms with substituents showing a positive induction effect.[83]

Mononuclear metal carbonyls form similar complexes with thiourea-type molecules. Examples include $Mo(CO)_3\{SC(NH_2)_2\}_3$[84] and $Re(CO)_3(Cl)\{SC(NH_2)_2\}_2$.[85] Reactions involving the hexacarbonyl compounds of W and Cr with both thiourea and its substituted derivatives under UV irradiation produced compounds of the kind $M(CO)_5SC(NR^1R^2)_2$ (R^1 = R^2 = H, R^1 = H, R^2 = Ph or ^{t}Bu, R^1 = R^2 = Me) [86] For $W(CO)_6$ the disubstituted *cis*-$W(CO)_4\{SC(NHR)_2\}_2$ compounds where R = Ph, ^{t}Bu, could also be isolated. Thermolysis of the Cr derivative, $Cr(CO)_5\{SC(NHPh)_2\}$, in the presence of additional $SC(NHPh)_2$, resulted in substitution of all carbonyl groups and NH activation to produce *fac*-$Cr\{SC(NPh)(NHPh)\}_3$, in which the thiourea is bound in a bidentate fashion to the central metal.

Multinuclear metal clusters containing thiourea-type ligands are less common. The dinuclear $Mn_2(CO)_{10}$ is known to react with tetramethylthiourea resulting in substitution of one carbonyl group to produce $Mn_2(CO)_9\{SC(NMe_2)_2\}$.[87] In contrast $Fe_2(CO)_9$ was shown to undergo fragmentation when exposed to thiourea reagents, producing mononuclear complexes with S-bonded thioureas.[88]

The reactions of thioureas $SC(NR^1R^2)_2$, with triruthenium dodecacarbonyl were first studied in this laboratory and produced a series of new and unique cluster complexes.[89] Trinuclear complexes of the type $(\mu_2\text{-H})(Ru_3(CO)_9(\mu_3,\eta^2\text{-RNCSNRH})$ were obtained from the reaction of $Ru_3(CO)_{12}$ with thiourea (R = H) and its dimethyl and diphenyl derivatives (R = Me, Ph). In the case of diethylthiourea, in addition to the analogous trinuclear cluster $Ru_3(CO)_9(\mu_2\text{-H})\text{-}(\mu_3,\eta^2\text{-EtNCSNHEt})$, the tetranuclear clusters $Ru_4(CO)_{8-n}(\mu_2\text{-CO})_3(\mu_4\text{-S})_2\{C(NRH)\}_n$ (n = 1,2) (R = Et) were isolated. With diisopropylthiourea the sole products were tetranuclear clusters of the same type (R = i-Pr). In the reaction of $Ru_3(CO)_{12}$ with ditertiarybutylthiourea, two complexes $Ru_3(CO)_8(\mu_2\text{-H})\text{-}(\mu_3\text{-S})(\eta^2\text{-}CH_2CMe_2NH\text{-}CNH^tBu)$ and $Ru_3(CO)_9(\mu_2\text{-H})\{(\mu_3\text{-S})Ru(CO)_3(\eta^2\text{-}CH_2CMe_2NHCNH^tBu)\}$ were isolated, in which not only C-S bond breaking of the thiourea is observed but also C-H activation of one of the t-butyl groups. Thus the nature of the thiourea substituent R, has a strong influence on the type of cluster formed. This is most likely a result of stabilization of one of the tautomeric forms of the thiourea (illustrated above) by the substituent R.

Among the trinuclear clusters containing the thiourea ligands in a μ_3,η^2 face-capping mode, the cluster in which R = Ph was isolated in a relatively high yield (59%).[104a] Furthermore this cluster, $(\mu_2\text{-H})(Ru_3(CO)_9(\mu_3,\eta^2\text{-SCNPhNPhH})$ (hereafter assigned as cluster **8**), was found to be relatively stable towards air. The interesting structural features of this cluster, as well as the ease with which it can be prepared and handled, render it a good candidate for an extended reactivity study.

3.2 Diphenylthiourea

The primary structural feature of cluster **8** is the diphenylthioureato ligand, therefore, a short discussion of the characteristics of this species is warranted. Diphenylthiourea is the commercially available, air-stable derivative of thiourea in which one proton on each of the

amine groups has been replaced with a phenyl group. Several routes to substituted thioureas exist but typically this product is synthesized by reaction of thiophosgene with aniline.[90]

$$CSCl_2 + 2PhNH_2 \rightarrow PhNHCSNHPh + 2HCl$$

It has been shown that the most energetically favorable conformation for the disubstituted molecule is the *cis-trans* form.[91] The presence of the two aryl groups has the advantage of producing a wider solubility range in standard organic solvents. Spectral analysis of thiourea and its substituted derivatives has led to assignment of the IR bands.[92] Keeping in mind the vibrational shift inevitable upon coordination to a metal center, the characteristic NH and NCN vibrations (at 3204 cm^{-1} and 1553 cm^{-1}, resp.) provide evidence of a thiourea type ligand in metal complexes. The (N)H and H(Ph) signals in ^1H NMR spectra also prove useful for this purpose.

3.3 The Triruthenium Cluster Complex (μ_2-H)$Ru_3(CO)_9(\mu_3,\eta^2$-SCNHPhNPh) (8).

Cluster **8** has been isolated and characterized previously.[89a] It is described as a trinuclear ruthenium carbonyl cluster containing a diphenylthioureato ligand bridging the metal skeleton in a μ_3,η^2-fashion, in addition to a μ_2-bridging hydride. Figure 15 shows a graphical representation of **8** and some relevant bond lengths and angles are listed in the caption. As pointed out in the introduction, sulfur-containing clusters offer numerous possibilities as catalysts for organic reactions. Thioureas are of notable interest owing to the proven catalytic activity of thiourea/PdX_2 complexes.[93] Investigations of the substitution reactions of cluster complexes with this ligand, in terms of both types and mechanisms, can often provide useful information regarding intermediates as well as mechanistic details of homogeneous catalytic processes. In addition, μ_3,η^2-face-capping ligands like that found in **8** have been shown to enforce cluster integrity, thus minimizing cluster fragmentation, a complication often encountered during the forcing conditions of some catalytic processes.[94] Recently Boroni *et al.*[95] have demonstrated the anchoring of a substituted dithiourea onto a Si support and its subsequent binding to metal species. Their ultimate goal is the use of such tethered species as catalysts. Furthermore the use of clusters containing thioureato ligands as models for the corrosion-inhibiting characteristics of thioureas towards metal surfaces is an intriguing aspect.[96] With these facts in mind, a reactivity study of cluster **8** was pursued.

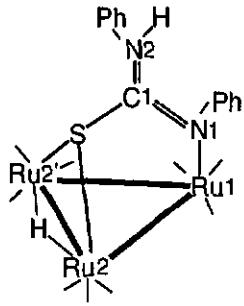

Figure 15: Graphical representation of $(\mu_2\text{-H})Ru_3(CO)_9(\mu_3,\eta^2\text{-SCNHPhNPh})$ (8). Some bond lengths: Ru1-Ru2; 2.7690(4)Å, Ru2-Ru2'; 2.8421(5)Å, Ru2-S; 2.4131(7)Å, Ru1-N1; 2.167(3)Å, S-C1; 1.776(4)Å, N1-C1; 1.2951(5)Å, N2-C1; 1.354(5)Å, Ru2-H; 1.81(4)Å. Some bond angles: Ru2-Ru1-Ru2'; 61.754(10)°, Ru2-Ru1-N1; 87.51(7)°, Ru1-Ru2-Ru2'; 59.123(7)°, Ru1-Ru2-S; 80.581(21)°, Ru2-S-Ru2'; 72.158(25)°, S-C1-N1; 120.1(3)°, S-C1-N2; 115.6(3)°, Ru1-N1-C1; 122.59(24), N1-C1-N2; 124.2(3)°, Ru2-H Ru2'; 103(3)°.

3.4 Reaction of $(\mu_2\text{-H})Ru_3(CO)_9(\mu_3,\eta^2\text{-SCNHPhNPh})$ (8) with Excess Diphenylthiourea.

Stirring a room temperature THF solution of the trinuclear species $(\mu_2\text{-H})Ru_3(CO)_9(\mu_3,\eta^2\text{-SCNHPhNPh})$ (8) with excess diphenylthiourea over an extended period resulted in formation of the mononuclear species 9 in 15.4% yield. This compound was also produced in long-term reactions of $Ru_3(CO)_{12}$ with excess diphenylthiourea (yield = 23.4%). Compound 9 was isolated from the reaction mixture by TLC as an UV band and could be recrystallized from mixed solvent systems. IR and ^{1}H NMR data are listed in Table 13 and indicate a mononuclear system with two intact diphenylthioureato ligands. The presence of an M^+ peak at 612 mass units in mass spectra of 9 supports this assignment. An independently published, x-ray structural analysis of the Os analogue $Os(CO)_2(pySH)_2$[97] showed the CO ligands to occupy *cis* positions and the sulfur ligands to occupy *trans* positions on a central Os atom. The appearance of two bands in the ν_{CO} region of the IR spectrum of 9 indicates a species of C_2 symmetry which requires the two carbonyl ligands to be placed in a *cis* orientation. A graphical representation of 9 is presented in Figure 16.

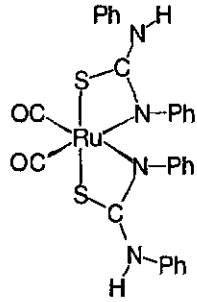

Figure 16: Graphical representation of $Ru(CO)_2(SCNHPhNPh)_2$ (**9**).

Table 13: IR and NMR data for $Ru(CO)_2(SCNHPhNPh)_2$ (**9**).

IR (c-hex, 298K)	$\{\nu_{CO}$ $(cm^{-1})\}$:	2039s	1973s
IR (KBr)	$\{\nu_{NH}$ $(cm^{-1})\}$:	3360m	
	$\{\nu_{NCN}$ $(cm^{-1})\}$:	1549m	
^1H NMR ($CDCl_3$, 298K)	$\{\delta(ppm)\}$:[a]	8.6(s, br, 1H)	
		7.5 - 7.0 (m, 10H)	

[a] 400 MHz

The valence requirements of the central Ru atom in **9** are fulfilled if the bidentate diphenylthioureato fragment is considered as a four-electron donor. This should result in decreased sp^2 character at the central C of the NCN portion of the ligand as compared to the trinuclear cluster **8** wherein the ligand serves as a five-electron donor. This aspect is supported by the observed low-energy shift of the NCN stretch in IR spectra of **9** as well as a high-energy shift for the NH stretch.

The Cr mononuclear complexes cited above are similar to **9**. However in the case of Cr, substitution of the carbooyl groups was complete, producing $Cr(\eta^2\text{-}SCNHPhNPh)_3$.[86] Mononuclear complexes entirely analogous to **9** have also been isolated from reactions of $Ru_3(CO)_{12}$ and pyridine-2-thione (pySH), but in cootrast to the diphenylthiourcato derivative described here, vigorous conditions were required to produce the complex $Ru(CO)_2(\eta^2pySH)_2$.[98] In that same publication, an alternative synthesis was outlined involving reductive carbonylation of $RuCl_3{\cdot}nH_2O$. The chlorocarbonyl complex thus formed was then allowed to react with the thiooe. The possibility of an increased yield and the rather high cost

of $Ru_3(CO)_{12}$ prompted an attempt of the same procedure to produce **9**. However this route was found to give even lower yields and was not pursued.

The mechanism postulated in the above reaction with $RuCl_3{\cdot}nH_2O$ is useful in explaining the low yields obtained in the diphenylthioureato case. Substitution of an axial Cl and CO on the ruthenium(II) chlorocarbonyl species (*fac*-$[RuCl_3(CO)_3]^-$) with two molecules of PySH, gives a six-coordinate intermediate wherein the PySH ligand is sulfur-bound and a proton resides on the ring nitrogen. Elimination of HCl via the chloride ligands *cis* to the pySH ligands and the pyridinium protons follows with formation of two bonds to the metal center through the pyridinato nitrogens to give the product. The less acidic nature of the NH protons of thiourea relative to the pyridinium protons is probably a contributing factor to the low yields obtained in similar reactions using diphenylthiourea.

Considering that formation of **9** occurs in better yields both from reactions of $Ru_3(CO)_{12}$ as well as of **8** with excess diphenylthiourea it follows that the trinuclear species **8** is a more productive precursor (as compared to the six-coordinate intermediate suggested above) in the formation of **9**. One might foresee a trinuclear species coordinating 2 or more diphenylthioureato ligands and then undergoing cluster fragmentation to yield the mononuclear product. The $Os(CO)_2(pySH)_2$ complex[99] could only be obtained from reactions of either $Os_3(CO)_{12}$ or $(\mu_2\text{-H})Os_3(CO)_9(pyS)$ with excess pySH.

A goal of some cluster chemists is the development of directed cluster synthesis. The need for these types of syntheses stem from the fact that often transition metal clusters are prepared using rather unselective methods, i.e. thermolysis reactions. Mononuclear complexes of type **9** could provide very useful starting materials for cluster build-up reactions, an approach successfully carried out with $Ru(CO)_2(pySH)_2$.[100]

3.5 Reactions of $(\mu_2\text{-H})Ru_3(CO)_9(\mu_3,\eta^2\text{-SCNHPhNPh})$ (8) with Triphenylphosphine.

3.5.1. Isolation and Characterization of $(\mu_2\text{-H})Ru_3(CO)_8(PPh_3)(\mu_3,\eta^2\text{-SCNHPhNPh})$ (10) and $(\mu_2\text{-H})Ru_3(CO)_7(PPh_3)_2(\mu_3,\eta^2\text{-SCNHPhNPh})$ (11).

Refluxing a THF solution of **8** containing one or two equivalents of PPh_3 over a period of 1h resulted in substitution of one or two carbonyl groups to produce the electronically saturated mono- or di-substituted clusters $(\mu_2\text{-H})Ru_3(CO)_8(PPh_3)(\mu_3,\eta^2\text{-SCNHPhNPh})$ (**10**) and $(\mu_2\text{-H})Ru_3(CO)_7(PPh_3)_2(\mu_3,\eta^2\text{-SCNHPhNPh})$ (**11**) respectively. An excess of PPh_3 produced no further substitution. These compounds are isoelectronic with the starting cluster **8**. Compounds **10** and **11** were separated from the reaction mixture using preparative TLC, eluting as two distinct orange bands. However ^1H NMR spectroscopy of the products isolated from the plates showed the presence of **11** in samples of **10** and vice versa. Pure, crystalline samples of **10** could be obtained by crystallization from CH_2Cl_2/C_6H_{14} solvent systems. The IR and ^1H NMR spectral data for **10** and **11** as well as those for a product **12** to be discussed in the next section are listed in Table 14.

Table 14: IR and NMR data for $(\mu_2\text{-H})Ru_3(CO)_8(PPh_3)(\mu_3,\eta^2\text{-SCNHPhNPh})$ (**10**), $(\mu_2\text{-H})Ru_3(CO)_7(PPh)_2(\mu_3,\eta^2\text{-SCNHPhNPh})$ (**11**) and $Ru_3(CO)_7(\mu_2,\eta^2\text{-}C_6H_4)(\mu_2\text{-}PPh_2)(PPh_3)(\mu_3\text{-S})$ **12**.

IR (c-hex, 298K)	{ν_{CO} (cm^{-1})}	**10**:	2064m	2029vs	1998m-s
			1979m	1970m	1946w,sh
		11:	2042vs	1996s	1986w
			1970s	1936m	
		12	2032m	2007vs	1982s
			1952s	1939vw	
IR (KBr)	{ν_{NH}(cm^{-1})}	**10**:	3354w-m		
		11:	3366w-m		
	{ν_{NCN}(cm^{-1})}	**10**:	1572m		
		11:	1571m		
^1H NMR ($CDCl_3$, 298K):[a]	{δ(ppm)}	**10**:	7.50-6.90(m, 25H)		
			6.08(s,hr, 1H)		
			-12.52(d, J=14Hz, 1H)		
		11:	7.60-6.70(m, 40H)		
			5.90(s,br, 1H)		
			-12.10(t, J=9Hz, 1H)		
^1H NMR (C_6D_6, 298K)[a]:	{δ (ppm)}	**12**	7.8-6.2(m)		
^{31}P NMR($CDCl_3$, 298K):[a]	{δ(ppm)}	**10**:	25.9(s)		
		11	29.0(s)		
^{31}P NMR (C_6D_6, 298K)[b]	{δ(ppm)}	**12**	215.0 (d, J = 6.7 Hz), 40.6 (s, hr).		

[a] 200 MHz
[b] *80.96 MHz*

The upfield shift of the phosphorous signals in ^{31}P NMR spectra of **10** and **11** indicates the phosphine ligand is bound to the metal through a σ-bond. This conclusion is also corroborated by the integrals of the ^{1}H NMR spectra, showing intact PPh_3 groups. The placement of the phosphine ligands on the clusters adjacent to the bridging hydride can be deduced from the presence of fine structure at the signals of their respective hydride ligands. Furthermore, the small values of the coupling constants indicate a *cis* orientation of the coupling groups.[101] From the presence of NH and NCN bands in solid-state IR spectra as well as the integrals of the ^{1}H NMR spectra in the phenyl region, it is clear that the diphenylthioureato ligand is undisturbed by substitution at the metal skeleton. Cabeza *et col.* prepared several phosphine and phosphite derivatives of trinuclear clusters containing the 2-amino-6-methylpyridinato (ampy) capping ligand,[102] as well as the pyridine-2-thiol (pyS) ligand.[98b] These reactions produced clusters similar to **10** and **11**, however no monosubstituted derivatives were structurally characterized.

The structure of cluster **10** was determined by X-ray structural analysis. The molecule crystallizes in the triclinic crystal system, in the space group $P\bar{1}$. There are two molecules per unit cell. The molecular structure of **10** is shown in Figure 17. Table 15 gives selected bond distances and angles.

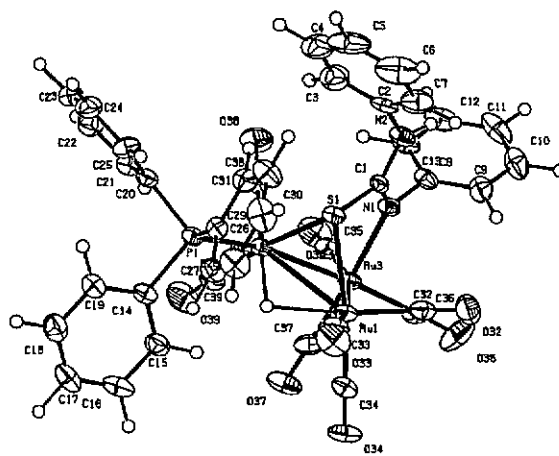

Figure 17: Molecular structure of $(\mu_2\text{-H})Ru_3(CO)_8(PPh_3)(\mu_3,\eta^2\text{-SCNHPhNPh})$ (**10**).

Table 15: Selected bond distances (Å) and angles (°) for (μ_2-H)$Ru_3(CO)_8(PPh_3)(\mu_3,\eta^2$-SCNHPhNPh) (**10**).

Ru(1)-Ru(2)	2.8592(11)	Ru(1)-Ru(3)	2.7642(10)
Ru(1)-S(1)	2.4128(17)	Ru(2)-Ru(3)	2.7614(11)
Ru(1)-H(1)	1.97(6)	Ru(2)-P(1)	2.3726(19)
Ru(2)-S(1)	2.4138(20)	Ru(3)-N(1)	2.149(5)
Ru(2)-H(1)	1.69(6)	Ru(3)-C(36)	1.933(9)
P(1)-C(14)	1.836(7)	S(1)-C(1)	1.775(6)
P(1)-C(26)	1.830(7)	P(1)-C(20)	1.830(7)
N(1)-C(8)	1.448(8)	N(1)-C(1)	1.298(8)
N(2)-C(2)	1.451(9)	N(2)-C(1)	1.357(8)
Ru(2)-Ru(1)-Ru(3)	58.79(3)	Ru(2)-Ru(1)-S(1)	53.69(5)
Ru(2)-Ru(1)-H(1)	35.3(18)	Ru(3)-Ru(1)-S(1)	80.48(5)
Ru(3)-Ru(1)-H(1)	83.4(18)	S(1)-Ru(1)-H(1)	79.2(19)
Ru(1)-Ru(2)-Ru(3)	58.89(3)	Ru(1)-Ru(2)-S(1)	53.66(5)
Ru(1)-Ru(2)-P(1)	106.81(5)	Ru(1)-Ru(2)-H(1)	42.1(21)
Ru(3)-Ru(2)-S(1)	80.52(5)	Ru(3)-Ru(2)-P(1)	165.12(5)
Ru(3)-Ru(2)-H(1)	88.6(22)	S(1)-Ru(2)-P(1)	94.16(7)
S(1)-Ru(2)-H(1)	84.5(22)	P(1)-Ru(2)-H(1)	77.0(22)
Ru(1)-Ru(3)-Ru(2)	62.32(3)	Ru(1)-Ru(3)-N(1)	88.36(14)
Ru(2)-Ru(3)-N(1)	86.94(15)	Ru(1)-S(1)-Ru(2)	72.65(5)
Ru(1)-S(1)-C(1)	106.16(22)	Ru(2)-S(1)-C(1)	103.00(22)
Ru(2)-P(1)-C(14)	114.51(23)	Ru(2)-P(1)-C(20)	116.03(23)
Ru(2)-P(1)-C(26)	116.08(23)	C(14)-P(1)-C(20)	101.5(3)
C(14)-P(1)-C(26)	103.7(3)	C(20)-P(1)-C(26)	103.2(3)
Ru(3)-N(1)-C(1)	122.6(4)	Ru(3)-N(1)-C(8)	120.0(4)
C(1)-N(1)-C(8)	117.4(5)	C(1)-N(2)-C(2)	123.8(6)
S(1)-C(1)-N(1)	120.0(5)	S(1)-C(1)-N(2)	116.6(5)
N(1)-C(1)-N(2)	123.3(6)	Ru(1)-H(1)-Ru(2)	102(3)

The triangular metal framework of cluster **10**, compared to that of **8**, is slightly perturbed by the presence of the PPh_3 ligand. In cluster **8** a mirror plane extends through Ru1 and the midpoint of the Ru2-Ru2' bond, entailing equidistant Ru1-Ru2 and Ru1-Ru2' bond lengths. Not only does the presence of the phosphine on only one side of the sulfur-bridged Ru-Ru bond destroy this symmetry, but it also renders each of the metal-metal bonds unequal. Specifically, the S-bridged Ru-Ru bond elongates relative to **8**, while the two remaining Ru-Ru bonds shorten slightly. At the hydride ligand, this asymmetry manifests itself in a noticeably shorter bond between the hydride and the phosphine bonded Ru (Ru(1)-H(1); 1.97(6)Å, Ru(2)-H(1); 1.69(6)Å). The atom H1 is found to fall 0.89(7)Å below the M_3 plane. Stated alternatively, the Ru1-H-Ru2 plane forms an angle of 51° with the M_3 plane. As implied by the ^{1}H NMR spectrum, the binding site of the PPh_3 is an equatorial position on one of the sulfur-bonded Ru atoms, *cis* to the bridging hydride.

Within the S-C-N base of the diphenylthioureato ligand, substitution at the metal framework has had little effect; the bond distances and angles there remain essentially unchanged. However, the Ru3-N1 bond is approximately 0.02 Å shorter in **10** (Ru1-N1, 2.167(3)Å in **8** vs. Ru3-N1, 2.149(5)Å in **10**). This shorter bond length does not change the Ru3-N1-C1 bond angle nor does it influence the remaining structural features of the diphenylthioureato ligand.

In the formation of the disubstituted cluster **11**, the second PPh_3 ligand is assumed to coordinate to the second sulfur-bonded Ru atom. The structure of the disubstituted PPh_3 derivative of $(\mu_2\text{-H})Ru_3(CO)_7(PPh)_2(\mu_3,\eta^2\text{-ampy})$ has been reported by Cabeza *et col.*.[102c] Therein one finds the two phosphine groups occupying equatorial positions on the nitrogen-bridged Ru atoms. The infrared data given for the Cabeza cluster show a ν_{CO} structure analogous to that of **11** as well as $J_{(\mu\text{-H})\text{-P}}$ coupling constants of the same order (8.3 Hz) as those found in spectra of **11**. Based on these observations, the two clusters can be assumed to be isostructural. The proposed molecular structure of **11** is illustrated in Figure 18.

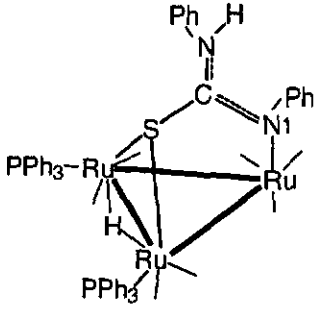

Figure 18: Graphical representation of $(\mu_2\text{-H})Ru_3(CO)_7(PPh_3)_2(\mu_3,\eta^2\text{-SCNHPhNPh})$ **11**.

Cabeza *et al.* also presented a trinuclear complex containing a μ_3,η^2-face-capping ligand derived from 2-mercaptobenzimidazole (mbim) in which two carbonyl groups are substituted with PPh_3 ligands.[102a] Unlike the diphenylthioureato derivative, this compound was

prepared via a room temperature reaction of the starting trinuclear cluster and PPh_3; thermal activation was not necessary. However, the disubstituted mbim cluster proved impossible to separate from its monosubstituted counterpart and was therefore never fully characterized.

3.5.2 Isolation and Characterization $Ru_3(CO)_6(\mu_2,\eta^2\text{-}C_6H_4)(\mu_2\text{-}PPh_2)(PPh_3)(\mu_3\text{-}S)$ (12).

Refluxing a toluene solution of **8** with 2 equivalents of PPh_3 produced the trinuclear cluster $Ru_3(CO)_6(\mu_2,\eta^2\text{-}C_6H_4)(\mu_2\text{-}PPh_2)(PPh_3)(\mu_3\text{-}S)$ (**12**). Similar results were obtained from thermolysis reactions of **11**. The product could be separated from the reaction mixture as a red band on Al_2O_3 TLC plates. Refluxing solutions of the reactants in a lower boiling solvent (i.e. THF) over extended periods of time resulted in formation of **12** but only in very small quantities; the major product was the PPh_3-substituted cluster, **10**.

According to infrared, ^1H and ^{31}P NMR spectroscopic data (see Table 14), cluster **12** differs structurally from clusters **10** and **11**. The IR spectrum in the carbonyl region is quite simple, showing only four strong bands and indicating extensive substitution at the metal framework. The nature of these substitutions becomes more apparent upon considering the NMR spectrum. In the ^1H NMR spectrum, a bridging hydride group is no longer observed and the number and nature of the phenyl groups has changed. The phenyl region is more complex than that observed for **8** or **10** and **11**. In addition the characteristic IR stretches of the diphenylthioureato ligand are absent. The presence of a phosphido bridge is verified by the downfield shift of one of the two peaks found in ^{31}P NMR spectra of **12**.[103] The remaining peak occurs in the region normally assigned to σ-bonded PPh_3.

Based on the coincidence of spectral data with their crystallographically characterized trinuclear cluster $Ru_3(CO)_6(\mu_2\text{-}Ph)(\mu_2\text{-}PPh_2)_2(\mu_3,\eta^2\text{-ampy})$,[102a] Cabeza *et. al.* identified the trinuclear cluster $[Ru_3(CO)_6(\mu_2\text{-}Ph)(\mu_2\text{-}PPh_2)_2(\mu_3,\eta^2\text{-mbim})]$, which contains two diphenylphosphido bridges, a bridging aryl group and a μ_3,η^2-mercaptobenzimidazolate ligand. The agreement of the ν_{CO} region of IR spectra of **12** with this mbim-based cluster, at first suggested a second structural analogue to the ampy cluster, however the lack of NH and NCN

bands typically associated with the diphenylthioureato ligands as well as the absence of nitrogen in elemental analyses of **12**, suggested the crystallographic characterization of this cluster was necessary.

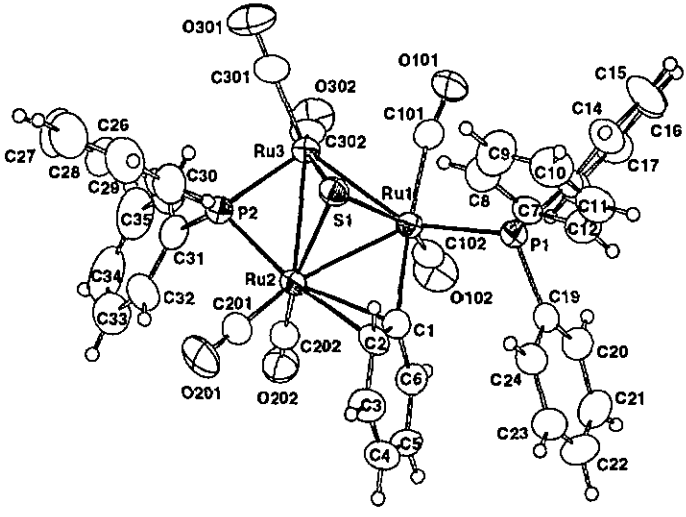

Figure 19: Molecular structure of $Ru_3(CO)_6(PPh_3)(\mu_2\text{-}PPh_2)(\mu_2,\eta^2\text{-}C_6H_5)(\mu_3\text{-}S)$(**12**).

Red, block crystals of **12** were found to crystallize in the monoclinic space group P $2_1/n$ with 4 complete molecules per unit cell. One molecule of dichloromethane was associated with each molecule of **12**. The molecular structure of **12** is presented in Figure 19 and relevant bond lengths and angles are summarized in Table 16.

Table 16: Selected bond distances (Å) and angles (°) for $Ru_3(CO)_6(PPh_3)(\mu_2\text{-}PPh_2)(\mu_2,\eta^2\text{-}C_6H_5)(\mu_3\text{-}S)$(**12**).

Ru(1)-Ru(2)	2.7738(8)	Ru(1)-Ru(3)	2.7032(7)
Ru(1)-P(1)	2.381(2)	Ru(1)-S(1)	2.441(2)
Ru(1)-C(1)	2.130(6)	Ru(2)-Ru(3)	2.8348(7)
Ru(2)-P(2)	2.292(2)	Ru(2)-S(1)	2.413(2)
Ru(2)-C(1)	2.355(6)	Ru(2)-C(2)	2.542(7)
Ru(3)-P(2)	2.243(2)	Ru(3)-S(1)	2.365(2)
P(1)-C(7)	1.825(7)	P(1)-C(13)	1.836(6)
P(1)-C(19)	1.838(6)	P(2)-C(25)	1.820(7)
P(2)-C(31)	1.818(7)	C(1)-C(2)	1.415(9)
C(1)-C(6)	1.440(9)	C(2)-C(3)	1.414(10)
C(3)-C(4)	1.360(11)	C(4)-C(5)	1.398(11)
C(5)-C(6)	1.375(9)		
Ru(1)-Ru(2)-Ru(3)	57.62(2)	Ru(1)-Ru(3)-Ru(2)	60.06(2)
Ru(1)-C(1)-Ru(2)	76.2(2)	Ru(2)-S(1)-Ru(1)	69.70(5)
Ru(2)-C(2)-H(2)	98(4)	Ru(3)-Ru(1)-Ru(2)	62.32(2)
Ru(3)-P(2)-Ru(2)	77.37(5)	Ru(3)-S(1)-Ru(1)	68.43(5)
Ru(3)-S(1)-Ru(2)	72.77(5)	P(1)-Ru(1)-Ru(2)	136.93(4)
P(1)-Ru(1)-Ru(3)	148.12(4)	P(1)-Ru(1)-S(1)	110.82(6)
P(2)-Ru(2)-S(1)	85.66(6)	P(2)-Ru(2)-C(1)	155.0(2)
P(2)-Ru(2)-C(2)	160.9(2)	C(1)-Ru(1)-S(1)	88.1(2)
C(1)-Ru(1)-Ru(3)	117.9(2)	C(1)-Ru(2)-C(2)	33.3(2)
C(1)-C(2)-Ru(2)	66.1(3)	C(1)-C(2)-H(2)	122(4)
C(2)-C(1)-Ru(1)	122.0(5)	C(2)-C(1)-Ru(2)	80.6(4)
C(2)-C(1)-C(6)	115.0(6)	C(3)-C(2)-C(1)	122.3(7)
C(3)-C(2)-H(2)	113(4)	C(31)-P(2)-C(25)	103.1(3)

The molecular structure of **12** shows the original trinuclear Ru framework where the only part of the diphenylthioureato ligand remaining is a capping μ_3-S. Further bridging ligands include a diphenylphosphido group spanning the Ru2-Ru3 bond and an aryl group bridging the Ru1-Ru2 vector. One terminal PPh_3 ligand is bound to Ru1 while six terminal carbonyl groups complete the coordination spheres of the remaining Ru atoms. Consistent with the ^1H NMR spectrum, no hydride ligands are present in the structure of **12**

The range of metal-metal bond lengths are on the average, consistent with single bonds (avg. Ru-Ru, 2.7706(7)Å), however they have shortened somewhat, relative to those of **8** (avg. Ru-Ru, 2.8177(5)Å). The Ru-S bonds show two typical Ru-S bond lengths and one rather short Ru-S distance (Ru3-S1, 2.365(2)Å). The bonding situation at the bridging aryl group is somewhat unusual and is illustrated with the associated bond lengths and atom orientations. The C1 bridge itself is asymmetric (Ru1-C1, 2.130(6)Å; Ru2-C1, 2.355(6)Å).

The calculated distance between the C2 atom of the bridging aryl group and Ru2 indicates a bonding interaction (Ru2-C2, 2.542(7)Å). Since the presence of the phenyl hydrogen atom on C2 was verified in difference maps (and refined), the C2 atom most likely takes part in a side-on π-interaction with Ru2 while the Ru1-C1 represents a σ-interaction. This σ,π-type interaction is further suggested by the tilting of the plane of the aryl group towards Ru2; the angle between the aryl plane and the Ru_3 plane is calculated as 67.97(14)°. On the other hand, the phosphido group represents a relatively symmetrical bridging ligand.

Treating the μ_3-S as a four-electron donor, the μ_2-PPh_2 group as a three-electron donor and the aryl group as a three-electron donor, cluster **12** contains a total of 48 electrons and is electronically saturated.

In assuming such an unusual bridging mode, the aryl group of **12** is somewhat unique. The compounds of Cabeza *et col.* mentioned above (reference 102) are the first examples of symmetrical bridging phenyl groups across Ru-Ru bonds. Other platinum group clusters with η^1-phenyl groups are also known.[104] As for a σ,π-interaction, the ampy bridged cluster of Cabeza has been shown to add diphenylacetylene in such a way that the acetylene carbon takes part in a σ-interaction with a Ru and the C=C double bond is involved in a π-interaction with the adjacent Ru.[105] Cluster **12** represents the first example of an aryl ligand employing combined bridging and side-on π- in a ruthenium cluster.

The formation of **12** from thermolysis reactions of **8** in the presence of PPh_3 has interesting implications. As will be shown later, thermolysis of **8** in the absence of PPh_3 leads to an entirely different group of products. This, in conjunction with formation of **12** in thermolysis reactions of **11**, suggests the intermediacy of a PPh_3 substituted derivative. The formation of a diphenylphosphido bridge is not unusual in thermolytic reactions of clusters with PPh_3 ligands, given the presence of a bridging hydride to provide for elimination of H_2.[106] The η^2-aryl ligand in **12** presumably results from orthometallation of one of the PPh_3 groups of **11** formed *in situ*, followed by elimination of H_2 via the metallated *ortho*-carbon and the bridging hydride. Elimination of the diaminocarbene fragment of the diphenylthioureato ligand could occur prior to or subsequent to P-C bond activation.

Both the ampy and mbim clusters of Cabeza underwent thermal activation of P-C bonds to form η^1-phenyl bridged species. The disubstituted PPh_3 ampy clusters required high temperatures and the presence of H_2 to initiate P-C bond cleavage while for the mbim clusters, refluxing a THF solution of the unsubstituted species in the presence of 2 equivalents of PPh_3 gave a product cited as analogous to the ampy-aryl cluster. Cluster 8 shows reactivity towards P-C bond activation intermediate between that of the ampy and the mbim clusters in that thermal activation is necessary but the presence of H_2 is not required.

3.6 Reaction of $(\mu_2\text{-H})Ru_3(CO)_9(\mu_3,\eta^2\text{-SCNHPhNPh})$ (8) with diphenylphosphinoethane.

Complex 8 reacts almost instantaneously with the difunctional phosphine diphenylphosphinoethane (dppe) to give the trinuclear cluster $(\mu_2\text{-H})Ru_3(CO)_7(Ph_2PCH_2CH_2PPh_2)(\mu_3,\eta^2\text{-SCNHPhNPh})$ (13) in high yield (80%). Cluster 13 could only be isolated by crystallization from the reaction solution; attempts to purify the compound with preparative TLC resulted in almost complete decomposition. The spectral characteristics of 13 are compiled in Table 17.

Table 17: IR and NMR data for $Ru_3(CO)_7(\mu_2\text{-}Ph_2PCH_2CH_2PPh_2)$ $(\mu_3,\eta^2\text{-SCNHPhNPh})$ (13).

IR (c-hex, 298K)	{ν_{CO}(cm^{-1})}:	2043s	1997vs	1968s
		1953m,	1938m	
IR (KBr)	{ν_{NH} (cm^{-1})}:	3340w-m		
	{ν_{NCN} (cm^{-1})}:	1573m		
^{1}H NMR ($CDCl_3$, 298K)[a]	{δ (ppm)}:	7.56-6.85 (m, 30H)		
		6.06 (s, 1H)		
		2.00 {d(J=12.5Hz), 4H}		
		-12.94 {t(J=13.0Hz), 1H}		
^{31}P NMR ($CDCl_3$, 298K)[a]		18.53(s)		

[a] 200 Mhz
[b] 80.96 MHz

The presence of only a single peak in ^{31}P NMR spectra indicates a symmetric dppe moiety. The most likely bonding site of the dppe is bridging the two sulfur-bound Ru atoms, a condition which would also satisfy the symmetry requirements. The triplet displayed by the hydride in the ^{1}H NMR spectrum confirms this placement and the small coupling constant of that multiplet suggests a hydride bridging the same Ru atoms as the dppe. An intact

diphenylthioureato ligand is inferred from its characteristic bands in the IR spectra. The doublet observed in the alkyl region of the ^{1}H NMR spectrum, which originates from the ethylene grouping of the dppe ligand, suggests either perfectly equivalent CH_2 groups or a certain degree of fluxionality. In contrast, a triplet is observed in ^{1}H NMR spectra of the unligated dppe.

Because no analogous structure was found in the literature, a single crystal X-ray structural analysis of **13** was undertaken. Crystals of **13** are monoclinic and belong to the space group $P2_1/n$. Four complete molecules are found in the unit cell. The molecular structure of **13** is presented in Figure 20 and selected bond distances and angles are presented in Table 18.

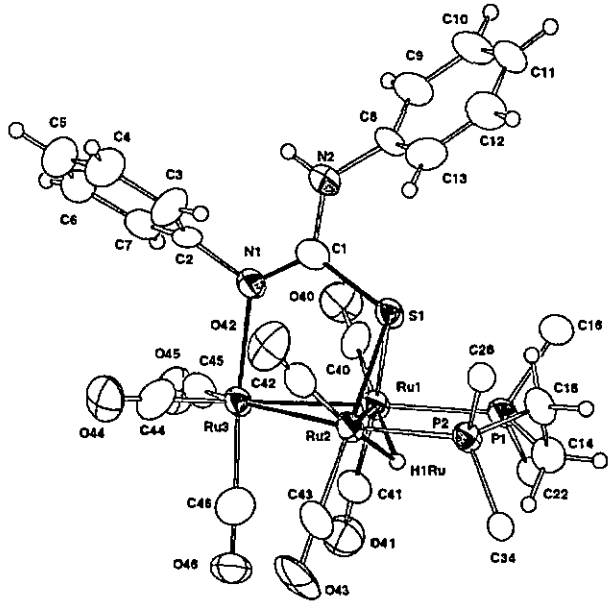

Figure 20: Molecular structure of $(\mu_2\text{-H})Ru_3(CO)_7(Ph_2PCH_2CH_2PPb_2)(\mu_3,\eta^2\text{-SCNHPhNPh})$ (**13**).

Figure 19 shows a trinuclear cluster similar to **8** except that substitution of two carbonyl ligands on adjacent Ru atoms has occurred and the vacant coordination sites have been taken up in σ-bonds to the two P atoms of dppe. The Ru-P bond lengths observed in **13** are typical for this ligand in Ru clusters. As suggested by the spectroscopic data, the dppe ligand is found spanning the S-bridged edge of the trinuclear cluster in a position *cis* to the bridging hydride and the bridging sulfur. In contrast to the changes in Ru-Ru bond lengths owing to substitution with a single PPh_3, the Ru-Ru bonds of **13** are little changed from those of **8**. The three Ru atoms and the two P atoms of the dppe ligand form a pentagonal base which is planar to within 0.053(1)Å. The bridging hydride (H1RU) assumes a position 0.75(7)Å below the M_3P_2 plane while C14 and C15 are positioned respectively , 0.53(1)Å below and 0.49(1)Å above.

Table 18: Selected bond lengths and angles of $(\mu_2\text{-H})Ru_3(CO)_7(Ph_2PCH_2CH_2PPh_2)(\mu_3,\eta^2\text{-SCNHPhNPh})$ (**13**).

Ru(1)-Ru(2)	2.843(2)	Ru(1)-Ru(3)	2.776(2)
Ru(1)-P(1)	2.357(3)	Ru(1)-S(1)	2.413(3)
Ru(1)-H(1RU)	1.79(3)	Ru(2)-Ru(3)	2.7601(13)
Ru(2)-P(2)	2.353(3)	Ru(2)-S(1)	2.417(3)
Ru(2)-H(1RU)	1.73(3)	Ru(3)-N(1)	2.178(9)
P(1)-C(22)	1.826(12)	P(1)-C(16)	1.828(12)
P(1)-C(14)	1.848(10)	P(2)-C(34)	1.812(11)
P(2)-C(28)	1.817(12)	P(2)-C(15)	1.830(12)
S(1)-C(1)	1.788(12)	N(1)-C(1)	1.284(14)
N(1)-C(2)	1.460(14)	N(2)-C(1)	1.353(14)
N(2)-C(8)	1.435(14)	C(14)-C(15)	1.58(2)
Ru(1)-S(1)-Ru(2)	72.13(9)	Ru(3)-Ru(1)-Ru(2)	58.82(4)
Ru(2)-Ru(3)-Ru(1)	61.80(4)	Ru(3)-Ru(2)-Ru(1)	59.38(4)
Ru(3)-Ru(1)-H(1RU)	86(2)	P(1)-Ru(1)-Ru(2)	104.05(8)
Ru(3)-Ru(2)-H(1RU)	87(2)	P(1)-Ru(1)-Ru(3)	162.87(8)
P(1)-Ru(1)-S(1)	90.08(11)	P(2)-Ru(2)-Ru(1)	102.99(8)
P(1)-Ru(1)-H(1RU)	79(2)	P(2)-Ru(2)-Ru(3)	162.08(8)
P(2)-Ru(2)-S(1)	86.88(10)	S(1)-Ru(1)-Ru(3)	79.58(8)
P(2)-Ru(2)-H(1RU)	78(3)	S(1)-Ru(1)-H(1RU)	78(2)
S(1)-Ru(1)-Ru(2)	54.00(7)	S(1)-Ru(2)-Ru(1)	53.87(7)
S(1)-Ru(2)-Ru(3)	79.84(7)	H(1)-Ru(3)-Ru(1)	88.6(3)
S(1)-Ru(2)-H(1RU)	79(2)	C(1)-S(1)-Ru(1)	105.9(4)
N(1)-Ru(3)-Ru(2)	88.0(2)	C(1)-N(1)-Ru(3)	122.4(8)
C(1)-S(1)-Ru(2)	106.5(4)	C(1)-N(2)-C(8)	129.0(10)
C(1)-N(1)-C(2)	118.6(10)	C(14)-P(1)-Ru(1)	114.8(4)
C(2)-N(1)-Ru(3)	118.8(7)	C(15)-P(2)-Ru(2)	115.7(4)
C(14)-C(15)-P(2)	114.1(8)	C(16)-P(1)-Ru(1)	120.3(4)
C(15)-C(14)-P(1)	112.8(8)	C(22)-P(1)-C(16)	102.1(5)
C(16)-P(1)-C(14)	101.0(5)	C(22)-P(1)-Ru(1)	113.0(4)
C(22)-P(1)-C(14)	103.5(5)	C(28)-P(2)-C(15)	101.3(5)
C(28)-P(2)-Ru(2)	112.8(4)	C(34)-P(2)-C(15)	100.9(5)
C(34)-P(2)-Ru(2)	119.7(4)	N(1)-C(1)-S(1)	119.1(9)
C(34)-P(2)-C(28)	104.2(5)	N(2)-C(1)-S(1)	116.2(9)
N(1)-C(1)-N(2)	124.7(11)		

Within experimental error the geometry of the diphenylthioureato ligand is similar to that observed previously (compounds **8** and **10** for example).

A pseudo mirror plane containing Ru3, N1, C1, and S1 bisects the Ru1-Ru2 and C14-C15 bonds. In the solid state, the dppe ligand distorts this symmetry element through the inequivalency of the methylene groups. However, the presence of only a doublet in the ^1H NMR spectrum, indicates that these groups must be considerably fluxional in solution. No symmetry restraints are presented by the phenyl groups of the ligated dppe. Those groups are forced to adopt a single orientation with respect to the metal cluster, which renders them equivalent.

Two molecules of CH_2Cl_2 as well as one molecule of H_2O were found to cocrystallize in the unit cell. The CH_2Cl_2 originates from the crystallization solvent (CH_2Cl_2/hexanes), while the source of the molecule of H_2O must be incompletely dried glassware.

The dppe ligand typically takes on a bridging mode in cluster complexes and in doing so lends a degree of stability to the resulting cluster molecule.[107] This was the case with the trinuclear cluster $(\mu_2\text{-H})Ru_3(CO)_7(Ph_2PCH_2PPh_2)(\mu_3,\eta^2\text{-ampy})$, prepared but not structurally characterized, by Cabeza and coworkers.[102b] Contrary to thermolysis of the disubstituted PPh_3 analogue (recall thermolysis under H_2 pressure produced P-C bond cleavage), exposure of the dppe/ampy cluster to elevated temperatures had no effect. The stabilizing effect of the dppe ligand is apparent. The behavior of cluster **13** under thermolytic conditions, however, does not suggest a significant stabilization effect from the dppe ligand. Refluxing a cyclohexane solution of **13** over a period of 1h resulted in formation of at least five different carbonyl clusters.

3.7 Concerning the Reactions of $(\mu_2\text{-H})Ru_3(CO)_9(\mu_3,\eta^2\text{-SCNHPhNPh})$ (8).

The added structural stability, originally perceived as possible with the face-capping diphenylthioureato ligand, has not always shown to be the case. Although under certain conditions, the diphenylthioureato ligand itself remains intact fragmentatioo has occurred even under extremely mild conditions. The phosphine-based reagents result in substitution of CO

groups. While the phosphine substituted derivatives of **8** undergo ligand transformations upon exposure to high temperatures, the original cluster nuclearity is maintained.

3.8 From Trinuclear to Hexanuclear Clusters

Cotton's general definition of a metal cluster offered as a group of two or more metal atoms in which substantial bonding occurs among the metals is useful in differentiating clusters from Werner-type coordination complexes.[108] In many of the later reviews of metal clusters however, this definition is narrowed to include only those species containing at least three metal atoms. The next step, from metal clusters to metal surfaces, is a more difficult distinction. The point at which one passes from a non-metallic state to a metallic state has been the subject of much research.[109] Localized versus delocalized bonding within the metal framework provides a starting point. It has been shown that when cluster nuclearity approaches six metal atoms, a localized bonding description no longer provides an adequate description.[110] At this point a delocalized bonding approach, more similar in nature to the band theory of metals, becomes necessary. Given such a position within the cluster hierarchy, the types of reactions and transformations undertaken by hexanuclear clusters offer a simplified model of those processes at the metal surface.

The full range of structural motifs displayed by hexanuclear cluster compounds is well documented.[110,111] The relationships between the observed geometries of these clusters and their closed-shell electronic requirements comprise a portion of the polyhedral skeletal electron pair theory (PSEPT).[112] The majority of M_6 clusters adopt an octahedral geometry, therefore not surprisingly, clusters of this type were among the first to be isolated and structurally characterized. The 86-electron octahedral cluster $Ru_6C(CO)_{17}$ is a typical example.[113] Many clusters have been isolated whose geometries are derived from standard polyhedra by capping or bridging in order to provide the additional vertices necessary to accommodate the additional metal atoms. These include the bicapped tetrahedral geometry and the capped square pyramid as exemplified by $Os_6(CO)_{17}(MeCN)$, $Os_6(CO)_{17}(\mu_4,\eta^2$-HCCEt) respectively.[114] These clusters contain a total of 84 and 86 valence electrons respectively, the numbers predicted from PSEPT. As opposed to the addition of vertices, the structures of some hexanuclear clusters must be considered as larger polyhedra with vertices missing, as in the case of the edge-bridged diminished pentagonal bipyramid found for (μ_2-

H)$Ru_6C(CO)_{15}(SEt)_3$.[115] Analogous to the boranes and carboranes, the opening-up of the polyhedral geometry requires additional skeletal electrons, thus the edge-bridged diminished pentagonal bipyramid shows an electron count of 92 electrons. Further variations are planar raft structures including both the triangular raft, $[(\mu_3\text{-H})Ru_6(CO)_{15}(\mu_3\text{-S})_3]^-$[89d] and the rhombic raft cluster, $(\mu_2\text{-H})_4(\mu_3\text{-H})_2Ru_6(CO)_{14}(\mu_3,\eta^2\text{-ampy})_2$.[116] The former cluster contains 92 valence electrons, two in excess of the number predicted from PSEPT. This feature has been used to explain the elongation of certain M-M bonds via population of antibonding cluster orbitals.[117] The latter also contains 92 valence electrons but this is in accord with its geometry. Distortion of the metal plane of the rhombic raft cluster results in alternative enre configurations. Some of these configurations resemble the various conformers of cyclohexane[118] while others represent structural intermediates between the stable conformations.[119] The majority of these latter raft-type clusters are either electron-rich or electron precise and all contain multiply bridging ligands.

From a simple thermolysis reaction of the trinuclear cluster $(\mu_2\text{-H})Ru_3(CO)_9(\mu_3,\eta^2$-SCNHPhNPh) (8), it was possible to isolate two hexanuclear thioureato clusters, each with a metal skeleton which mimics a known conformer of cyclohexane. The first of these is structurally similar to the *boat* conformer while the second is a structural analogue of the *sofa* conformer. The second, the sofa-like structure, is produced in relatively high yield (46%) for a preparative proceedure that is known for its lack of selectivity. Given easy access to reasonable amounts of the second hexanuclear species, it was considered an ideal opportunity to explore its reactivity towards a series of organic reagents.

3.9 Thermolysis of $(\mu_2$ H)$Ru_3(CO)_9(\mu_3,\eta^2$-SCNHPhNPh) (8)

3.9.1 Isolation and Characterization of $Ru_6(\mu_2\text{-CO})_2(CO)_{14}(\mu_3,\eta^2$-SCNHPhNPh) $(\mu_3,\eta^2$-NPhCNHPh) (14).[120]

From the thermolysis of the trinuclear cluster $(\mu_2\text{-H})Ru_3(CO)_9(\mu_3,\eta^2$-SCNHPhNPh) (8) in cyclohexane, a minor product could be isolated from the reacton mixture as a green-blue band on TLC plates. Interpretation of the spectroscopic data for this compound indicated a product more complex in nature than the starting material. These data are compiled in Table 19. This same product was isolated in approximately the same yield from the thermolysis of

an equimolar solution of $Ru_3(CO)_{12}$ and $(PhNH)_2CS$. Crystals of the compound could be obtained from CH_2Cl_2/C_5H_{12} solutions maintained at -18°C over a period of 1 week. An X-ray structural analysis of the compound identified it as $Ru_6(\mu_2\text{-}CO)_2(CO)_{14}(\mu_4\text{-}S)(\mu_3,\eta^2\text{-}SCNHPhNPh)(\mu_3,\eta^2\text{-}NPhCNHPh)$ (**14**), the metal framework of which presents an hexagonal boat-like arrangement of the six metal atoms.

Table 19: IR and NMR data for $Ru_6(\mu_2\text{-}CO)_2(CO)_{14}(\mu_4\text{-}S)(\mu_3,\eta^2\text{-}SCNHPhNPh)(\mu_3,\eta^2\text{-}NPhCNHPh)$ (**14**).

IR(c-hex, 298K)	{$\nu_{CO}(cm^{-1})$}:	2082m	2057s	2036vs
		2005m	1976m	1854m,br
IR(KBr)	{$\nu_{NH}(cm^{-1})$}:	3343w	3304w	
	{$\nu_{NCN}(cm^{-1})$}:	1558m	1498m	
^{1}H NMR ($CDCl_3$, 298K)*	{δ(ppm)}:	7.72-6.41 (m, 20H, Ph-*H*)		
		6.28 (s,br,1H,N*H*)		
		6.22 (s,br,1H,N*H*)		

* 400 MHz

Aside from the presence of a bridging carbonyl group in solution IR spectra of **14**, few differences from the starting material are observed in the carbonyl region. The two separate signals in the NH region of the IR spectrum are ambiguous in that they could imply either two different NCN-type linkages in which NH activatioo has occurred or a single $C(NHPh)_2$ type ligand. However the two peaks observed in the NCN region of solid state IR spectra indicate at least two different NCN-type linkages and the complexity of the phenyl region of the ^{1}H NMR spectrum of **14** further supports this conclusion.

The X-ray structural analysis of 14 produced the molecular structure presented in Figure 21. Crystals of **14** are triclinic and belong to the space group $P\bar{1}$. All non-hydrogen atoms were located in difference maps and refined. Hydrogen atoms were placed in calculated positions. Important bond lengths and angles for **14** are given in Table 20.

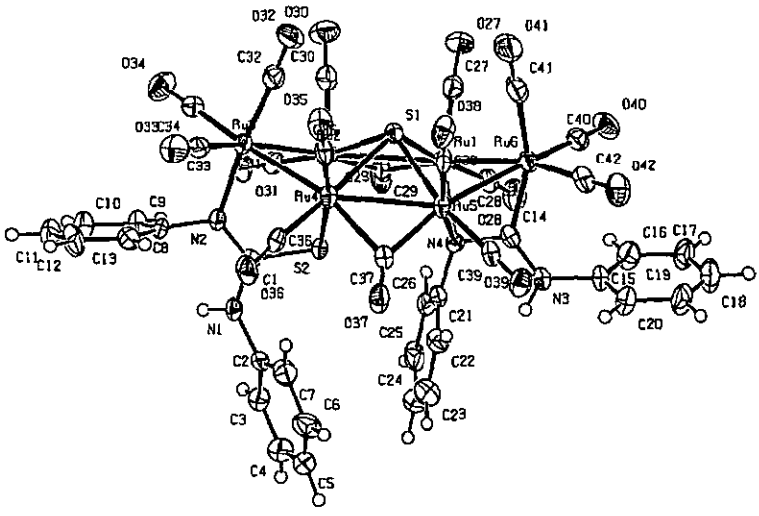

Figure 21: Molecular structure of $Ru_6(\mu_2\text{-}CO)_2(CO)_{14}(\mu_4\text{-}S)(\mu_3,\eta^2\text{-}SCNHPhNPh)(\mu_3,\eta^2\text{-}NPhCNHPh)$ (14).

Table 20: Selected bond lengths (Å) and angles (°) of compound $Ru_6(\mu_2\text{-}CO)_2(CO)_{14}(\mu_4\text{-}S)(\mu_3,\eta^2\text{-}SCNHPhNPh)(\mu_3,\eta^2\text{-}NPhCNHPh)$ (14).

Ru(1)-Ru(2)	2.9163(11)	Ru(4)-C(37)	2.182(7)
Ru(1)-Ru(6)	2.7708(13)	Ru(5)-Ru(6)	2.7670(11)
Ru(1)-Ru(5)	3.2234(11)	Ru(5)-S(1)	2.4365(20)
Ru(1)-S(1)	2.4311(18)	Ru(5)-N(4)	2.269(5)
Ru(1)-N(4)	2.268(5)	Ru(5)-C(37)	2.079(7)
Ru(1)-C(29)	2.130(7)	Ru(6)-C(14)	2.044(7)
Ru(2)-Ru(3)	2.7504(10)	S(2)-C(1)	1.794(7)
Ru(2)-Ru(4)	3.0374(11)	N(1)-C(2)	1.437(9)
Ru(2)-S(1)	2.5050(20)	N(1)-C(1)	1.328(9)
Ru(2)-S(2)	2.4712(20)	N(2)-C(1)	1.298(9)
Ru(2)-C(29)	2.133(7)	N(2)-C(8)	1.458(8)
Ru(3)-Ru(4)	2.7529(11)	N(3)-C(14)	1.324(9)
Ru(3)-N(2)	2.142(6)	N(3)-C(15)	1.461(8)
Ru(4)-Ru(5)	2.8972(11)	N(4)-C(14)	1.399(8)
Ru(4)-S(1)	2.5021(19)	N(4)-C(21)	1.442(9)
Ru(4)-S(2)	2.4544(19)		

Table 20 (cont.):

Ru(1)-Ru(2)-Ru(3)	144.19(3)	Ru(4)-Ru(5)-S(1)	55.14(5)
Ru(1)-Ru(2)-S(1)	52.62(4)	Ru(4)-Ru(3)-N(2)	87.38(15)
Ru(1)-Ru(2)-C(29)	46.80(18)	Ru(4)-Ru(5)-N(4)	99.65(13)
Ru(1)-Ru(2)-Ru(4)	91.47(3)	Ru(4)-S(2)-C(1)	101.73(21)
Ru(1)-Ru(2)-S(2)	92.62(5)	Ru(4)-Ru(5)-C(37)	48.67(20)
Ru(1)-Ru(5)-Ru(6)	54.46(3)	Ru(4)-C(37)-Ru(5)	85.6(3)
Ru(1)-Ru(5)-N(4)	44.72(14)	Ru(5)-Ru(1)-Ru(6)	54.35(3)
Ru(1)-Ru(5)-Ru(4)	88.17(3)	Ru(5)-Ru(1)-S(1)	48.60(5)
Ru(1)-Ru(5)-S(1)	48.46(4)	Ru(5)-Ru(1)-N(4)	44.73(13)
Ru(1)-Ru(5)-C(37)	122.64(19)	Ru(5)-Ru(1)-C(29)	126.06(20)
Ru(1)-Ru(6)-C(14)	67.14(19)	Ru(5)-Ru(4)-S(1)	53.04(5)
Ru(1)-Ru(6)-Ru(5)	71.19(3)	Ru(5)-Ru(4)-S(2)	93.18(5)
Ru(1)-N(4)-C(14)	93.2(4)	Ru(5)-Ru(6)-C(14)	67.06(17)
Ru(1)-N(4)-Ru(5)	90.54(19)	Ru(5)-N(4)-C(14)	92.9(4)
Ru(1)-C(29)-Ru(2)	86.3(3)	Ru(6)-Ru(1)-S(1)	84.12(5)
Ru(2)-Ru(1)-Ru(5)	88.17(3)	Ru(6)-Ru(1)-N(4)	68.03(13)
Ru(2)-Ru(1)-Ru(6)	138.18(3)	Ru(6)-Ru(5)-S(1)	84.10(5)
Ru(2)-Ru(3)-Ru(4)	67.00(3)	Ru(6)-Ru(5)-N(4)	68.09(13))
Ru(2)-Ru(4)-Ru(3)	56.46(3)	Ru(6)-C(14)-N(3)	131.6(5)
Ru(2)-Ru(4)-Ru(5)	92.19(3)	Ru(6)-C(14)-N(4)	110.3(4)
Ru(2)-Ru(4)-S(1)	52.70(5)	S(1)-Ru(1)-N(4)	88.83(14)
Ru(2)-Ru(4)-S(2)	52.18(5)	S(1)-Ru(2)-S(2)	91.64(6)
Ru(2)-Ru(3)-N(2)	86.50(14)	S(1)-Ru(4)-S(2)	92.11(6)
Ru(2)-S(2)-Ru(4)	76.15(6)	S(1)-Ru(5)-N(4)	88.69(14)
Ru(3)-Ru(2)-Ru(4)	56.540(25)	S(2)-C(1)-N(1)	117.0(5)
Ru(3)-Ru(4)-Ru(5)	144.70(3)	S(2)-C(1)-N(2)	118.8(5)
Ru(3)-Ru(2)-S(1)	92.30(5)	N(1)-C(1)-N(2)	124.1(6)
Ru(3)-Ru(4)-S(1)	92.30(5)	N(3)-C(14)-N(4)	118.1(6)
Ru(3)-N(2)-C(1)	123.8(4)	C(1)-N(1)-C(2)	127.7(6)
Ru(3)-N(2)-C(8)	118.2(4)	C(1)-N(2)-C(8)	118.0(6)
Ru(4)-Ru(5)-Ru(6)	138.34(3)	C(14)-N(3)-C(15)	124.1(6)
Ru(4)-Ru(2)-S(1)	52.61(5)		

Of the six Ru atoms comprising the cluster framework, four of them form an approximately square base. Opposing sides of this trapezoid are bridged by the remaining two Ru atoms. Significant deviations from a square geometry occur at the edges bridged by the metal atoms; here the longer metal-metal bonds are observed [Ru2-Ru4 (3.037(1)Å) and Ru1-Ru5 (3.223(1)Å)]. The remaining Ru-Ru bond lengths fall within the range 2.750(1)Å-2.916(1)Å. The same sequence of long-short metal bond lengths is observed in the boat clusters cited previously.[118b,121] The square cluster base is planar within 0.02Å. The Ru atoms not lying in the plane of the square base, form an angle with that substructure of 17.27(2)° for Ru3 and 19.80(2)° for Ru6. The overall result is a metal framework resembling the boat conformer of cyclohexane.

The square base is capped by a μ_4-sulfur (average Ru-S1 distance 2.469(2)Å). The surface of the cluster opposite to the μ_4-sulfur contains a μ_3,η^2-diphenylthioureato ligand spanning the trianglar substructure composed of Ru2, Ru3 and Ru4. Compared to the diethylthioureato cluster analogue[118d], the Ru-S bonds are slightly longer but the Ru-N bond is of the same magnitude [Ru3-N2 (2.142(6)Å)]. The unsaturation at C1 is relieved through formation of a double bond to N2 (N2-C1, 1.298(9)Å). The hydrogen located on N1 (H1) takes part in a hydrogen-bonding interaction with the oxygen (O31), of a CO ligand from a neighboring molecule (d(H··O), 2.43Å). This feature probably originates from a shift of electron density from the N into a delocalized double bond over the NCN system, similar to what has been suggested for the unligated thiourea. This shift in electron densitty would leave H1 with a slight positive charge and more susceptible to hydrogen bonding.

On the same side of the cluster, but spanning the second triangular substructure containing Ru1, Ru5 and Ru6, is a μ_3,η^2-diaminocarbene fragment. Here the Ru-N bonds are identical to those of the previously published diethylthioureato boat cluster (avg. 2.268(5)Å), while the carbene carbon atom bound to Ru6 shows a markedly shorter bond to the metal [Ru6-C14 (2.044(7)Å)]. The C-N bond lengths within this ligand show a lesser degree of sp^2 character compared to the diethylthioureato ligand [C14-N3 (1.324(9)Å), C14-N4 (1.399(8)Å)] and this is most likely responsible for the observed shortening of the Ru6-C14 bond. Bridging carbonyl ligands are found spanning the Ru1-Ru2 bond as well as the Ru4-Ru5 bond and fall just below the plane of the four-membered trapezoid (avg. distance to the plane 0.9(1)Å). Terminal carbonyl ligands complete the coordination sphere of the remaining ruthenium atoms.

Two dichloromethane molecules were found to crystallize in the unit cell. Non-bonded distance calculations[122] have shown relevant H-bonding interactions between the hydrogens of these solvent molecules and the oxygens of the CO ligands. In the most significant of these interactions a hydrogen atom of solvent molecule, H1Sb, is shown to approach O41 at 2.49Å, a distance significantly shorter than the sum of these atoms' VDW radii (2.72Å). Similar to cluster **4**, these hydrogen-bonding interactions reveal the important role the crystallization solvent can play in crystal formation.

Following the principles of PSEPT as put forth by Mingos[110], a hexanuclear cluster of this type can formally be considered as a bi-edge-bridged square and requires 92 electrons to satisfy its closed-shell requirements. If one considers the μ_4-S as a 4-electron donor and the diphenylthioureato and the diaminocarbene ligands as 5-electron donors then cluster **14** contains a total of 94 electrons. Electrons in excess of those required seem to characterize the hexanuclear Ru-based *boat*-type clusters cited here. The most straightforward explanation assigns a bond order of 0.5 to the longer Ru-Ru bonds (Ru1-Ru5 and Ru2-Ru4 in **14**) thus accounting for the elongation of those bonds and at the same time satisfying the effective atomic number rule for the entire cluster. Adams *et al.* restated this concept by postulating that the two additional electrons occupy a delocalized antibonding orbital on the central Ru_4 square resulting in bond weakening of those Ru-Ru bonds similar to the situation in the 92 electron hexanuclear raft clusters[123]. From the bond length data, it appears this effect is most dominant at the non-carbonyl-bridged edges, however, without calculations this becomes conjecture.

3.9.2 Isolation and Characterization of $(\mu_2\text{-H})Ru_6(CO)_{16}(\mu_5\text{-S})$-$(\mu_3,\eta^2\text{-SCNHPhNPh})$ (15).[118d]

From the thermolysis of $(\mu_2$ H$)Ru_3(CO)_9(\mu_3,\eta^2$-SCNHPhNPh) (**8**) in THF the major product is the hexanuclear cluster $(\mu_2$ H$)Ru_6(CO)_{16}(\mu_5$-S$)(\mu_3,\eta^2$-SCNHPhNPh) (**15**) (46%). The compound **15** could be easily isolated from the reaction mixture as a red band by chromatography on TLC plates. Spectroscopic data for **15** are presented in Table 21.

Table 21: IR and NMR data for $(\mu_2$ H$)Ru_6(CO)_{16}(\mu_5$-S$)(\mu_3,\eta^2$-SCNHPhNPh) (**15**).

IR(c-hex, 298K)	{ν_{CO}(cm^{-1})}:	2092m	2070s	2061s
		2046m	2023m	2012s
		1949m		
IR(KBr)	{ν_{NH}(cm^{-1})}:	3374m		
	{ν_{NCN}(cm^{-1})}:	1565m		
^{1}H-NMR($CDCl_3$, 298K)[a]	{δ(ppm)}:	7.63-7.11 (m,10H,Ph-*H*)		
		6.84 (s,br,1H,Ph-*H*)		
		-22.24(s, 1H, Ru_2*H*)		

[a] 200 MHz

It is immediately obvious from the carbonyl region of solution IR spectra of **15**, that the nature of this product differs significantly from that of the starting material. Specifically

the appearance of new bands indicates that a condensation to form a species of higher nuclearity has occurred. The remaining IR data indicate an intact diphenylthioureato ligand as do the phenyl and NH peaks in the ^{1}H NMR spectrum. The single bridging hydride is shifted significantly upfield from that of compound **8** (-12.90 ppm) and suggests a proton in the vicinity of a larger number of metal atoms.

Red, block crystals of **15** could be easily obtained from slow evaporation at room temperature of a CH_2Cl_2 solution. An X-ray structural analysis of one of these crystals was carried out and the molecular structure thus determined is presented in Figure 22. The cluster **15** was found to crystallize in the monoclinic system in the space group $P2_1/n$; Z = 4. All non-hydrogen atoms and the single bridging hydride (H), were located in difference maps and subsequently refined. The remaining hydrogen atoms were fixed in calculated positions. Relevant bond lengths and angles are assembled in Table 22.

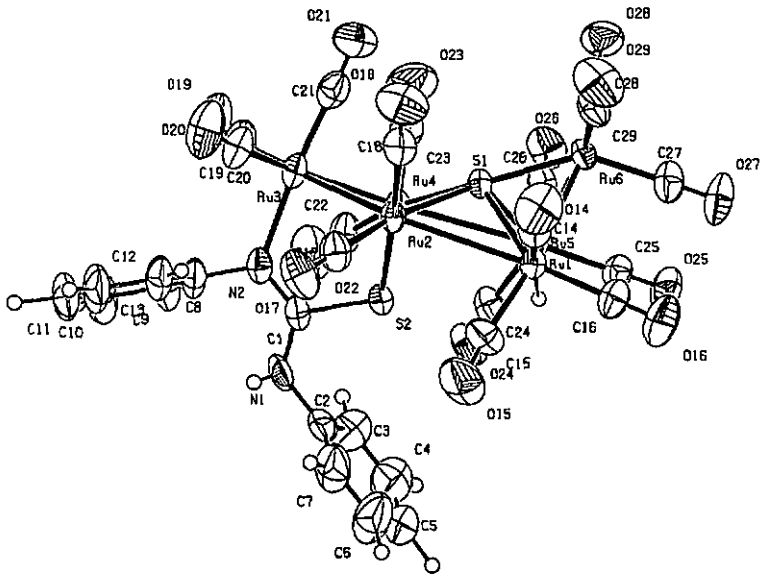

Figure 22: Molecular structure of $(\mu_2\ H)Ru_6(CO)_{16}(\mu_5\text{-}S)(\mu_3,\eta^2\text{-}SCNHPhNPh)$ (**15**).

Table 22: Selected bond lengths and angles for (μ_2 H)$Ru_6(CO)_{16}(\mu_5$-S)-(μ_3,η^2-SCNHPhNPh) (**15**).

Ru(1)-Ru(2)	3.1713(6)	Ru(1)-Ru(5)	2.9221(5)
Ru(1)-Ru(6)	2.7807(6)	Ru(1)-S(1)	2.4068(12)
Ru(1)-H	1.73(6)	Ru(2)-Ru(3)	2.7156(6)
Ru(2)-Ru(4)	2.9208(5)	Ru(2)-S(1)	2.3909(12)
Ru(2)-S(2)	2.4213(14)	Ru(3)-Ru(4)	2.7268(6)
Ru(3)-N(2)	2.146(5)	Ru(4)-Ru(5)	3.0817(5)
Ru(4)-S(1)	2.4312(12)	Ru(4)-S(2)	2.4086(13)
Ru(5)-Ru(6)	2.7858(5)	Ru(5)-S(1)	2.3890(12)
Ru(5)-H	1.80(6)	Ru(6)-S(1)	2.3126(12)
S(2)-C(1)	1.779(5)	N(1)-C(1)	1.336(8)
N(1)-C(2)	1.451(9)	N(2)-C(1)	1.295(7)
N(2)-C(8)	1.433(7)		

Ru(1)-Ru(2)-S(2)	81.72(3)	Ru(1)-Ru(5)-Ru(4)	90.377(15)
Ru(1)-Ru(5)-Ru(6)	58.250(14)	Ru(1)-Ru(5)-S(1)	52.74(3)
Ru(1)-Ru(5)-H	33.2(18)	Ru(1)-Ru(6)-Ru(5)	63.329(14)
Ru(1)-N-Ru(5)	112(3)	Ru(2)-Ru(1)-Ru(5)	89.474(15)
Ru(2)-Ru(1)-Ru(6)	96.588(17)	Ru(2)-Ru(1)-S(1)	48.41(3)
Ru(2)-Ru(3)-Ru(4)	64.916(14)	Ru(2)-Ru(3)-N(2)	88.06(11)
Ru(2)-Ru(4)-Ru(3)	57.356(14)	Ru(2)-Ru(4)-Ru(5)	91.266(15)
Ru(2)-Ru(4)-S(1)	52.09(3)	Ru(2)-Ru(4)-S(2)	52.99(3)
Ru(2)-S(1)-Ru(4)	74.56(4)	Ru(2)-S(1)-Ru(5)	127.80(5)
Ru(2)-S(1)-Ru(6)	142.29(5)	Ru(2)-Ru(1)-H	102.7(19)
Ru(2)-S(2)-Ru(4)	74.42(4)	Ru(3)-Ru(2)-Ru(4)	57.728(14)
Ru(3)-Ru(2)-S(1)	101.67(3)	Ru(3)-Ru(2)-S(2)	79.79(3)
Ru(3)-Ru(4)-Ru(5)	147.988(18)	Ru(3)-Ru(4)-S(1)	100.30(3)
Ru(3)-Ru(4)-S(2)	79.78(3)	Ru(3)-N(2)-C(1)	121.1(4)
Ru(4)-S(2)-C(1)	104.29(18)	Ru(4)-Ru(2)-S(1)	53.35(3)
Ru(4)-Ru(2)-S(2)	52.59(3)	Ru(4)-Ru(3)-N(2)	89.21(12)
Ru(4)-Ru(5)-Ru(6)	100.003(16)	Ru(4)-Ru(5)-S(1)	50.86(3)
Ru(4)-Ru(5)-H	101.1(19)	Ru(4)-S(1)-Ru(5)	79.48(4)
Ru(4)-S(1)-Ru(6)	143.00(5)	Ru(5)-Ru(1)-Ru(6)	58.421(14)
Ru(5)-Ru(1)-S(1)	52.18(3)	Ru(5)-Ru(1)-H	34.7(18)
Ru(5)-Ru(4)-S(1)	49.66(3)	Ru(5)-Ru(4)-S(2)	86.04(3)
Ru(5)-Ru(6)-S(1)	54.94(3)	Ru(5)-S(1)-Ru(6)	72.65(4)
Ru(6)-Ru(1)-S(1)	52.35(3)	Ru(6)-Ru(1)-H	89.0(18)
Ru(6)-Ru(5)-S(1)	52.41(3)	Ru(6)-Ru(5)-H	87.5(18)
S(1)-Ru(1)-H	82.8(19)	S(1)-Ru(2)-S(2)	85.89(4)
S(1)-Ru(4)-S(2)	85.29(4)	S(1)-Ru(5)-H	81.9(19)
S(2)-C(1)-N(1)	115.3(4)	S(2)-C(1)-N(2)	119.9(4)
N(1)-C(1)-N(2)	124.8(5)	N(1)-C(2)-C(3)	119.3(6)
C(1)-N(1)-C(2)	125.5(5)	C(1)-N(2)-C(8)	117.3(5)

The metal framework of **15** consists of a unique arrangement of six metal atoms which can be considered analogous to the sofa conformer of cyclohexane. The base of the hexanuclear skeleton forms an approximately planar array of five ruthenium atoms (Ru1, Ru2, Ru3, Ru4 and Ru5), arranged in an envelope-like fashion with Ru4 occupying the flap position and showing the most significant deviation from the plane of the remaining atoms

(0.1071(5)Å). The Ru1-Ru5 edge is bridged by a sixth ruthenium atom, Ru6, arranged at an angle of approximately 90° with respect to the plane of the other ruthenium atoms. A penta-coordinate sulfur bridges four of the in-plane ruthenium atoms (Ru1, Ru2, Ru4 and Ru5) and the out-of-plane ruthenium atom (Ru6). The pentacoordinate sulfur forms a plane with ruthenium atoms 2, 4 and 6 and itself shows the maximum deviation from that plane of 0.0459(12)Å. The opposing side of the cluster base contains a μ_3,η^2-diphenylthioureato ligand in which the sulfur spans Ru2 and Ru4 and the nitrogen atom is bound in a terminal fashion to Ru3. A bridging hydride is found between Ru1 and Ru5. Each ruthenium coordination sphere is completed with terminal carbonyl groups, two in the case of the metal atoms Ru2 and Ru4 and three for Ru1, Ru3, Ru5 and Ru6. The molecule possesses an approximate mirror-plane passing through atoms Ru6, S1, S2, C1, N2 and Ru3, and distortion to that symmetry element is due to a slight twisting of the molecule probably resulting from the unusual coordination of the sulfido ligand.

In **15** the metal-metal bond distances span a wide range. The longest metal-metal bonds are found between Ru1 and Ru2 (3.1713(6)Å) and Ru4 and Ru5 (3.0817(5)Å). Although distances of this magnitude have been previously cited as bonding in S-containing Ru clusters[124], they are particularly long. Alternatively, one might suggest two trinuclear Ru units linked together by the μ_5-S. However, in this case both trinuclear units would be unsaturated; that containing the diphenylthioureato ligand would contain only 45 valence electrons (48 valence electrons are required for a triangular array of metal atoms). Somewhat shorter, though almost identical, metal-metal bond lengths are found opposite the longest Ru-Ru bonds (Ru2-Ru4, 2.9208(5)Å; Ru1-Ru5, 2.9221(5)Å); the longer of these contains the bridging hydride. Shorter but relatively consistent bonds are found to the apical Ru6 and the bridging Ru3 (average Ru-Ru, 2.7522Å). Among the two types of sulfur atoms, metal-sulfur bond distances vary from 2.3126(12)Å (Ru6-S1) to 2.4312(12)Å (Ru4-S1). Surprisingly both the long and the short metal-sulfur bonds are associated with the pentacoordinate sulfur, further suggesting the unique coordination mode adopted by this atom.

Table 22 shows the lengths of the Ru-Ru bonds spanned by the thioureato ligand of **15** are significantly different from the same bonds in **8**.[89a] However the nature of the diphenylthioureato ligand remains undisturbed in that metal-sulfur bond lengths are comparable to **8** and the double bond character between C(1) and N(2) is retained. As found in **14**, the

acidic nature of the amine proton (H1), manifests itself in a hydrogen-bonding interaction to the O atom of the CO on an adjacent cluster molecule. The distance calculated between H1 and O25 is 2.56Å, indicating an interaction less significant than found in **14**.

In considering ruthenium-sulfur bond distances one observes a range of some 12 pm and, as stated, the shortest and longest are associated with S1. The shortest of these metal-sulfur bonds can be rationalized in part through electron counting procedures. Donation of all six valence electrons on S(1) is necessary to satisfy the effective atomic number rule for the cluster and specifically two of these valence electrons are donated to Ru(6) thus resulting in an increased bond order and a corresponding decrease in bond length. Finding all the noticeably short Ru-S bonds to the pentacoordinate sulfur lends further support to full electron donation by S(1). Through electron donation sulfur may subsequently decrease the bond order of the adjacent metal-metal bonds and thus contribute to their lengthening. Bridging hydride atoms have also been shown to increase metal-metal bond lengths and this effect must also be considered.[125] Furthermore, given such a framework geometry, the pentacoordinate sulfur atom in bonding to Ru6 is forced to accept a position only 1.0968(12)Å above the plane of the five basal ruthenium atoms. Such an exceptionally close approach by S(1) could contribute further to lengthening the metal-metal bonds of the rectangular base.[126]

Examples of pentacoordinate sulfur in metal cluster complexes exist. In the early seventies, the structure of a mineral known as argentian pentlandite, which displayed pentacoordinate sulfur in a square pyramidal coordination was published.[127] More recently Adams *et al.* have identified several complexes in which a sulfur ligand bridges four ruthenium or osmium atoms and also coordinates a molybdenum atom in a fifth axial position, again assuming a square pyramidal coordination mode.[128] Further examples involve either hexacoordinate sulfur[129] or encapsulation of the chalcogen by multiple metal atoms.[126,130]

Compound **15** contains a unique example of μ_5-sulfur spanning five mutually bonded ruthenium atoms. Considering only the metal framework of **15** and S1, an analogy to a chemisorbed sulfur atom can be drawn. Indeed, definitive studies of atomic adsorption on metal surfaces establish multicenter metal-adsorbate atom interactions.[131] The atypical coordination of S(1), as exemplified by the diverse bond lengths and unusual geometry exhibited throughout its coordination sphere, demonstrate the tenacity with which sulfur can

bind to a metal surface and thus render it "sulfur-poisoned". Evidence of the strength of the Ru-S bonds is provided from reactions which failed to affect these bonds.

From the thermolysis of [(μ_2-H)Ru_3(CO)$_9$(μ_3,η^2-SCNHPhNPh)] (**8**) the primary product is the hexanuclear sofa-like cluster **15** (46%). The hexanuclear boat-like cluster **14** is also obtained from this reaction, but for this product the yield varies inversely with the duration of the reaction (5%-3%). Previously it was postulated that the formation of **14** and **15** proceeded through the intermediacy of the trinuclear cluster **8**.[118d] Thus both **14** and **15** are available from **8** upon heating. From **8**, a condensation with elimination of H_2 and CO to produce the boat-like **14** was suggested. Further elimination of the diaminocarbene fragment and coordination of the fifth Ru atom to the capping sulfur would produce **15** (see Scheme II), an hypothesis which would explain the varying yields of **14** with respect to reaction time.

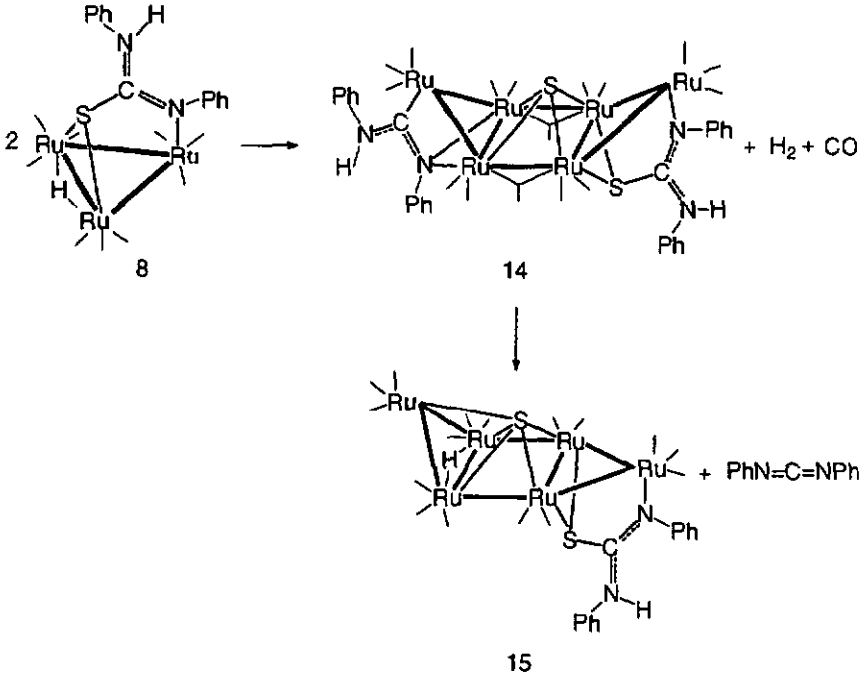

Scheme II.

However, the eliminated $(PhNH)_2C$ has not been detected in the reaction mixture. Furthermore, if **14** alone is subjected to thermolysis at 130°C, it is converted to **15** but only in

low yield (6%). Although this does not rule out the possibility of **14** as an intermediate in the formation of **15**, this mechanism cannot be stated with certainty.

3.10 Reaction of $(\mu_2\text{-H})Ru_6(CO)_{16}(\mu_5\text{-S})(\mu_3,\eta^2\text{-SCNHPhNPh})$ (15) with H_2; $(\mu_2\text{-H})_6Ru_6(CO)_{14}(\mu_3,\eta^2\text{-SCNHPhNPh})_2$ (16)[120]

Exposing a CH_2Cl_2 solution of **15** to moderate pressures of H_2 (5bar), over a period of 6h, caused the reaction solution to change from deep, burgundy red to bright red. Chromatographic work-up of the solution on TLC plates allowed the isolation of 3 products. First to elute was a yellow band, identified as the known compound $(\mu_2\text{-H})_2Ru_3(CO)_9(\mu_3\text{-S})$.[132] Second was the trinuclear cluster $(\mu_2\text{-H})Ru_3(CO)_9(\mu_3,\eta^2\text{-SCNHPhNPh})$ (**8**). The major product was a bright red band found in the lower third of the plates. This band was isolated and characterized as the hexanuclear cluster $(\mu_2\text{-H})_6Ru_6(CO)_{14}(\mu_3,\eta^2\text{-SCNHPhNPh})_2$ (**16**).

Spectroscopic data for **16** are summarized in Table 23. The carbonyl region of the IR spectrum is relatively simple, suggesting a somewhat symmetric structure. Typical NH and NCN bands, due to the presence of the diphenylthioureato ligand are apparent. Because cluster **16** is less soluble in chloroform, NMR spectra were carried out in [D_6]acetone. These spectra also indicate an intact diphenylthioureato ligand. In the hydride region of the ^{1}H NMR spectrum, one observes three signals occurring over the range of -12 to -16 ppm, a region indicative of metal-bridging hydrides. Each hydride signal showed a coupling interaction with the other. The coupling interactions of the bridging hydrides, in addition to the relatively wide range of their chemical shifts, suggest a species containing Ru-Ru bonds of significantly different character than those of **15**.

Red, block crystals of **16** were grown from 3:1 acetone:heptane solutions, maintained at -18°C over a period of approximately 1 week. This allowed for the single crystal, X-ray structural characterization of **16**, which showed the crystals as triclinic and of the space group $P\bar{1}$. The unit cell contains one complete molecule of **16** with C_i symmetry. The non-hydrogen atoms and two of the bridging hydrides could be located in difference maps and were refined. The phenyl and the amine hydrogens were placed in calculated positions. A ZORTEP

illustration of this cluster with a schematic of the metal framework is presented in Figure 23. Relevant bond lengths and angles are compiled in Table 24.

Table 23: IR and NMR spectroscopic data for $(\mu_2\text{-H})_6Ru_6(CO)_{14}(\mu_3,\eta^2\text{-SCNHPhNPh})_2$ (**16**).

IR(c-hex, 298K)	$\{\nu_{CO}(cm^{-1})\}$:	2073m	2061vs	2049s
		2010s	1989s,br	
IR(KBr)	$\{\nu_{NH}(cm^{-1})\}$:	3370m		
	$\{\nu_{NCN}(cm^{-1})\}$:	1563m		
^{1}H NMR(C_2D_6O, 298K)[a]	{δ(ppm)}:	8.35 (s, br, 1H, N-*H*)		
		7.66-7.08 (m, 10H, Ph-*H*)		
		-12.48 (m, 1H, Ru_2H)		
		-13.14 (d(d),J=5.86(1.86)Hz,1H,Ru_2H)		
		-16.05(m, 1H, Ru_2H)		

[a] 400 MHz

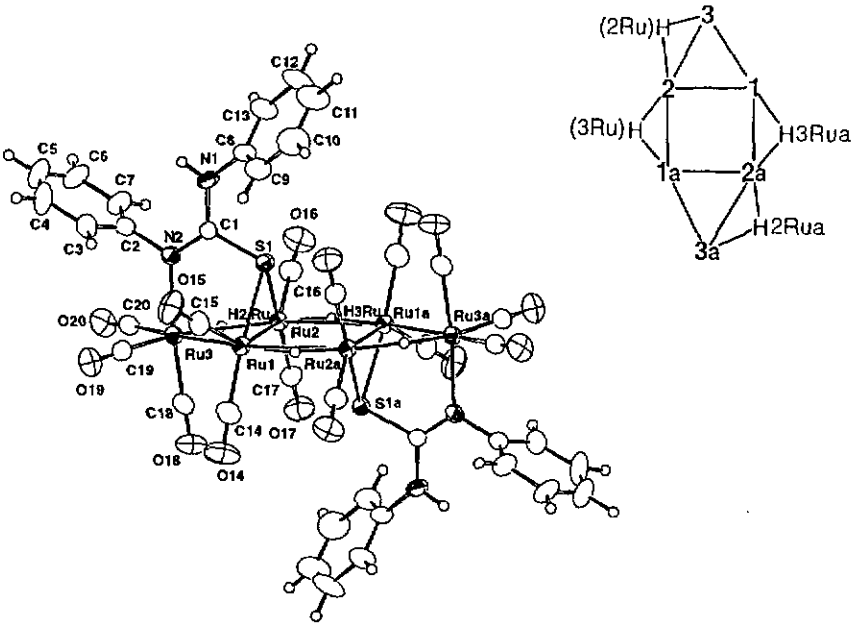

Figure 23: Molecular structure of $(\mu_2\text{-H})_6Ru_6(CO)_{14}(\mu_3,\eta^2\text{-SCNHPhNPh})_2$ (**16**).

Table 24: Important bond lengths (Å) and angles (°) for $(\mu_2\text{-H})_6Ru_6(CO)_{14}(\mu_3,\eta^2\text{-SCNHPhNPh})_2$ (**16**).

Ru(1)-Ru(2)	2.8507(9)	Ru(1)-Ru(2)a	3.2218(9)
Ru(1)-Ru(3)	2.7657(9)	Ru(1)-S(1)	2.4056(20)
Ru(1)-H(3R)	1.83(8)	Ru(2)-Ru(3)	2.9489(9)
Ru(2)-S(1)	2.4165(20)	Ru(2)-H(2R)	1.59(9)
Ru(2)-H(3R)a	1.48(8)	Ru(3)-N(2)	2.145(6)
Ru(3)-N(2R)	1.55(9)	S(1)-C(1)	1.784(8)
N(2)-C(1)	1.299(9)	N(2)-C(2)	1.441(10)
N(1)-C(1)	1.357(9)	N(1)-C(8)	1.422(10)
Ru(1)-Ru(2)-Ru(1)a	86.034(24)	Ru(1)-Ru(2)-Ru(3)	56.934(22)
Ru(1)-Ru(2)-S(1)	53.58(5)	Ru(1)-Ru(3)-Ru(2)	59.744(23)
Ru(1)-Ru(3)-N(2)	87.14(16)	Ru(1)-S(1)-C(1)	104.39(24)
Ru(1)-S(1)-Ru(2)	72.48(6)	Ru(1)a-Ru(2)-Ru(3)	142.97(3)
Ru(1)-N(3R)-Ru(2)a	154(5)	Ru(2)-Ru(1)-Ru(3)	63.322(23)
Ru(1)a-Ru(2)-S(1)	80.27(5)	Ru(2)-H(2R)-Ru(3)	139(6)
Ru(2)-Ru(1)-Ru(2)a	93.97(3)	Ru(2)a-Ru(1)-S(1)	84.96(5)
Ru(2)-Ru(1)-S(1)	53.94(5)	Ru(2)-Ru(3)-N(2)	87.32(17)
Ru(2)-S(1)-C(1)	107.88(24)	Ru(3)-Ru(1)-S(1)	81.57(5)
Ru(2)a-Ru(1)-Ru(3)	157.29(3)	Ru(3)-Ru(2)-S(1)	77.64(5)
Ru(3)-N(2)-C(1)	123.5(5)	Ru(3)-N(2)-C(2)	118.8(4)
S(1)-C(1)-N(2)	120.2(5)	S(1)-C(1)-N(1)	115.3(5)
N(2)-C(1)-N(1)	124.5(7)	C(1)-N(1)-C(8)	126.4(6)
C(1)-N(2)-C(2)	117.6(6)		

Symmetry operator a) 1-x, -y, -z.

Figure 23 shows a basal raft structure for **16** defined by six ruthenium atoms. Here two equivalent triangular ruthenium units related by an inversion center are held together by relatively long metal-metal bonds [Ru1-Ru2a (3.2218(9)Å)]. Unsaturation at Ru1 and Ru2 (and necessarily Ru1a and Ru2a) requires these bonds. These same metal-metal bonds are bridged by hydride ligands (H3R and H3Ra) which lie to the exterior of the metal ring. The six-membered, metal ring is planar to within 0.02(1)Å with H3R and H3Ra in that plane (deviation from the Ru_6 plane = 0.02Å). Bridging hydrides span the Ru2-Ru3 and Ru2a-Ru3a bonds (H2R, H2Ra resp.) located on the periphery of the metal skeleton but also lying in the Ru_6 plane. Presumably these hydrides contribute to the lengthening of the Ru2-Ru3 and Ru2a-Ru3a bonds (2.9489(9)Å) as compared to the same bond of the trinuclear complex **8** (2.77(1)Å) which contains no bridging hydride at this position. The Ru1-Ru3 bond in the triangular substructure is of the same magnitude (Ru1-Ru3, 2.7657(9)Å), as its analogue in complex **8**, while the Ru1-Ru2 bond is longer (Ru1-Ru2, 2.8507(9)); a contributing factor to this lengthening will be discussed. The hexanuclear raft cluster of Cabeza *et al.*[116b] contains slightly longer metal-metal bonds between the two triangular subunits and μ_3- hydrides positioned so as to connect the two trinuclear units. No evidence for a μ_3-type hydride was found for **16**.

Bonded in a centrosymmetric fashion to each triangular end of the complex are μ_3,η^2-diphenylthioureato ligands, one above the metal plane, the other below. The atom N2, terminally bound to Ru3 shows bonds typical for this arrangement (Ru3-N2, 2.14(1)Å) as does the bridging S (avg. Ru-S, 2.41(1)A). Double bond character is retained between C1 and N2 (1.30(1)Å). The coordination sphere of each ruthenium atom is completed with terminal carbonyl ligands. The complex crystallized with four molecules of acetone per unit cell.

As per Figure 23, this structure represents an unsaturated 90 electron cluster. Like the clusters **14** and **15** this cluster can be considered a bi-edge-bridged square for which PSEPT predicts 92 electrons. Although unsaturated hexanuclear clusters are not uncommon[133], ^{1}H NMR spectra for cluster **16** suggested two bridging hydrides in addition to the four located crystallographically. The two spectroscopically identified hydrides (H1R and H1Ra) are believed to bridge the Ru1-Ru2 and Ru1a-Ru2a. The hydride region of ^{1}H NMR spectra for **4** is displayed in Figure 24 and shows three hydride resonances which are assigned as follows: the upfield multiplet at -16.05 ppm is assigned to the hydrides H1R (H1Ra), the doublet of doublets at -13.14 ppm is assigned to H2R (H2Ra) while the multiplet (appearing as a broad singlet) at -12.48 ppm, results from H3R (H3Ra). COSY spectra indicate mutual coupling between all three protons. To clarify the nature of these interactions, decoupling experiments were carried out. Most significantly, decoupling at the -12.48 ppm signal (H3R, H3Ra) results in doublets for the two remaining hydride signals at -13.14 and -16.05 ppm, each doublet displaying the same coupling constant of 5.86 Hz. The fine splitting generating the doublet at -13.14 ppm with the smaller coupling constant (J=1.66Hz) must therefore result from coupling to protons H3R (H3Ra), while the larger J value of 5.86 Hz is from coupling to H1R (H1Ra). The larger coupling constant produced by the H1R protons as well as the upfield shift in their signal, suggests a different chemical environment compared to that of the H2R and H3R protons. Given the postulated positions of the H1R protons, that is in the interior of the ruthenium framework where anisotropy due to the surrounding metal atoms would be large, these effects might be expected. The location of these hydrides is further implied by the elongation of the metal-metal bonds in question (Ru1-Ru2; 2.92(1)Å).[125b] The addition of these two hydride ligands to the structure results in a total of 92 electrons as predicted for this type of cluster.

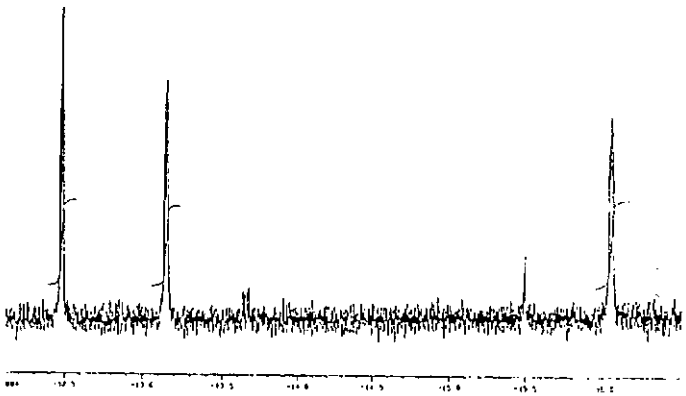

Figure 24: ^{1}H NMR ($CDCl_3$ at 400 MHz) of the hydride region of compound **16**; H3R at -12.48, H2R at -13.14 and, H1R at -16.05.

Since the known cluster $(\mu_2\text{-H})_2Ru_3(CO)_9(\mu_3\text{-S})$[134] is also formed in this reaction, it can be assumed that upon hydrogenation the hexanuclear framework of **15** breaks down to $(\mu_2\text{-H})_2Ru_3(CO)_9(\mu_3\text{-S})$ and an unsaturated 46-electron trinuclear fragment which dimerizes to give **16**. Such oligomerizations to relieve unsaturation have been observed previously.[135] Alternatively, the intermediate trinuclear species may pick up CO with subsequent H_2 elimination to form **8**, also found in the reaction mixture. That formation of **16** in reactions of the trinuclear cluster **8** with molecular hydrogen does not occur, implies a carbon-monoxide deficient intermediate not accessible from **8**.

3.11 Conclusions Concerning the Hexanuclear Clusters 14-16.

The isolation and characterization of the three hexanuclear clusters, **14-16** provides a short series of structural variations for the six-membered rhombic raft geometry. The changes in the metal skeleton configuration reflect the structural flexibility inherant in metal clusters of medium nuclearity and their tendency to adopt an arrangement which most appropriately accommodates the multi-site bonded ligands present while at the same time satisfying the

effective atomic number rule for each of the metal atoms. For cluster **14**, the two ligands are bonded to the same side of the rhombic raft cluster but their steric demands require the triangular edges of the metal framework to bend up, thus allowing them a larger volume. The geometry of the sofa-like cluster **15**, possessing only one sterically demanding ligand, is determined primarily by its electronic requirements. This geometry allows five of the Ru atoms to bond to the naked sulfur, subsequently fulfilling the valence requirements of the cluster. The planar cluster **16**, adopts a configuration which allows electronic saturation as well as the presence of two sterically demanding ligands.

3.12 Thermolysis of $(\mu_2\text{-H})Ru_3(CO)_9(\mu_3,\eta^2\text{-SCNHMeNMe})$

With the isolation of the two hexanuclear clusters **14** and **15** from thermolysis reactions of **8** and the isolation of a boat-like cluster from thermolysis reactions of the ethyl analogue of **8**[118d], the question of similar clusters, available from thermolysis reactions of the methyl analogue of 8, $(\mu_2\text{-H})Ru_3(CO)_9(\mu_3,\eta^2\text{-SCNHMeNMe})$ arises. If a THF solution of $(\mu_2\text{-H})Ru_3(CO)_9(\mu_3,\eta^2\text{-SCNHMeNMe})$ is heated at 130°C in a pressure Schlenk tube, and the resulting reaction mixture chromatographed on TLC plates, a small amount of a green compound elutes. However, this compound was extremely unstable and nearly impossible to characterize. The major component of the reaction mixture is a compound present as an orange band, midway up the plates. This band was isolated and characterized spectroscopically and by a single-crystal X-ray analysis as the tetranuclear cluster $Ru_4(CO)_7(\mu_2\text{-CO})_3(\mu_4\text{-S})_2C(NHMe)_2$ (**17**). Spectral data are given in Table 25.

Table 25: Spectroscopic data for $Ru_4(CO)_7(\mu_2\text{-CO})_3(\mu_4\text{-S})_2C(NHMe)_2$ (**17**).

IR(c-hex, 298K)	$\{\nu_{CO}(cm^{-1})\}$:	2074m	2046s	2035s
		2008vs	1997vs	1972s
		1952m	1877w	1850m
		1830w		
IR(KBr)	$\{\nu_{NH}(cm^{-1})\}$:	3427m	3401m	
	$\{\nu_{NCN}(cm^{-1})\}$:	1566m	1506m	
^{1}H NMR (C_2D_6O, 298K)[a]:	$\{\delta(ppm)\}$	6.01 (s,br,1H, N-*H*)		
		4.87 (s,br,1H, N-*H*)		
		3.53 (s, J=4.47Hz, 3H, CH_3-*H*)		
		2.75 (d, J=4.48Hz, 3H, CH_3-*H*)		

[a] 200 MHz

The presence of two peaks in the IR region corresponding to bridging carbonyl groups demands the presence of at least two of these ligands, each distinct from the other. A minimum of two μ_2-CO groups, coupled with the large number of terminal CO bands would also necessitate an augmentation of cluster nuclearity. The ^{1}H NMR spectrum coupled with the relevant IR vibrations of the dimethythiourea ligand, reveals the nature of the reaction. Two separate NH signals and two separate CH_3 signals in ^{1}H NMR spectra imply a dialkyldiaminocarbene fragment, but in contrast to the dialkyldiaminocarbene fragment of **14**, neither N atom is metal bound. Nevertheless, the spectra do not indicate whether there are two of these fragments bound in a nonsymmetric fashion to two metal centers, or if there is only one dialkyldiaminocarbene fragment bound in a way which prohibits free rotation.

The extent of substitution was resolved through X-ray structural analysis. Preliminary scans identified the orange, block crystals of **17** as triclinic, belonging to the space group $P\bar{1}$; Z = 2. All non-hydrogen atoms were located in difference maps and refined. The hydrogen atoms were placed in calculated positions. The molecular structure of **17** is given in Figure 25. Selected bond lengths and angles are found in Table 26.

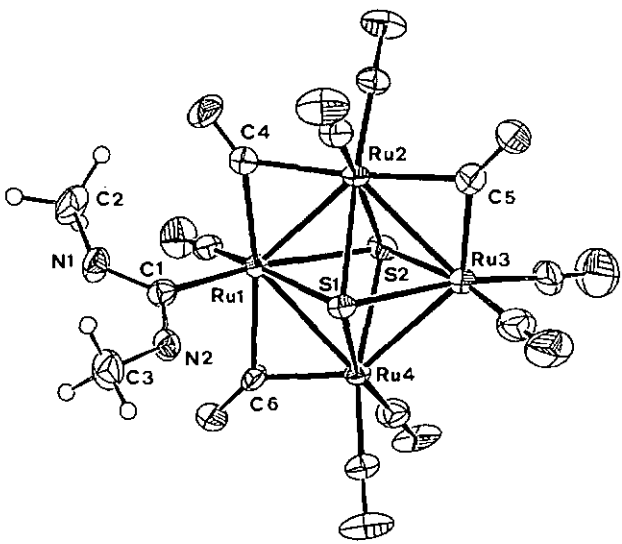

Figure 25: Molecular structure of $Ru_4(CO)_7(\mu_2\text{-}CO)_3(\mu_4\text{-}S)_2C(NHMe)_2$ (**17**).

Table 26: Selected bond lengths and angles for $Ru_4(CO)_7(\mu_2\text{-}CO)_3(\mu_4\text{-}S)_2C(NHMe)_2$ (**17**).

Ru(1)-Ru(2)	2.7530(8)	Ru(1)-Ru(4)	2.7448(7)
Ru(1)-S(1)	2.5877(14)	Ru(1)-S(2)	2.5526(13)
Ru(1)-C(1)	2.064(5)	Ru(1)-C(4)	2.032(5)
Ru(1)-C(6)	2.186(5)	Ru(2)-Ru(3)	2.7480(7)
Ru(2)-S(1)	2.4994(13)	Ru(2)-S(2)	2.4886(12)
Ru(2)-C(4)	2.168(5)	Ru(2)-C(5)	2.181(5)
Ru(3)-Ru(4)	2.8266(8)	Ru(3)-S(1)	2.4598(13)
Ru(3)-S(2)	2.4512(14)	Ru(3)-C(5)	1.980(6)
Ru(4)-S(1)	2.4522(12)	Ru(4)-S(2)	2.4565(13)
Ru(4)-C(6)	2.009(5)	C(4)-O(4)	1.149(7)
C(5)-O(5)	1.177(7)	C(6)-O(6)	1.157(6)
N(1)-C(1)	1.342(7)	N(1)-C(2)	1.462(7)
N(2)-C(1)	1.325(6)	N(2)-C(3)	1.472(7)
Ru(1)-Ru(2)-Ru(3)	92.235(21)	Ru(1)-S(1)-Ru(2)	65.50(3)
Ru(1)-Ru(4)-Ru(3)	90.727(21)	Ru(1)-S(1)-Ru(4)	65.93(3)
Ru(1)-S(1)-Ru(3)	103.51(5)	Ru(1)-S(2)-Ru(3)	104.80(5)
Ru(1)-S(2)-Ru(2)	66.19(3)	Ru(1)-C(1)-N(1)	116.1(3)
Ru(1)-S(2)-Ru(4)	66.42(3)	Ru(1)-C(4)-Ru(2)	81.84(19)
Ru(1)-C(1)-N(2)	129.5(4)	Ru(2)-Ru(1)-Ru(4)	89.295(21)
Ru(1)-C(6)-Ru(4)	81.62(17)	Ru(2)-S(1)-Ru(3)	67.29(4)
Ru(2)-Ru(3)-Ru(4)	87.736(21)	Ru(2)-S(2)-Ru(3)	67.59(4)
Ru(2)-S(1)-Ru(4)	102.57(5)	Ru(2)-C(5)-Ru(3)	82.50(20)
Ru(2)-S(2)-Ru(4)	102.76(5)	Ru(3)-S(2)-Ru(4)	70.33(4)
Ru(3)-S(1)-Ru(4)	70.26(4)	S(1)-Ru(1)-C(1)	95.85(14)
S(1)-Ru(1)-S(2)	73.76(4)	S(1)-Ru(3)-S(2)	77.83(4)
S(1)-Ru(2)-S(2)	76.41(4)	C(1)-N(1)-C(2)	125.6(4)
S(1)-Ru(4)-S(2)	77.88(4)	N(1)-C(1)-N(2)	114.4(4)
C(1)-N(2)-C(3)	129.0(5)		

A tetranuclear Ru base consisting entirely of Ru-Ru single bonds, capped on each side by a μ_4-S makes up the cluster skeleton of **17**. The four Ru atoms and the two S atoms are arranged in a pseudo-octahedral geometry. The square base comprised of Ru1-Ru4, is relatively planar, with Ru3 showing the largest distance to the calculated plane (0.0089(6)Å). The two S atoms, S1 and S2, are 1.552(1)Å and 1.553(1)Å above and below the Ru_4 plane. Three of the Ru-Ru edges are bridged by μ_2-CO groups. For all practical purposes, the bridging CO groups lie within the metal plane (C6 lies furthest from the plane at 0.064(5)Å). Bonded to one of the Ru atoms (Ru1), located between two of the bridging carbonyls, is a dimethyldiaminocarbene (dmac) ligand. The dmac ligand lies 1.503(5)Å above the Ru_4 plane. Cluster **17** has no symmetry elements and thus belongs to the C_1 symmetry group.

The structure of an entirely analogous cluster containing a diisopropyldiaminocarbene ligand has been published. In comparing the two structures very few differences in bond lengths and angles are observed at the metal framework. In fact, there are no metal-metal

bond lengths differing by more than 0.005 Å among the two structures. With the exception of bonds to Ru1, similar lengths are also observed among the Ru-S bonds of **17**. At Ru1, the Ru-S bonds differ among themselves to a larger degree (Ru1-S1, 2.5877(14)Å and Ru1-S2 2.5526(13)Å in **17**) but overall are longer than those of the isopropyl derivative. Continuing towards the dmac ligand, the differences between the methyl and isopropyl derivatives become more pronounced. The distance between the carbene carbon (C1) and Ru1 is significantly shorter in **17** (Ru1-C1, 2.064(5)Å in **17** vs. 2.099(3)Å in the diisopropyl derivative). Both the C1-N1 and C1-N2 bonds are longer in the dmac derivative **17** (1.342(7)Å and 1.462(7)Å respectively). There is a difference of *ca.* 0.12 Å between these two bond lengths. The same bonds in the isopropyl derivative are of approximately the same magnitude. The bond angles around C1 also spread out more in **17** (**17**: Ru1-C1-N1, 116.1(3)°, Ru1-C1-N2, 129.5(4)°). These differences suggest a shifting of double bond character from the C-N bonds to the Ru-C bonds, providing for greater electron donation by the carbene carbon atom. This results in weaker Ru-S bonds.

Several other tetranuclear Ru clusters containing $[C(NR_2)_2]$ ligands have been isolated and structurally characterized. Specifically $Ru_4(\mu_2\text{-}CO)_2(CO)_{9-n}(\mu_4\text{-}S)_2\{C(NMe_2)\}_n$ (n = 1,2) and $Ru_4(\mu_2\text{-}CO)_3(CO)_{8-n}(\mu_4\text{-}S)_2\{C(NHR)\}_n$ (*n* = 1,2) (R = Et, i-Pr)[89b] result from thermal reactions of tetramethylthiourea with $Ru_3(CO)_{12}$ and room temperature reactions of diethyl- and diisopropylthiourea with $Ru_3(CO)_{12}$ respectively. To generate these clusters, a C-S bond cleavage of the thiourea compounds must occur to generate both the sulfido ligand and the $[C(NR_2)_2]$ fragment. Whether these bond breaking processes precede or succeed the formation of a Ru_4 framework has not been addressed.

Because **17** results from thermolysis of the trinuclear species $\{(\mu_2\text{-}H)Ru_3(CO)_9(\mu_3,\eta^2\text{-}SCNHMeNMe)\}$, the mechanism of formation most likely involves opening of the Ru-N bond followed by C-S bond cleavage to generate an unsaturated sulfido cluster and a [C(NHMe)(NMe)] fragment, similar to what occurs in the formation of **14** and **15**. However, for the methyl derivative subsequent reaction does not favor direct condensation with a second molecule of the trinuclear species to give hexanuclear products. Adams *et al.* were able to generate tetranuclear clusters from reactions of trinuclear sulfido clusters with $Ru(CO)_5$ followed by substitution of a CO group to yield $Ru_4(\mu_2\text{-}CO)_2(CO)_7\{C(NMe_2)Ph\}(\mu_4\text{-}S)$.[136] These results suggest a reaction route involving an intermediate trinuclear fragment and an

ambient [$Ru(CO)_4$] species to yield a tetranuclear species which then undergoes substitution of a CO group with the previously generated [C(NHMe)(NMe)] fragment. Obviously, the nature of the R substituents on the thiourea influence significantly the final outcome of thermolysis reactions of the trinuclear species $(\mu_2\text{-H})Ru_3(CO)_9(\mu_3,\eta^2\text{-SCNHRNR})$.

3.13 Reactions of $(\mu_2\ H)Ru_6(CO)_{16}(\mu_5\text{-S})(\mu_3,\eta^2\text{-SCNHPhNPh})$ (15); Reactivity at the μ_5-Sulfur.

In light of the unusual coordination mode of the μ_5-S in cluster **15**, an investigation into the reactivity of this structural feature was undertaken. Previous results have shown the versatile nature of the sulfur ligand often allows for the construction of higher nuclearity or mixed-metal clusters. Adams *et al.*[128c] were able to add $W(CO)_4(PMe_2Ph)$ and $W(CO)_5$ (generated photochemically), to the quadruply bridging sulfido ligand of some Ru clusters to produce herteronuclear metal complexes with penta-coordinate sulfur atoms. Another series of reactions resulted in addition of $Ru(CO)_4$ fragments to the μ_3-S of a trinuclear Ru cluster to produce a μ_4-S and augment the cluster nuclearity by one unit.[137] An interesting question was whether the μ_5-S of **15** would coordinate another Lewis acid-type atom in a sixth coordination site, or if an existing Ru-S bond would open to allow cluster build-up.

Initial attempts involved reactions of **15** with $W(CO)_6$ under UV irradiation. The relevant amount of $W(CO)_6$ was dissolved in THF and the reactive species, $W(CO)_5$ generated photochemically. The presence of $W(CO)_5$ was indicated by a color change of the solution and verified by the appearance of two CO bands is IR solution spectra as opposed to one. One equivalent of **15**, dissolved in the same solvent, was then added. The THF solvent was removed and the residue redissolved in CH_2Cl_2 and allowed to stir at room temperature for 12h. From this solution, the starting material could be recovered almost quantitatively.

Pursuing a more reactive species, the addition of a $Ru(CO)_4$ fragment was attempted. $Ru(CO)_5$ is easily generated from $Ru_3(CO)_{12}$ by photolytic cleavage in the presence of excess CO (following the route of Bor[138]). Immediately, upon adding **15** to a solution containing the $Ru(CO)_5$, the solution color went from red to deep blue. This same result was obtained if instead of $Ru(CO)_5$, $Fe_2(CO)_9$ or $Co_2(CO)_8$ was used, however, with those reagents the formation of the blue species occurred over a longer period of time. As will be shown later,

this was the result of the reaction of **15** with CO, a process which occurs in the presence of even a slight excess of CO. Given the difficulty of producing $Ru(CO)_5$ without CO as well as the liklihood of generating CO in reactions of $Fe_2(CO)_9$ or $Co_2(CO)_8$, this approach was not pursued.

In further attempts to induce reaction at the μ_5-S, the adduct $Me_2S{\cdot}BH_3$ was employed. Stirring solutions of **15** for an extended period of time in the presence of $Me_2S{\cdot}BH_3$, yielded several products, all of which could be isolated using prepratory TLC. Those present in significant quantity were, in reverse order of elution on the plates, $\{(\mu_2\text{-}H)_2Ru_3(CO)_8(\mu_3\text{-}S)\}_3$ (**18**), $(\mu_2\text{-}H)Ru_6(CO)_{15}(Me_2S)(\mu_3,\eta^2\text{-}SCNHPhNPh)$ (**19**), $(\mu_2\text{-}H)Ru_3(CO)_9(\mu_3,\eta^2\text{-}SC{<}\ {>}NHPhNPh)$[89a] (**8**), and $(\mu_2\text{-}H)_2Ru_3(CO)_9(\mu_3\text{-}S)$[134]. The first two products were present as yellow and deep red bands respectively. The spectroscopic data for these two products, **18** and **19**, are summarized in Table 27. Yellow, block crystals of **18** could be isolated from CH_2Cl_2/pentane solution, maintained at -18°C for approximately 5days.

Table 27: IR and NMR data for $\{(\mu_2\text{-}H)_2Ru_3(CO)_8(\mu_3\text{-}S)\}_3$ (**18**) and $(\mu_2\text{-}H)\text{-}Ru_6(CO)_{15}(Me_2S)(\mu_3,\eta^2\text{-}SCNHPhNPh)$ (**19**)

IR (c-hex, 298K)	$\{\nu_{CO}(cm^{-1})$	**18**:	2085m	2050vs	2009s
			2003s-m		
		19:	2085m	2058vs	2043s
			2026vs	2013w	2002m
			1988m	1981w	1956m
			1930w		
IR (KBr)	$\{\nu_{NH}(cm^{-1})\}$		3355m		
	$\{\nu_{NCN}(cm^{-1})\}$		1565m		
^{1}H NMR ($CDCl_3$, 298K)[a]	{δ(ppm)}	**18**:	-18.15(s,3H,Ru_2-*H*)		
			-18.98(s,3H,Ru_2-*H*)		
		19:	7.10-7.70(m,10H,Ph-*H*)		
			6.85(s,br,1H,N-*H*)		
			2.06(s,6H,CH_2-*H*)		

[a] 200 MHz

Based on the IR data collected for **18**, this product had not been previously characterized. Initial ^{1}H NMR data for **18** were of limited value, given the presence of impurities which produced a series of peaks in the phenyl region, implying the presence of the diphenylthioureato ligand. Therefore an x-ray structural analysis was carried out, yielding the

molecular structure illustrated in Figure 26. A summary of bond lengths and angles are provided in Table 28. Crystals of **18** are triclinic and belong to the space group $P\bar{1}$.

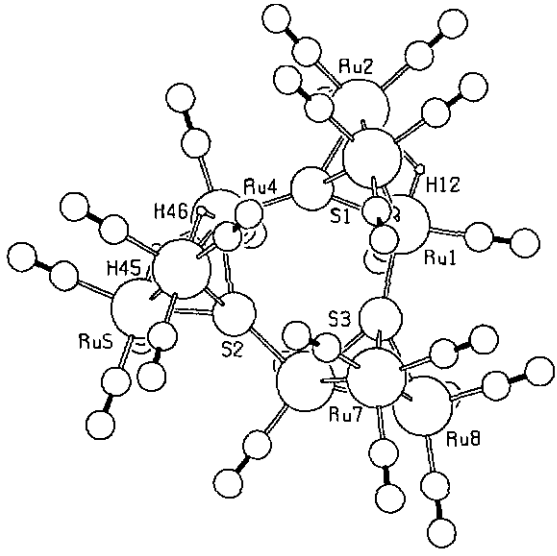

Figure 26: Pluto plot of the molecular structure of $\{(\mu_2\text{-H})_2Ru_3(CO)_8(\mu_4\text{-S})\}_3$ (**18**).

Table 28: Selected bond distances (Å) and angles (°) for $\{(\mu_2\text{-H})_2Ru_3(CO)_8(\mu_4\text{-S})\}_3$ (**18**).

Ru(1)-Ru(2)	2.8747(13)	Ru(1)-Ru(3)	2.9075(14)
Ru(1)-S(1)	2.350(3)	Ru(1)-S(3)	2.401(3)
Ru(2)-Ru(3)	2.7492(15)	Ru(2)-S(1)	2.326(3)
Ru(2)-H(12)	2.0150(10)	Ru(3)-S(1)	2.350(3)
Ru(3)-H(31)	1.4727(9)	Ru(4)-Ru(5)	2.8561(14)
Ru(4)-Ru(6)	2.8980(15)	Ru(4)-S(1)	2.389(3)
Ru(4)-S(2)	2.359(3)	Ru(4)-H(45)	1.7331(10)
Ru(4)-H(46)	1.9054(9)	Ru(5)-Ru(6)	2.7555(15)
Ru(5)-S(2)	2.339(3)	Ru(5)-H(45)	1.5130(10)
Ru(6)-S(2)	2.363(3)	Ru(6)-H(46)	1.5761(10)
Ru(7)-Ru(8)	2.8635(14)	Ru(7)-Ru(9)	2.9050(15)
Ru(7)-S(2)	2.410(3)	Ru(8)-Ru(9)	2.7440(14)
Ru(7)-S(3)	2.363(3)	Ru(9)-S(3)	2.366(3)
Ru(8)-S(3)	2.327(3)		

Table 28: cont.

Ru(1)-Ru(2)-Ru(3)	62.21(3)	Ru(4)-Ru(5)-Ru(6)	62.16(4)
Ru(7)-Ru(8)-Ru(9)	62.36(4)	Ru(1)-S(1)-Ru(2)	75.87(9)
Ru(1)-S(1)-Ru(4)	131.53(12)	Ru(2)-S(1)-Ru(4)	128.44(12)
Ru(3)-S(1)-Ru(4)	145.19(12)	Ru(4)-S(2)-Ru(5)	74.88(8)
Ru(4)-S(2)-Ru(6)	75.71(8)	Ru(4)-S(2)-Ru(7)	129.75(12)
Ru(5)-S(2)-Ru(6)	71.75(8)	Ru(5)-S(2)-Ru(7)	131.10(12)
Ru(6)-S(2)-Ru(7)	145.87(13)	Ru(1)-S(3)-Ru(7)	132.05(12)
Ru(1)-S(3)-Ru(8)	130.44(12)	Ru(1)-S(3)-Ru(9)	144.22(13)
Ru(7)-S(3)-Ru(8)	75.25(9)	Ru(7)-S(3)-Ru(9)	75.79(9)
Ru(8)-S(3)-Ru(9)	71.55(8)	Ru(1)-H(12)-Ru(2)	113.88(4)
Ru(1)-H(31)-Ru(3)	122.72(5)	Ru(4)-H(45)-Ru(5)	123.11(4)
Ru(4)-H(46)-Ru(6)	112.35(5)		

This same ruthenium cluster was isolated and structurally characterized by Adams *et al.*.[135b] These authors determined the same space group for their sample and bond lengths and angles for the two determinations are consistent. However, the IR data reported are significantly different between the two samples. Furthermore, the synthesis described by Adams involves the thermolysis or photolysis of $(\mu_2\text{-H})_2Ru_3(CO)_9(\mu_3\text{-S})$, producing **18** in yields of roughly the same magnitude as reported here (25-27%).

The cluster **18** is described as a cyclic trimer of $(\mu_2\text{-H})_2Ru_3(CO)_9(\mu_3\text{-S})$.[134] As shown in Figure 26, one of the principal structural features is a six-membered ring composed of alternating Ru-S linkages. Each Ru atom of the six-membered ring is further bonded to two additional Ru atoms which comprise trinuclear fragments. Four edge-bridging hydride ligands could be located along the edges of the ring to non-ring metal atoms (Ru1-Ru2, Ru1-Ru3, Ru4-Ru5, Ru4-Ru6). The Adams structure includes two additional edge-bridging hydrides, located and refined along the Ru7-Ru8 and Ru7-Ru9 edges. Peaks consistent with the presence of these additional hydrides were found in ^{1}H NMR spectra of **18**. The trinuclear fragments are capped with sulphido ligands acting locally as three-electron donors. These S atoms donate an additional electron in bonds to the Ru atoms of adjacent trinuclear fragments resulting in the central six-membered ring and acting overall as four-electron donors. Altogether, cluster **18** has C_3 symmetry.

Consistent with the results found by Adams, longer M-M bonds occur along the hydride bridged edges. Likewise, the M-S bond lengths linking the trinuclear units are longer than those found within the monomeric units.

The mechanism for the formation of **18**, as for the formation of **16**, involves oligomerization undertaken to relieve unsaturation. Although speculative, the following mechanism is suggested. The BH_3 serves as a hydrogen source, causing cluster fragmentation and producing the known compound $(\mu_2\text{-H})_2Ru_3(CO)_9(\mu_3\text{-S})$ [134] and the unsaturated fragment "$HRu_3(CO)_7(\mu_3,\eta^2\text{-SCNHPhNPh})$". The unsaturated fragment may then take up CO, either from the reaction solution or by abstraction from a neighboring $(\mu_2\text{-H})_2Ru_3(CO)_9(\mu_3\text{-S})$. This accounts for the presence of **8** in the final solution and would provide a reactive "$(\mu_2\text{-H})_2Ru_3(CO)_8(\mu_3\text{-S})$" fragment, which could then undergo oligomerization to produce **18**. Adams *et al.* also proposed an intermediate "$(\mu_2\text{-H})_2Ru_3(CO)_8(\mu_3\text{-S})$" but sampling of the reaction solution at various intervals via ^1H NMR, showed no evidence for its existence. However, Adams pointed out that **18** could be converted quantitatively back to $(\mu_2\text{-H})_2Ru_3(CO)_9(\mu_3\text{-S})$ by exposure to CO.

No suitable crystals of the second new product of this reaction, **19**, could be obtained. The characterization of this product is based on spectral and analytical data. IR spectra in the carbonyl region contain a large number of bands, implying either a product of low symmetry or a number of isomers. Single NH and NCN vibrations are observed in KBr spectra of **19** and these are only slightly shifted from the corresponding bands of **15**. The amine proton is well-defined in the ^1H NMR spectrum and integrates precisely with the phenyl protons. These data indicate an intact diphenylthioureato ligand. The presence of a single Me_2S group is based on the single peak in the ^1H NMR spectrum and corroborated by the analytical data (see experimental section). Even though a variety of solvents and spectral parameters were used, the hydride peak could not be positively identified. This compound could also be obtained in a higher yield from reactions of **15** with an excess of Me_2S.

The proposed structure of **19** is presented graphically in Figure 27. Based on the results obtained from substitution reactions of the trinuclear cluster **8**, few conclusions can be drawn from NH or NCN shifts in IR spectra. For steric reasons, substitution at a site relatively well-removed from the diphenylthiourea ligand would be expected. Presumably this would involve an axial site on either of the apical Ru atoms. The placement of the Me_2S group on the N-bound Ru atom will be discussed in conjunction with PPh_3, $P(OR)_3$ and ^{t}BuNC substituted derivatives, characterized definitively by X-ray structural analysis.

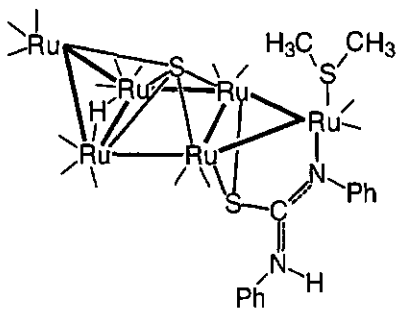

Figure 27: Graphical representation of $(\mu_2\text{-H})Ru_6(CO)_{15}(Me_2S)(\mu_3,\eta^2\text{-SCNHPhNPh})$ (**19**)

3.14 Reactions of $(\mu_2\text{-H})Ru_6(CO)_{16}(\mu_5\text{-S})(\mu_3,\eta^2\text{-SCNHPhNPh})$ (15); Reactions at the Metal Core.

3.14.1 $(\mu_2$ H)$Ru_6(CO)_{16}(\mu_5\text{-S})(\mu_3,\eta^2\text{-SCNHPhNPh})$ (15) in the Presence of CO.

Facile addition of CO to **15**, was first observed in attempts to place a metal carbonyl fragment on the naked sulfur, where even small quantities of CO resulted in reaction. In reproducing this reaction, it was found that bubbling CO through a RT solution of **15** (i.e. acetone, CH_2Cl_2 or c-hexane) for *ca.* 30 minutes, produced a deep blue solution. IR spectra indicated the presence of only a single species (**20**). If left under an N_2 atmosphere, the blue solution converted back to its original red color and IR spectra indicated the only species present was **15**. However, if a CO atmosphere was maintained and the solution cooled to -30°C a crystalline solid precipitated. While preparative TLC (with precautions taken to maintain the highest possible ambient concentration of CO) could be used to purify **20**, a great deal of product was lost in conversion back to **15** if this route was pursued, thus precipitation offered the most practical means of isolation. Once in solid form, **20** proved relatively stable. Spectroscopic data for the blue solid thus isolated (**20**), are presented in Table 29.

Table 29: Spectroscopic data for compound **20**.

IR (c-hex, 298K)	{$\nu_{CO}(cm^{-1})$}:	2102m	2070vs	2045vs
		2032s	2009m	1993w
		1973w,br	1865w,br	
IR (KBr)	{$\nu_{NH}(cm^{-1})$}:	3347m		
	{$\nu_{NH}(cm^{-1})$}:	1557m		
^{1}H NMR ($CDCl_3$)[a]	{δ(ppm)}	7.70-7.00 (m,10H,Ph-*H*)		
		6.58 (s,br,1H,N-*H*)		
		-20.97 (s,1H,Ru_2-*H*)		
Mass spectrum (NBA)[b]	M^+	M^+=1316		

[a] 200 Mhz
[b] FAB

A ν_{CO} band in the bridging carbonyl region is the most obvious feature in spectra of **20**. That aside, analogies to the carbonyl region in spectra of **15** can be drawn. With one exception, the same number of major peaks is present in IR spectra of **20**, and these show similar intensity variations to those of **15**. The diphenylthioureato ligand shows its characteristic peaks in KBr-IR and ^{1}H NMR spectra. A peak signifying a slightly less shielded μ_2-H also appears in the ^{1}H NMR spectrum. As previously stated, mass spectra of multi-nuclear Ru compounds are somewhat complicated, but are useful in indicating cluster nuclearity. The fragmentation pattern often provides clues to molecular structure. Mass spectra of **20** indicate a hexanuclear metal cluster with an M^+ peak at 1316 mass units. The fragmentation pattern indicates several structural features in common with **15**. Coincidence with the MW of **15** may be the result of initial loss of the first carbonyl group to give the M^{+2} peak, a phenomenon often observed in mass spectra of carbonyl cluster compounds.[139] Based on these data, a tentative structure for **20** involving an opened Ru-Ru bond (Ru1-Ru2 in **15**) opposite to a μ_2-CO bridged Ru-Ru bond, is proposed (see Figure 28).

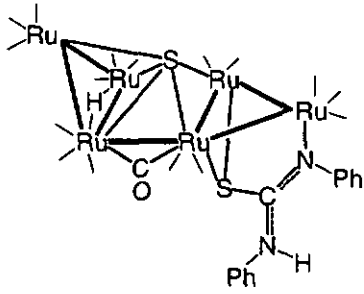

Figure 28: Graphical representation of compound **20**; "(μ_2-H)Ru_6 (μ_2-CO)$(CO)_{16}$(μ_5-S) (μ_3,η^2-SCNHPhNPh)".

The only formal difference in the proposed structure of **20** and that of **15**, is the presence of an extra carbonyl ligand. This additional CO takes a bridging position between atoms Ru3 and Ru4 in the corresponding structure of **15**. In Figure 28, the Ru1-Ru2 vector is no longer represented as a bond. In order to satisfy the effective atomic number rule for the six Ru atoms in a cluster with 7 metal-metal bonds, like that proposed for **20**, a total of 94 electrons would be required. The total number of electrons, donated by the ligands of **20** is 94, and the cluster can be considered electronically saturated.

The following alterations at the Ru skeleton, upon formation of **20** could be expected. In addition to a larger separation between Ru1 and Ru2, one might expect the distance between Ru3-Ru4 to shorten. Vahrenkamp *et col.* have reported reversible M-M bond cleavage with addition of 2-electron donor ligands to $FeCo_2$ clusters with μ_3-capping phosphine ligands.[140] Their report included addition of CO to the trinuclear cluster $(\mu_3\text{-PMe})FeCo_2(CO)_7(PMe)_2$ with concurrent bond opening, entirely analogous to that postulated for **20**. Addition of CO to trinuclear clusters (M = Ru, Os) containing multiply bridging ligands with simultaneous M-M bond formation has also been observed.[141] The numerous examples of M-M edge opening processes have led to the proposal of a "breathing mode" for clusters.[142] The ability of clusters to behave like breathing objects is based on the presence of a non-fluxional bridging ligand producing distortions of the metal atom polyhedron, and thus facilitating the occurrence of reversible M-M edge opening processes under mild conditions. Cluster **15** presents a likely candidate for such behavior. The μ_5-S is a non-fluxional ligand, and the long M-M bonds between the two trinuclear substructures provide a likely site for an edge-opening process.

The reversible nature of the CO addition and implied framework deformation in **20**, has some interesting aspects. The Ru1-Ru2 vector of the original cluster **15**, is quite long, however the electronic requirements of the cluster necessitate a bonding interaction at this position. The addition of CO across the opposite Ru-Ru bond with opening of the Ru1-Ru2 bond, offers an alternative to this weak interaction. Nevertheless the energy difference between these two options cannot be too large, resulting in the ease with which the two species interconvert.

Although crystalline solids precipitated from several different solvent systems, none produced X-ray quality crystals. An X-ray structural determination would provide definitive proof of a framework distortion. In pursuing a derivative of **15** which would exhibit the same reversible CO binding, but produce X-ray quality crystals of the final product, results were obtained which lend support to the structure proposed for **20**.

3.14.2 Reaction of $(\mu_2\text{-H})Ru_6(CO)_{16}(\mu_5\text{-S})(\mu_3,\eta^2\text{-SCNHPhNPh})$ (15) with Triphenylphosphine.

Reaction of **15** with 1 or 2 equivalents of PPh_3 over a period of 12h, at RT in a non-polar solvent (i.e. CH_2Cl_2 or c-hexane) gave three different products. Preparative TLC separated these compounds, in order of elution, as a bright red band, a yellow band and a brick-red band. The bright red band was identified by its IR spectrum, as the previously isolated compound $Ru_3(CO)_6(PPh_3)(\mu_2,\eta^2\text{-}C_6H_5)(\mu_2\text{-}PPh_2)(\mu_3\text{-S})$ (**12**), available from thermal reactions of the trinuclear cluster 8 with PPh_3 or direct thermolysis of the disubtituted derivative $(\mu_2\text{-H})Ru_3(CO)_7(PPh_3)_2(\mu_3,\eta^2\text{-SCNHPhNPh})$ (**11**). The IR and NMR data distinguished the yellow band as the dinuclear Ru complex $Ru_2(CO)_4(PPh_3)_2(\mu_3,\eta^2\text{-SCNHPhNPh})$ (**21**). Spectral data indicated the brick-red compound to be the monosubstituted PPh_3 derivative of **15**, $(\mu_2\text{ H})Ru_6(CO)_{15}(PPh_3)(\mu_5\text{-S})(\mu_3,\eta^2\text{-SCNHPhNPh})$ (**22**). The IR and NMR data for **21** and **22** are summarized in Table 30.

Table 30: IR and NMR data for $Ru_2(CO)_4(\mu_2,\eta^2\text{-SCNHPhNPh})(PPh_3)_2$ (**21**) and $(\mu_2\text{-H})Ru_6(CO)_{15}(PPh_3)(\mu_5\text{-S})(\mu_3,\eta^2\text{-SCNHPhNPh})$ (**22**).

IR (c-hex, 298K)	{ν_{CO} (cm^{-1})}	**21**:	2019vs	1987m	1956s
		22:	2061vs	2040s	2004s
			1989w,br	1943m,hr	
IR (KBr)	{ν_{NH}(cm^{-1})}	**22**:	3333m		
	{ν_{NCN}(cm^{-1})}	**21**:	1624m	1588m	
		22:	1564m		
^{1}H NMR ($CDCl_3$)[a]	{δ(ppm)}	**21**:	7.48-6.85(m,25H,Ph-*H*)		
			5.72(s,br,1H,N-*H*)		
		22:	7.60-7.07(m,25H,Ph-*H*)		
			6.74(s,br,1H, N-*H*)		
			-17.50(s,br,1H,Ru_2-*H*)		
^{31}P NMR($CDCl_3$)[b]	{δ(ppm)}	**21**:	24.47(s)		
		22:	34.48(s)		

[a] 400 MHz, [b] 80.96 MHz.

Symmetrically substituted dinuclear Ru complexes have been isolated and characterized previously.[143] The carbonyl region of IR and hoth ^{1}H and ^{31}P NMR spectra of **21** are consistent with a complex of this type. Based on these data, the structure presented in Figure 29 is proposed for **21**. In complex **21** two diphenylthioureato ligands span the Ru-Ru vector, bonding in a terminal fashion through the S and the N. A PPh_3 ligand is σ-bonded to each Ru atom. The ^{1}H and ^{31}P NMR data support this conclusion. The N-H stretch in IR spectra of **21** could not be located due to the presence of H_2O in the sample.

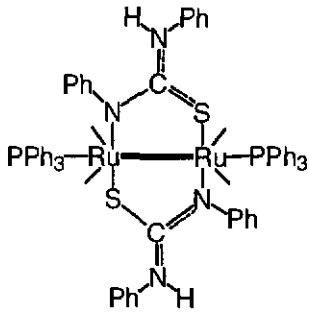

Figure 29: Graphical representation of $Ru_2(CO)_4(\mu_2,\eta^2\text{-}SCNHPhNPh)(PPh_3)_2$ (**21**).

If the diphenylthioureato ligand is considered a three-electron donor, then the dinuclear species **21** is electron precise with a total of 34 valence electrons.

Spectroscopic data for **22** show a relatively simple carbonyl region; only five hands are observed suggesting a more open polyhedral arrangement, relative to that of **15**. The presence of an undisturbed diphenylthioureato ligand is clear from IR and ^{1}H NMR data. Integration of the phenyl and the NH region of the ^{1}H NMR, combined with the ^{31}P NMR spectrum, leads to a single, σ-bonded PPh_3 group. Room temperature ^{1}H NMR spectra of **22** in $CDCl_3$ show a broad, poorly defined peak for the μ_2-hydride ligand at -17.50 ppm. The downfield shift of the signal denotes a chemical environment for this proton less affected hy the anisotropy of the metal core. Upon cooling CD_2Cl_2 samples to -70°C, two well-defined singlets at -17.70 ppm and -17.73 ppm (400 MHz) in an approximately 1:1 ratio can be seen.

This result is consistent with the presence of two interconverting isomers in room temperature solutions.

An X-ray structural characterization of **22** provided the exact location of the PPh_3 ligand on the hexanuclear framework, and also revealed some interesting structural features. Deep-red, plate crystals of **22** were grown from CH_2Cl_2/hexanes(xs) solutions. Crystals of **22** are triclinic and belong to the space group $P\bar{1}$. The molecular structure of **22** is illustrated in Figure 30, while important bond lengths and angles are summarized in Table 31.

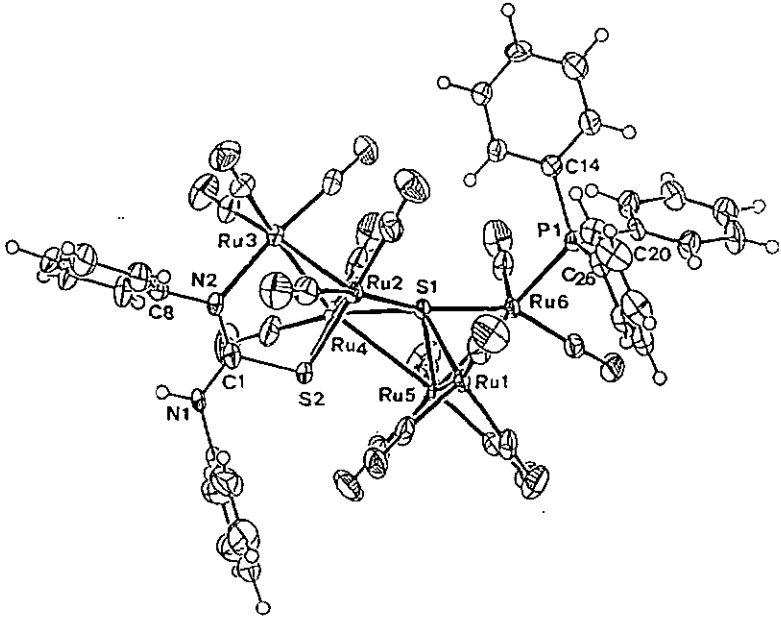

Figure 30: Molecular structure of $(\mu_2\text{-H})Ru_6(CO)_{15}(PPh_3)(\mu_5\text{-S})(\mu_3,\eta^2\text{-SCNHPhNPh})$ (22)

Table 31: Important bond lengths (Å) and angles (°) for (μ_2 H)$Ru_6(CO)_{15}(PPh_3)(\mu_5$-S) ($\mu_3,\eta^2$-SCNHPhNPh) (**22**).

Ru(1)-Ru(2)	3.3729(11)	Ru(1)-Ru(5)	2.7904(10)
Ru(1)-Ru(6)	2.9529(10)	Ru(1)-S(1)	2.3762(17)
Ru(2)-Ru(4)	2.9106(10)	Ru(2)-Ru(3)	2.7206(10)
Ru(2)-S(2)	2.4287(18)	Ru(2)-S(1)	2.4089(17)
Ru(3)-N(2)	2.164(5)	Ru(3)-Ru(4)	2.7100(10)
Ru(4)-Ru(5)	3.0870(11)	Ru(4)-S(1)	2.4285(18)
Ru(4)-S(2)	2.4091(19)	Ru(5)-Ru(6)	2.7885(11)
Ru(5)-S(1)	2.3646(16)	Ru(6)-P(1)	2.3743(18)
Ru(6)-S(1)	2.3381(18)	C(1)-N(1)	1.362(9)
S(2)-C(1)	1.781(7)	P(1)-C(20)	1.835(6)
P(1)-C(14)	1.816(6)	N(1)-C(2)	1.417(9)
P(1)-C(26)	1.830(7)	N(2)-C(8)	1.452(9)
N(2)-C(1)	1.272(9)		
Ru(1)-Ru(2)-Ru(4)	86.12(3)	Ru(1)-Ru(2)-Ru(3)	143.01(3)
Ru(1)-Ru(5)-Ru(6)	63.92(3)	Ru(1)-Ru(5)-Ru(4)	94.01(3)
Ru(1)-Ru(6)-Ru(5)	58.07(3)	Ru(1)-Ru(5)-S(1)	54.14(4)
Ru(1)-Ru(6)-P(1)	109.26(5)	Ru(1)-Ru(6)-S(1)	51.79(4)
Ru(1)-S(1)-Ru(6)	77.56(5)	Ru(1)-S(1)-Ru(2)	89.64(6)
Ru(2)-Ru(1)-Ru(6)	92.75(3)	Ru(2)-Ru(1)-Ru(5)	88.11(3)
Ru(2)-Ru(3)-N(2)	88.12(15)	Ru(2)-Ru(3)-Ru(4)	64.82(3)
Ru(2)-Ru(4)-Ru(5)	91.73(3)	Ru(2)-Ru(4)-Ru(3)	57.767(25)
Ru(2)-Ru(4)-S(2)	53.32(5)	Ru(2)-Ru(4)-S(1)	52.70(4)
Ru(2)-S(2)-Ru(4)	73.97(5)	Ru(2)-S(1)-Ru(4)	73.98(5)
Ru(3)-Ru(2)-Ru(4)	57.415(24)	Ru(2)-S(2)-C(1)	103.87(23)
Ru(3)-Ru(4)-Ru(5)	148.62(3)	Ru(3)-Ru(2)-S(2)	80.03(5)
Ru(3)-Ru(4)-S(2)	80.59(5)	Ru(3)-Ru(4)-S(1)	101.18(5)
Ru(3)-N(2)-C(8)	119.1(4)	Ru(3)-N(2)-C(1)	121.6(4)
Ru(4)-Ru(2)-S(2)	52.70(5)	Ru(4)-Ru(2)-S(1)	53.32(4)
Ru(4)-S(1)-Ru(5)	80.18(5)	Ru(4)-Ru(5)-Ru(6)	96.87(3)
Ru(4)-S(2)-C(1)	103.48(24)	Ru(5)-Ru(1)-Ru(6)	58.011(24)
Ru(5)-Ru(1)-S(1)	53.75(4)	Ru(5)-Ru(6)-S(1)	54.07(4)
Ru(5)-Ru(6)-P(1)	167.05(5)	Ru(5)-S(1)-Ru(6)	72.73(5)
Ru(6)-Ru(1)-S(1)	50.64(4)	Ru(6)-Ru(5)-S(1)	53.20(4)
Ru(6)-P(1)-C(14)	120.24(23)	Ru(6)-P(1)-C(20)	111.10(20)
Ru(6)-P(1)-C(26)	113.29(21)	S(2)-C(1)-N(2)	120.3(5)
S(1)-Ru(2)-S(2)	85.61(6)	N(2)-C(1)-N(1)	125.2(6)
S(2)-C(1)-N(1)	114.5(5)	C(1)-N(2)-C(8)	119.3(6)

The metal framework of **22** consists of six Ru atoms, arranged similarly to those of **15**. A pentacoordinate sulfur ligand S1, remains bonded through five σ-bonds to Ru1, Ru2 and Ru4, Ru5 and Ru6. A μ_3,η^2-diphenylthioureato ligand spans the Ru2-Ru4 triangular substructure; the S (S2) bridges Ru2 and Ru4 and the N (N2) is bound terminally to Ru3 A CO ligand on the apical Ru6 has been replaced with a PPh_3 ligand. The PPh_3 occupies a position which is equatorial with respect to the Ru_3 triangular substructure composed of Ru1,Ru5, and Ru6. An appropriate number of terminal CO ligands were located on each of the six Ru atoms.

Yet, the original sofa-like configuration of **15** has been somewhat distorted in **22**. The distance between Ru1 and Ru2 (3.3729(11)Å) has increased by *ca.* 0.20Å from that of **15**. While in general, M-M bond lengths vary significantly among bonds of the same order[144], the distance between Ru1 and Ru2 clearly does not allow for a formal Ru-Ru bond. This result demonstrates the inherant weakness of the Ru1-Ru2 interaction. Within the Ru1-Ru5-Ru6 triangular substructure, the sequence of long-short bond lengths has changed with respect to that of **15**, further suggesting alterations in the Ru-Ru bonding scheme. The Ru1-Ru6 vector elongates by *ca.* 0.17Å, while Ru1-Ru5 shortens by *ca.* 0.13Å. However, these changes do not affect the relative M-M bond orders amongst those bonds. In opening the Ru1-Ru2 bond, the cluster now assumes the appearance of two trinuclear units linked through the μ_3-S and a single, long but reasonable Ru-Ru bond (Ru4-Ru5, 3.0870(11)Å).

Although a bridging hydride could not be located crystallographically, the NMR data are consistent with the placement of this ligand spanning the Ru1-Ru5 vector; no coupling to the P is observed. The downfield shift of the hydride's ^{1}H NMR signal results from the opening-up of the cluster which allows the hydride to avoid the anisotropy due to the metal centers. As stated above, room temperature ^{1}H NMR spectra of **22** show a broad, poorly defined peak in the hydride region. Low temperature spectra, on the other hand, reveal two closely-spaced peaks in an approximately 1:1 ratio. The two separate peaks, centered at -17.71 ppm (CD_2Cl_2, 400 MHz), reflect the presence of two isomers in solutions of **22**. One (**22a**), represented by the molecular structure shown in Figure 30, has the PPh_3 ligand in an apical position on Ru6 pointing away from the bridging hydride. The other isomer (**22b**), has the PPh_3 ligand on the same Ru atom (Ru6) but the ligand is now rotated ~180°, and approaches the bridging hydride more closely. Although this structural variation is relatively removed from the bridging hydride, the difference in the chemical environment is significant enough to cause a separate peak for the hydride of each isomer. The hydride of isomer **22a** is assigned to the downfield signal at -17.71ppm. while that of isomer **22b** is assigned to the upfield signal at -17.73ppm.

With seven Ru-Ru bonds, the cluster **22** requires 94 electrons to achieve electronic saturation. There are no changes in the bond lengths or angles of the diphenylthioureato ligand which could indicate an alteration in its role as a five-electron donor. The same is true for the sulfide ligand, which continues to donate all six of its electrons to the cluster. Like the CO

ligands, PPh_3 is a two-electron donor. Overall, cluster **22** contains 92 electrons, the same number as **15**, thus it must be considered to be an electronically unsaturated cluster.

When exposed to CO, **22** does not undergo the same transformation as **15**. Instead cluster fragmentation occurs to generate the trinuclear species $(\mu_2\text{-H})Ru_3(CO)_9(\mu_3,\eta^2\text{-SCNHPhNPh})$ (**8**). Presumably, the CO coordinates at the highly unsaturated Ru2, causing the Ru2-S1 bond to open. Further bond scission ensues with the eventual abstraction of an ambient hydride to produce **8**. The addition of CO at Ru2 is facillitated in **22** by the opening-up of the Ru1-Ru2 bond which provides an alternative to the μ_2-interaction assumed in **20**. Given the lack of any other products in reactions of **15** with excess PPh_3, it can be assumed that cluster **22** does not coordinate an additional phosphine ligand at the electron defincient Ru centers. The different stereochemical demands of PPh_3 versus CO may be a contributing factor.

3.14.3 Reactions of 15 with $P(n\text{-}Bu)_3$, $P(OMe)_3$, $P(OPh)_3$, and ^tBuNC.

In contrast to reactions of **15** with PPh_3, addition of $P(n\text{-}Bu)_3$, either of the phosphites $P(OMe)_3$ or $P(OPh)_3$, or ^tBuNC, gave as the major product analogous monosubstituted derivatives of **15**. The duration of the reaction has very little effect on the product yields. These derivatives are all easily isolated using preparative TLC. Spectral data (summarized in Table 32) clearly show that the site of substitution in these derivatives differs from that of **22**.

Table 32: IR and NMR data for $(\mu_2\text{-H})Ru_6(CO)_{15}(R)(\mu_5\text{-S})(\mu_3,\eta^2\text{-SCNHPhNPh})$; R = $P(n\text{-}C_4H_9)_3$ (**23**), $P(OMe)_3$ (**24**), $P(OPh)_3$ (**25**), $(CH)_3CNC$ (**26**).

IR (c-hex, 298K)	{ν_{NC}(cm^{-1})}	**26**:	2166w		
	{ν_{CO}(cm^{-1})}	**23**:	2083m	2056vs	2041s
			2023vs	2011w	2001m
			1985m,br	1953m	1925w
		24:	2084m	2057vs	2041s
			2030s	2015m	2001m
			1989m	1966w,br	1937w,br
		25:	2085m	2058vs	2042s
			2031s,sh	2016m	2002m
			1990m	1976w,br	1942w,br
		26:	2084m	2057vs	2042s
			2033s	2016m	2001m
			1989s,br	1976w,br	1939w,br

Table 32: cont.

IR(KBr):	{$\nu_{NH}(cm^{-1})$}	**23**:	3362m
		24:	3339m
		25:	3355m
		26:	3361w
	{$\nu_{NCN}(cm^{-1})$}	**23**:	1552m
		24:	1554m
		25:	1556m
IR(KBr):	{$\nu_{NCN}(cm^{-1})$}	**26**:	1564m
^{1}H NMR($CDCl_3$)[a]	{δ(ppm)}	**23**:	7.40-7.10 (m,Ph-*H*)
			6.81 (s,br,N-*H*)
			1.43-0.84 (m,C_4-H_9)
			-22.07 (s,Ru_2-*H*)
		24:	7.57-7.10(m, 10H, Ph-*H*)
			6.78(s,br, 1H, N-*H*)
			3.45(d,J=11.2Hz, 9H, CH_2-*H*)
			-22.0(s,1H, Ru_2-*H*)
		25:	7.43-6.67(m,25H, Ph-*H*)
			6.78(s,br,1H, N-*H*)
			-22.1(s,1H, Ru_2-*H*)
		26:	7.60-7.12 (m,10H, Ph-*H*)
			6.76 (s,br,0.8H) 6.74 (s,hr,0.2H); N-*H*
			1.54 (s,0.2H,) 1.50 (s,0.8H); C-H_3
			-21.91 (s,1H, Ru_2-*H*)
^{31}P NMR($CDCl_3$)[b]		**23**:	20.81(s)
		24:	121.8(s)
		25:	107.7(s)
FAB-MS (NBA)	M^+	**23**:	1486
		24:	1409
		25:	1598

[a] 200 MHz, 298K
[b] 80.96 MHz, 298K.

The data assembled in Table 32 show trends indicating substitution of a CO by these 2-electron donor ligands at a site different from that of **22**. The large number of bands in the carbonyl region results from perturbations to the pseudo mirror-plane symmetry of **15**. Insignificant spectral shifts of relevant signals for the diphenylthioureato ligand in **23-26**, as compared to the same data for **15**, establish its bonding mode as unchanged. The hydride signals also show insignificant spectral shifts. The coincidence of the spectral data for **23-26** with that of **19** suggests that these species are isomorphic. Thus the dimethylsulfide derivative **19**, may be included in this series of derivatives. The NH and CH_3 signals in the ^{1}H NMR spectrum of cluster **26**, indicate the presence of isomers. A schematic representation of clusters **23-26** is presented in Figure 31.

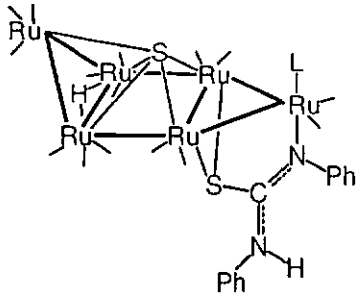

L = P(n-Bu)3
= P(OMe)3
= P(OPh)3
= t-BuNC

Figure 31: Schematic representation of clusters **23-26**.

Verification of the site of substitution in **23-26** was provided by structural analysis of the ^{t}BuNC substituted derivative, **26**. Deep red, plates of **26** could be isolated from 3:1 acetone-heptane solutions maintained at 5°C for 3d. These crystals were triclinic of the space group $P\bar{1}$. An ORTEP plot of **26** is presented in Figure 32 and selected bond lengths and angles are given in Table 33. An area of disordered solvent was associated with each molecule of **26**.

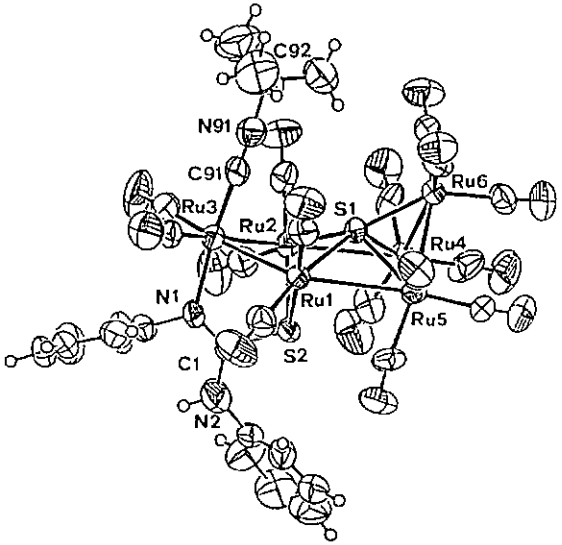

Figure 32: Molecular structure of $(\mu_2\text{-}H)Ru_6(CO)_{15}\{^t BuNC\}(\mu_5\text{-}S)(\mu_3,\eta^2\text{-}SCNHPhNPh)$ (**26**).

Tahlc 33: Selected bond lengths (Å) and angles (°) of (μ_2-H)$Ru_6(CO)_{15}$\{^{t}BuNC\}(μ_5-S)(μ_3,η^2-SCNHPhNPh) (**26**).

Ru(1)-Ru(2)	2.929(2)	Ru(1)-Ru(3)	2.728(2)
Ru(1)-Ru(5)	3.190(2)	Ru(1)-S(1)	2.392(3)
Ru(1)-S(2)	2.420(3)	Ru(2)-Ru(3)	2.720(2)
Ru(2)-Ru(4)	3.152(2)	Ru(2)-S(1)	2.401(3)
Ru(2)-S(2)	2.417(3)	Ru(3)-N(1)	2.166(11)
Ru(3)-C(91	1.96(2)	Ru(4)-Ru(5)	2.907(2)
Ru(4)-Ru(6)	2.783(2)	Ru(4)-S(1)	2.394(3)
Ru(5)-Ru(6)	2.784(2)	Ru(5)-S(1)	2.393(3)
Ru(6)-S(1)	2.312(3)	S(2)-C(1)	1.802(12)
N(1)-C(1)	1.28(2)	N(1)-C(2)	1.45(2)
N(2)-C(1)	1.34(2)	N(2)-C(8)	1.44(2)
N(91)-C(92)	1.49(2)	C(91)-N(91)	1.14(2)
Ru(1)-Ru(2)-Ru(4)	90.56(4)	Ru(1)-S(1)-Ru(2)	75.34(9)
Ru(1)-S(1)-Ru(4)	129.22(14)	Ru(1)-S(1)-Ru(5)	83.64(10)
Ru(2)-Ru(1)-Ru(5)	89.04(4)	Ru(2)-Ru(3)-Ru(1)	65.04(4)
Ru(2)-S(2)-Ru(1)	74.53(10)	Ru(3)-Ru(1)-Ru(2)	57.35(4)
Ru(3)-Ru(1)-Ru(5)	145.65(5)	Ru(3)-Ru(2)-Ru(1)	57.62(4)
Ru(3)-Ru(2)-Ru(4)	147.09(5)	Ru(4)-Ru(5)-Ru(1)	90.20(4)
Ru(4)-Ru(6)-Ru(5)	62.96(4)	Ru(4)-S(1)-Ru(2)	82.20(10)
Ru(5)-Ru(4)-Ru(2)	90.17(4)	Ru(5)-S(1)-Ru(2)	127.26(14)
Ru(5)-S(1)-Ru(4)	74.80(10)	Ru(6)-Ru(4)-Ru(2)	97.25(4)
Ru(6)-Ru(4)-Ru(5)	58.54(4)	Ru(6)-Ru(5)-Ru(1)	96.08(4)
Ru(6)-Ru(5)-Ru(4)	58.50(4)	Ru(6)-S(1)-Ru(1)	142.29(14)
Ru(6)-S(1)-Ru(2)	142.35(14)	Ru(6)-S(1)-Ru(4)	72.49(9)
Ru(6)-S(1)-Ru(5)	72.56(9)	S(1)-Ru(1)-S(2)	85.50(11)
S(1)-Ru(2)-S(2)	85.36(11)	N(1)-C(1)-N(2)	125.8(11)
N(1)-C(1)-S(2)	118.7(9)	N(2)-C(1)-S(2)	115.6(10)
N(91)-C(91)-Ru(3)	179.5(13)	N(91)-C(92)-C(94)	106.3(14)
N(91)-C(92)-C(95)	107(2)	N(91)-C(92)-C(93)	108(2)
C(1)-N(1)-Ru(3)	123.2(8)	C(1)-N(1)-C(2)	117.9(11)
C(1)-N(2)-C(8)	127.5(11)	C(2)-N(1)-Ru(3)	118.9(9)
C(91)-Ru(3)-Ru(1)	87.9(4)	C(91)-N(91)-C(92)	177(2)

The molecular structure of **26** shows a derivative of **15** resulting from CO suhstitution hy the two-electron donor group ^{t}BuNC. The cluster skeleton of **26**, like that of **15**, consists of five Ru atoms arranged in a pentagonal-shaped polyhedron with a sixth Ru atom bridging the Ru-Ru edge opposite to the apex. The sixth Ru atom sits above the planar hase at an angle of 85°. The pentacoordinate S atom remains bonded to five metal atoms, four from the square base (Ru1, Ru2, Ru4, Ru5) and the out-of-plane, apical Ru atom (Ru6). The triangular substructure composed of Ru1, Ru2, and Ru3 is spanned by the μ_3,η^2-diphenylthinureato ligand. In contrast to the monosubtituted PPh_3 derivative **22**, the isonitrile ligand in **26** occupies an axial pnsition on the in-plane apical Ru atom of the hexanuclear framework (Ru3). The C91-N91-C92 bond of the ligand resides perpendicular to the cluster base. Terminal carbonyl ligands are found on each of the Ru atoms. A bridging hydride could not be located

in the refinement of the structural data of **26** but the ^{1}H NMR spectral data show a single peak in the hydride region essentially unchanged from that of **15** (as per Fig. 31). Thus, it is likely that a hydride ligand bridges the Ru4-Ru5 vector (Ru1-Ru5 in **15**).

The bond lengths and angles determined in **26** show little change from those of **15**. The two triangular substructures consist of Ru-Ru single bonds wherein the multiply bridged sides (Ru4-Ru5 and Ru1-Ru2) are elongated. The two trinuclear units are connected by two long Ru-Ru bonds (Ru1-Ru5 and Ru2-Ru4) however, the bond lengths still provide for an interaction between the relevant atoms. As in the case of **15**, this interaction relieves unsaturation at Ru1 and Ru2 (Ru2 and Ru4 in **15**). The two long Ru-Ru bonds connecting the triangular units, while slightly longer than those of **15** (~0.05Å longer), are closer in absolute value compared to those of **22**, a result related to the better σ-donor characteristics of the isonitrile ligand. The unsaturation at Ru1 and Ru2 is slightly less significant in the presence of such a ligand. The noticeable changes in the Ru-Ru bond lengths apparent in **22**, are absent in the derivative **26**. On average, the Ru-S1 bond lengths display a more uniform distribution when compared to those of **15** (avg. Ru-S1, 2.378(3)Å).

The presence of isomers in solutions of **26**, as implied by the ^{1}H NMR spectrum, are due to differing orientations of the ^{t}BuNC group. The situation is similar to that described for **22**. Steric requirements should favor an orientation in which the ^{t}BuNC group occupies an axial coordination site on Ru3, as determined crystallographically. The phenyl group on N2 would interact to a lesser extent with an axial ^{t}BuNC group than one with that group in an equatorial position. The axial isomer is assigned as **26a** and produces the NH signal at 6.76 ppm and the CH_3 signal at 1.50 ppm. The isomer containing the ^{t}BuNC group in an equatorial coordination site occurs also and is responsible for the NH peak at 6.74 ppm and the CH_3 peak at 1.54 ppm. That binding at the equatorial site still occurs in **26b**, can be traced to the large separation between the N2-bound phenyl and the ^{t}Bu methyls, provided by the C-N-^{t}Bu linkage. No NMR evidence was found for the existence of isomers in solutions of **23-25**.

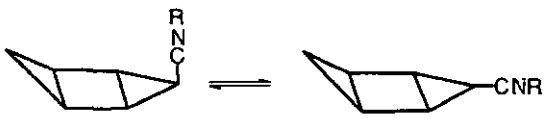

26a 26b

3.15 Reactions of $(\mu_2\text{-H})Ru_6(CO)_{15}(L)(\mu_5\text{-S})(\mu_3,\eta^2\text{-SCNHPhNPh}$ (23-26) with CO.

Each of the monosubstituted derivatives of **15** (**23-26**), exhibited reversible addition of CO. In reactions entirely analogous to that outlined in section 3.10.1, CO was bubbled through room temperature solutions of **23-26**, causing the solution color to change from deep red to dark blue and producing an IR spectrum different from that of the relevant starting material, in that a ν_{CO} in the bridging carbonyl region was evident. If left under an N_2 atmosphere, the solution color reverted back to red and IR spectra indicated the presence of only the original monosubstituted compound. Some of these derivatives were slightly more stable than **20** and could be purified with preparative TLC, provided the solvent used was first saturated with CO and a CO atmosphere maintained during the chromatography. Once in solid form, the phosphite derivatives did not lose CO. However, the n-butylphosphine derivative was the least stable and reformed the red starting material even in the solid form. The ^{t}BuNC derivative always produced a mixture of two blue compounds. The first of these ^{t}BuNC derivatives to elute on the TLC plates was the only one stable enough to isolate and characterize. These compounds are designated as **27** {L = $P(n\text{-}Bu)_3$}, **28** {L = $P(OMe)_3$}, **29** {L = $P(OPh)_3$} and **30** (L = $^tBu_3NC$) and their spectral data are outlined in Table 34.

The species **27-30** provide spectral data consistent with a monosubstituted derivative of **20**. Specifically, one band is missing in the ν_{CO} region of their IR spectra, but the bridging ν_{CO} is still present. The characteristic IR vibrations of the diphenylthioureato ligand are consistently shifted to lower wavenumbers in **27-30**, relative to those of **23-26**, analogous to observations made for **15** and **20**. Furthermore, the NH and μ_2-H signals in ^{1}H NMR spectra of the starting compound and the final product, also show frequency shifts analogous to **15** and **20**. Most telling however, are the shifts observed in ^{31}P NMR spectra of **26-29**.

It has been noted previously that ^{31}P NMR chemical shifts tend to shift downfield as the cluster framework opens up.[140] Chemical shift data of ^{31}P NMR spectra for **26-29** are consistent with the proposed structures of the CO adducts in which the Ru-Ru bond opposite to the bridging CO group is considerably longer. The most stable of the CO adducts, the $P(OPh)_3$ derivative (**29**), was subjected to FAB mass spectral analysis and analytical data was obtained. As found for **20**, a fragmentation pattern similar to the parent compound, **25**, as well as the same molecular ion (1596) was observed. Elemental analysis shows little difference

from those obtained for **25**. These observations lead to the structures presented in Figure 33 for compounds **26-30**.

Table 34: IR and NMR data for **27** - **30**.

IR(c-hex, 298K)	{ν_{NC}(cm^{-1})}:	**30**:	2177w			
	{ν_{CO}(cm^{-1})}:	**27**:	2091m	2056m	2039s	2029vs
			1986m	1953w-m	1849w,br	
		28:	2093m	2057m	2039vs	2031s
			1986m,br	1976m,br	1854w,br	
		29:	2094m	2059w	2040vs	2032s
			1988m,br	1978sh	1855w,br	
		30:	2091m	2058m	2038vs	2026s
			1986m,br	1964w-m	1861w,br	
IR (KBr)	{ν_{NH}(cm^{-1})}:	**27**:	3355m			
		28:	3359m			
		29:	3342m			
		30:	3357m			
	{ν_{NCN}(cm^{-1})}:	**27**:	1545m			
		28:	1549m			
		29:	1546m			
		30:	1558m			
^{1}H NMR($CDCl_3$)	{δ(ppm)}		[a]**28**:	7.57-7.00 (m,10H,Ph-*H*)		
				6.65 (s,1H,N-*H*)		
				3.51 (d,J = 11.2Hz,9H,C-H_3		
				-21.6 (s,1H,Ru_2-*H*)		
			[b]**29**:	7.55-6.66 (m,25H,Ph-*H*)		
				6.60 (s,1H,N-*H*)		
				-21.3 (s,1H,Ru_2-*H*)		
			[a]**30**:	7.57-6.94 (m, Ph-*H*)		
				6.51 (s,br, N-*H*)		
				1.51 (s, C-H_3)		
				-21.1 (s,Ru_2-*H*)		
^{31}P NMR($CDCl_3$)	{δ(ppm)}		[c]**28**:	125.2 (s)		
			[c]**29**:	110.6 (s)		
Mass spectrum[c]	(M^+)		**29**:	1596		

[a] 400 MHz, 298K.
[b] 200 MHz, 298K.
[c] 80.97 MHz, 298K.
[d] NBA as matrix.

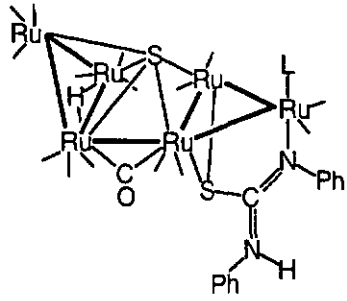

L = P(n-Bu)3(**27**)
= P(OMe)3(**28**)
= P(OPh)3 (**29**)
= t-BuNC (**30**)

Figure 33: Proposed molecular structures of **26-30**.

3.16 Reactions of 15 with Two-Electron Donor Ligands.

It is established that the weakest points in transition metal carbonyl clusters are the metal-metal bonds.[110] Reactions of the hexanuclear "sofa" cluster **15**, with PPh_3 demonstrate the truly sensitive nature of these structural features. In this reaction, the effects of replacing CO with the isoelectronic PPh_3, are seen relatively far-removed from the substitution site. Most significantly, this perturbation is enough to alter the Ru-Ru interaction one bond removed. Phosphor-based reagents other than PPh_3 result in substitution, but not at the same Ru atom and moreover, the Ru framework remains unchanged from that of **15**. The same results are obtained when a CO group is substituted with the isoelectronic RNC group. Clearly, steric interactions are not responsible for the variation in the site of substitution, given the same results with $P(OPh)_3$ as with CN'Bu. Pi backbonding also cannot be responsible as PPh_3 is a better pi acceptor than $P(n\text{-}Bu)_3$. For the derivatives of **15**, **23-26**, the single consistent difference between the substituent groups and that of **22**, is increased σ-donor properties. Placing the substituent groups in a series of increasing σ-bonding tendencies shows the following progression: $CNR > P(OPh)_3 > P(OMe)_3 > P(n\text{-}Bu)_3 > PPh_3$.

The formation of **20** demonstrates the utility of the CO ligand in transition metal clusters. Its ability to serve as a two-electron donor in either a terminal or a bridging mode is

truly its most advantageous feature. In assuming a bridging mode the CO ligand also serves to decrease electron density at the metal cluster through increased π-backbonding. None of the alternative two-electron donor ligands of **22-26**, with perhaps the exception of the isonitrile[145], are able to function both as bridging ligands and effective π-acceptors, therefore, the conversion analogous to **15** → **20**, is not observed. However, the substitution of an alternative two-electron donor in a position which results in no essential change to the metal framework of **15**, does not inhibit the addition of a bridging CO across one of the longer Ru-Ru bonds. The series of reactions producing the clusters **20** and **22-30** are presented in Scheme IV.

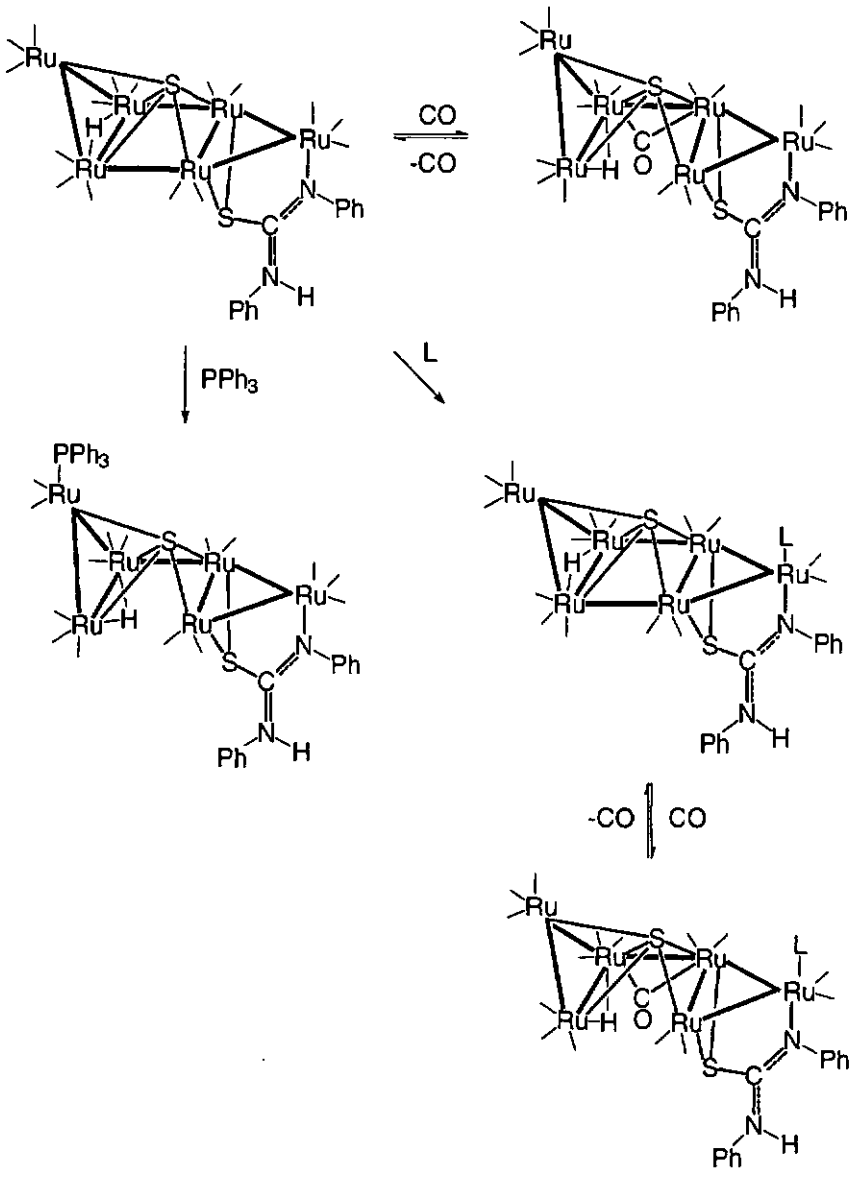

Scheme IV.

[81] Fackler J.P., Moyer T., Costamagna J.A., Latorre R., Granifo J., *Inorg. Chem.*, **1987**, *26*, 836.

[82] Sauerbrunn R.D., Sandell E.B., *J. Am. Chem. Soc.*, **1953**, *75*, 3554.

[83] Cristiani F., Diaz A., *Inorg. Chim. Acta*, **1977**, *24*, L7

[84] Cotton F.A., Zingales F., *Inorg. Chem.*, **1962**, *1*, 145.

[85] Hieber W., Rohm W., *Chem. Ber.*, **1969**, *102*, 2787.

[86] Bodensieck U., *Doctoral Thesis*, Université de Neuchâtel, **1992**.

[87] Carriedeo C., Sanchez M.V., Carriedo G.A., Riera V., Solans X., Valin M.V., *J. Organomet. Chem.*, **1987**, *331*, 53

[88] Alper H., Chan A.S.K., *Inorg. Chem.*, **1974**, *13*, 225,

[89] a. Bodensieck U., Stoeckli-Evans H., Süss-Fink G., *Chem. Ber.*, **1990**, *123*, 1603.

b. Bodensieck U., Santiago J., Stoeckli-Evans H., Süss-Fink G., *J.C.S., Dalton Trans.*, **1992**, 255.

c. Bodensieck U., Stoeckli-Evans H., Süss-Fink G., *J. Chem. Soc., Chem. Commun.*, **1990**, 267.

d. Bodensieck U., Stoeckli-Evans H., Süss-Fink G., *Angew. Chem.*, **1991**, *103*, 1147; *Angew. Chem. Int. Ed. Engl.*, **1991**, *30*, 1126.

e. Bodensieck U., Meister G., Stoeckli-Evans H., Süss-Fink G., *J. Chem. Soc., Dalton Trans.*, **1992**, 2131.

f. Bodensieck U., Stoeckli-Evans H., Süss-Fink G., *J. Organomet. Chem.*, **1992**, *433*, 149.

g. Bodensieck U., Stoeckli-Evans H., Rheinwald G., Süss-Fink G., *J. Organomet. Chem.*, **1992**, *433*, 167.

[90] Schroeder D.C., *Chem. Rev.*, **1955**, *55*, 181.

[91] Terol A., Alberola S., Jeanjean B., Sabon F., Jumes J.C., *Acta Cryst.*, **1982**, *B38*, 636.

[92] Stewart J.E., *J. Chem. Phys.*, **1951**, *26(2)*, 248.

[93] a. Chiusoli G.P., Costa M., Pergreffi Pl, Reverberi S., Salerno G., *Gazz. Chim. Ital.*, **1985**, *115*, 691.

b. Chiusoli G.P., Costa M., Masarati E., Salerno G., *J. Organomet. Chem.*, **1983**, *255*, C35.

[94] a. Haines R.J., Steen N.D.C.T., English R.B., *J. Chem. Soc., Dalton Trans.*, **1984**, 515

b. Andreu P.L., Cabeza J.A., Riera V., Bois C., Jeannin Y., *J. Chem. Soc., Dalton Trans.*, **1990**, 2201.

[95] Boroni E., Predieri G., Tiripicchio A., Tiripicchio-Camellini M., *J. Organomet. Chem.*, **1993**, *451*, 163.

[96] Jeannin Y., Jeannin, Lavigne G., *Inorg. Chem.*, **1978**, *17(8)*, 2103.

[97] Deeming A.J., Meah M.N., Randle N.P., *J. Chem. Soc., Dalton Trans.*, **1989**, 2211.

[98] a. Deeming A.J., Karim M., *Polyhedron*, **1991**, *10(8)*, 837.

b. Andreu P.L., Cabeza J.A., Fernández-Colinas J.M., Riera V., *J. Chem. Soc., Dalton Trans.*, **1990**, 2927.

[99] Deeming A.J., Meah M.N., Randle N.P., *J. Chem. Soc., Dalton Trans.*, **1989**, 2211.

[100] Hardcastle K.I., Cockerton B.R., Deeming A.J., Karim M., *J. Chem. Soc., Dalton Trans.*, **1992**, 1607.

[101] Aime S., Gobetto R., Osella D., Milone L., Rosenberg E., *Organomet.*, **1982**, *1*, 640

[102] a. Cabeza J.A., Franco R.J., Llamazares A., Riera V., Pérez-Carreno E., Van der Maelen J.F., *Organometallics*, **1994**, *13*, 55.

b.. Andreu P.L., Cabeza J.A., Cuyás J.L.,Riera V., *J. Organomet. Chem.*, **1992**, *427*, 363.

c. Andreu P.L., Cabeza J.A., Pellinghelli A., Riera V., Tiripicchio A., *Inorg. Chem.*, **1991**, *30*, 4611.

d. Andreu P.L., Cabeza J.A., Riera V., Bois C., Jeannin Y., *J. Chem. Soc., Dalton Trans.*, **1990**, 3347.

[103] Carty A.J.; MacLaughlin S.A.; Nucciarone D., *Phosphorous-31 NMR Spectroscopy in Stereochemical Analysis*; Berkade J.G., Quin L.D., Ed.; VCH Publishers Inc.: 1987; chap. 16.

[104] a. Bradford C.W.; Nyholm R.S., *J. Chem. Soc., Dalton Trans.*, **1973**, 529.

b. Bender R.; Braunstein P.; Tiripicchio A.; Tiripicchio-Camellini M., *Angew. Chem. Int. Ed.*, **1985**, *24*, 861.

c. Garding M.M.; Nicholls B.S.; Smith A.K., *J. Chem. Soc., Dalton Trans.*, **1983**, 1479.

[105] Briard P., Cabeza J.A., Llamazares A., Ouahab L., Riera V., *Organometallics*, **1993**, *12*, 1006.

[106] Lugan N., Ibers J.A., Bonnet J.-J., *J. Am. Chem. Soc.*, **1985**, *107*, 4484.

[107] Braunstein P., *Perspectives in Coordination Chemistry*, Williams A.F., Floriani C., Merhach A.E., Ed., VCH Publishers Inc., 1992, pg. 78.

[108] Cotton F.A., *Quart. Rev.*, **1966**, *20*, 389.

[109] Schmid G., *Struct. Bond.*, **1985**, *62*, chap. 2.

[110] Mingos D.M.P., Wales D.J. in "Introduction to Cluster Chemistry"; Grimes R.N., Ed.; Prentice Hall International Editions: Inc. New Jersey, **1990**, chap. 2.

[111] a. Ma, L.; Williams, G.K.; Shapley, J.R., *Coordn. Chem. Rev.* **1993**, *128*, 261.
b. *Metal Clusters*; Moskovits, M., Ed.; John Wiley & Sons: New York, 1986.

[112] a. Williams R.E., *Prog. Inorg. Chem. Radiochem.*, **1976**, *18*, 67.
b. Wade K., *Adv. Inorg. Chem. Radiochem.*, **1976**, *18*, 1.
c. Mingos D.M.P., *Acc. Chem. Res.*, **1984**, *17*, 311.
d. Rudolph R.W., *Acc. Chem. Res.*, **1976**, *9*, 446.

[113] Johnson B.F.G., Johnston R.D., Lewis J., *J. Chem. Soc. A*, **1968**, 2856.

[114] Gomez-Sal, M.P.; Johnson, B.F.G.; Kamarudin, R.A.; Lewis, J.; Raithby, J. *J. Chem. Soc., Chem. Commun.*, **1985**, 1622.

[115] Johnson, B.F.G.; Lewis, J.; Wong, K.; McPartlin, M. *J. Organomet. Chem.*, **1980**, *185*, C17.

[116] a. Cifuentes, M.P.; Jeynes, T.P.; Humphrey, M.G.; Skelton, B.W.; White, A.H., *J. Chem. Soc., Dalton. Trans.*, **1994**, 925.
b. Caheza, J.A.; Fernández-Colinas, F.M.; García-Granda, S.; Llamazares, A.; López-Ortíz,F.; Riera, V.; Van der Maelen, J.F., *Organometallics*, **1994**, *13*, 426

[117] Boag N.M., Knobler C.B., Kaesz G.D., *Angew. Chem. Int. Ed. Engl.*, **1983**, *22*, 249.

[118] a. Gervasio, G.; Rossetti, R.; Stanghellini, P.L.; Bor G. *Inorg. Chem.*, **1984**, *23*, 2073
b. Adams, R.D.; Babin, J.E.; Tasi, M., *Inorg. Chem.*, **1987**, *26*, 2561.
c. Cockerton, B.R.; Deeming, A., *Polyhedron*, **1994**, *13(13)*, 2085.
d. Bodensieck, U.; Hoferkamp, L.; Stoeckli-Evans, H.; Süss-Fink, G., *J. Chem. Soc., Dalton Trans.*, **1993**, 127

[119] Jeannin S.; Jeannin Y.; Robert F.; Rosenberger C., *Inorg. Chem.*, **1994**, *33*, 243.

[120] Hoferkamp L., Rheinwald G., Stoeckli-Evans H., Süss-Fink G., *Inorg. Chem.*, in press.

[121] Cockerton, B.R.; Deeming, A. *Polyhedron* **1994**, *13(13)*, 2085.

[122] Spek, A.L., *Acta Crystallogr.*, **1990**, *A46*, C34.

[123] Boag N.M., Knobler C.B., Kaesz H.D., *Angew. Chem., Intl. Ed. Engl.*, **1983**, *22*, 249.

[124] a. Adams R.D., Babin J.E., Tasi M., Wolfe T.A., *New J. Chem.*, **1988**, *12*, 481.

b. Adams R.D., Chen G., Tanner J.T., Yin J., *Organometallics*, **1990**, *9*, 1240.

[125] a. Churchill M.R., Ziller J.W., Dalton D.M., Keister J.B., *Organometallics.*, **1987**, *6*, 806.

b. Churchill M.R., Deboer B.G., Rotella F.J., *Inorg. Chem.*, **1976**, *15*, 1843

[126] Vidal J.L., Fiato R.A., Cosby L.A., Pruett R.L., *Inorg. Chem.*, **1978**, *17(9)*, 2774.

[127] Hall S.R., Stewart J.M., *Can. Mineral.*, **1973**, *12*, 169.

[128] a. Adams R.D., Babin J.E., Natarajan K., Tasi M., Wang J.G., *Inorg. Chem.*, **1987**, *26*, 3708.

b. Adams R.D., Babin J.E., Natarajan K., *J. Am. Chem. Soc.*, **1986**, *108*, 3518.

c. Adams R.D., Babin J.E., Wang J.G., *Polyhedron*, **1989**, *8*, 2351.

[129] Wu X., Wang B., Zheng Y. Lu J., *Jiegou Huaxue*, **1988**, *7*, 47.

[130] Ciani G., Garlaschelli L., Sironi A., *J. Chem. Soc., Chem. Commun.*, **1989**, 563.

[131] Muetterties E.L., Rhodin T.N., Band E., Brucker C.F., Pretzer W.R., *Chem. Rev.*, **1979**, *79(2)*, 91.

[132] Sappa E, Gambino O., Cetini G., *J. Organomet. Chem.*, **1972**, *35*, 375.

[133] a. Adams R.D., Horvath I.T., Mathur P., *Organometallics*, **1984**, *3*, 623.

b. Adams R.D., Foust D.F., Segmüller B.E., *Organometallics*, **1983**, *2*, 308.

[134] Sappa E., Gambino O., Cetini G., *J. Organomet. Chem.*, **1972**, *35*, 375.

[135] a. Adams R.D., Babin J.E., Wolfe T.A., *Polyhedron*, **1989**, *8*, 1123.

b. Adams, R.D., Manig, D.,Segmüller B.E., *Organometallics*, **1983**, *2*, 149.

[136] Adams R.D., Babin J.E., Tasi M., *Inorg. Chem.*, **1986**, *25*, 4514.

[137] Adams R.D., Babin J.E., Tasi M., *Organometallics*, **1988**, 7, 503.

[138] Koelliker R., Bor G., *J. Organomet. Chem.*, **1991**, *417*, 439.

[139] Ferrari R.P., Vaglio G.A., Valle M., J. Chem. Soc., Dalton Trans., 1978, 1164.

[140] Planalp R.P., Vahrenkamp H., *Organometallics*, **1987**, *6*, 492.

[141] Carty A.J., Maclaughlin S.A., Taylor N.J., *J. Organomet. Chem.*, **1981**, *204*, C27.

[142] Knoll K., Huttner G., Zsolnai L., Orama O., *Angew. Chem. Int. Ed. Engl.*, **1986**, *25*, 1119.

[143] Beguin A., Rheinwald G., Stoeckli-Evans H., Süss-Fink G., *Helv. Chim. Acta*, **1994**, *77*, 525.

[144] Johnson B.F.G., Rodgers A. in "*The Chemistry of Metal Cluster Complexes*"; Shriver D.F., Kaesz H.D., Adams R.D., Ed.; VCH Puhlishers Inc., **1990**, chap 6.

[145] Elschenbroich Ch., Salzer A. in "*Organometallics, a Concise Introduction*"; Weller M.G., Ed.; VCH Verlagsgesellschaft, Weinheim (Federal Republic of Germany) and VCH Publishers, New York, NY (USA), **1989**, pg 240.

4 Experimental Part

4.1 Apparatus

Manipulations were carried out using standard schlenk techniques[146] under an N2 atmosphere. Thermolysis reactions were performed in a high pressure schlenk tube able to withstand 8 bars of internal pressure. Reactions which required an accurate knowledge of the pressure were carried out in 100 ml or 500 ml autoclaves equipped with glass sleeves. An Heräus Hg-vapor lamp was used in photochemical reactions.

In appropriate cases thin layer chromatography (TLC) was used to purify compounds.[147] TLC plates were prepared by placing a uniform 0.5 mm layer of the appropriate support (Al_2O_3 or SiO_2; G or G/UV_{254}, Macherey-Nagel) on 20x20 cm glass plates.[148] After charging the plates with the support they were allowed to air dry for ~1h and then dried in an oven at 125°C for 12h. When strictly anhydrous conditions were necessary, freshly activated plates were used. Unless otherwise stated the reaction mixtures were loaded onto the plates as CH_2Cl_2 solutions. The solvent mixture used to elute the products was determined using Macherey-Nagel test TLC plates (5 x 2 cm) of the appropriate support.

4.2 Solvents and Gases

Standard laboratory solvents were purified and dried according to standard laboratory practices.[149] Distillation of solvents was carried out under an N_2 atmosphere; the inert atmosphere over the solvent was maintained thereafter. Laboratory gases were purchased from Carbagas, Messer Griesheim, and used directly from the cylinders without further purification.

4.3 Starting Materials

Tritutheniumdodecacarbonyl $Ru_3(CO)_{12}$[150], triosmiumdodecacarbonyl $Os_3(CO)_{12}$[151], $(\mu_2\text{-H})Ru_3(CO)_9(\mu_3,\eta^2\text{-SCNHPhNPh})$[152], and $Ru_3(CO)_{11}(tBuNC)$[153] were prepared according to published procedures. Other chemicals were purchased from the vendors indicated below and used as received.

Borane-methyl sulfide complex (Aldrich, 10-10.2 M BH_3 in Me_2S)*

Borane Tetrahydrofuran Complex Solution (Fluka, 1M in THF)*

n-Butyllithium (Aldrich, 1.6M in hexane)*

t-Butylisonitrile (Fluka, 98%)*

Diironnonacarbonyl (Aldrich, 98%)*

Diphenylacetylene (Fluka, 99%)

1,2-Bis(diphenylphosphino)ethane (97%)

Methyl sulfide (Fluka, 99%)

N,N'-Dimethylthiourea (Merck, 98%)

N,N'-Diphenylthiourea (Fluka, 98%)

Triirondodecacarbonyl (Aldrich, stabilized with 5% MeOH)*

Ruthcniumchloride-hydrate (Johnson-Matthey)

Trimethylphosphite (Fluka, 99%)*

Triphenylphosphite (Fluka, 99%)*

Tri n-butylphosphine (Fluka, 99%)*

Triphenylphosphine (Merck, 98%)

1,3,5-Trithiane (Fluka, 98%)

*Stored under N_2.

4.4 Instrumentation and Analyses

4.4.1 Infrared Spectroscopy

Infrared spectra were obtained using a PERKIN-ELMER 1720 X spectrometer in transmission mode where the absorptions are given in reciprocal centimeters (cm^{-1}). Solution spectra were measured in a 0.1 mm CaF_2 cell. A standard press was used to produce KBr pellets. Intensity data are described with the following abbreviations: vs = very strong, s = strong, m = medium, w = weak, vw = very weak and sh = shoulder.

4.4.2 Standard NMR Spectroscopy

The ^{1}H, ^{13}C and ^{31}P NMR spectra used in characterization, were acquired with either a BRUKER AMX 400 or a VARIAN Gemini 200 BB spectrometer and the measurement temperature indicated. Chemical shift data is quoted according to the δ-scale and given in ppm. The ^{13}C NMR spectra measured at variable temperature and used to determine rate constants for the merry-go-round process of the carbonyls in **2** and **3** were recorded using a BRUKER AC-200 spectrometer (4.7 T) working at 50.323 MHz. 1H NMR spectra were calibrated with respect to the signal of the residual non-deuterated solvent. ^{31}P NMR spectra were calibrated with respect to H_3PO_4. Signal multiplicity is described with the following abbreviation: s = singlet, d = doublet, t = triplet, q = quartet, m = multiplet, hr = broad. Deuterated solvents (99.8% deuteration) were purchased from ICN Chemicals.

4.4.3 High-Pressure NMR Spectroscopy

The variable-pressure experiments were performed by Dr. G. Laurenczy at the Institut de Chimie Minèrale et Analytique, Universitè de Lausanne in Lausanne, Switzerland using a BRUKER AM-400 spectrometer (9.4 T) working at 100.626 MHz. The measurements were made up to 2000 bar using a home-built high-pressure probe, designed for a BRUKER wide-bore cryomagnet.[154] A built-in Pt resistor allowed temperature measurements with an accuracy of ± 1K. By pumping a thermostated liquid through the homb, the temperature was stabilized to ± 0.2K at 253.1K for **2** or 279.5K for **3**. The spectra were obtained hy using 32 K data points resulting from 17,000 to 25,000 scans accumulated over a total spectral width of 17 kHz for **3** or 23 kHz for **2**. To improve the signal to noise ratio, exponential filters (line-broadening) of 1 Hz for **2** or 10 Hz for **3** were used. Carbon-13 chemical shifts are referred to Me_4Si and measured with respect to the THF signal at 68.6 ppm. The EXSY ^{13}C NMR spectra of **3** were obtained in (D_8) THF at 263K from NOESY experiments using TPPI.[155] The spectral width was 7575.7 Hz in both F12 and F2 domains, a shifted squared cosine hell was applied in both domains prior to *Fourier* transformation. The mixing time was 100 ms.

4.4.4 X-Ray Structural Analyses

X-ray structural data were collected on a Stoe-Siemens AED 2 four-circle diffractometer using graphite monochromatized Mo-Kα radiation (λ = 0.71073Å). Low temperature measurements were carried out using controlled temperature nitrogen gas-flow. Crystal structure data were analyzed using the SHELXS[156] and NRCVAX[157] program packages of the VAX-Cluster of the Département de Calcul of the Université de Neuchâtel. Illustrations of molecular structure were drawn with either PLUTO[158] or SHAKAL[159] programs. Illustrations showing thermal motion ellipsoids were drawn using the PLATON[160] or ZORTEP[161] program. Complete tables of atomic coordinates and isotropic thermal parameters for all structurally characterized molecules are presented in chapter VI. Additional data for those structures published in scientific journals has been deposited with the Cambridge Crystallographic Data Centre, 12 Union Rd, GB-Cambridge CB2 1EW (UK).

4.4.5 Elemental Analyses

Elemental analyses were performed by the Mikroelementaranalytisches Laboratorium, ETH, Zurich, Switzerland.

4.4.6 Mass Spectra

FAB mass spectra were measured by Professor T.A. Jenny of the University of Fribourg, Fribourg Switzerland using 3-Nitrobenzyl alcohol (NBA) as the matrix.

4.5 Syntheses

Trithiane Clusters of the Group VIII Metals

4.5.1 Synthesis of the Ligand 2,4,6-Tribenzyl-1,3,5-Trithiacyclohexane

This ligand was prepared according to the procedure outlined by Edema et. al. (II,38).

4.5.2 Synthesis of $Fe_2(CO)_6(\mu_2\text{-}S_3C_3H_6)$ (1)

A solution of $Fe_3(CO)_{12}$ (113 mg, 0.213 mmol) and trithiane (31 mg, 0.240 mmol) in benzene (25 ml) was placed under vigorous reflux for 2h. After removing the solvent the residue was redissolved in CH_2Cl_2 and chromatographed on SiO_2 TLC plates. Elution with 1:3 CH_2Cl_2:C_6H_{12} produced **1** as a yellow-orange band (17.2 mg, 12.9%).

Anal. calcd. for $C_9H_6Fe_2O_6S_3$ (418.0): C, 25.9; H, 1.45. Found: C, 26.0; H, 1.20.

4.5.3 Synthesis of $Ru_3(\mu_2\text{-}CO)_3(CO)_6(\mu_3,\eta^3\text{-}S_3C_3H_6)$ (2)

A solution of $Ru_3(CO)_{12}$ (64.3 mg, 0.101 mmol) and 1,3,5-trithiacyclohexane (14.7 mg, 0.106 mmol) in THF (25 ml) was refluxed for three hours. The resulting yellow solution was allowed to cool to room temperature and the volume of THF reduced to 5 ml. To the THF solution was then added 25 ml CH_2Cl_2 producing a finely divided yellow precipitate. The solid was isolated, dissolved in 2 ml THF and chromatographed on Al_2O_3 TLC plates. Elution with CH_2Cl_2/THF 1:3, gave **2** (49.6 mg, 71.1 %) and some unreacted $Ru_3(CO)_{12}$. Isolating **2** required rinsing the Al_2O_3 with alternating portions of THF and CH_3OH. Yellow crystals of **2** were obtained by slow evaporation of a THF solution. The filtrate from the original separation contained no products in any significant concentration.

Anal. calc. for $C_{12}H_6O_9Ru_3S_3 \cdot 0.15\ C_4H_8O$ (704.32): C, 21.49; H, 1.03. Found: C, 21.53; H, 1.06.

4.5.4 Synthesis of $Ru_3(\mu_2\text{-}CO)_3(CO)_5(tBuNC)(\mu_3,\eta^3\text{-}S_3C_3H_6)$ (3)

A solution of $Ru_3(CO)_{11}(tBuNC)$ (50 mg, 0.072 mmol) and 1,3,5-trithiacyclohexane (10.5 mg, 0.076 mmol) in hexane (30 ml) was refluxed in a for 8h resulting in a light yellow precipitate and solution. The yellow solid was isolated by filtration and chromatographed on Al_2O_3 TLC plates in CH_2Cl_2 producing two yellow bands. The lower band contained **2**, while the fast-moving band contained the desired product **3** (24 mg, 44%).

Anal. calc. for $C_{16}H_{15}NO_8Ru_3S_3 \cdot 0.5\ C_4H_8O$ (784.7): C, 27.55; H, 2.44; N, 1.78. Found: C, 27.51; H, 2.47; N, 1.78.

4.5.5 Synthesis of $Ru_3(\mu_2\text{-}CO)_3(CO)_6\{\mu_3,\eta^3\text{-}S_3(CHCH_2Ph)_3\}$ (4)

A solution of $Ru_3(CO)_{12}$ (160 mg, 0.250 mmol) and 1,3,5-thithia-2,4,6-tribenzyl-cyclohexane (106 mg, 0.260 mmol) in THF (30 ml) was refluxed under nitrogen for 8h resulting in a dark yellow solution. After removing the solvent, the residue was dissolved in CH_2Cl_2 and chromatographed on Al_2O_3 TLC plates in 8% acetonitrile in toluene. A wide yellow band was the only major band and was collected and isolated with CH_2Cl_2 to yield **4** as a yellow solid (144 mg, 60%).

Anal. calc. for $C_{33}H_{24}O_9Ru_3S_3$ (963.9): C, 41.12; H, 2.51. Found: C, 41.03; H, 2.58.

4.5.6 Synthesis of $Os_3(CO)_{11}(S_3C_3H_6)$ (5), $(\mu_2\text{-}H)Os_3(CO)_{10}(\mu_2\text{-}OH)$ (6) and $(\mu_2\text{-}H)Os_3(CO)_9(\mu_3,\eta_2\text{-}SCHS_2C_2H_4)$ (7)

A solution of $Os_3(CO)_{12}$ (100 mg, 0.110 mmol), $S_3C_3H_6$ (16 mg, 0.115 mmol) and anhydrous trimethylamineoxide (12 mg, 0.115 mmol) in THF (25 ml) was stirred at room temperature for 24h. After removing the THF from the light yellow solution, the residue was dissolved in CH_2Cl_2 and chromatographed on SiO_2 plates in 1:1 CH_2Cl_2:C_6H_{12}. The major product **5** migrated as yellow band just below the solvent front followed by compounds **6** and **7**, also present as yellow bands. Each was isolated with CH_2Cl_2: **5**, 58.2 mg, 52%; **6** (2.5 mg, 2.6%); **7** (2.5 mg, 2.4%). If the schlenk tube was flame-dried prior to use and the $Os_3(CO)_{12}$ added to a stirring solution of trithiane and trimethylamineoxide but the remaining conditions left unaltered then the yields of the products were found to change as follows: **5** (34.4 mg, 30.7%), **6** (9.0 mg, 9.5%), **7** (12.3 mg, 11.6).

5 Anal. calc. for $C_{14}H_6O_{11}Os_3S_3{\cdot}0.25\ C_4H_8O$ (1047.1): C, 17.41; H, 0.80. Found: C, 17.43; H, 0.86.

6 Anal. calc. for $C_{10}H_2O_{11}Os_3$ (868.1): C, 13.8; H, 0.23. Found: C, 14.02; H, 0.20.

7 Anal. calc. for $C_{12}H_6O_9Os_3S_3{\cdot}0.25\ C_6H_{12}$ (981.9): C, 16.5; H, 0.92. Found: C, 16.32; H, 0.94.

Thiourea Clusters of Ruthenium

4.5.7 Synthesis of $Ru(CO)_2(\eta^2\text{-}SCNHPhNPh)_2$ (9)

Direct Synthesis: A solution of $Ru_3(CO)_{12}$ (40.5 mg, 0.0633 mmol) and $(PhNH)_2CS$ (86.4 mg, 0.39 mmol) in THF (20 ml) was stirred at room temperature for 7d. The solvent was removed and the residue redissolved in CH_2Cl_2 and chromatographed on Al_2O_3 TLC plates in 1:1 CH_2Cl_2:C_6H_{12} yielding in order of elution, **9** (26.6 mg, 23%) as a UV band and **8** (5.6 mg, 11.3%) as an orange band.

Reaction of **8** with $(PhNH)_2CS$: A solution of **8** (36.2 mg, 0.046 mmol) and $(PhNH)_2CS$ (13.2 mg, 0.058 mmol) in THF (20 ml) was stirred at room temperature for 4d. After removing the solvent **9** was isolated as a UV band by TLC (Al_2O_3, 1:1 CH_2Cl_2:C_6H_{12}); (13.1 mg, 15.4%).

Anal. calcd. for $C_{28}H_{22}N_4O_2RuS_2{\cdot}0.25\ CH_2Cl_2$ (632.9): C, 53.6; H, 3.58; N, 8.85. Found: C, 53.84; H, 3.58; N, 8.90.

4.5.8 Synthesis of $(\mu_2\text{-}H)Ru_3(CO)_8(PPh_3)(\mu_3,\eta^2\text{-}SCNHPhNPh)$ (10)

A solution of 8 (78.4 mg, 0.100 mmol) and PPh_3 (27.6 mg, 0.105 mmol) in THF (20 ml) was stirred at room temperature for 24h. The solvent was removed and the residue dissolved in CH_2Cl_2 and chromatographed on TLC plates (Al_2O_3, 30:70 CH_2Cl_2:C_6H_{12}). Two major bands eluted. The first band contained compound **11** (trace). The second band was primarily compound **10** (69.9 mg, "68.7%") slightly contaminated with **11**. Crystals of **10** were obtained from CH_2Cl_2 solutions at room temperature.

Anal. calcd. for $C_{39}H_{27}N_2O_8Ru_3PS$ (1018): C, 46.0%; H, 2.67%; N, 2.75%. Found: C, 45.7%; H, 2.78%; N, 2.46%.

4.5.9 Synthesis of $(\mu_2\text{-}H)Ru_3(CO)_7(PPh_3)_2(\mu_3,\eta^2\text{-}SCNHPhNPh)$ (11)

A solution of $Ru_3(CO)_{12}$ (50.0 mg, 0.064 mmol) and PPh_3 (35.2 mg, 0.134 mmol) in THF (20 ml) was stirred at room temperature for 24h. The solvent was removed and the residue dissolved in CH_2Cl_2 and chromatographed on TLC plates (Al_2O_3, 30:70 CH_2Cl_2:C_6H_{12}). Only one major band migrated and consisted primarily of **11** (27mg, 34%) but

contained traces of **10**. It was not possible to obtain a pure sample of compound **11**; a trace amount of **10** was persistently present, therefore, no elemental analysis was carried out on **11**.

4.5.10 Synthesis of $Ru_3(CO)_6(\mu_2,\eta^2\text{-}C_6H_5)(\mu_2\text{-}PPh_2)(PPh_3)(\mu_3,\eta^2\text{-}SCNHPhNPh)$ (12)

A solution of **8** (48 mg, 0.061 mmol) and PPh_3 (17 mg, 0.064 mmol) in toluene (20 ml) was refluxed for 2h forming a deep red solution. The solvent was removed and the residue dissolved in CH_2Cl_2 and chromatographed on TLC plates (Al_2O_3, 30:70 CH_2Cl_2:C_6H_{12}). Compound **12** was isolated from a major red band located approximately half-way up the plate (20.5 mg, 32.0%). Alternatively, a refluxing, toluene solution of **11** produced **12** in approximately the same yield.

Anal. calcd. for $C_{43}H_{29}O_7Ru_3P_2S\cdot0.5CH_2Cl_2$ (1099.3): C, 47.5%; H, 2.75%.
Found: C, 47.0%; H, 2.94%.

4.5.11 Synthesis of $(\mu_2\text{-}H)Ru_3(CO)_7(\mu_2,\eta^2Ph_2PCH_2CH_2PPh_2)$ $(\mu_3,\eta^2\text{-}SCNHPhNPh)$ (13)

A solution of compound **8** (30 mg, 0.038 mmol) and diphenylphosphinoethane (16 mg, 0.040 mmol) in CH_2Cl_2 (ml) was stirred for 30 minutes. The solvent volume was reduced to approximately 3 ml and an excess of hexanes layered on top. After 24h, the product could be collected as an orange crystalline solid (35.3 mg, 82.5%).

Anal. calcd. for $C_{46}H_{36}N_2O_7Ru_3P_2S\cdot(0.5CH_2Cl_2)$: C, 47.7; H, 3.19; N, 2.39.
Found: C, 47.7; H, 3.39; N, 1.91.

4.5.12 Synthesis of $Ru_6(\mu_2\text{-}CO)_2(CO)_{14}(\mu_4\text{-}S)(\mu_3,\eta^2\text{-}SCNHPhNPh)(\mu_3,\eta^2\text{-}NPhCNHPh)$ (14)

A solution of compound **8** (65 mg, 0.083 mmol) in cyclohexane (25 ml) was prepared in a pressure Schlenk tube. The tube was placed in a preheated 130°C oil-bath and allowed to stir for 30 minutes. Following evaporation of the solvent, the residue was dissolved in dichloromethane and the products separated by preparative TLC (cyclohexane-dichloromethane 75:25). Elution of the solvent gave **13** (46%) as a red band and **14** as a blue band (5% yield) (in order of elution). Compound **14** was isolated from a dichloromethane-

cyclohexane solution; a dichloromethane-pentane solution of **14** at -18°C produced blue-black x-ray quality crystals.

Anal. calcd. for $C_{42}H_{22}N_4O_{16}Ru_6S_2 \cdot 1.00\ CH_2Cl_2\ 0.66\ C_6H_{12}$: C, 34.2; H, 1.95; N, 3.40. Found: C, 34.51; H, 2.19; N, 3.47.

4.5.13 Synthesis of $(\mu_2\text{-H})Ru_6(CO)_{16}(\mu_5\text{-S})(\mu_3,\eta^2\text{-PhNCSNHPh})$ (15)

Direct Synthesis: A solution of $Ru_3(CO)_{12}$ (50 mg, 0.078 mmol) and $(C_6H_5NH)_2CS$ (19 mg, 0.083 mmol) in 25 ml of THF was prepared in a pressure Schlenk tube. The tube was placed in a preheated 130° C oil bath and allowed to stir for 35 minutes. Following evaporation of the solvent, the residue was dissolved in dichloromethane and the products separated by preparative TLC (CH_2Cl_2/C_6H_{12}; 25/75) yielding **15** as the major product (20 mg, 39%).

Thermolysis of $(\mu_2\text{-H})Ru_3(CO)_9(\mu_3,\eta^2\text{-SCNHPhNPh})$ (**8**): A solution of 8 (34 mg, 0.04 mmol) in THF (20 ml) was prepared in a pressure Schlenk tube. The tube was placed in a preheated 130°C oil-bath and the solution stirred for 35 minutes. Following evaporation of the solvent, the residue was dissolved in dichloromethane and the products separated by preparative TLC (CH_2Cl_2/C_6H_{12}; 25/75). Elution of the solvent mixture allowed the separation of **15** as the major product. The fast-moving band contained the previously reported compound $[(\mu_2\text{-H})_2Ru_3(CO)_9(\mu_3\text{-S})]$. The band immediately following contained **15** (13.3 mg, 46%). The remaining two bands contained in order of elution, **14** (1.7 mg, 5.6%) and an unidentified green compound (9.6 mg). Compound **15** was recrystallized from dichloromethane.

Anal. calcd. for $C_{29}H_{12}N_2O_{16}Ru_6S_2$ (1315): C, 26.5%; H, 0.9%; N, 2.1%. Found: C, 26.97%; H, 0.78%; N, 1.90%.

4.5.14 Synthesis of $(\mu_2\text{-H})_6Ru_6(CO)_{14}(\mu_3,\eta^2\text{-SCNHPhNPh})_2$ (16)

A solution of **15** (50 mg, 0.038 mmol) was prepared in an autoclave in CH_2Cl_2 (10 ml). The autoclave was charged with 5bars of H_2 and the solution stirred for 6 hours. After releasing the pressure, the solution volume was reduced and the products separated by

preparative TLC (CH_2Cl_2/C_6H_{12}; 25/75). The fast-moving band contained the previously reported compound $(\mu_2\text{-}H)_2Ru_3(CO)_9(\mu_3\text{-}S)$ (31%). Just below was a band containing the trinuclear complex **8** (25%). Compound **16** was isolated from a bright red band above the residue (13%). Orange-red crystals of **16** were obtained from acetone:heptane solutions (75:25) at -18°C.

Anal. calcd for $C_{40}H_{28}N_4O_{14}Ru_6S_2{\cdot}CH_2Cl_2$: C, 31.9; H, 1.93; N, 3.63. Found: C, 31.9; H, 2.08; N, 3.62.

4.5.15 Synthesis of $Ru_4(\mu_2\text{-}CO)_3(CO)_7(\mu_4\text{-}S)_2\{C(NHCH_3)_2\}$ (17)

A solution of $Ru_3(CO)_{12}$ (128 mg, 0.201 mmol) and $(CH_3NH)_2CS$ (22.6 mg, 0.217 mmol) in THF (30 ml) were prepared in a pressure schlenk tube. The tube was placed into a 130° oil-bath and allowed to stir for 35 minutes. Following evaporation of the solvent the residue was dissolved in CH_2Cl_2 and the products separated by preparative TLC (CH_2Cl_2/C_6H_{12} : 25/75) yielding **17** as a dark orange band (15.5mg, 12.6%). Orange crystals of **17** were grown at room temperature from a CH_2Cl_2 solution.

Anal. calcd. for $C_{13}H_8N_2O_{10}Ru_4S_2$ (820.6): C, 19.02; H, 0.98; N, 3.41. Found: C, 20.0; H, 1.21; N, 3.59.

4.5.16 Synthesis of $(\mu_2\text{-}H)Ru_6(CO)_{15}(\mu_5\text{-}S)(Me_2S)(\mu_3,\eta^2\text{-}SCNHPhNPh)$ (19)

A solution of **15** (30 mg, 0.023 mmol) and Me_2S (0.075 mmol) in CH_2Cl_2 (10 ml) was stirred at room temperature for 7d. After removing the solvent the residue was redissolved in CH_2Cl_2 and chromatographed on Al_2O_3 TLC plates in 1:3 CH_2Cl_2:C_6H_{12}. The first band contained unreacted **15** while the dark red band just below that was contained **19** (12.6 mg, 40.6%).

Anal. calcd. for $C_{30}H_{18}N_2O_{15}Ru_6S_3$ (1353.4): C, 26.71; H, 1.34; N, 2.08. Found: C, 26.58; H, 1.50; N, 1.98.

4.5.17 Synthesis of $(\mu_2\text{-H})Ru_6(\mu_2\ CO)(CO)_{16}(\mu_5\text{-S})$ $(\mu_3,\eta^2\text{-SCNHPhNPh})$ 20.

Carbon monoxide was bubbled through a room temperature solution of compound **15** (50 mg, 0.038 mmol) in CH_2Cl_2 (10 ml). Upon exposure to CO, the solution color went immediately from red to dark blue. After 30 minutes of CO purge there remained no **15** according to IR spectra of the reaction mixture. The volume of CH_2Cl_2 was reduced to approximately 2 ml by a stream of CO. The remaining solution could be chromatographed on TLC plates (Al_2O_3, 35:65 CH_2Cl_2/C_6H_{12} {CO saturated, CO atmosphere})resulting in the migration of a major blue band. The band was rinsed from the Al_2O_3 support with CH_2Cl_2 into a CO filled schlenk tube. The CH_2Cl_2 used to isolate the substance from the TLC support was removed by a stream of CO. The reversible nature of the CO binding did not allow thorough removal of residual solvent and therefore no accurate weight of the isolated substance could be obtained. Furthermore, an undetermined amount of product was lost to decomposition and conversion back to **15**, thus crystallization provided the most effective means of isolations. According to the IR spectra of the final solution, the reaction was at least 90% complete. Crystallization of dark blue **20** occurred from either CH_2Cl_2, diethylether or acetone maintained under a CO atmosphere at -30°C over a period of 1 week, however none of the crystals thus isolated were suitable for x-ray analysis.

Anal.; calcd. for $C_{30}H_{12}N_2O_{17}Ru_6S_2$ (1343): C, 26.8%; H, 0.9%; N, 2.1%. Found: C, 25.93; H, 1.19; N, 1.84.

4.5.18 Synthesis of $Ru_2(CO)_4(PPh_3)_2(\mu_2,\eta^2\text{-SCNHPhNPh})$ (21) and $(\mu_2\text{-H})Ru_6(CO)_{15}(PPh_3)(\mu_5\text{-S})(\mu_3,\eta^2\text{-SCNHPhNPh})$ (22)

A solution of **15** (64 mg, 0.049 mmol) and PPh_3 (26.8 mg, 0.102 mmol) in C_6H_{12} (20 ml) was stirred for 24h. The solvent was removed and the residue dissolved in CH_2Cl_2 and the products separated by TLC (Al_2O_3, 40/60 Et_2O/C_6H_{12}. Compound **21** was isolated from a leading yellow band (<3% yield) while compound **22** was isolated from a red-brown band (29 mg, 38.2%) located just below a faint red band consisting of the trinuclear compound **12** (trace). Crystals of **22** were grown at room temperature from a 3:1 CH_2Cl_2:C_7H_{16} solution.

22: Anal. calcd. for $C_{46}H_{28}N_2O_{15}PRu_6S_2$ (1550.3): C, 35.64; H,1.82; N,1.81. Found: C, 35.92; H, 1.62; N, 1.86.

4.5.19 Synthesis of $(\mu_2\text{-H})Ru_6(CO)_{15}(L)(\mu_5\text{-S})(\mu_3,\eta^2\text{-SCNHPhNPh})$; L = $P(n\text{-}C_4H_9)_3$ (23), $P(OMe)_3$ (24), $P(OPh)_3$ (25), $(CH)_3CNC$ (26).

A solution of **15** (**23**; 59 mg, 0.045 mmol, **24**; 33.5 mg, 0.025 mmol, **25**; 67.4 mg, 0.051 mmol, **26**; 62.0 mg, 0.047 mmol) in a solvent (cyclohexane, CH_2Cl_2 or THF produced similar results) (20 ml) was prepared in a dried schlenk tube. Under N_2 flow, a solution of the appropriate reagent (**23**: $P(n\text{-}C_4H_9)_3$; 12.0 μL, 0.048 mmol, **24**: $P(OMe)_3$; (3.0 μL, 0.027 mmol, **25**: $P(OPh)_3$; 14μL, 0.054 mmol, **26**: $(CH)_3CNC$; 6 μL, 0.053 mmol) in the appropriate solvent(10 ml) was added dropwise to the stirring solution. The solution color immediately turned a deeper shade of red. The reaction solution was stirred at room temperature for 4-6h. After removing the solvent, the residue was redissolved in CH_2Cl_2 and chromatographed on TLC plates (Al_2O_3, 40:/60 Et_2O/C_6H_{12}). Compounds **23-26** were isolated from prominent red bands located in the lower half of the TLC plates. **23**; 15.3 mg, 22.8%, **24**; 12.2 mg, 34.0%, **25**; 53.4 mg, 65.2%, and **26**; 37.0 mg, 53.0%. Samples for elemental analyses were prepared by recrystallization of the products from CH_2Cl_2 layered with an excess of heptane.

24: Anal. calcd. for $C_{31}H_{21}N_2O_{18}PRu_6S_2$ (1411.0): C, 26.4; H, 1.50; N, 1.99. Found: C,27.15; H, 1.58; N, 2.05.

25: Anal. calcd. for $C_{31}H_{21}N_2O_{18}PRu_6S_2$ (1411.0): C, 26.4; H, 1.50; N, 1.99. Found: C, 27.15; H, 1.58; N, 2.05.

26: Anal. calcd. for $C_{33}H_{21}N_3O_{15}S_2Ru_6{\cdot}0.5\ C_7H_{16}$ (1420.1): C, 30.87; H, 2.06; N, 2.96. Found: C, 29.92; H, 2.02; N, 2.96.

4.5.20 Synthesis of $(\mu_2\text{-H})Ru_6(\mu_2\ CO)(CO)_{15}(L)(\mu_5\text{-S})$ $(\mu_3,\eta^2\text{-SCNHPhNPh})$: L = $P(n\text{-Bu})_3$ 27, $P(OMe)_3$ 28, $P(OPh)_3$ 29, ^{t}BuNC 30.

These syntheses were entirely analogous to the preparation of compound **20**. CO was bubbled through a solution of the appropriate hexanuclear compound (**23-25** and **26**). After 30 minutes the solvent volume was reduced with a stream of CO and the solution purified through preparative TLC carried out in a CO atmosphere with CO saturated solvents. These compounds generally showed greater stability during chromatography than **20**, but thorough removal of solvent was still not possible. Only the CO adduct of **25** (compound **29**) was isolated in a large enough quantity, of sufficient purity for the collection of analytical data.

29: Anal. calcd. for $C_{47}H_{27}N_2O_{19}PS_2Ru_6$ $0.5{\cdot}C_6H_{14}$ (1597.0): C, 36.0; H, 2.05; N, 1.69. Found: C,36.4; H,2.11; N,1.75.

[146] Herzog S., Dehnert J., *Z. Chem.* **1969**, *4*, 1.

[147] Stahl E., *Dünnschichtchromatographie. Ein Laboratoriumshandbuch*, 2. Aufl., Springer, Berlin, **1967**.

[148] Merck, *Mitteilungen zur Dünnschichtchromatographie*, **1985**.

[149] Perrin D.D., Armarego W.L.F., *Purification of Laboratory Chemicals*, 3, Ed., Pergamon Press, Oxford, **1988**.

[150] Bruce M.I., Jensen C.M., Jones N.L., *Inorg. Synth.*, **1989**, *25*, 259.

[151] *Inorg. Synth.*, **1972**, *13*, 92.

[152] Bodensieck U. Chem. Ber.

[153] Bruce M.I., Matisons J.G., Wallis R.C., *Aust. J. Chem.*, **1982**, *35*, 935.

[154] Frey U., Helm L., Merbach A., *High Pres. Res.*, **1990**, *2*, 237.

[155] Bodenhausen G., Kogler H., Ernst R.R., *J. Magn. Res.*, **1984**, *58*, 370.

[156] Sheldrick G.M:, SHELXS-86, *Program for Crystal Structure Determination*, University of Göttingen, **1986**.

[157] Gabe E.J., Le Page Y., Charland J.-P., Lee F.L, *NRCVAX-an Interactive Program System for Structure Analysis, J. Appl. Crystallogr.*, **1989**, *22*, 384.

[158] Gabe E.J., Le Page Y., Charland J.-P., Lee F.L., *NRCVAX-an Interactive Program System for Structure Analysis, J. Appl. Crystallogr.*, **1989**, *22*, 384.

[159] Keller E., SCHAKAL 88, *a* FORTRAN *Program for the Graphical Representation of Molecular and Crystallographic Models*, University Freiburg, **1988**.

[160] Spek A.L., *Acta Crystallogr.*, **1990**, *A46*, C34.

[161] Johnson C.K., ORTEP, Oak Ridge National Laboratory, Oak Ridge, TN, USA, modified for PC (ZORTEP) by L. Zsolnai and H. Pritzkow, University of Heidelberg, Germany, 1994.

V Summary

It was the goal of the present work to investigate the reactions of some sulfur-containing molecules with the group VIII trinuclear metal carbonyls and to explore the reactions of some well-characterized tri- and hexanuclear ruthenium clusters containing the diphenylthioureato ligand.

It has been shown that the cyclic thioether 1,3,5-trithiacyclohexane (ttch), reacts differently with each of the group VIII trinuclear metal carbonyls, $M_3(CO)_{12}$ (M = Fe, Ru, Os). Reaction with $Fe_3(CO)_{12}$ results in fragmentation of the starting cluster and C-S bond cleavage of the ttch to produce the dinuclear species, $Fe_2(\mu_2,\eta^3\text{-}SCH_2SCH_2SCH_2)$ (**1**). In compound **1**, the ttch ligand is bound to the two Fe atoms in a μ_2-mode through one S, and with σ-bonds involving another S and a C atom. The same dinuclear compound has been isolated from reactions of $Fe(CO)_5$ with ttch.[II.47] Triruthenium-dodecacarbonyl reacts with ttch under slightly more mild conditions with substitution of one CO on each Ru atom to yield the trinuclear ttch capped cluster, $Ru_3(\mu_2\text{-}CO)_3(CO)_6(\mu_3,\eta^3\text{-}S_3C_3H_6)$ (**2**).[II.47] X-ray structural analysis of this product shows the intact ttch is bound to the Ru_3 framework through three Ru-S bonds. The resulting higher electron density at the cluster core is compensated by the formation of three bridging carbonyl groups. Different yet, in room temperature reactions, triosmium-dodecacarbonyl substitutes only one CO group to form an Os-S σ-bond with the ttch, to give the substitution product $Os_3(CO)_{11}(S_3C_3H_6)$ (**5**). If Me_3NO is used in the osmium reactions, then C-H bond activation occurs to a limited extent, to produce the cluster $(\mu_2\text{-}H)Os_3(CO)_9(\mu_3,\eta^2\text{-}SCH_2SCH_2SCH)$ (**7**). The previously identified cluster $(\mu_2\text{-}H)Os_3(CO)_{10}(\mu_2\text{-}OH)$ (**6**)[II.73] is found as a side-product in the reaction with Me_3NO. These reactions and their corresponding products are outlined in Figure 35.

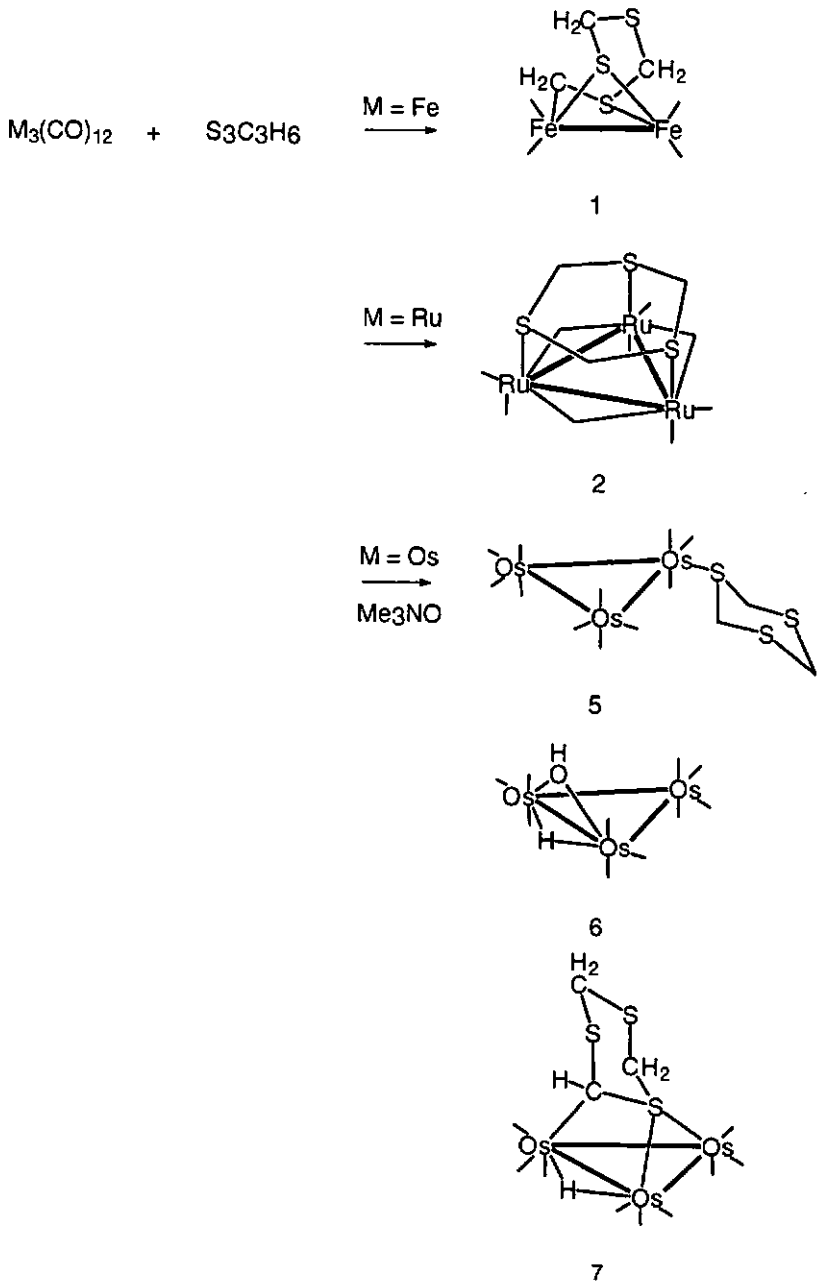

Figure 35: Reactions of $M_3(CO)_{12}$ (M = Fe, Ru, Os) with 1,3,5-trithiacyclohexane.

The question of carbonyl fluxionality in trinuclear, binary transition-metal carbonyl clusters became relevant with the advent of high resolution nuclear magnetic resonance techniques. An established theory describing the mechanism by which this fluxionality proceeds is the "merry-go-round" process.[II.65] This theory postulates intermediate stages in the intramolecular exchange of CO groups among metal atoms of a cluster involving bridging carbonyls. The molecular structure of **2** reveals a set of three bridging carbonyl groups and two sets consisting of three terminal groups each, and models the postulated bridging intermediate. Changes in the ^{13}C NMR spectra with temperature, indicated that **2** was undergoing CO exchange via the "merry-go-round" process. Rate constants and activation parameters for this process in **2**, were obtained from detailed variable temperature ^{13}C NMR experiments, while the types of transition states employed in the fluxional process were provided by variable pressure ^{13}C NMR results.[II.60] Changes in the exchange mechanism due to alterations in the ligand envelope were investigated by substitution of an axial carbonyl group with the two-electron donor t-butylisonitrile to give the cluster $Ru_3(\mu_2\text{-}CO)_3(CO)_5(^tBuNC)(\mu_3,\eta^3\text{-}S_3C_3H_6)$ (**3**), and carrying out the same experiments.

The NMR determined rates for CO exchange in **2** and **3** show a slower process in the ^{t}BuNC substituted cluster. This result can be rationalized by acknowledging the better σ-donor and weaker π-acceptor properties of ^{t}BuNC, which ultimately stabilize the CO-bridged ground-state of **3** relative to that of **2**. On the other hand, the activation volumes determined for **2** and **3** can be considered equal to within experimental error and offer no comparisons among themselves. However, by comparing the results for **2** and **3** with those obtained in similar experiments using the tetranuclear Ir clusters $Ir_4(\mu_2\text{-}CO)_3(CO)_6(\mu_3,\eta^3\text{-}S_3C_3H_6)$ and $Ir_4(CO)_9(\mu_3,\eta^3\text{-}S_3C_3H_6)$,[II.71] it is possible to propose a transition state of the merry-go-round for clusters **2** and **3** with a geometry closer to the limiting dissociative case. That is to say, an intermediate consisting mostly of terminal CO groups is implied. These results are illustrated graphically in Figure 36.

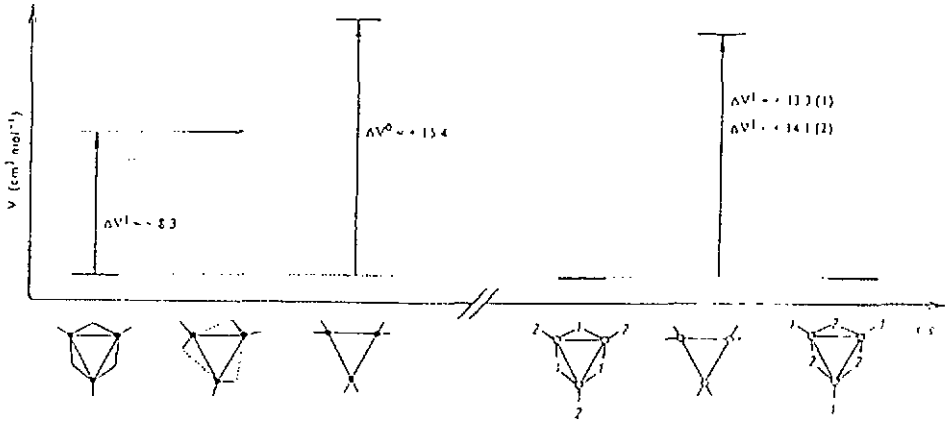

Figure 36: Volume profiles for the merry-go-round process a) in $Ir_4(CO)_9(\mu_3,\eta^3\text{-}S_3C_3H_6)$ (• = Ir) and b) in **2** and **3** (∘ = Ru). Only the basal face of the Ir cluster is shown: r.c. = reaction coordinate.

A derivative of the ligand ttch was prepared by substituting one of each of the methylene hydrogens with benzyl groups to give 2,4,6-tribenzyl-1,3,5-trithiacyclohexane. This new ligand was then reacted with $Ru_3(CO)_{12}$, producing the μ_3 capped cluster $Ru_3(\mu_2\text{-}CO)_3(CO)_6\{\mu_3,\eta^3\text{-}S_3(CHCH_2C_6H_5)_3\}$ (**4**), which exhibits better solubility in common organic solvents as compared to **2**. Single-crystal X-ray structural analysis of **4**, shows the ligand to bind to the Ru_3 skeleton in a manner entirely analogous to **2**, with only slight changes in Ru-Ru or Ru-S bond lengths. One of the methylene hydrogen atoms on each of the benzyl groups, if placed in appropriately calculated position, approaches the oxygen atom of the bridging carbonyl group directly beneath it, at a distance which implies a significant hydrogen bonding interaction. In determining this interaction, it was realized that the oxygen atom of the acetone molecule which crystallized with **4**, displays a significant interaction with the apical hydrogen atoms remaining on the S_3C_3 ring. Furthermore, an intermolecular hydrogen-bonding network was found in the crystal lattice of **4**. The phenyl hydrogens of the pendant benzyl groups were found to interact with the carbonyl oxygens on bridging CO groups of neighboring molecules. A graphical representation of **4** is presented in Figure 37. Reexamination of these types of

contacts in **2** show a similar network, but for **2** the atoms involved are the methylene protons of the tich ligand and the oxygen atoms of the bridging carbonyl groups.

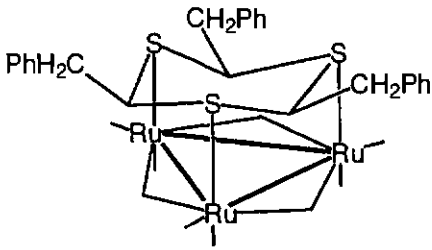

Figure 37: Graphical representation of **4**.

Investigations into the reactivity of the previously isolated, trinuclear ruthenium cluster (μ_2-H)$Ru_3(CO)_9(\mu_3,\eta^2$-SCNHPhNPh) (**8**), comprise the second part of this work. The cluster **8**, is obtained from room temperature reaction of $Ru_3(CO)_{12}$ with $(PhHN)_2CS$ and contains a μ_3,η^2-diphenylthioureato ligand spanning the Ru_3 framework. The S atom is μ_2-bridging while the N is bound in a terminal fashion. A bridging hydride spans the S-bridged Ru-Ru bond.[111,89a]

Reactions of **8** with excess diphenylthiourea result in binding of additional diphenylthioureato ligands with cluster fragmentation to give the mononuclear complex $Ru(CO)_2(SCNHPhNPh)_2$ (**9**). Complex **9** contains the somewhat unusual feature of bidentate diphenylthioureato ligands. Compex **9** is shown graphically in Figure 38.

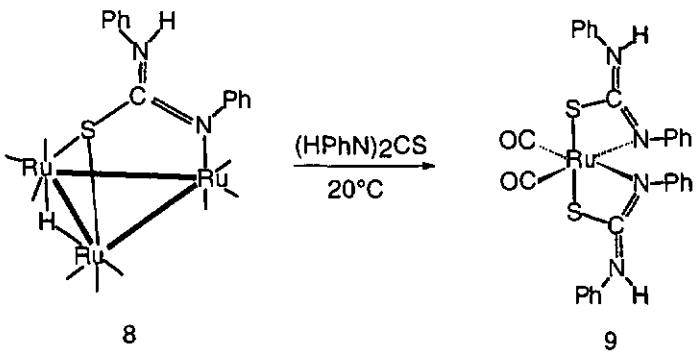

8 9

Figure 38: Reactions of **8** with excess diphenylthiourea.

Substitution of CO ligands on **8** with the two-electron donor ligand PPh_3 was straightforward and took place under relatively mild conditions. One or two equivalents of PPh_3 resulted in substitution at one or both sulfur-bound Ru atoms respectively, to yield the clusters $(\mu_2\text{-H})Ru_3(CO)_8(PPh_3)(\mu_3,\eta^2\text{-SCNHPhNPh})$ (**10**) and $(\mu_2\text{-H})Ru_3(CO)_7(PPh_3)_2(\mu_3,\eta^2\text{-SCNHPhNPh})$ (**11**), wherein the phosphine groups are located *cis* to the bridging sulfur and bridging hydride atoms. A crystal structure determination of **10** showed phosphine substitution of a single CO group produces changes in Ru-Ru and Ru-H-Ru bond lengths but has little effect on the diphenylthioureato ligand. Thermolysis of the disubstituted cluster **11** in toluene, caused P-C bond activation, forming the trinuclear cluster $Ru_3(CO)_6(\mu_2,\eta^2\text{-}C_6H_5)(\mu_2\text{-}PPh_2)(PPh_3)(\mu_3,\eta^2\text{-SCNHPhNPh})$ (**12**) in good yield. Cluster **12** provides only the second example of a σ-π-bridging phenyl group in cluster chemistry. The difunctional phosphine ligand dppe, also replaces equatorial CO groups on the two S-bound Ru atoms of **8** with σ-bonds to the P atoms producing $(\mu_2\text{-H})Ru_3(CO)_8(\mu_2,\eta^2\text{-}Ph_3CH_2CH_2PPh_3)(\mu_3,\eta^2\text{-SCNHPhNPh})$ (**13**). A crystal structure determination of **13** shows a trinuclear cluster wherein the symmetrically bonded dppe ligand has no effect on either the framework bond lengths or the diphenylthioureato ligand. The mirror plane symmetry present in the starting cluster **8** is slightly perturbed by the *zigzag* nature of the P1-C14-C15-P2 linkage. These substitution reactions of cluster **8** are summarized in Figure 39-40.

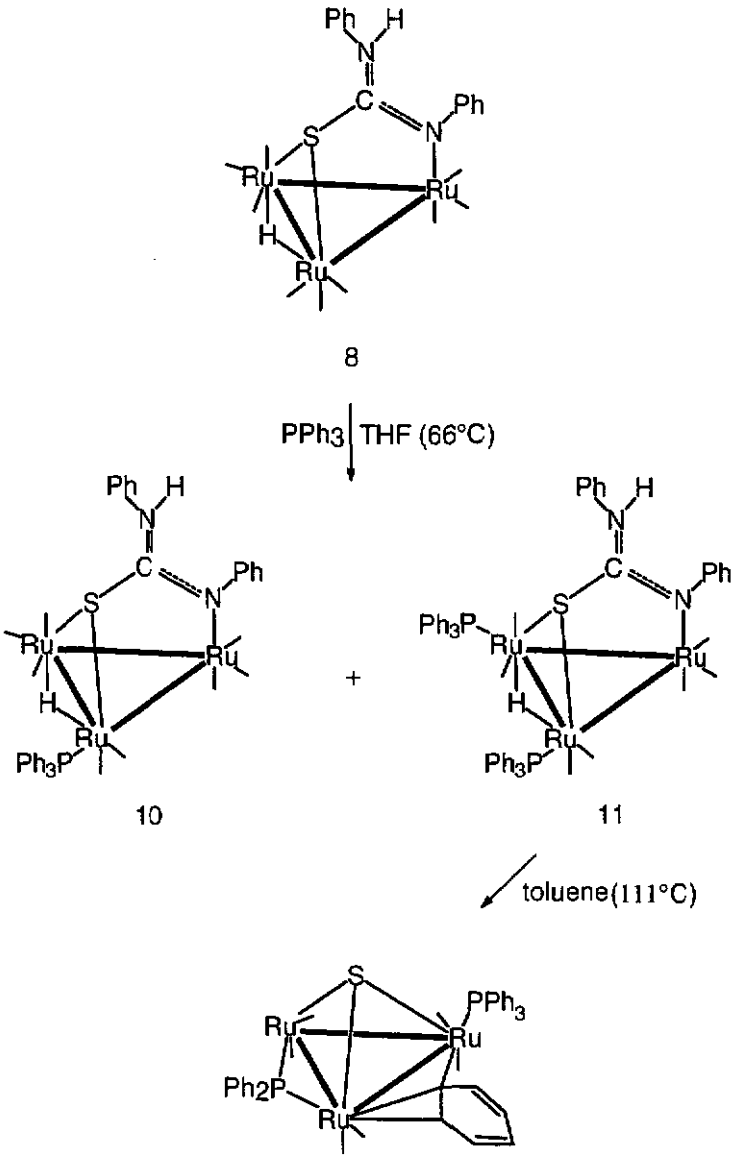

Figure 39: Reactions of $(\mu_2\text{-H})Ru_3(CO)_9(\mu_3,\eta^2\text{-SCNHPhNPh})$ (**8**) with PPh_3.

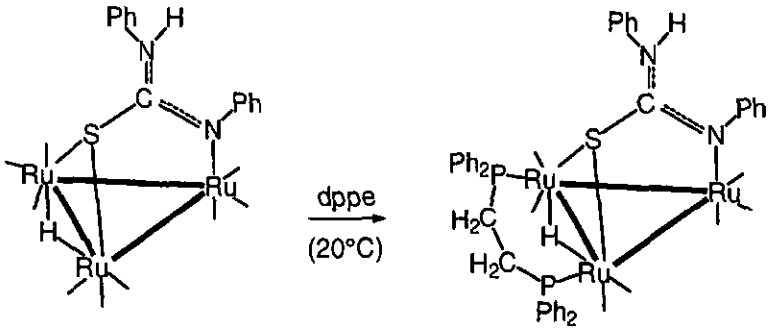

8 13

Figure 40: Reactions of $(\mu_2\text{-H})Ru_3(CO)_9(\mu_3,\eta^2\text{-SCNHPhNPh})$ (**8**) with diphenylphosphinoethane (dppe).

Thermolysis reactions of **8** resulted in several products, two of which were successfully characterized through single-crystal X-ray structural analysis.[111,116d,120] These are hexanuclear clusters, each containing diphenylthioureato ligands in combination with other ligands.

The first is a low-yield product which falls into the category of hexanuclear Ru *boat*-type clusters, and was identified as $Ru_6(\mu_2\text{-CO})_2(CO)_{14}(\mu_4\text{-S})(\mu_3,\eta^2\text{-NPhCNHPh})(\mu_3,\eta^2\text{-SCNHPhNPh})$ (**14**). Its molecular structure (see Figure 41) shows a square base of four Ru atoms capped with a μ_4-S, and bridged on opposite edges by two additional Ru atoms. One triangular Ru_3 substructure is spanned by a diphenylthioureato ligand, μ_2-bridging through the S and terminally bound through the N and lying on the side of the metal framework opposite to the μ_4-S. Still on the surface opposite to the μ_4-S and spanning the other triangular Ru_3 substructure is a diaminocarbene fragment, wherein the N atom bridges two Ru atoms and the C is terminally bound. The presence of these two comparatively large ligands causes the triangular substructures to bend up relative to the Ru_4 plane, resulting in the *boat*-like arrangement of the Ru_6 skeleton. A bridging carbonyl group spans each of the bonds connecting the triangular substructures while terminal groups complete the coordination sphere of the remaining Ru atoms. In combination with the carbonyl groups, the ligands donate 46 electrons to the cluster, two in excess of the number needed for a cluster with this polyhedral

arrangement. The electron excess is most likely responsible for the longer Ru-Ru edges. Recently, these clusters are found more often in the final reaction mixtures of thermolyses of lower nuclearity clusters.

The second compound identified from thermolysis reactions of **8** is the principal product and was identified as the hexanuclear Ru cluster $(\mu_2\text{-H})Ru_6(CO)_{16}(\mu_5\text{-S})(\mu_3,\eta^2\text{-}$SCNHPhNPh) (**15**) (see Figure 41). This hexanuclear cluster also consists of a planar Ru_4 base in which each Ru atom is bound to a capping S atom and opposing edges are bridged by additional Ru atoms. One diphenylthioureato ligand was identified in the molecular structure of **15**. As in cluster **14**, the diphenylthioureato ligand spans one of the Ru_3 substructures in a μ_3,η^2-fashion, on the side of the cluster framework opposite to the capping S. The remaining triangular substructure contains only a bridging hydride spanning the Ru bridged edge of the square base. This bridging hydride provides no steric interaction for the diphenylthioureato ligand, thus, the diphenylthioureato-bonded triangular substructure is planar with the Ru_4 square base. In contrast, the apical Ru atom of the remaining Ru_3 triangular substructure forms an angle of 90° with the square base, which in turn allows for a bond between it and the capping sulfur, resulting in a μ_5-S and an overall framework geometry resembling the *sofa* conformer of cyclohexane. If the μ_5-S is considered as a six-electron donor and the diphenylthioureato ligand as a five-electron donor, then together with the hydride, the carbonyl ligands, and the six Ru atoms, **15** contains 92 electrons. For a hexanuclear cluster containing eight metal-metal bonds 92 electrons are required, implying **15** is electronically saturated. However, one of the Ru-Ru bonds connecting the two triangular substructures is quite long and leaves open to question, the possibility of an unsaturated 92-electron cluster with six Ru atoms and only seven metal-metal bonds. Cluster **15** represents not only the sole published example of a hexanuclear Ru cluster displaying a *sofa*-like skeletal arrangement, but also the first example of a pentacoordinate S atom spanning five mutually bonded Ru atoms.

A mechanism for the formation of the hexanuclear clusters **14** and **15** is suggested. Since both these species are isolated from thermolysis reactions of the trinuclear cluster **8**, it is proposed that **14** is the product of condensation of two molecules of **8** with C-S bond cleavage at one of the diphenylthioureato ligands, resulting in the μ_4-S and the diaminocarbene ligand, which both bond to the hexanuclear cluster. The cluster **14** then goes on to eliminate the diaminocarbene fragment, causing the apical Ru atom to form a fifth bond to the capping sulfur

to give **15**. The conversion of **14** to **15** could only be realized in very low yield, a result which does not completely rule out the proposed mechanism.

Exposing the hexanuclear cluster **15** to 5 bars of H_2 pressure for approximately six hours, results in formation of a hexanuclear cluster containing diphenylthioureato ligands and several bridging hydrides. A combination of X-ray structural analysis and NMR decoupling experiments gave the exact molecular formula as $(\mu_2\text{-H})_6Ru_6(CO)_{14}(\mu_3,\eta^2\text{-SCNHPhNPh})_2$ (**16**) (see Figure 41). The framework geometry of **16** is again a square base, bridged on opposing edges by two additional Ru atoms, however, this hexagonal arrangement of Ru atoms is now perfectly planar. The Ru_3 triangular substructures are spanned by μ_3,η^2-diphenylthioureato ligands, each bound in a centrosymmetric fashion to opposite sides of the Ru_6 plane. Four bridging hydrides were located in difference Fourier maps during refinement of the crystal data. Two additional bridging hydride atoms were identified in ^{1}H NMR spectra of **16**. These were positioned according to their coupling interactions and symmetry requirements indicated in the NMR spectrum. As stated above, a Ru_6 cluster requires 92 electrons, if eight metal-metal bonds are assumed. In combination the diphenylthioureato ligands, the carbonyl groups and the hydrides, provide 44 electrons and with the Ru atoms the electron count is 92. Similar to the situation in cluster **15**, the extremely long Ru-Ru bonds which connect the two trinuclear substructures are necessary to relieve what would otherwise be unsaturation. In fact the formation of **16** is believed to result from the oligomerization of two highly unsaturated trinuclear fragments produced upon hydrogenation of **15**.

Clusters **14**-**16** are assembled in Figure 41 and represent a series of structural variations in hexanuclear Ru clusters containing diphenylthioureato ligands. Each cluster has assumed a framework geometry which best allows it to accommodate the multiply bridging ligands bonded to it.

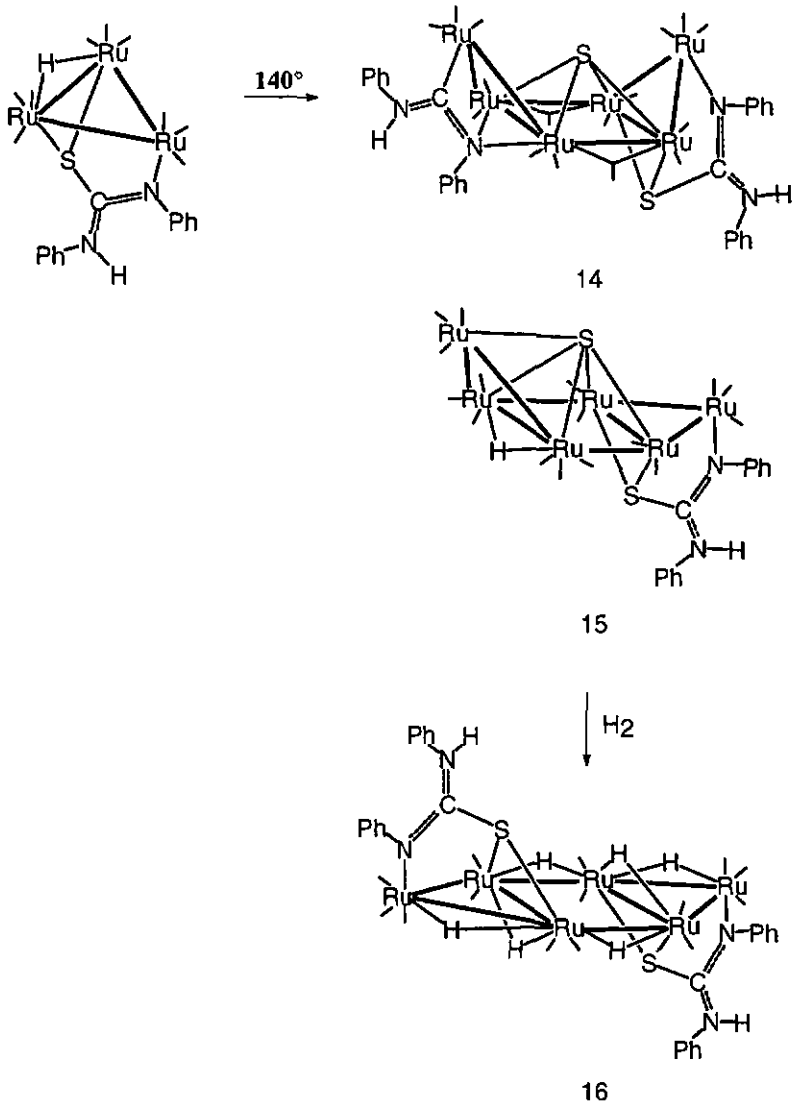

Figure 41: Graphical representation of the three hexanuclear clusters **14-16** showing different framework geometries.

Anticipating a hexanuclear *boat*-like cluster, thermolysis reactions of the trinuclear dimethylthiourea analogue of **8**, $(\mu_2\text{-H})Ru_3(CO)_9(\mu_3,\eta^2\text{-SCNHMeNMe})$, were carried out. Although traces of a hexanuclear species were found in the final reaction mixture, the major product of these reactions was the tetranuclear cluster $Ru_4(\mu_2\text{-CO})_3(CO)_7(\mu_4\text{-S})(C(NHMe_2)_2)$ (**17**). Structural analysis of this product identified the number of diaminocarbene ligands present as one. This cluster is illustrated in figure 42.

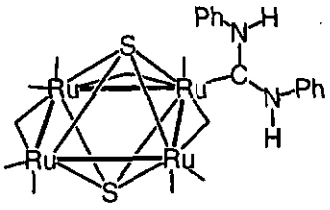

Figure 42: Thermolysis reactions of $(\mu_2\text{-H})Ru_3(CO)_9(\mu_3,\eta^2\text{-SCNHMeNMe})$ to produce cluster $Ru_4(\mu_2\text{-CO})_3(CO)_7(\mu_4\text{-S})(C(NHMe_2)_2)$ (**17**).

Pursuing the possibility of reactions at the naked sulfur in cluster **15**, several attempts were made to add Lewis acid-type species at this site. None of the reagents used succeeded in adding to the capping sulfur. In reactions of **15** with different sources of BH_3, the reagent was shown to behave as a hydrogen source, producing unsaturated intermediates which underwent oligomerization to relieve their electron deficiencies. In contrast to reactions with molecular hydrogen however, the portion of **15** spanned by the diphenylthiourea ligand was not involved in the oligomerization. In this instance, unsaturated trinuclear sulfur-capped species were generated which combined to produce the previously isolated $\{Ru_3(CO)_8(\mu_4\text{-S})\}_3$ (**18**)[III.135b]. When the source of BH_3 used was the adduct $Me_2S{\cdot}BH_3$, then carbonyl substitution of **15** was also observed to give the product $(\mu_2\text{-H})Ru_6(CO)_{15}(Me_2S)(\mu_5\text{-S})(\mu_3,\eta^2\text{-SCNHPhNPh})$ (**19**). This same product was found in reactions of **15** with Me_2S. The site of substitution was later confirmed by X-ray structural analysis of the t-butylisonitrile derivative. The reactions of **15** with these various reagents are outlined in Figure 43.

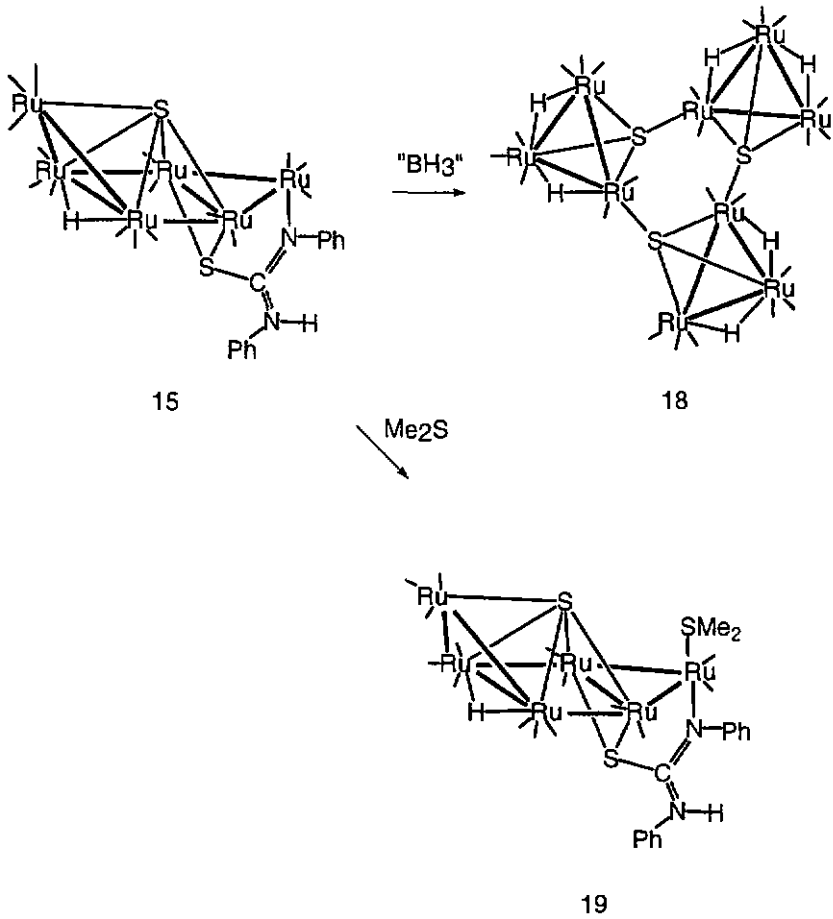

Figure 43: Reactions of **15** with sources of BH_3 and Me_2S.

In manipulations of **15**, it was realized that even a slight excess of CO caused the formation of a deep blue species with an IR indicating structural difference from **15**. By passing CO through solutions of **15** for short periods of time, this blue species could be generated almost quantitatively. If the blue solution was left under an N_2 atmosphere, quantitative conversion back to **15** occurred. Preparative TLC under a CO atmosphere could be used to isolate the blue compound, but the highly reversible nature of the reaction left direct

crystallization as a more productive route. Unfortunately, none of the crystals produced in this manner were of X-ray quality and so definitive identification of the blue species was not possible. Through spectral analysis (IR, ^{1}H NMR and FAB-MS) as well as analytical data (elemental analysis), a simple addition of CO across one of the longer Ru-Ru bonds of **15** to produce the cluster (μ_2-H)Ru$_6$(μ_2-CO)(CO)$_{16}$(μ_5-S)(μ_3,η^2-SCNHPhNPh) (**20**) is offered. A graphical representation of this product is presented in Figure 44. The cluster **20** is most likely a hexanuclear Ru cluster with seven metal-metal bonds and a bridging CO group. The combination of ligands in **20** provide 46 electrons and allow for an electron count of 94. The ease with which **15** and **20** interconvert indicates that the potential energy surface along the reaction coordinate (**15** ↔ **20**) has a very low barrier.

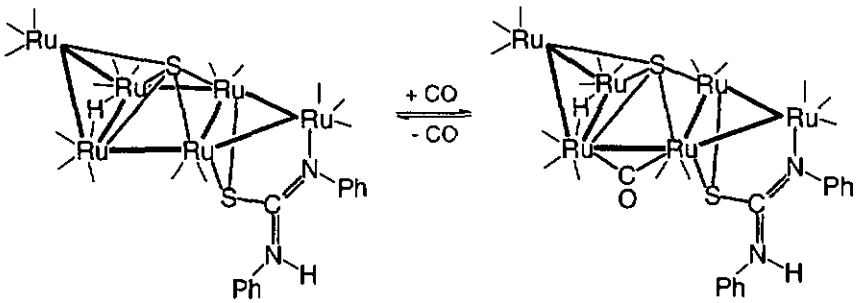

Figure 44: Proposed addition of CO to **15**.

Oftentimes, a simple substitution of CO with an alternative two-electron donor produces an isoelectronic species which will crystallize more efficiently than the parent compound. With this in mind, a series of derivatives of **15** were prepared, hoping that they too would display reversible CO binding but generate X-ray quality crystals. While a slightly more stable CO adduct was discovered in the phosphite derivatives, some interesting differences in the behavior of **15** towards the various two-electron donor ligands was also found.

In room temperature reactions of **15** with PPh$_3$, the monosubstituted derivative was isolated but two other products were also present in non-negligible quantities. The first was the trinuclear cluster Ru$_3$(CO)$_6$(μ_2-C$_6$H$_5$)(μ_2-PPh$_2$)$_2$(μ_3,η^2-SCNHPhNPh) (**12**) (see Figure 39), isolated in thermolysis reactions of (μ_2-H)Ru$_3$(CO)$_7$(PPh$_3$)$_2$(μ_3,η^2-SCNHPhNPh) (**11**). The

second was a dinuclear compound of the form, $Ru_2(CO)_4(PPh_3)_2(\mu_3,\eta^2\text{-}SCNHPhNPh)$ (**21**) (see Figure 45). These two species further suggest the multitude of reactive intermediates available from **15**. The third product was characterized through a single-crystal X-ray structural determination as $(\mu_2\text{-}H)Ru_6(CO)_{15}(Me_2S)(\mu_5\text{-}S)(\mu_3,\eta^2\text{-}SCNHPhNPh)$ (**22**). The molecular structure of **22** shows substitution of a CO group on the μ_5-S bound Ru atom occupying the apical position. The diphenylthioureato ligand remains undisturbed by this substitution. The bridging hydride however, experiences a different chemical environment as evidenced by the downfield shift in its ^{1}H NMR signal.

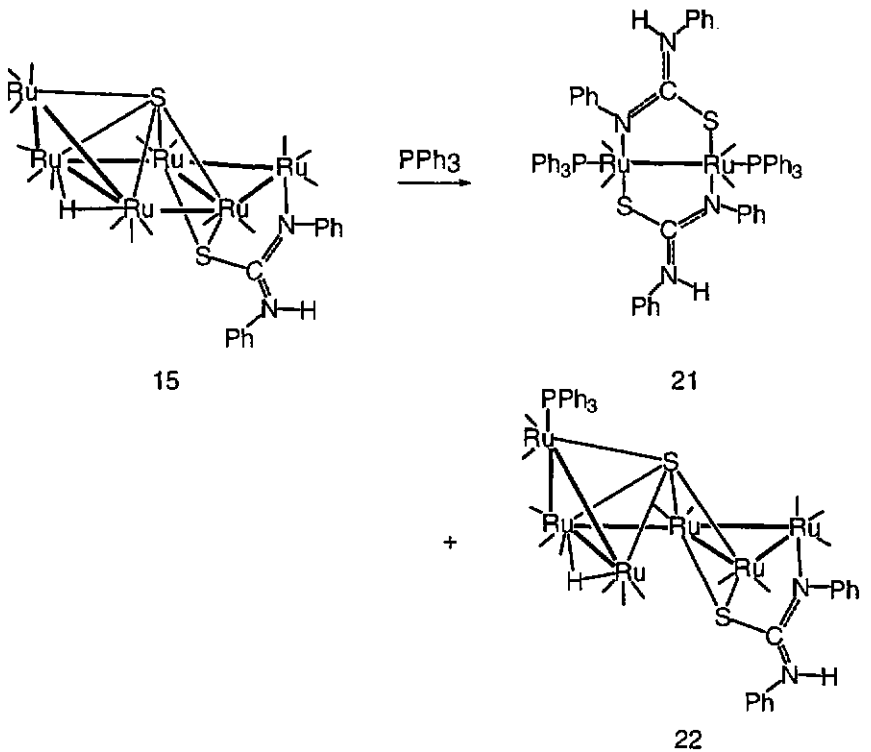

Figure 45: Reactions of **15** with PPh_3 and the subsequent reaction of **22** with CO.

Low-temperature NMR spectra indicated the presence of two isomers of **22**. These are believed to differ only by a rotation of the PPh_3 ligand. At the metal framework itself, one observes significant changes in Ru-Ru bond lengths. One of the Ru-Ru bonds between the two

triangular substructures elongates by approximately 20 pm. This opening-up of the cluster framework changes the chemical environment experienced by the bridging hydride. Moreover, this result shows the weak nature of this metal-metal interaction in **15**. The change in the skeletal structure of the cluster no longer allows for reversible binding of CO. Exposing **22** to one atmospheres of CO resulted in limited reaction, wherein the major product was the trinuclear cluster **8**. The reactions of **15** with PPh_3 are outlined in Figure 45.

Carbonyl substitution at an alternative metal center in **15** occurs in the presence of any of the two-electron donor ligands $P(n\text{-}Bu)_3$, $P(OMe)_3$, $P(OPh)_3$ and ^{t}BuNC (and Me_2S as mentioned previously) to produce the compounds $(\mu_2\text{-}H)Ru_6(CO)_{15}(P(n\text{-}Bu)_3)(\mu_5\text{-}S)(\mu_3,\eta^2\text{-}SCNHPhNPh)$ (**23**), $(\mu_2\text{-}H)Ru_6(CO)_{15}(P(OMe)_3)(\mu_5\text{-}S)(\mu_3,\eta^2\text{-}SCNHPhNPh)$ (**24**), $(\mu_2\text{-}H)Ru_6(CO)_{15}(P(OPh)_3)(\mu_5\text{-}S)(\mu_3,\eta^2\text{-}SCNHPhNPh)$ (**25**), and $(\mu_2\text{-}H)Ru_6(CO)_{15}(^t\text{BuNC})(\mu_5\text{-}S)(\mu_3,\eta^2\text{-}SCNHPhNPh)$ (**26**). An X-ray structural determination of **26** confirmed the site of substitution at the apical Ru atom of the diphenylthioureato spanned triangular substructure of **15**. The Ru-Ru bond lengths as well as the structural features of the diphenylthioureato ligand show little change from those of the parent cluster **15**. These reactions are shown in Figure 46.

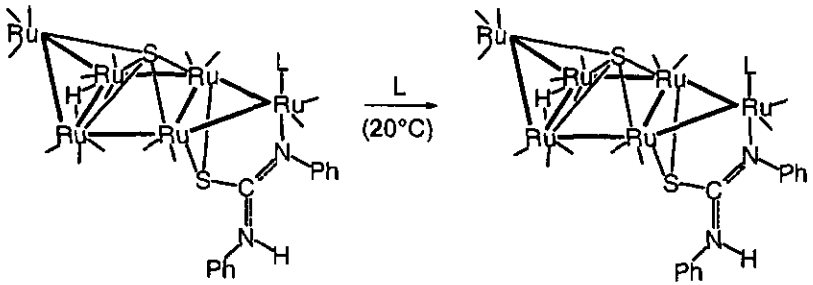

L = P(n-Bu)3(**23**)
= P(OMe)3(**24**)
= P(OPh)3 (**25**)
= t-BuNC (**26**)

Figure 46: Reactions of **15** with $P(n\text{-}Bu)_3$, $P(OMe)_3$, $P(OPh)_3$ and ^{t}BuNC.

The monosubstituted products **23-26** display the same tendencies toward addition of CO as that observed for **15**. That is to say, exposing a solution of any of **23-26** to CO, caused formation of a blue species showing a similar IR spectrum with a ν_{CO} in the bridging carbonyl region. All these blue species were converted easily back to their respective monosubstituted starting clusters. The n-butylphosphine derivative was the least stable of the CO adducts while the phosphite derivatives were stable enough that they could be effectively purified with preparative TLC (provided the eluting solvent was CO saturated and a relatively high concentration of CO was maintained in the TLC cuvette). The t-butylisonitrile derivative could also be purified with preparative TLC, but two blue species were observed, only one of which was stable enough to characterize. As for **20**, crystallization was possible but no X-ray quality crystals could be obtained. However, FAB-MS and elemental analysis of the triphenylphosphite derivative show results analogous to those obtained for **20**, thus, the following molecular formulas for the products, **27-30**, are proposed; $(\mu_2\text{-H})Ru_6(\mu_2\text{-CO})(CO)_{15}\{P(n\text{-Bu})_3\}(\mu_5\text{-S})(\mu_3,\eta^2\text{-SCNHPhNPh})$ **(27)**, $(\mu_2\text{-H})Ru_6(\mu_2\text{-CO})(CO)_{15}\{P(OMe)_3\}(\mu_5\text{-S})(\mu_3,\eta^2\text{-SCNHPhNPh})$ **(28)**, $(\mu_2\text{-H})Ru_6(\mu_2\text{-CO})(CO)_{15}\{P(OPh)_3\}(\mu_5\text{-S})(\mu_3,\eta^2\text{-SCNHPhNPh})$ **(29)** and $(\mu_2\text{-H})Ru_6(\mu_2\text{-CO})(CO)_{15}(^t\text{BuNC})(\mu_5\text{-S})(\mu_3,\eta^2\text{-SCNHPhNPh})$ **(30)**. A general representation of **27-30** is presented in Figure 47.

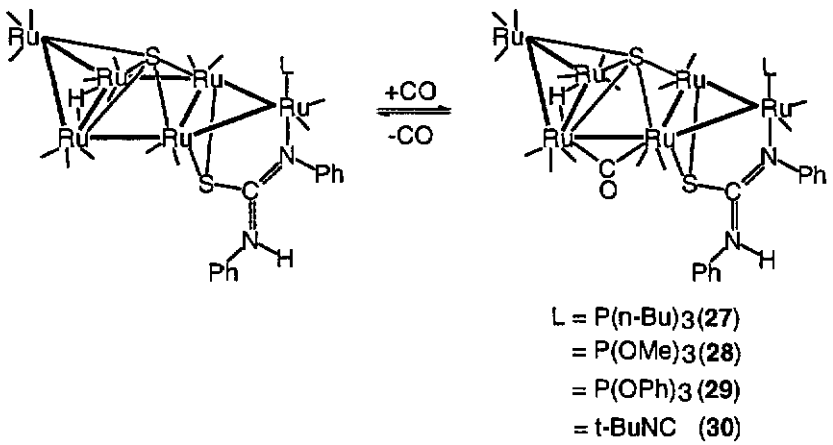

Figure 47: Basic structure of clusters **27-30**.

Résumé

Le but de cette étude était d'étudier les réactions des molécules contenant du soufre avec les clusters trinucléaires carbonylés des métaux de transition du huitième groupe ainsi que de caractériser les réactions de certains clusters de ruthénium hexa- et tri-nucléaires et contenant le ligand diphénylthiourea.

La première partie de ce travail est consacrée aux réactions du thioéther cyclique, 1,3,5-trithiacyclohexane (ttch) avec les carbonyles trinucléaires $M_3(CO)_{12}$ (M = Fe, Ru, Os). La réaction de $Fe_3(CO)_{12}$ avec ttch résulte principalement à une fragmentation du cluster original ainsi qu'à une activation de la liaison C-S de ttch et produit le composé dinucléaire $Fe_2(CO)_6(\mu_2,\eta^2\text{-}SCH_2SCH_2SCH_2)$ (**1**). Dans le composé **1**, le ligand du ttch est lié par une liaison μ_2-S et par des liaisons simples avec un autre atome de soufre ainsi qu'avec l'atome de carbone à côté. Le même composé a été isolé par des réactions de $Fe(CO)_5$ avec du ttch.[II.47] Le dodécacarbonyle de triruthénium réagit avec le ttch sous des conditions plus douces avec substitution d'un groupe carbonyle de chaque atome de ruthénium, afin de produire le cluster trinucléaire, $Ru_3(\mu_2\text{-}CO)_3(CO)_6(\mu_3,\eta^2\text{-}S_3C_3H_6)$ (**2**).[II.47] Une analyse structurale par rayons X du produit **2** montre que le ligand ttch intact est lié à l'ossature du Ru_3 par trois liaisons Ru-S. La densité plus élevée au noyau de cluster qui en résulte, est compensée par la formation de trois groupe carbonyles pontés. Dans les réactions à température ambiante le triosmium dodécacarbonyle substitue un groupement CO seulement, en créant une liaison simple entre l'osmium et le soufre afin de produire $Os_3(CO)_{11}(S_3C_3H_6)$ (**5**). Au cas où le Me_3NO est utilisé dans les réactions de $Os_3(CO)_{12}$, une activation limitée de la liaison C-H produit le cluster (μ_2-$H)Os_3(CO)_9(\mu_3,\eta^2\text{-}SCH_2SCH_2SCH)$ (**7**). Le cluster $(\mu_2\text{-}H)Os_3(CO)_{10}(\mu_2\text{-}OH)$[II.73] (**6**), précédemment identifié est un produit secondaire de la réaction avec le Me_3NO. Ces réactions ainsi que les produits correspondants sont présentés à l'illustration 35.

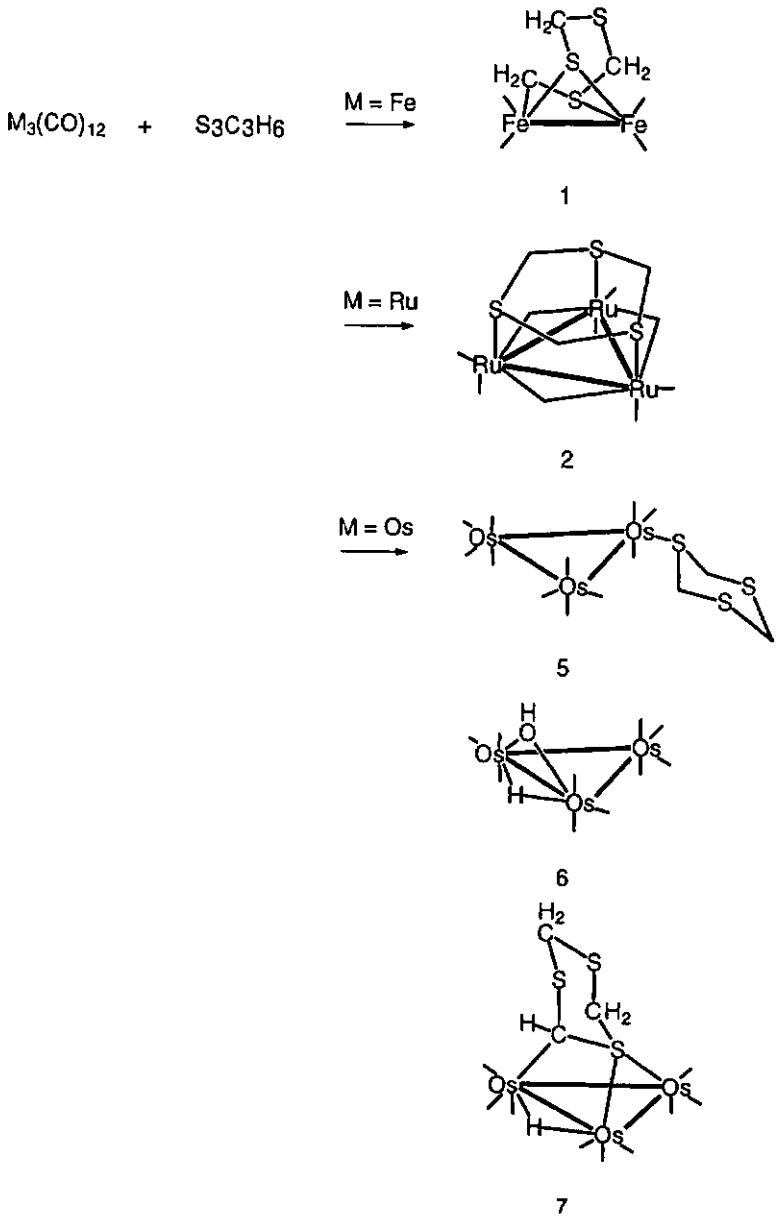

Figure 35: Les réactions de $M_3(CO)_{12}$ (M = Fe, Ru, Os) avec ttch.

La question de la fluxionalité des carbonyles dans les clusters carbonyles trinucléaires s'est posée avec l'arrivée de la résonance magnétique nucléaire de haute résolution. Une théorie établie décrivant le mecanisme de cette fluxionalité est celle du procédé dit "merry-go-round".[II,65] Cette théorie postule des étapes intermédiaires à l'échange intramoléculaire des groupes CO entre les atomes métalliques d'uo cluster qui contient des carbonyles en pont. La structure moléculaire de **2** révèle une série de trois groupes carbonyles pontants ainsi que deux séries qui chacune consiste de trois groupes carbonyles terminaux qui sert de modèle pour l'intermédiaire ponté postulé.[II,54] Les changements de spectre RMN en fonction de la température indiquent que **2** subi uo échange de CO en suivant le procédé "merry-go-round". Les constantes de vitesse ainsi que les paramètres d'activation de ce procédé pour **2** ont été obtenus à travers des expériences ^{13}C RMN à pression variable.[II,60] Les changements du mécanisme d'échange dû à des modifications de la sphère des ligands ont été étudiés par substitution d'un groupe carbonyle axial avec le donneur de deux électrons, t-butylisonitrile, afin de produire le cluster $Ru_3(\mu_2\text{-}CO)_3(CO)_5(^tBuNC)(\mu_3,\eta^3\text{-}S_3C_3H_6)$ (**3**), et en réalisant les mêmes expériences.

Les constantes de vitesse pour l'échange des groupes CO de **2** et **3**, déterminées par RMN, indiquent un cours d'échange plus lent pour le cluster **3** qui contient le ligand t-BuNC. L'abaissement de la constante de vitesse pour l'échange des groupes CO de **3** vient des meilleurs propriétés σ-donneurs du ligand t-BuNC ainsi que de ses propriétés π-accepteur plus faible. Ces caractéristiques rendent l'état non-excité, avec les groupes CO pontantss de **3**, plus stable comparé au même état de **2**. Par contre les volumes d'activation déterminés pour les clusters **2** et **3** doivent être considérés comme étant égaux dans la limite d'erreur expérimentale. En comparant les volumes d'activation des composés **2** et **3** à eux obtenus lors d'une expérience analogue en utilisant le cluster $Ir(CO)_9(\mu_3,\eta^3\text{-}S_3C_3H_6)$,[II,71] il est possible de proposer un état de transition pour le "merry-go-round" de **2** et **3** ayant un géométrie plus proche du cas limité dissociatif. Ces résultats son présentés à la figure 36.

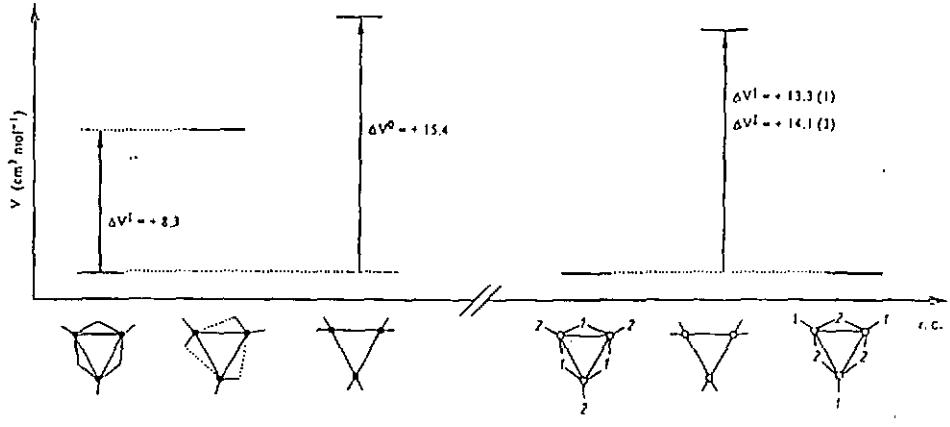

Figure 36: Les "volume profiles" pour le processus "merry-go-round" de a) $Ir_4(CO)_9(\mu_3,\eta^3\text{-}S_3C_3H_6)$ (• = Ir) et b) pour **2** et **3** (○ = Ru).

Un dérivé du ligand ttch a été préparé par substitution d'un de chaque hydrogène méthylène avec les groupes benzylique en donnant 2,4,6-tribenzyl-1,3,5-trithiacyclohexane. Le nouveau ligand réagit avec le dodécacarbonyle de triruthénium afin de produire le cluster $Ru_3(\mu_2\text{-}CO)_3(CO)_5\{\mu_3,\eta^3\text{-}(SCHCH_2C_6H_5)_3\}$ (**4**) qui contient le ligand de ttch substitué lié de la même façon μ_3 que le cluster **2** (Fig. 37). Le cluster **4** est plus soluble dans les solvants organiques typiques (CH_2Cl_2, THF, etc.) comparé à **2**. La détermination de la structure moléculaire de **4** par rayons X indique très peu de changement de la longueur des liaisons Ru-Ru ou Ru-S quoique le ligand soit rattaché a l'ossature Ru_3 d'une manière analogue à **2**. La distance entre un des atomes hydrogène des groupes méthylènes et l'atome d'oxygène du groupe CO situé directement dessous indique la formation d'une liaison hydrogène importante. En déterminant cette intéraction il a été réalisé que l'atome d'oxygène de la molécule d'acétone qui se trouve dans la maille élémentaire interagit avec les hydrogènes apicaux de l'anneau S_3C_3. De plus un système de liaisons hydrogène intermoléculaire a été trouvé dans le réseau cristallin de **4**. Ces intéractions intermoléculaires se passent entre les hydrogènes phénylique des groupes benzylique et les atomes d'oxygène CO appartiennent à une molécule voisine. En ré-examinant les contacts intermoléculaires de **2**, un réseau similaire a été trouvé. Pour

le cluster **2**, ce sont les hydrogènes méthlyléniques du ligand ttch qui interagissent avec les atomes d'oxygènes d'un groupe CO ponté.

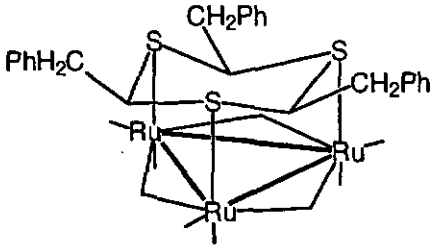

Figure 37: La representation graphique de **4**.

Dans la deuxième partie de cette thèse quelques réactions du cluster trinucléaire de ruthénium, $(\mu_2\text{-H})Ru_3(CO)_9(\mu_3,\eta^2\text{-SCNHPhNPh})$ (**8**), ont été étudiées. Le cluster **8** a été précédement isolé à partir des réactions à température ambiante avec le $Ru_3(CO)_{12}$ et le $(PhHN)_2CS$.[II,104a] Ce cluster contient un ligand μ_3,η^2-thiouréato pontant une ossature métallique triangulaire. L'atome de soufre du ligand lie deux atomes de ruthénium alors que l'atome d'azote est coordonné d'une manière terminale au troisième atome de Ru. Un ligand hydrure traverse la liaison Ru-Ru qui contient le pont soufré.

La réaction de **8** avec un excès de $(PhHN)_2CS$ à température ambiante aboutit à une fragmentation du cluster original pour produire le complexe mononucléaire $Ru(CO)_2(SCNHPhNPh)_2$ (**9**). Le complexe **9** contient de ligands bidentés thiouréatos et est présenté dans la figure 38.

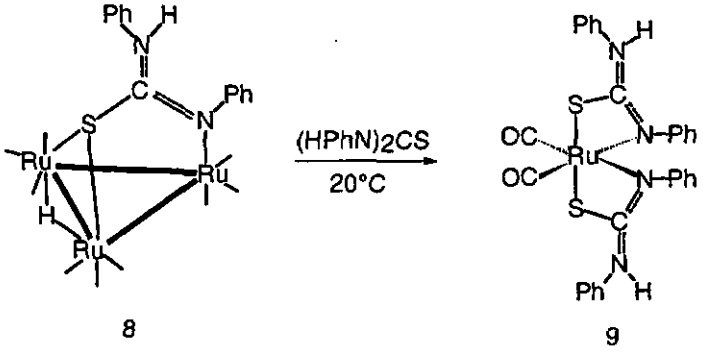

8 9

Figure 38: La reaction de **8** avec un excès de diphéoylthiourea.

La substitution des groupes CO de **8** par le ligand PPh_3 a été simple et directe. Les réactions de **8** avec un ou deux équivalents de PPh_3 ont donné le produit mono- ou disubstitué respectivement, $(\mu_2\text{-H})Ru_3(CO)_8(PPh_3)(\mu_3,\eta^2\text{-SCNHPhNPh})$ (**10**) et $(\mu_2\text{-H})Ru_3(CO)_7(PPh_3)_2(\mu_3,\eta^2\text{-SCNHPhNPh})$ (**11**), dans lequel les groupes PPh_3 sont situés aux atomes de ruthénium pontés par le soufre. Une détermination structurale par rayons X du cluster **10** montre que la substitution d'un groupe CO par une phosphine n'a aucune influence sur le ligand diphénylthioureato quoique elle modifie les longueurs des liaisons Ru-Ru et Ru-H-Ru. La thermolyse du cluster **11** disubstitué dans du toluène cause l'activation de la liaison P-C en formant le cluster trinucléaire $Ru_3(CO)_6(\mu_2\text{-}C_6H_5)(\mu_2\text{-}PPh_2)_2(\mu_3,\eta^2\text{-SCNHPhNPh})$ (**12**) avec un bon rendement. Le cluster **12** est le second exemple d'un groupe phénylique ponté de façon "σ-π" dans la chimie du ruthénium. Le ligand de phosphine bifonctionnel dppe remplace les groupe CO équatoriaux qui sont rattachés aux deux atomes Ru, pontés par un soufre, de la molécule **8** par une liaison simple avec les atomes de phosphore en produisant $(\mu_2\text{-H})Ru_3(CO)_7(\mu_2,\eta^2\text{-}Ph_3PCH_2CH_2PPh_3)(\mu_3,\eta^2\text{-SCNHPhNPh})$ (**13**). Une détermination structurale de **13** montre un cluster trinucléaire dans lequel le ligand dppe qui est lié symétriquement n'a aucun effet ni sur la longueur des liaisons métalliques ni sur le ligand diphénylthioureato. La symétrie par rapport au plan miroir du cluster **8** est modérément perturbé par la nature "zigzag" de la chaîne P1-C14-C15-P2. Ces réactions de substitutions du cluster **8** sont présentées a la figure 39-40.

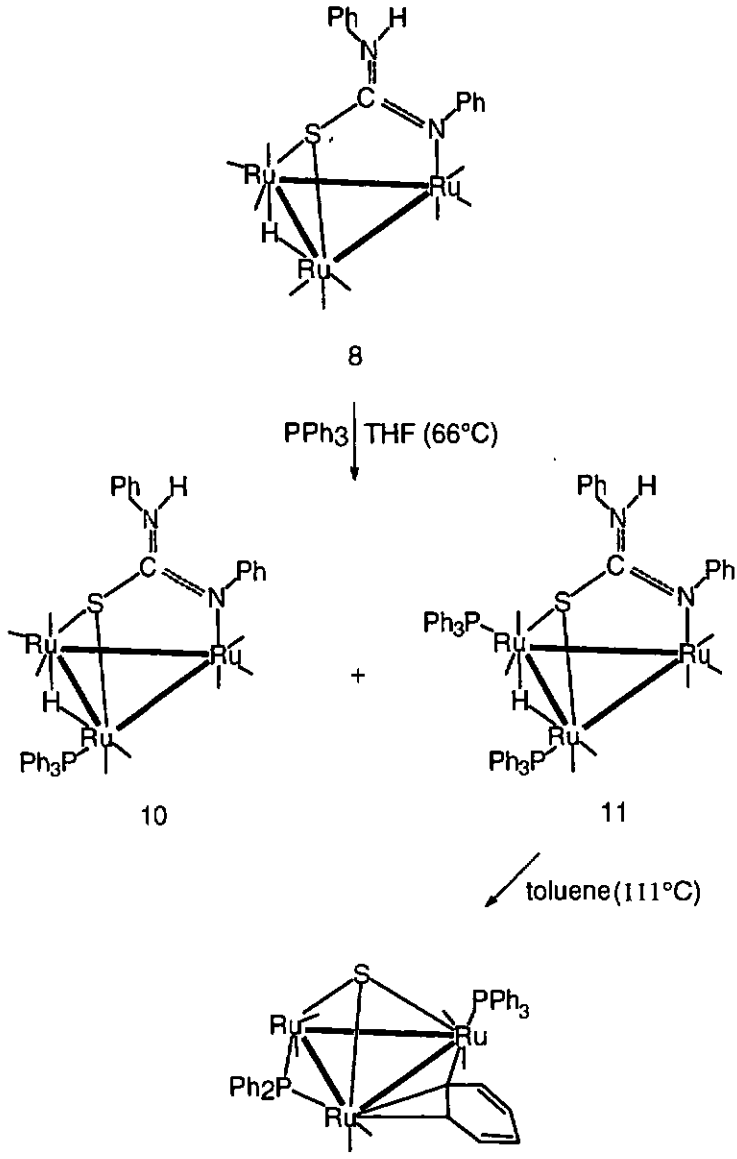

Figure 39: Les réactions de **8** avec le PPh_3.

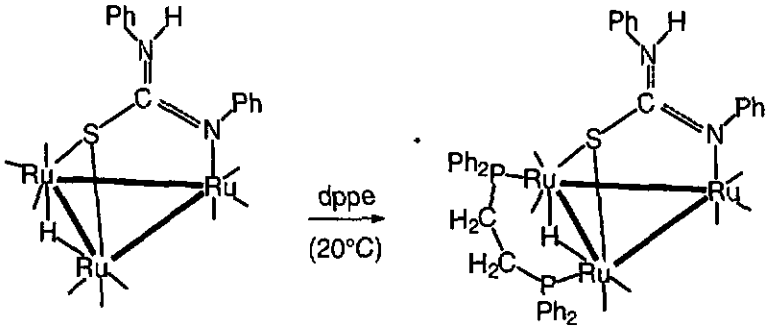

8 13

Figure 40: La réaction de (**8**) avec diphénylphosphinoéthane (dppe).

Les réactions de thermolyse de **8** ont donné plusieurs produits parmi lesquels deux clusters ont été caractérisés par une analyse structurale aux rayons X.[111,118,120] Ceux-ci sont des clusters hexanucléaires chacun contenant un ligand diphénylthioureato en combinaison avec d'autres ligands.

Le premier est un produit de bas rendement qui appartient à la catégorie des clusters hexanucléaires du ruthénium de type bateau et a été identifié comme étant $Ru_6(\mu_2\text{-}CO)_2(CO)_{14}(\mu_4\text{-}S)(\mu_3,\eta^2\text{-}NPhCNHPh)(\mu_3,\eta^2\text{-}SCNHPhNPh)$ (**14**). Sa structure moléculaire (voir illustration 41) montre une base carré de quatre atomes de ruthénium coiffée par un μ_4-S et ponté sur les extrêmités opposés par deux atomes de ruthénium additionnels. Une substructure triangulaire Ru_3 est liée sous forme de pont par un ligand μ_3-η^2-diphénylthioureato qui se trouve au côté opposé de l'ossature Ru_6. De plus, sur la surface opposée à μ_4-S se trouve un fragment diaminocarbène qui lie sous forme de pont l'autre substructure triangulaire Ru_3 de façon μ_3-η^2. La présence de ces ligands qui sont relativement grands a comme effet de plier les substructures triangulaires par rapport au plan Ru_4 en résultant a l'arrangement de type bateau du squelette Ru_6. Un groupe CO lie les deux liaisons Ru-Ru les plus longs alors que des groupes CO terminaux complètent la sphère de coordination des atomes Ru restants. En combinaison avec les groupes CO les ligands donnent 46 électrons au cluster, deux de plus que le nombre nécessaire pour un cluster avec cet

arrangement polyhédral. L'élongation des liaisons Ru-Ru pontées par les CO est probablement due a l'excès électrons. Récemment ces clusters sont trouvés plus fréquemment dans les produit finaux des réactions de thermolyse des clusters à basse nucléarité.

Le second composé isolé par des réactions de thermolyse de **8** est le produit principal et a été identifié comme étant le cluster hexanucléaire de ruthénium $(\mu_2\text{-H})Ru_6(CO)_{16}(\mu_5\text{-S})(\mu_3,\eta^2\text{-SCNHPhNPh})$ (**15**) (voir illustration 41). Ce cluster hexanucléaire a une base plate de Ru_4 également dont chaque atome de ruthénium est lié avec un soufre coiffe alors que les extrêmes opposés sont pontés par des atomes de Ru additionnels. Néanmoins un seul ligand diphénylthioureato a été identifié dans la structure moléculaire de **15**. Comme pour le cluster **14**, le ligand diphenylthioureato est lié à une des substructures Ru_3 de façon $\mu_3\text{-}\eta^2$, à l'extrêmité de la structure du cluster opposée au soufre coiffé. La substructure triangulaire restante contient un seul hydrure qui ponte les deux ruthénium, déjà pontés par un autre Ru, de la base carrée. Le hydrure ponte ne montre pas d'intéraction avec le ligand diphénylthioureato, c'est pourquoi la substructure triangulaire liée par le $\mu_3\text{-}\eta^2$-diphénylthiouréato se trouve sur le même plan. Par contre l'atome de ruthénium apical de la substructure triangulaire Ru_3 restante forme un angle de 90° avec la base carrée, en formant une liaison entre cet atome et le soufre coiffé, avec comme résultat un μ_5-S et une géométrie de l'ossature qui ressemble la conformation *sofa* de cyclohexane. Si le μ_5-S est considéré comme un donneur de six électrons et le ligand comme un donneur de cinq électrons alors en tenant compte de l'hydrure, des ligands CO ainsi que des six atomes de ruthénium **15** contient 92 électrons. Pour un cluster hexanucléaire avec huit liaisons métal-métal 92 électron sont requis; ceci implique que **15** est électroniquement saturé. Néanmoins une des liaisons Ru-Ru qui lie les deux substructures triangulaires étant très longue pointé vers la possibilité d'un cluster à 92 électrons insaturé contenant six atomes de Ru et seulement sept liaisons métal-métal. Le cluster **15** est le seul exemple publié d'un cluster hexanucléaire qui a un arrangement d'ossature de type *sofa* ainsi que le premier exemple d'un μ_5-S qui ponte cinq atomes de ruthénium mutuellement liés.

Un mécanisme pour la formation des clusters hexanucléaires **14** et **15** est proposé. Ces deux molécules étant isolées à partir de réactions de thermolyse du cluster trinucléaire **8**, il est proposé que **14** est le produit de condensation de deux molécules de **8** avec une coupure d'une

liaison C-S d'un des ligands diphénylthioureato. Ceci résulte à une liaison μ_4-S ainsi qu'à un ligand diaminocarbène qui sont liés au cluster hexanucléaire. Le fragment diaminocarbène du cluster **14** est ensuite éliminé aboutissant à la formation d'une cinquième liaison de l'atome de ruthénium apical avec le μ_5-S pour produire **15**. La conversion de **14** à **15** a un rendement très bas, ceci n'étant pas contraire au mécanisme proposé.

La réaction de **15** sous un atmosphère de cinq bars de H_2 pendant à peu près six heures aboutit à la formation d'un cluster hexanucléaire contenant le ligand diphénylthioureato ainsi que plusieurs hydrures pontés. Une analyse structurale aux rayons X combinée avec des expériences de découplage RMN ont révélé la formule moléculaire exacte, $(\mu_2\text{-}H)_6Ru_6(CO)_{14}(\mu_3,\eta^2\text{-}SCNHPhNPh)_2$ (**16**) (voir illust. 41). La géométrie de l'ossature de **16** est également une base carrée, ayant les extrêmités opposées pontées par deux atomes de Ru additionnels, néanmoins cet arrangement hexagonal des atomes de Ru est parfaitement plate. Les substructures triangulaires Ru_3 sont liées à deux ligands μ_3-η^2-diphénylthioureato, chacun étant lié de façon centrosymmétrique aux cotés opposés du plan Ru_6. Quatre hydrures pontés ont été localisés dans des cartes Fourier de différence lors de l'affinement des données du cristal. Deux hydrures pontant additionnels ont été identifiés dans **16** par RMN. Les positions de ces hydrures ont été établies par rapport à leurs intéractions de couplage et les contraintes de symétrie indiquées au spectre RMN. Comme il a déjà été indiqué, un cluster Ru_6 requièrt 92 électrons en supposant l'existence de huit liaisons métal-métal. En combinant les ligands diphénylthioureato, les groupes CO et les hydrures, on obtient 44 électrons et, avec l'addition des atomes de Ru, on arrive à 92 électrons. Similairement au cluster **15**, les liaisons Ru-Ru qui sont extrêmement longues sont nécessaires pour éviter un déficit électronique. En effet, il a été postulé que la formation de **16** résulte d'une oligomérisation de deux fragments hautement insaturés qui sont produits par l'hydrogénation de **15**.

Les clusters **14-16** présentés à la figure 41 représentent une série de variations structurelles des clusters hexanucléaires de ruthénium qui contiennent des ligands diphénylthioureato. Chaque cluster a une géométrie d'ossature qui lui permet d'accommoder les ligands pontants qui lui sont rattachés.

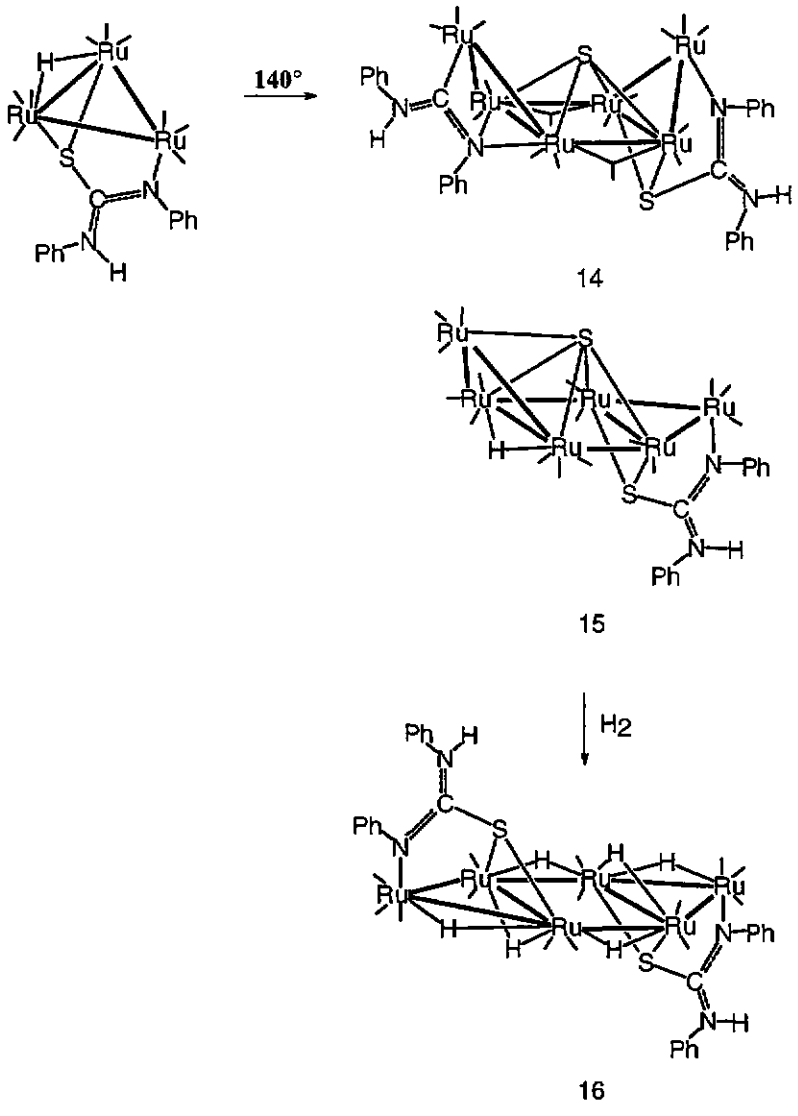

Figure 41: Représentation graphique des clusters **14-16**.

En escomptant un cluster de type *boat*, des réactions de thermolyse de l'analogue diméthylthiourea trinucléaire de **8** (μ_2-H)$Ru_3(CO)_9(\mu_3,\eta^2$-SCNHMeNMe) ont été exécutés. Quoique des traces de la molécule hexanucléaire aient été isolées parmi les produits de ces réactions, le produit principal est le cluster tétranucléaire $Ru_4(\mu_2\text{-}CO)_3(CO)_7(\mu_4\text{-}S)(C(NHMe_2)_2)$(**17**). Une analyse structurale de ce produit a révélé la présence d'un seul ligand diaminocarbène. Ce cluster est présente à la figure 42.

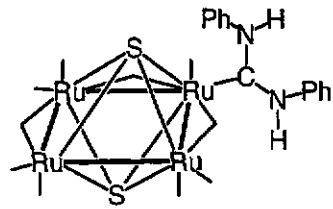

Figure 42: La représentation graphique du cluster **17**.

En étudiant la possibilité de réaction du μ_5-S du cluster **15**, plusieurs essais d'addition de molécules de type acide de Lewis ont été effectués. Le μ_5-S n'a réagi avec aucun des réactifs utilisés. Dans les réactions de **15** avec plusieurs sources du fragment BH_3, le réactif s'est comporté comme une source d'hydrogène en produisant des intermédiaires insaturés qui ont subi une oligomérisation afin d'assouplir leurs déficiences électroniques. Cependant, contrairement aux réactions avec l'hydrogène moléculaire, la partie du **15** contenant le ligand diphénylthioureato n'était pas impliquée dans l'oligomérisation. Dans ce cas les espèces insaturées trinucléaires avec un soufre coiffant produites se sont combinées afin de produire la molécule $\{Ru_3(CO)_8(\mu_4\text{-}S)\}_3$ **18** précédemment isolées. Quand la source de BH_3 utilisée était le $Me_2S{\cdot}BH_3$, la substitution d'un CO du **15** a également donné le produit (μ_2-H)$Ru_6(CO)_{15}(Me_2S)(\mu_5\text{-}S)(\mu_3,\eta^2$-SCNHPhNPh) (**19**). Ce même produit a été isolé dans les réactions de **15** avec Me_2S. La position exacte de substitution a été confirmée plus tard par analyse structurelle aux rayons X du dérivé t-butylisonitrile. Les réactions de **15** avec ces divers réactifs sont présentés à la figure 43.

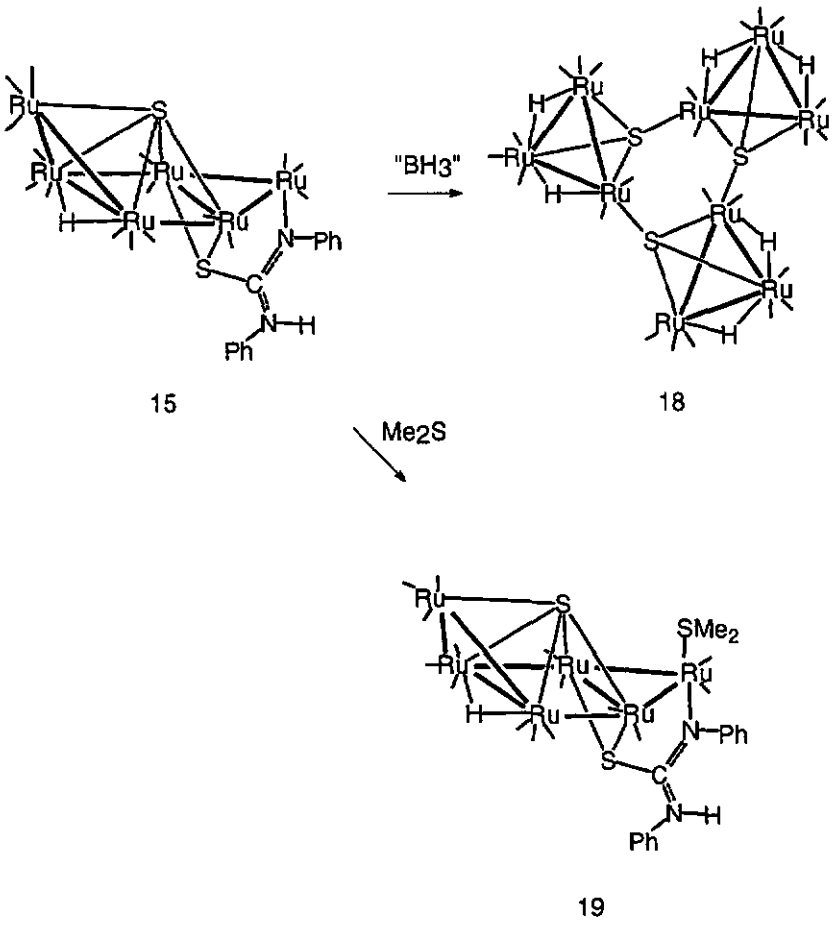

Figure 43: Les réactions de **15** avec BH_3 et Me_2S pour produire **18** et **19**.

En manipulant **15** il a été constaté que même des traces de CO initient la formation d'une espèce bleu-foncé tandis que le spectre IR indique des modifications de la structure par rapport a celle de **15**. En passant du CO à travers des solutions de **15** pendant de courtes périodes, cette espèce de couleur bleue a été générée de façon quasi-quantitative. Si la solution bleue est conservée sous une atmosphère d'azote une conversion quantitative a **15** est observée. La chromatographie sur couche mince sous une atmosphère de CO peut être utilisée pour isoler la molécule bleue cependant la nature hautement réversible de cette réaction rend la

cristallisation directe plus productive. Malheureusement aucun des cristaux produit de cette manière avait la qualité requise pour être analyse par rayons X donc l'identification définitive de l'espèce bleue n'a pas été possible. Une analyse spectroscopique ainsi qu'une analyse élémentaire suggèrent l'addition simple d'un CO à travers une des liaisons Ru-Ru les plus longues afin de produire le cluster (μ_2-H)Ru_6(μ_2-CO)$(CO)_{16}$(μ_5-S)(μ_3,η^2-SCNHPhNPh) (**20**) présenté à la figure 44. Le cluster **20** est probablement un cluster de ruthénium hexanucléaire avec sept liaisons métal-métal et un groupe CO pontant. La combinaison des ligands de **20** fourni 46 électrons et permet un nombre d'électrons total de 94. La facilite avec laquelle **15** et **20** s'interconvertissent indique que la surface de l'énergie potentielle le long de cette coordonnée de réaction a une très basse barrière.

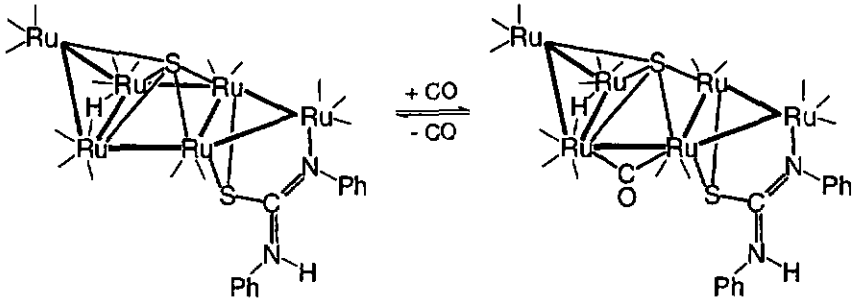

Figure 44: La structure proposée pour **20**.

Souvent une simple substitution du CO par un donneur à deux électrons produit une molécule isoélectronique qui se cristallise mieux que la molécule d'origine. Une série de dérivés de **15** a été préparée, en espérant que ceux-ci également montrent une addition de CO réversible, dans le but de générer des cristaux de qualité adéquate pour une analyse par rayons X. Un composé d'addition de CO un peu plus stable a été isolé dans les dérivés de phosphites, de plus quelques différences intéressantes dans les réactions de **15** avec les différents ligands donneurs de deux électrons ont été trouvé.

Dans les réactions a température ambiante de **15** avec PPh_3 le dérivé monosubstitué a été isolé, cependant deux autres produits étaient présents dans des petites quantités. Le premier était le cluster trinucléaire $Ru_3(CO)_6$(μ_2-C_6H_5)(μ_2-PPh_2)$_2$(μ_3,η^2-SCNHPhNPh) (**12**)

(voir figure 39), isolé par les réactions de thermolyses de $(\mu_2\text{-H})Ru_3(CO)_7(PPh_3)_2(\mu_3,\eta^2\text{-SCNHPhNPh})$ **(11)**, tandis que le deuxième était le cluster dinucléaire $Ru_2(CO)_4(PPh_3)_2(\mu_3,\eta^2\text{-SCNHPhNPh})$**(21)** (*voir figure 45*). Ces deux molécules postulent la présence de plusieurs intermédiaires réactifs à partir de **15**. Le dérivé monosubstitué de **15** avec la PPh_3 a été caractérisé par une analyse structurelle par rayoos X comme étant $(\mu_2\text{-H})Ru_6(CO)_{15}(Me_2S)(\mu_5\text{-S})(\mu_3,\eta^2\text{-SCNHPhNPh})$ **(22)**. La structure moléculaire de **22** montre la substitution d'un groupe CO sur le Ru lié à μ_5-S occupant la position apicale. Le ligand diphénylthioureato n'est pas influence par cette substitution tandis que l'hydrure pontant est influencé par le nouvel environnement chimique comme indiqué par le déplacement du signal ^{1}H RMN.

Les spectres RMN à basse température indiquent la présence de deux isomères de **22** qui diffèreot seulement en la rotation du ligand PPh_3. A l'ossature métallique on observe des modifications significatives des longueurs des liaisons Ru-Ru. Une des liaisons Ru-Ru entre les deux substructures triangulaires s'allonge d'approximativement 20 pm. Cette ouverture de l'ossature du cluster modifie l'environnement chimique autour de l'hydrure pontant. De plus ce résultat démontré la faiblesse de cette intéraction métal-métal dans **15**. La modification de l'ossature de ce cluster ne permet plus l'addition réversible du CO. En exposant **22** à une atmosphère de CO une réactioo limitée n'a produit que le cluster trinucléaire **8**. Les réactions de **15** avec PPh_3 soot présentées à l'figure 45.

La substitution d'un CO à un autre centre métallique de **15** se fait en présence de n'importe lequel des ligands donneurs de deux électrons $P(n\text{-Bu})_3$, $P(OMe)_3$, $P(OPh)_3$ et ^{t}BuNC (ainsi que Me_2S comme mentionné précédemment) afin de produire les molécules $(\mu_2\text{-H})Ru_6(CO)_{15}(P(n\text{-Bu})_3)(\mu_5\text{-S})(\mu_3,\eta^2\text{-SCNHPhNPh})$ **(23)**, $(\mu_2\text{-H})Ru_6(CO)_{15}(P(OMe)_3)(\mu_5\text{-S})(\mu_3,\eta^2\text{-SCNHPhNPh})$ **(24)**, $(\mu_2\text{-H})Ru_6(CO)_{15}(P(OPh)_3)(\mu_5\text{-S})(\mu_3,\eta^2\text{-SCNHPhNPh})$ **(25)**, and $(\mu_2\text{-H})Ru_6(CO)_{15}(^t\text{BuNC})(\mu_5\text{-S})(\mu_3,\eta^2\text{-SCNHPhNPh})$ **(26)**. Une analyse structurale par rayons X de **26** a démootré que la substitution se fait sur l'atome de ruthénium apical de la substructure triangulaire de **15** ponté par le diphénylthioureato. Des modifications importantes des liaisons de l'ossature métallique ainsi que des ligands n'ont pas été observées. Ces réactions soot présentées à la figure 46.

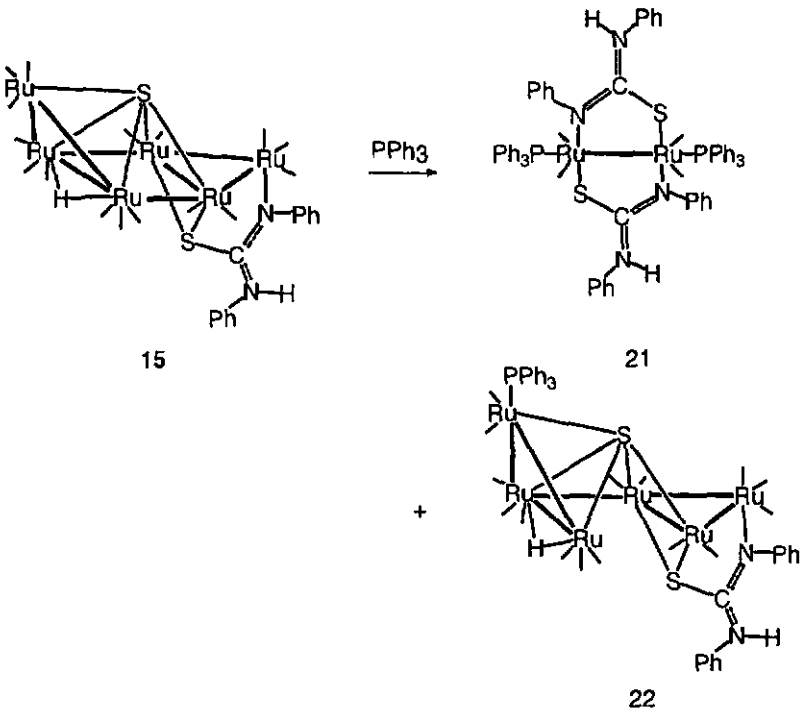

Figure 45: Les réactions de **15** avec le PPh_3.

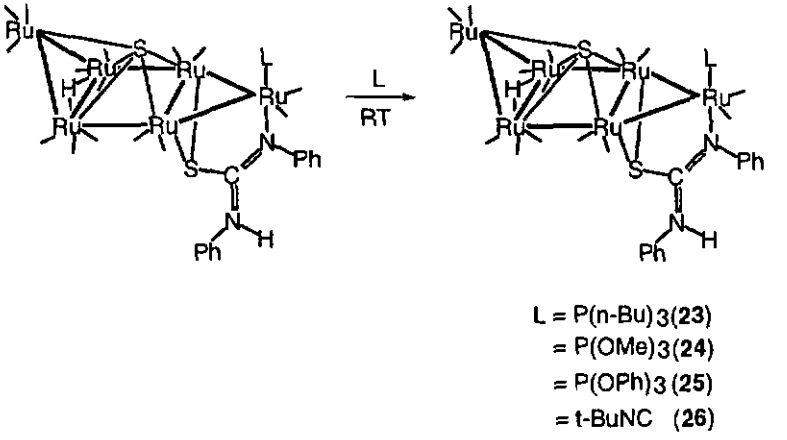

Figure 46: Les réactions de **15** avec $P(n\text{-}Bu)_3$, $P(OMe)_3$, $P(OPh)_3$ et ^{t}BuNC.

Les produits monosubstitués **23-26** montrent les mêmes tendances en ce qui concerne l'addition de CO comme celles de **15**. C'est à dire en exposant une solution de **23-26** à une atmosphère de CO, la formation d'une molécule bleue ayant un spectre IR similaire à celui de **20** a été observée. Toutes ces molécules bleues ont montré la même réversibilité par rapport à l'addition de CO. Le dérivé n-butylphosphine était le moins stable parmi les adduits de CO tandis que les dérivés de phosphites était assez stables pour être purifiés par chromatographie sur couche mince. Le dérivé t-butylisonitrile a également été purifié par chromatographie sur couche mince cependant deux molécules bleus ont été observées parmi lesquelles une seule était assez stable pour être caractérisée. En ce qui concerne **20**, les cristaux obtenus n'avaient pas la qualité requise pour une analyse a rayons X. Cependant FAB-MS et l'analyse élémentaire du dérivé $P(OPh)_3$ donnent des résultats analogue à que ceux obtenus pour **20**, ce qui nous conduit à proposer les formules moléculaires suivantes pour **27-30**; ; $(\mu_2\text{-H})Ru_6(\mu_2\text{-CO})(CO)_{15}\{P(n\text{-Bu})_3\}(\mu_5\text{-S})(\mu_3,\eta^2\text{-SCNHPhNPh})$ **(27)**, $(\mu_2\text{-H})Ru_6(\mu_2\text{-CO})(CO)_{15}\{P(OMe)_3\}(\mu_5\text{-S})(\mu_3,\eta^2\text{-SCNHPhNPh})$ **(28)**, $(\mu_2\text{-H})Ru_6(\mu_2\text{-CO})(CO)_{15}\{P(OPh)_3\}(\mu_5\text{-S})(\mu_3,\eta^2\text{-SCNHPhNPh})$ **(29)** and $(\mu_2\text{-H})Ru_6(\mu_2\text{-CO})(CO)_{15}(^t\text{BuNC})(\mu_5\text{-S})(\mu_3,\eta^2\text{-SCNHPhNPh})$ **(30)**. La représentation générale de **27-30** est présentée à l'illustration 47.

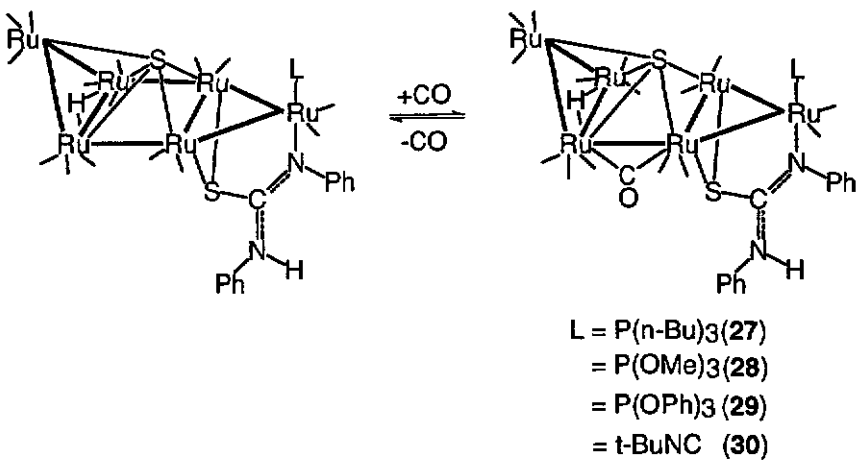

Figure 47: La représentation générale de **27-30**.

VI Supplementary data

6.1 Crystal structure data tables

Compound	2	4
Molecular formula	$C_{12}O_9Ru_3S_3$	$C_{33}H_{14}O_9Ru_3S_3\ C_3H_6O$
MW	687.51	1022 .01
Z	4	2
Crystal dimensions/mm	0.42x0.34x0.30	0.46x0.38x0.15
Crystal color/habit	yellow/blocks	yellow/blocks
Crystal system	orthorhombic	monoclinic
space group	$P\ na2_1$	$P\ 2_1$
a/Å	12.7535(4)	9.903(3)
b/Å	12.7835(4)	17.772(5)
c/Å	11.2755(6)	11.521(3)
α/°	90°	90°
β/°	90°	108.410(20)°
γ/°	90°	90°
V/Å^3	1838.29(13)	1923.9(9)
D_c/g cm^{-3}	2.484	1.764
μ(Mo-Kα)/mm^{-1}	2.76	2.69
T of data collection (K)	298	193
F(000)	1319.88	1895.81
Index limits h,k,l	0 15, 0 15, 0 13	-13 13, -24 24, -16 16
Absorption correction	none	none
No. of unique data	1711	11172
No. of obs. data used [$F_o>2.5\sigma(F_o)$]	1622	11085
$2\theta_{min}/2\theta_{max}$(°)	3/50.0	3/60.0
Instrumental error factor k[b]	0.0005	0.001
R(R')[c]	0.024(0.035)	0.035(0.05)
Residual electron-density difference features: (max., min.)/e Å^{-3}	0.39, -0.99	0.720, -0.570

[a] Details in common: data collected on a Stoe-Siemens AED 2 four-circle diffractometer; graphite-monochromated Mo-Kα radiation, λ = 0.71073 Å; scan mode ω-θ.

[b] Refinement was by full-matrix least squares with a weighting scheme of the form $w^{-1} = \sigma^2(F_o) + k(F_o^2)$.

[c] $R = \Sigma||F_o| - |F_c||/\Sigma|F_o|$, $R' = [\Sigma w(|F_o| - |F_c|)^2/\Sigma w(|F_o|)^2]^{1/2}$

Compound	5[d]	6[d]
Molecular formula	$C_{14}H_6O_{11}Os_3S_3$	$C_{10}H_2O_{11}Os_3$
MW	1016.97	868.72
Z	4	4
Crystal dimensions/mm	0.49x0.35x0.30	0.38x0.19x0.19
Crystal color/habit	yellow/blocks	orange/blocks
Crystal system	monoclinic	monoclinic
space group	$P2_1/a$	$P2_1/n$
a/Å	13.078(7)	7.371(2)
b/Å	9.671(5)	25.010(9)
c/Å	18.469(10)	9.037(3)
α/°	90	90
β/°	107.63(4)	107.07(3)
γ/°	90	90
V/Å^3	2226(2)	1592.6(9)
D_c/g cm^{-3}	3.034	3.623
μ(Mo-Kα)/mm^{-1}	17.414	23.930
T of data collection (K)	293(2)	293(2)
F(000)	1816	1512
Index limits h,k,l	16 16, 0 12, 0 24	-8 8, 0 29, 0 10
Absorption correction	empirical/DIFABS	empirical/DIFABS
T_{max}/T_{min}	1.000/0.322	1.000/0.627
No. of unique data	5105	2803
No. of obs. data used [$F_o>2.5\sigma(F_o)$]	3765	2247
$2\theta_{min}$, $2\theta_{max}$(°)	3/55	3/50
$R(>2\sigma F^2)/R1(all)$[b]	0.0621(0.0957)	0.0462(0.0676)
$wR2(>2\sigma F^2)/wR2(all)$[c]	0.1350 (0.1479)	0.0863 (0.0931)
wa/wb	0.0655/35.3061	0.0291/26.4214
Residual electron-density difference features: (max., min.)/e Å^{-3}	1.777, -1.755	1.272, -1.198

[a] Details in common: data collected on a Stoe-Siemens AED 2 four-circle diffractometer; graphite-monochromated Mo-Kα radiation, λ = 0.71073 Å; scan mode ω-θ.

[b] $R = \Sigma||F_o| - |F_c||/\Sigma|F_o|$

[c] $wR2 = [\{\Sigma[w(F_o^2 - F_c^2)^2]/\Sigma[w(F_o)^4]\}]^{1/2}$, $w^{-1} = [\sigma^2(F_o^2) + (waP)^2 + wbP]$, $P = (F_o^2 + 2F_c^2)/3$

[d] data refinement using SHELXL 93.

Compound	**10**	**12**	**13**[d]
Molecular formula	$C_{39}H_{26}N_2O_8PRu_3S$	$C_{42}H_{30}O_6P_2Ru_3S\cdot CH_2Cl_2$	$C_{46}H_{38}N_2O_6P_2Ru_3S\ 2CH_2Cl_2$
MW	1016.88	1112.8	1313.85
Z	2	4	4
Crystal dimensions/mm	0.34x0.27x0.23	0.68x0.53x0.42	0.99x0.65x0.61
Crystal color/habit	orange/blocks	black/blocks	orange-red/blocks
Crystal system	triclinic	monoclinic	monclinic
space group	$P\bar{1}$	P $2_1/n$	$P2_1/n$
a/Å	10.014(2)	10.824(1)	17.667(7)
b/Å	14.449(4)	19.193(5)	17.681(5)
c/Å	14.573(4)	20.953(2)	18.049(4)
α/°	100.38(2)	90	90
β/°	98.70(2)	97.44(1)	108.06(2)
γ/°	107.20(2)	90	90
V/Å^3	1933.8(8)	4316.2(13)	5360(3)
D_c/g cm^{-3}	1.746	1.712	1.628
μ(Mo-Kα)/mm^{-1}	2.56	1.329	1.184
T of data collection (K)	193	293	203(2)
F(000)	2003.75	2200	2616
Absorption correction	empirical	semi-emp/psi scans	semi-emp/psi scans
T_{max}/T_{min}	0.5936/0.4826	0.2756/0.1875	0.1715/0.1176
Index limits h,k,l	-11 11, 0 17, -17 17	-12 12, 0 22, 0 24	-20 19, 0 21, 0 21
No. of unique data	6781	7595	9410
No. of obs. data used [$F_o>2.5\sigma(F_o)$]	5278	7056	5111
$2\theta_{min}$, $2\theta_{max}$(°)	3/50	3/50	3/55
Instrumental error factor k[b]	0.0005		
R(R')[c] (**10**)	0.036(0.055)		
R(>2σF^2)/R1(all) (**12,13**)[e]		0.0506(0.0726)	0.0754(0.1526)
wR2(>2σF^2)/wR2(all)[f]		0.1263 (0.1402)	0.1666(0.2044)
wa/wb		0.0835/0.000	0.0964/0.000
Residual electron-density difference features: (max., min.)/e Å^{-3}	0.70, -0.55	1.247, -0.884	1.678, -1.133

[a] Details in common: data collected on a Stoe-Siemens AED 2 four-circle diffractometer; graphite-monochromated Mo-Kα radiation, λ = 0.71073 Å; scan mode ω-θ.

[b] Refinement was by full-matrix least squares with a weighting scheme of the form $w^{-1} = \sigma^2(F_o) + k(F_o^2)$.

[c] $R = \Sigma||F_o| - |F_c||/\Sigma|F_o|$, $R' = [\Sigma w(|F_o| - |F_c|)^2/\Sigma w(|F_o|)^2]^{1/2}$

[d] data refinement using SHELXL 93.

[e] $R = \Sigma||F_o| - |F_c||/\Sigma|F_o|$

[f] $wR2 = [\{\Sigma[w(F_o^2 - F_c^2)^2]/\Sigma[w(F_o)^4]\}]^{1/2}$, $w^{-1} = [\sigma^2(F_o^2) + (waP)^2 + wbP]$, $P = (F_o^2 + 2F_c^2)/3$

Compound	14	15
Molecular formula	$C_{42}H_{22}N_4O_{15}Ru_6S_2 \cdot 2CH_2Cl_2$	$C_{29}H_{12}N_2O_{16}S_2Ru_6$
MW	1679.1	1314.9
Z	2	4
Crystal dimensions/mm	0.57x0.46x0.46	0.57x0.53x0.38
Crystal color/habit	deep red/rectangular rods	red/rectangular rods
Crystal system	triclinic	monoclinic
space group	$P\bar{1}$	$P\,2_1/n$
a/Å	12.141(3)	9.2712(4)
b/Å	12.449(4)	20.727(2)
c/Å	19.712(6)	20.438(1)
α/°	90.22(3)	90
β/°	99.50(2)	92.561(4)
γ/°	111.61(2)	90
V/Å^3	2725.1(14)	3923.4(4)
D_d/g cm^{-3}	2.046	2.226
μ(Mo-Kα)/mm^{-1}	1.93	2.38
T of data collection (K)	193	298
F(000)	1619.81	2491.71
Absorption correction	none	none
Index limits h,k,l	-15 14, 0 16, -25 25	-11 11, 0 24, 0 24
No. of unique data	12196	6878
No. of obs. data used [$F_o > 2.5\sigma(F_o)$]	8354	5746
$2\theta_{min}$, $2\theta_{max}$(°)	3/55	3/50
Instrumental error factor k[b]	0.0015	0.003
R(R')[c]	0.045(0.059)	0.034(0.057)
Residual electron-density difference features: (max., min.)/e Å^{-3}	1.63/-1.22	0.62/-1.66

[a] Details in common: data collected on a Stoe-Siemens AED 2 four-circle diffractometer; graphite-monochromated Mo-Kα radiation, λ = 0.71073 Å; scan mode ω-θ.

[b] Refinement was by full-matrix least squares with a weighting scheme of the form $w^{-1} = \sigma^2(F_o) + k(F_o^2)$.

[c] $R = \Sigma||F_o| - |F_c||/\Sigma|F_o|$, $R' = [\Sigma w(|F_o| - |F_c|)^2/\Sigma w(|F_o|)^2]^{1/2}$

Compound	**16**	**17**
Molecular formula	$C_{40}H_{26}N_4O_{14}Ru_6S_2$ 4$(CH_3)_2CO$	$C_{13}H_8N_2O_{10}Ru_4S_2$
MW	1689.50	820.6
Z	1	2
Crystal dimensions/mm	0.30x0.23x0.15	0.57x0.34x0.23
Crystal color/habit	orange-red/blocks	orange/blocks
Crystal system	triclinic	triclinic
space group	$P\bar{1}$	$P\bar{1}$
a/Å	9.799(1)	9.636(2)
b/Å	12.594(2)	10.635(2)
c/Å	14.466(1)	12.005(3)
α/°	112.45(1)	70.95(1)
β/°	92.71(1)	83.46(1)
γ/°	102.05(1)	70.40(1)
V/Å^3	1597.6(3)	1095.5(4)
D_c/g cm^{-3}	1.756	2.488
μ(Mo-Kα)/mm^{-1}	2.91	6.60
T of data collection (K)	203	298
F(000)	1197.86	2579.69
Absorption correction	none	none
Index limits h,k,l	-12 12, 0 16, -18 17	-10 11, 0 12, -13 14
No. of unique data	7333	3866
No. of obs. data used [F_o>2.5σ(F_o)]	3993	3432
$2\theta_{min}$, $2\theta_{max}$(°)	3/55	3/50
Instrumental error factor k[b]	0.001	0.003
R(R')[c]	0.042(0.048)	0.045(0.075)
Residual electron-density difference features: (max., min.)/e Å^{-3}	0.63/-0.76	0.65/-4.70

[a] Details in common: data collected on a Stoe-Siemens AED 2 four-circle diffractometer; graphite-monochromated Mo-Kα radiation, λ = 0.71073 Å; scan mode ω-θ.

[b] Refinement was by full-matrix least squares with a weighting scheme of the form $w^{-1} = \sigma^2(F_o) + k(F_o^2)$.

[c] $R = \Sigma||F_o| - |F_c||/\Sigma|F_o|$, $R' = [\Sigma w(|F_o| - |F_c|)^2/\Sigma w(|F_o|)^2]^{1/2}$

Compound	19	22	26
Molecular formula	$C_{24}H_4O_{24}S_3Ru_6$	$C_{46}H_{26}N_2O_{15}PRu_6\,CH_2Cl_2$	$C_{33}H_{20}N_3O_{13}Ru_6S_2{\cdot}C_{1.5}O_{0.5}$
MW	1682.1	1633.1	1398.1
Z	2	2	2
Crystal dimensions/mm	0.30x0.15x0.15	0.38x0.38x0.15	0.72x0.42x0.06
Crystal color/habit	yellow/rods	deep-red/plates	red/plates
Crystal system	triclinic	triclinic	triclinic
space group	$P\bar{1}$	$P\bar{1}$	$P\bar{1}$
a/Å	11.347(3)	9.808(2)	9.431(2)
b/Å	12.606(3)	10.285(2)	15.794(2)
c/Å	18.970(6)	27.48(1)	16.772(2)
α/°	87.09(1)	91.97(2)	87.94(1)
β/°	72.97(1)	90.02(2)	84.72(1)
γ/°	63.880(1)	94.52(2)	76.70(1)
V/Å^3	2319.9(11)	2761.8(13)	2420.6(7)
D_c/g cm^{-3}	2.408	1.964	1.928
μ(Mo-Kα)/mm^{-1}	3.00	3.66	1.827
T of data collection (K)	298	213	293
F(000)	1543.73	3103.66	1346
Absorption correction	none	empirical/psi scans	empirical/difabs
T_{max}/T_{min}		0.4833/0.2971	1.000/0.227
Index limits h,k,l	-9 10, 0 12, -18 18	-11 11, 0 12, -32 32	-11 11, -18 18, 0 19
No. of unique data	4318	9724	8485
No. of obs. data used [$F_o>2.5\sigma(F_o)$]	3392	7123	8483
$2\theta_{min}$, $2\theta_{max}$(°)	3/40	3/50	3/55
Instrumental error factor k[b]	0.001	0.0015	none
R(R')[c]	0.032(0.046)	0.039(0.052)	none
R(>2σF^2)/R1(all)[c]	none	none	0.071(0.131)
wR2(>2σF^2)/wR2(all)[d]	none	none	0.171(0.193)
wa/wb	none	none	0.111/0.00
Residual electron-density difference features: (max., min.)/e Å^{-3}	0.74/-0.71	1.29/-1.21	1.397/-1.203

[a] Details in common: data collected on a Stoe-Siemens AED 2 four-circle diffractometer; graphite-monochromated Mo-Kα radiation, λ = 0.71073 Å; scan mode ω-θ.

[b] Refinement was by full-matrix least squares with a weighting scheme of the form $w^{-1} = \sigma^2(F_o) + k(F_o^2)$.

[c] $R = \Sigma||F_o| - |F_c||/\Sigma|F_o|$, $R' = [\Sigma w(|F_o| - |F_c|)^2/\Sigma w(|F_o|)^2]^{1/2}$

[d] $wR2 = [\{\Sigma[w(F_o^2 - F_c^2)^2]/\Sigma[w(F_o)^4]\}]^{1/2}$, $w^{-1} = [\sigma^2(F_o^2) + (waP)^2 + wbP]$, $P = (F_o^2 + 2F_c^2)/$

6.2 Atomic coordinates and thermal parameters (B_{iso} or U_{eq})

Table 35: Atomic coordinates and B_{iso} for **2**.

	x	y	z	Biso
RU 1	0.89267(4)	0.45524(4)	0.09369	1.843(20)
RU 2	0.69864(4)	0.54285(4)	0.01182(7)	1.977(21)
RU 3	0.72851(4)	0.50007(4)	0.25581(9)	1.845(22)
S 1	0.97043(12)	0.62752(13)	0.11854(17)	2.00 (6)
S 2	0.76580(14)	0.71994(13)	0.02845(18)	2.31 (6)
S 3	0.79378(14)	0.67515(14)	0.29317(18)	2.14 (6)
C 1	0.9086 (5)	0.7207 (6)	0.0216 (7)	2.4 (3)
C 2	0.7515 (5)	0.7632 (5)	0.1784 (8)	2.7 (3)
C 3	0.9329 (5)	0.6783 (5)	0.2617 (6)	2.01 (24)
C 4	0.8345 (6)	0.4876 (6)	-0.0820 (8)	2.3 (3)
O 4	0.8579 (5)	0.4692 (6)	-0.1774 (6)	3.8 (3)
C 5	0.5995 (6)	0.5647 (6)	0.1632 (8)	2.4 (3)
O 5	0.5153 (4)	0.5920 (4)	0.1824 (6)	3.40 (24)
C 6	0.8820 (6)	0.4323 (6)	0.2799 (7)	2.3 (3)
O 6	0.9298 (5)	0.3946 (4)	0.3551 (6)	3.48 (24)
C11	1.0347 (6)	0.4144 (6)	0.0661 (7)	2.9 (3)
O11	1.1200 (4)	0.3936 (5)	0.0517 (7)	4.0 (3)
C12	0.8541 (6)	0.3147 (6)	0.0686 (7)	2.7 (3)
O12	0.8350 (5)	0.2294 (4)	0.0510 (8)	4.7 (3)
C21	0.6209 (6)	0.5978 (6)	-0.1162 (8)	3.1 (3)
O21	0.5717 (7)	0.6306 (7)	-0.1939 (8)	6.0 (4)
C22	0.6272 (6)	0.4177 (6)	-0.0144 (7)	2.5 (3)
O22	0.5802 (5)	0.3439 (5)	-0.0300 (7)	4.3 (3)
C31	0.6791 (7)	0.4991 (5)	0.4142 (9)	2.8 (3)
O31	0.6476 (7)	0.4920 (5)	0.5083 (7)	5.0 (4)
C32	0.6743 (6)	0.3635 (6)	0.2434 (7)	2.8 (3)
O32	0.6447 (5)	0.2801 (5)	0.2421 (6)	4.3 (3)

Biso is the Mean of the Principal Axes of the Thermal Ellipsoid

Table 36: Atomic coordinates and B_{iso} for **4**.

	x	y	z	Biso
RU1	0.25508(4)	0.67599	0.48009(4)	1.730(16)
RU2	0.35303(4)	0.79185(3)	0.35544(4)	1.730(16)
RU3	0.37858(4)	0.80837(3)	0.60714(4)	1.718(14)
S1	0.01662(14)	0.72969(9)	0.42663(12)	1.75 (5)
S2	0.11938(14)	0.85289(9)	0.29082(12)	1.70 (5)
S3	0.14919(14)	0.87239(9)	0.55951(12)	1.59 (4)
C1	-0.0220 (5)	0.7863 (4)	0.2887 (5)	1.80 (19)
C2	-0.0570 (7)	0.7375 (4)	0.1722 (5)	2.44 (23)
C3	-0.1818 (6)	0.6859 (4)	0.1619 (5)	2.51 (23)
C4	-0.1567 (8)	0.6112 (5)	0.1986 (7)	3.5 (3)
C5	-0.2694 (12)	0.5628 (5)	0.1936 (9)	4.9 (4)
C6	-0.4082 (11)	0.5899 (7)	0.1500 (11)	5.6 (5)
C7	-0.4324 (9)	0.6617 (7)	0.1098 (12)	6.1 (6)
C8	-0.3195 (8)	0.7102 (5)	0.1152 (9)	4.2 (4)
C9	0.0981 (6)	0.9162 (3)	0.4093 (5)	1.65 (18)
C10	0.1747 (6)	0.9911 (3)	0.4152 (5)	1.93 (19)
C11	0.1280 (6)	1.0341 (3)	0.2977 (5)	2.04 (21)
C12	0.2111 (7)	1.0367 (4)	0.2216 (6)	2.9 (3)
C13	0.1696 (8)	1.0789 (5)	0.1135 (6)	3.6 (3)
C14	0.0415 (10)	1.1155 (5)	0.0795 (7)	3.6 (3)
C15	-0.0452 (9)	1.1134 (4)	0.1543 (6)	3.3 (3)
C16	-0.0018 (8)	1.0731 (4)	0.2628 (6)	2.9 (3)
C17	0.0027 (5)	0.8054 (3)	0.5291 (4)	1.69 (18)
C18	-0.0108 (6)	0.7737 (3)	0.6492 (5)	2.03 (21)
C19	-0.0333 (6)	0.8364 (4)	0.7306 (5)	2.10 (21)
C20	-0.1519 (7)	0.8835 (4)	0.6878 (6)	2.50 (23)
C21	-0.1716 (8)	0.9420 (5)	0.7620 (8)	3.4 (3)
C22	-0.0786 (11)	0.9538 (5)	0.8755 (8)	4.4 (4)
C23	0.0401 (11)	0.9068 (7)	0.9167 (6)	4.8 (4)
C24	0.0628 (9)	0.8477 (5)	0.8464 (7)	3.5 (3)
C25	0.3072 (6)	0.7070 (4)	0.6673 (6)	2.27 (21)
O25	0.3154 (5)	0.6786 (3)	0.7606 (4)	2.80 (19)
C26	0.4262 (7)	0.8649 (4)	0.7535 (7)	3.0 (3)
O26	0.4581 (7)	0.8964 (4)	0.8447 (6)	5.3 (3)
C27	0.5595 (6)	0.7636 (4)	0.6667 (6)	2.50 (22)
O27	0.6672 (5)	0.7351 (3)	0.7060 (6)	3.76 (23)
C28	0.4522 (6)	0.8775 (4)	0.4892 (7)	2.42 (23)
O28	0.5296 (5)	0.9272 (3)	0.4953 (5)	2.88 (19)
C29	0.5393 (7)	0.7536 (4)	0.3919 (6)	2.65 (25)
O29	0.6544 (5)	0.7360 (4)	0.4129 (6)	3.88 (25)
C30	0.3686 (6)	0.8271 (4)	0.2065 (6)	2.7 (3)
O30	0.3819 (6)	0.8455 (4)	0.1141 (5)	4.0 (3)
C31	0.2732 (6)	0.6827 (4)	0.2987 (5)	2.16 (20)
O31	0.2655 (5)	0.6416 (3)	0.2189 (5)	2.86 (19)
C32	0.4301 (6)	0.6248 (3)	0.5168 (6)	2.31 (23)
O32	0.5317 (6)	0.5927 (3)	0.5353 (6)	3.74 (24)
C33	0.1626 (6)	0.5824 (4)	0.4776 (6)	2.23 (22)
O33	0.1081 (6)	0.5259 (3)	0.4785 (5)	3.54 (23)
O34	-0.2598 (5)	0.9041 (4)	0.2917 (5)	4.1 (3)
C34	-0.3149 (7)	0.9450 (5)	0.2062 (7)	3.2 (3)
C35	-0.2696 (8)	0.9441 (7)	0.0930 (7)	4.3 (4)
C36	-0.4267 (9)	0.9991 (5)	0.2084 (11)	5.0 (5)

Biso is the Mean of the Principal Axes of the Thermal Ellipsoid

Table 37: Atomic coordinates (x 10^4) and U_{eq} (x 10^3) ($Å^2$) for **5**.

	x	y	z	U(eq)
Os(1)	1135(1)	3983(1)	2384(1)	35(1)
Os(2)	1254(1)	6850(1)	2848(1)	31(1)
Os(3)	2581(1)	4789(1)	3816(1)	31(1)
S(1)	-240(4)	4454(5)	1223(3)	43(1)
S(2)	-1201(5)	3212(8)	-339(3)	73(2)
S(3)	-2662(5)	4260(7)	529(4)	65(2)
C(1)	-236(16)	3073(28)	570(11)	64(7)
C(2)	-2402(21)	2941(28)	-67(14)	74(7)
C(3)	-1517(16)	4059(25)	1357(11)	57(6)
C(11)	121(18)	3507(21)	2904(12)	55(6)
O(11)	-514(15)	3129(20)	3184(10)	86(6)
C(12)	1399(20)	2057(22)	2355(12)	57(6)
O(12)	1614(18)	933(16)	2341(10)	87(6)
C(13)	2202(15)	4359(19)	1909(10)	41(4)
O(13)	2825(13)	4439(16)	1563(9)	62(4)
C(21)	67(15)	6430(22)	3227(12)	51(5)
O(21)	-594(12)	6288(20)	3488(10)	81(6)
C(22)	317(14)	7840(19)	2029(10)	39(4)
O(22)	-206(12)	8458(18)	1522(9)	66(4)
C(23)	2342(13)	7175(19)	2369(10)	39(4)
O(23)	2957(12)	7434(16)	2062(9)	60(4)
C(24)	1762(15)	8257(22)	3563(10)	47(5)
O(24)	2032(14)	9147(17)	3981(9)	72(5)
C(31)	1457(15)	4620(18)	4309(10)	41(4)
O(31)	846(11)	4488(16)	4647(8)	55(4)
C(32)	3404(16)	5848(21)	4649(12)	48(5)
O(32)	3964(16)	6450(20)	5174(10)	96(7)
C(33)	3682(16)	5031(21)	3325(12)	51(5)
O(33)	4363(12)	5170(18)	3062(9)	67(4)
C(34)	3095(15)	3008(18)	4199(11)	41(4)
O(34)	3382(17)	1945(17)	4418(12)	91(6)

Table 38: Atomic coordinates (x 10^4) and U_{eq} (x 10^3) ($Å^2$) for **6**.

	x	y	z	U(eq)
Os(1)	50(1)	5891(1)	2220(1)	31(1)
Os(2)	-1229(1)	6134(1)	-953(1)	31(1)
Os(3)	-3176(1)	6546(1)	1075(1)	32(1)
O(1)	-1282(14)	5398(4)	252(12)	31(3)
C(11)	2335(27)	5454(7)	2842(20)	40(4)
O(11)	3732(19)	5230(6)	3277(17)	66(4)
C(12)	-1126(27)	5571(7)	3600(20)	43(5)
O(12)	-1862(20)	5381(6)	4413(16)	65(4)
C(13)	1118(27)	6409(8)	3696(22)	51(5)
O(13)	1709(23)	6746(6)	4591(18)	74(5)
C(21)	-3577(26)	6034(6)	-2566(22)	38(4)
O(21)	-5004(20)	5975(6)	-3450(18)	69(4)
C(22)	405(27)	5848(8)	-2067(20)	46(5)
O(22)	1350(21)	5703(7)	-2782(17)	71(5)
C(23)	-1025(25)	6815(8)	-1740(20)	43(4)
O(23)	-966(22)	7242(6)	-2211(16)	69(5)
C(31)	-3574(27)	6635(7)	3055(22)	44(5)
O(31)	-3820(26)	6685(6)	4236(17)	79(5)

Table 38: cont.

C(32)	-4648(27)	5887(7)	603(20)	39(4)
O(32)	-5510(18)	5517(6)	236(18)	60(4)
C(33)	-5304(36)	6956(9)	-200(25)	62(6)
O(33)	-6580(23)	7199(7)	-838(23)	94(6)
C(34)	-1346(32)	7141(8)	1316(22)	51(5)
O(34)	-314(21)	7478(6)	1432(18)	62(4)

Table 39: Atomic coordinates and B_{iso} for **10**.

	x	y	z	Biso
RU1	0.22446(6)	0.12269(4)	0.16974(4)	1.94 (3)
RU2	0.21500(6)	0.28756(4)	0.30735(4)	1.765(25)
RU3	0.14197(6)	0.09788(4)	0.33881(4)	1.96 (3)
S1	0.03900(17)	0.19799(13)	0.16148(12)	1.91 (8)
P1	0.30529(18)	0.43234(14)	0.25007(13)	1.90 (8)
N1	-0.0735 (6)	0.0771 (4)	0.2691 (4)	2.0 (3)
N2	-0.2375 (6)	0.1111 (4)	0.1594 (4)	2.5 (3)
C1	-0.1022 (7)	0.1211 (5)	0.2022 (5)	1.8 (3)
C2	-0.2715 (7)	0.1742 (6)	0.0991 (5)	2.5 (3)
C3	-0.2525 (9)	0.2725 (7)	0.1377 (6)	3.9 (4)
C4	-0.2875 (10)	0.3315 (7)	0.0804 (8)	4.6 (5)
C5	-0.3400 (10)	0.2941 (9)	-0.0141 (9)	5.2 (6)
C6	-0.3592 (11)	0.1962 (10)	-0.0536 (7)	5.6 (7)
C7	-0.3256 (9)	0.1343 (7)	0.0035 (6)	3.8 (5)
C8	-0.1933 (7)	0.0157 (5)	0.2995 (5)	2.3 (3)
C9	-0.2585 (8)	-0.0834 (6)	0.2520 (6)	3.0 (4)
C10	-0.3720 (9)	-0.1427 (6)	0.2818 (7)	3.8 (4)
C11	-0.4173 (9)	-0.1032 (7)	0.3602 (7)	4.2 (5)
C12	-0.3501 (9)	-0.0043 (7)	0.4086 (6)	3.7 (5)
C13	-0.2382 (7)	0.0558 (6)	0.3772 (5)	2.7 (4)
C14	0.5015 (7)	0.4867 (5)	0.2782 (5)	2.1 (3)
C15	0.5874 (8)	0.4317 (6)	0.3043 (6)	2.9 (4)
C16	0.7368 (8)	0.4772 (7)	0.3315 (6)	3.7 (4)
C17	0.7997 (8)	0.5742 (6)	0.3342 (6)	3.3 (4)
C18	0.7154 (8)	0.6295 (6)	0.3080 (6)	3.5 (4)
C19	0.5684 (8)	0.5856 (6)	0.2817 (5)	2.8 (4)
C20	0.2544 (7)	0.5398 (5)	0.2984 (5)	2.2 (3)
C21	0.2522 (7)	0.5610 (6)	0.3959 (5)	2.6 (4)
C22	0.2261 (8)	0.6449 (6)	0.4372 (5)	2.8 (4)
C23	0.1991 (8)	0.7088 (6)	0.3829 (6)	3.3 (4)
C24	0.1998 (8)	0.6883 (6)	0.2859 (6)	3.1 (4)
C25	0.2267 (8)	0.6051 (6)	0.2440 (5)	2.7 (4)
C26	0.2564 (7)	0.4172 (5)	0.1208 (5)	2.2 (3)
C27	0.3543 (8)	0.4148 (6)	0.0624 (5)	2.8 (4)
C28	0.3091 (9)	0.3972 (7)	-0.0359 (6)	3.6 (4)
C29	0.1681 (10)	0.3814 (7)	-0.0767 (6)	4.0 (5)
C30	0.0692 (8)	0.3816 (6)	-0.0196 (6)	3.5 (4)
C31	0.1134 (8)	0.3993 (6)	0.0789 (5)	2.7 (4)
C32	0.0975 (8)	-0.0106 (6)	0.1206 (5)	2.8 (4)
O32	0.0229 (6)	-0.0902 (5)	0.0908 (4)	4.1 (3)
C33	0.2776 (8)	0.1574 (6)	0.0537 (5)	2.7 (4)
O33	0.3116 (6)	0.1698 (5)	-0.0154 (4)	4.5 (3)
C34	0.3812 (8)	0.0797 (6)	0.2006 (5)	2.7 (4)
O34	0.4766 (6)	0.0523 (5)	0.2164 (4)	3.8 (3)
C35	0.1009 (8)	0.1293 (6)	0.4629 (6)	2.7 (4)

Table 39:cont.

O35	0.0853	(6)	0.1477	(5)	0.5388	(4)	4.3	(3)
C36	0.1012	(8)	-0.0443	(7)	0.3210	(6)	3.0	(4)
O36	0.0815	(8)	-0.1269	(5)	0.3091	(5)	5.4	(4)
C37	0.3379	(8)	0.1297	(6)	0.3915	(5)	2.8	(4)
O37	0.4562	(6)	0.1492	(5)	0.4256	(4)	4.0	(3)
C38	0.0800	(8)	0.3170	(6)	0.3715	(5)	2.6	(3)
O38	-0.0084	(6)	0.3324	(5)	0.4074	(4)	4.3	(3)
C39	0.3545	(8)	0.3380	(6)	0.4212	(5)	2.6	(4)
O39	0.4361	(6)	0.3701	(5)	0.4927	(4)	4.3	(3)
H1	0.333	(7)	0.259	(5)	0.245	(5)	2.5	(15)

Table 40: Atomic coordinates (x 10^4) and U_{eq} (x 10^3) ($Å^2$) for **12**.

	x	y	z	U(eq)
Ru(1)	1243(1)	1654(1)	4450(1)	32(1)
Ru(2)	2499(1)	2488(1)	5403(1)	33(1)
Ru(3)	-137(1)	2400(1)	5193(1)	36(1)
S(1)	1131(2)	2923(1)	4489(1)	38(1)
P(1)	1547(1)	1267(1)	3402(1)	34(1)
P(2)	1059(2)	2920(1)	6011(1)	37(1)
C(1)	3218(6)	1742(3)	4638(3)	40(2)
C(2)	3849(6)	2359(4)	4504(3)	41(2)
C(3)	5163(7)	2416(4)	4613(4)	56(2)
C(4)	5862(7)	1860(5)	4843(4)	63(2)
C(5)	5288(6)	1232(4)	4972(3)	53(2)
C(6)	4011(6)	1175(4)	4885(3)	48(2)
C(7)	1538(6)	1905(4)	2756(3)	40(2)
C(8)	1071(8)	2572(4)	2816(4)	57(2)
C(9)	1000(9)	3025(4)	2309(4)	73(3)
C(10)	1366(8)	2845(5)	1738(4)	69(2)
C(11)	1840(7)	2194(5)	1668(4)	62(2)
C(12)	1930(7)	1726(4)	2174(3)	52(2)
C(13)	341(6)	647(3)	3068(3)	39(2)
C(14)	-376(7)	758(4)	2476(3)	55(2)
C(15)	-1339(8)	301(5)	2257(4)	72(2)
C(16)	-1589(7)	-265(4)	2616(4)	62(2)
C(17)	-878(7)	-381(4)	3199(4)	58(2)
C(18)	61(6)	70(3)	3424(3)	48(2)
C(19)	3046(6)	827(3)	3370(3)	36(1)
C(20)	3225(6)	123(4)	3485(3)	46(2)
C(21)	4392(8)	-175(4)	3527(4)	59(2)
C(22)	5423(7)	243(4)	3453(4)	60(2)
C(23)	5252(6)	942(4)	3335(3)	50(2)
C(24)	4086(6)	1237(4)	3299(3)	43(2)
C(25)	911(6)	3859(3)	6095(3)	44(2)
C(26)	362(8)	4133(4)	6601(4)	64(2)
C(27)	193(11)	4850(5)	6648(5)	94(3)
C(28)	572(10)	5299(5)	6187(5)	88(3)
C(29)	1083(9)	5021(4)	5688(5)	77(3)
C(30)	1261(7)	4312(4)	5635(4)	58(2)
C(31)	1148(7)	2611(3)	6836(3)	45(2)
C(32)	2270(8)	2663(4)	7241(3)	59(2)
C(33)	2399(10)	2399(5)	7852(4)	82(3)
C(34)	1429(13)	2099(5)	8089(4)	93(4)
C(35)	290(11)	2054(5)	7712(4)	79(3)

Table 40:cont.

C(36)	164(8)	2304(4)	7084(4)	59(2)
C(101)	-554(6)	1525(4)	4213(3)	45(2)
O(101)	-1538(4)	1371(3)	4013(3)	71(2)
C(102)	1336(6)	776(4)	4852(3)	44(2)
O(102)	1367(5)	263(3)	5134(3)	69(2)
C(201)	3670(6)	3200(4)	5683(3)	44(2)
O(201)	4357(5)	3622(3)	5869(3)	73(2)
C(202)	3090(6)	1820(4)	6044(3)	44(2)
O(202)	3397(5)	1403(3)	6410(3)	60(1)
C(301)	-1461(6)	3034(4)	5121(3)	46(2)
O(301)	-2252(5)	3429(3)	5065(3)	76(2)
C(302)	-918(6)	1711(4)	5644(3)	47(2)
O(302)	-1444(5)	1287(3)	5875(3)	70(2)
Cl(1)	4875(17)	4412(6)	4309(5)	476(9)
Cl(2)	3065(8)	4406(6)	3365(7)	410(7)
C(15)	3579(26)	4959(12)	4030(12)	366(24)
H(2)	3449(58)	2728(34)	4215(31)	41(18)

Table 41: Atomic coordinates (x 10^4) and U_{eq} (x 10^3) ($Å^2$) for **13**.

	x	y	z	U(eq)
Ru(1)	-374(1)	3762(1)	3066(1)	30(1)
Ru(2)	900(1)	3309(1)	2514(1)	31(1)
Ru(3)	895(1)	2923(1)	3994(1)	32(1)
P(1)	-1231(2)	4443(2)	2016(2)	32(1)
P(2)	574(2)	3880(2)	1277(2)	31(1)
S(1)	729(2)	4544(2)	3014(2)	31(1)
N(1)	1519(6)	3979(5)	4405(5)	36(2)
N(2)	1690(6)	5272(5)	4249(6)	41(3)
C(1)	1391(7)	4583(7)	3990(6)	35(3)
C(2)	2151(7)	3985(6)	5153(6)	31(3)
C(3)	2927(7)	4079(8)	5168(7)	47(3)
C(4)	3535(8)	4026(8)	5866(8)	57(4)
C(5)	3357(9)	3890(8)	6546(8)	58(4)
C(7)	1974(8)	3878(6)	5836(7)	39(3)
C(6)	2592(9)	3807(7)	6528(7)	54(4)
C(8)	1611(7)	5971(6)	3828(7)	36(3)
C(9)	1316(8)	6585(7)	4100(7)	46(3)
C(10)	1274(8)	7264(7)	3743(8)	52(4)
C(11)	1548(9)	7355(7)	3114(8)	54(4)
C(12)	1839(8)	6732(8)	2831(8)	54(4)
C(13)	1876(8)	6035(8)	3191(7)	50(4)
C(14)	-1041(7)	4308(7)	1073(6)	41(3)
C(15)	-197(7)	4610(7)	1082(6)	39(3)
C(16)	-1280(7)	5475(7)	2057(6)	33(3)
C(17)	-822(8)	5882(7)	2699(7)	42(3)
C(18)	-895(8)	6674(7)	2731(7)	42(3)
C(19)	-1430(8)	7040(7)	2120(8)	46(3)
C(20)	-1888(9)	6658(7)	1474(8)	53(4)
C(21)	-1807(7)	5876(7)	1449(7)	42(3)
C(22)	-2274(7)	4175(6)	1805(6)	34(3)
C(23)	-2558(10)	3500(9)	1421(9)	69(5)
C(24)	-3337(10)	3290(11)	1294(9)	80(5)
C(25)	-3845(9)	3683(9)	1540(8)	61(4)
C(26)	-3559(9)	4313(9)	1967(11)	77(5)
C(27)	-2779(9)	4553(9)	2089(9)	73(5)

Table 41:cont.

C(29)	1460(9)	5170(7)	1158(7)	49(4)
C(28)	1400(7)	4405(7)	1129(6)	36(3)
C(30)	2110(10)	5542(8)	1070(8)	62(4)
C(31)	2725(9)	5151(9)	973(8)	59(4)
C(32)	2688(9)	4356(10)	938(8)	61(4)
C(33)	2025(7)	3982(8)	1022(8)	48(3)
C(34)	212(7)	3303(6)	408(6)	29(3)
C(35)	354(7)	3493(7)	-302(6)	38(3)
C(36)	-4(8)	3094(7)	-972(7)	47(3)
C(37)	-490(8)	2500(8)	-971(7)	48(3)
C(38)	-666(8)	2292(8)	-294(8)	54(4)
C(39)	-277(8)	2709(7)	387(7)	43(3)
C(40)	-593(7)	4249(7)	3894(6)	36(3)
O(40)	-727(6)	4515(5)	4427(5)	57(3)
C(41)	-1091(8)	2994(7)	3069(7)	43(3)
O(41)	-1556(6)	2546(6)	3073(6)	64(3)
C(42)	1992(9)	3351(7)	2872(7)	45(3)
O(42)	2696(5)	3420(6)	3111(5)	62(3)
C(43)	931(8)	2305(7)	2183(8)	48(3)
O(43)	957(7)	1690(5)	1962(6)	79(4)
C(44)	1884(8)	2413(8)	4417(7)	47(3)
O(44)	2482(6)	2094(6)	4678(5)	61(3)
C(45)	408(7)	2863(7)	4781(7)	40(3)
O(45)	61(5)	2762(6)	5228(5)	58(3)
C(46)	371(8)	2036(8)	3517(7)	48(3)
O(46)	75(7)	1494(5)	3251(5)	69(3)
C(1S)	3627(14)	6278(15)	5691(13)	144(9)
Cl(1S)	2810(3)	6155(3)	5948(3)	107(2)
Cl(2S)	3540(4)	6553(7)	4811(4)	219(5)
C(2S)	-5997(14)	4805(11)	2915(10)	118(8)
Cl(3S)	-5368(4)	4302(4)	2547(4)	138(2)
Cl(4S)	-5675(4)	4807(4)	3934(4)	130(2)
O(1W)	-5541(19)	4601(22)	-49(16)	366(27)

Table 42: Atomic coordinates and B_{iso} for **14**.

	x	y	z	Biso
RU1	0.02631(4)	0.37026(5)	0.21175(3)	2.066(21)
RU2	-0.20085(5)	0.33300(5)	0.11985(3)	2.026(21)
RU3	-0.40851(5)	0.37838(5)	0.10413(3)	2.134(22)
RU4	-0.31612(5)	0.36589(5)	0.23982(3)	2.033(21)
RU5	-0.09737(5)	0.40556(5)	0.33835(3)	2.085(21)
RU6	0.14776(5)	0.48067(5)	0.33970(3)	2.284(22)
S1	-0.10472(15)	0.47480(14)	0.22288(9)	1.89 (7)
S2	-0.31765(14)	0.18408(14)	0.19025(8)	1.80 (6)
N1	-0.5252 (5)	0.0126 (5)	0.1374 (3)	2.5 (3)
N2	-0.5029 (5)	0.1946 (5)	0.0998 (3)	1.89 (23)
N3	0.1038 (5)	0.2300 (5)	0.3783 (3)	2.23 (24)
N4	-0.0442 (5)	0.2632 (4)	0.2992 (3)	1.73 (24)
C1	-0.4646 (6)	0.1258 (6)	0.1375 (3)	1.9 (3)
C2	-0.5202 (6)	-0.0611 (6)	0.1928 (4)	2.3 (3)
C3	-0.5261 (7)	-0.1709 (7)	0.1773 (4)	3.2 (4)
C4	-0.5300 (8)	-0.2463 (7)	0.2292 (5)	4.0 (4)
C5	-0.5290 (8)	-0.2112 (8)	0.2962 (5)	4.2 (4)
C6	-0.5202 (8)	-0.1009 (8)	0.3120 (4)	3.8 (4)
C7	-0.5162 (7)	-0.0234 (7)	0.2598 (4)	3.2 (4)
C8	-0.6180 (6)	0.1440 (6)	0.0529 (3)	2.0 (3)
C9	-0.6240 (6)	0.0921 (7)	-0.0108 (4)	2.5 (3)
C10	-0.7286 (7)	0.0554 (7)	-0.0583 (4)	3.1 (4)
C11	-0.8292 (7)	0.0687 (8)	-0.0425 (4)	3.4 (4)
C12	-0.8251 (7)	0.1175 (8)	0.0218 (5)	3.7 (4)
C13	-0.7193 (7)	0.1534 (7)	0.0700 (4)	2.7 (3)
C14	0.0684 (6)	0.3051 (6)	0.3426 (3)	1.9 (3)
C15	0.2175 (6)	0.2617 (6)	0.4267 (4)	2.4 (3)
C16	0.3212 (7)	0.2761 (8)	0.4012 (4)	3.4 (4)
C17	0.4294 (7)	0.3073 (9)	0.4472 (5)	4.1 (4)
C18	0.4331 (8)	0.3239 (9)	0.5152 (5)	4.4 (5)
C19	0.3288 (8)	0.3067 (8)	0.5400 (4)	3.8 (4)
C20	0.2187 (7)	0.2761 (7)	0.4949 (4)	3.0 (4)
C21	-0.1092 (6)	0.1399 (6)	0.2976 (4)	2.2 (3)
C22	-0.1695 (6)	0.0924 (6)	0.3505 (4)	2.6 (3)
C23	-0.2221 (8)	-0.0272 (8)	0.3522 (5)	3.9 (4)
C24	-0.2156 (8)	-0.0998 (7)	0.3024 (5)	3.6 (4)
C25	-0.1573 (7)	-0.0525 (7)	0.2491 (5)	3.6 (4)
C26	-0.1026 (7)	0.0674 (6)	0.2465 (4)	2.6 (3)
C27	0.1199 (7)	0.4924 (7)	0.1653 (4)	2.7 (3)
O27	0.1777 (5)	0.5663 (5)	0.1389 (3)	4.0 (3)
C28	0.1389 (6)	0.2995 (6)	0.2121 (4)	2.4 (3)
O28	0.2021 (5)	0.2518 (5)	0.2107 (3)	3.5 (3)
C29	-0.0638 (6)	0.2646 (6)	0.1189 (4)	2.4 (3)
O29	-0.0420 (5)	0.2079 (5)	0.0819 (3)	3.4 (3)
C30	-0.1312 (6)	0.4578 (7)	0.0661 (4)	2.5 (3)
O30	-0.0926 (5)	0.5310 (5)	0.0332 (3)	3.9 (3)
C31	-0.2819 (6)	0.2398 (6)	0.0389 (4)	2.4 (3)
O31	-0.3267 (5)	0.1837 (5)	-0.0113 (3)	3.1 (3)
C32	-0.3099 (7)	0.5382 (7)	0.1141 (4)	2.8 (3)
O32	-0.2541 (5)	0.6346 (5)	0.1177 (3)	3.8 (3)
C33	-0.5438 (6)	0.4113 (6)	0.1238 (4)	2.6 (3)
O33	-0.6182 (5)	0.4344 (5)	0.1377 (3)	4.0 (3)
C34	-0.4472 (6)	0.3763 (6)	0.0057 (4)	2.7 (3)
O34	-0.4736 (6)	0.3726 (5)	-0.0526 (3)	4.0 (3)
C35	-0.3265 (6)	0.5071 (6)	0.2630 (4)	2.6 (3)

Table 42;cont.

O35	-0.3379 (5)	0.5919 (5)	0.2762 (3)	3.8	(3)
C36	-0.4765 (6)	0.2904 (6)	0.2484 (3)	2.2	(3)
O36	-0.5726 (4)	0.2406 (5)	0.2560 (3)	3.2	(3)
C37	-0.2769 (6)	0.3109 (6)	0.3430 (4)	2.3	(3)
O37	-0.3367 (4)	0.2555 (5)	0.3795 (3)	3.4	(3)
C38	-0.0962 (6)	0.5506 (6)	0.3664 (4)	2.6	(3)
O38	-0.0976 (5)	0.6391 (5)	0.3796 (3)	3.7	(3)
C39	-0.0614 (6)	0.3748 (6)	0.4317 (4)	2.4	(3)
O39	-0.0420 (5)	0.3573 (5)	0.4878 (3)	3.3	(3)
C40	0.3003 (6)	0.4909 (6)	0.3199 (4)	2.7	(3)
O40	0.3896 (5)	0.4985 (5)	0.3078 (3)	3.6	(3)
C41	0.1630 (7)	0.6374 (7)	0.3177 (5)	3.3	(4)
O41	0.1668 (6)	0.7272 (5)	0.3053 (4)	5.3	(4)
C42	0.2049 (7)	0.5226 (7)	0.4368 (4)	2.9	(3)
O42	0.2433 (5)	0.5489 (5)	0.4928 (3)	3.8	(3)
C1S	0.096 (3)	0.8146 (18)	0.1622 (11)	16.8	(24)
C2S	0.7671 (19)	0.0351 (15)	0.5772 (9)	10.9	(13)
CL1	0.1507 (4)	0.9652 (3)	0.21041(20)	8.6	(3)
CL2	0.1113 (4)	0.8275 (4)	0.08521(21)	9.0	(3)
CL3	0.7070 (5)	0.1109 (5)	0.5222 (3)	11.7	(4)
CL4	0.9194 (4)	0.0526 (4)	0.5686 (3)	12.5	(3)

Biso is the Mean of the Principal Axes of the Thermal Ellipsoid

Table 43: Atomic coordinates and B_{iso} for **15**.

	x	y	z	Biso
RU1	0.70291(4)	0.202928(19)	0.358325(20)	2.860(16)
RU2	0.60941(4)	0.136388(19)	0.223282(19)	2.767(16)
RU3	0.68672(4)	0.054999(21)	0.126795(20)	3.206(17)
RU4	0.89919(4)	0.081621(19)	0.219422(19)	2.761(16)
RU5	0.98333(4)	0.138945(18)	0.354926(18)	2.571(17)
RU6	0.76112(4)	0.089679(20)	0.427512(19)	2.899(18)
S1	0.75534(12)	0.09812 (6)	0.31459 (6)	2.65 (4)
S2	0.82615(14)	0.18944 (6)	0.18902 (6)	3.01 (5)
N1	0.8573 (7)	0.2400 (3)	0.0718 (3)	4.52 (25)
N2	0.7515 (5)	0.13795 (22)	0.07259 (21)	3.61 (18)
C1	0.8097 (6)	0.1874 (3)	0.10200 (24)	3.38 (20)
C2	0.9342 (7)	0.2933 (3)	0.1035 (3)	4.2 (3)
C3	1.0744 (8)	0.2843 (4)	0.1269 (4)	5.6 (3)
C4	1.1436 (11)	0.3355 (5)	0.1574 (5)	8.1 (5)
C5	1.0786 (14)	0.3942 (4)	0.1624 (4)	7.9 (5)
C6	0.9380 (15)	0.4017 (4)	0.1387 (5)	10.0 (7)
C7	0.8658 (13)	0.3510 (4)	0.1094 (4)	7.6 (5)
C8	0.7404 (8)	0.1392 (3)	0.0024 (3)	4.6 (3)
C9	0.8603 (8)	0.1249 (4)	-0.0334 (3)	5.7 (3)
C10	0.8421 (12)	0.1235 (5)	-0.1019 (4)	8.1 (5)
C11	0.7114 (14)	0.1356 (5)	-0.1335 (4)	7.9 (6)
C12	0.5941 (13)	0.1510 (4)	-0.0966 (4)	7.7 (5)
C13	0.6090 (8)	0.1518 (4)	-0.0296 (3)	5.5 (3)
C14	0.5022 (6)	0.1954 (3)	0.3733 (3)	4.4 (3)
C15	0.6778 (8)	0.2730 (3)	0.2962 (3)	4.9 (3)
C16	0.7284 (7)	0.2537 (3)	0.4356 (3)	4.6 (3)
C17	0.4903 (7)	0.1793 (3)	0.1623 (3)	4.6 (3)
C18	0.4509 (6)	0.0882 (3)	0.2478 (3)	4.18 (25)
C19	0.7925 (7)	-0.0023 (4)	0.0718 (3)	4.9 (3)

Table 43: cont.

C20	0.5073 (7)	0.0459 (3)	0.0783 (3)	4.7 (3)
C21	0.6412 (7)	-0.0136 (3)	0.1825 (3)	4.5 (3)
C22	1.0335 (7)	0.0805 (3)	0.1558 (3)	4.5 (3)
C23	0.9485 (8)	-0.0031 (3)	0.2405 (3)	4.8 (3)
C24	1.1081 (6)	0.1758 (3)	0.2914 (3)	3.73 (23)
C25	1.0799 (6)	0.1728 (3)	0.4315 (3)	3.73 (23)
C26	1.0887 (6)	0.0610 (3)	0.3676 (3)	3.57 (22)
C27	0.8282 (7)	0.1263 (3)	0.5082 (3)	4.6 (3)
C28	0.8334 (6)	0.0072 (3)	0.4502 (3)	3.80 (22)
C29	0.5675 (6)	0.0733 (3)	0.4531 (3)	4.22 (24)
O14	0.3852 (5)	0.1938 (3)	0.3847 (3)	7.4 (3)
O15	0.6590 (9)	0.3183 (3)	0.2651 (3)	9.3 (4)
O16	0.7411 (7)	0.2849 (3)	0.4805 (3)	7.6 (3)
O17	0.4181 (6)	0.2060 (3)	0.1248 (3)	6.6 (3)
O18	0.3547 (5)	0.0588 (3)	0.2613 (3)	7.0 (3)
O19	0.8545 (6)	-0.0374 (3)	0.0439 (3)	7.8 (3)
O20	0.3981 (5)	0.0367 (3)	0.0522 (3)	7.3 (3)
O21	0.6102 (7)	-0.0561 (3)	0.2141 (3)	7.0 (3)
O22	1.1151 (6)	0.0806 (3)	0.1153 (3)	7.4 (3)
O23	0.9831 (8)	-0.05540 (24)	0.2525 (4)	8.4 (4)
O24	1.1915 (5)	0.2003 (3)	0.26022 (23)	5.51 (22)
O25	1.1342 (5)	0.1931 (3)	0.47671 (24)	5.92 (23)
O26	1.1546 (5)	0.01540 (23)	0.37672 (24)	5.34 (20)
O27	0.8759 (6)	0.1481 (3)	0.55498 (24)	6.5 (3)
O28	0.8761 (6)	-0.04422 (22)	0.4625 (3)	5.94 (23)
O29	0.4529 (5)	0.0645 (3)	0.4663 (3)	7.6 (3)
H1	0.835 (8)	0.248 (3)	0.043 (4)	4.7 (17)
H	0.886 (6)	0.214 (3)	0.352 (3)	4.0 (13)

Biso is the Mean of the Principal Axes of the Thermal Ellipsoid

Table 44: Atomic coordinates and B_{iso} for **16**.

	x	y	z	Biso
RU1	0.49654(6)	0.02996(5)	0.15119(5)	1.86(3)
RU2	0.28281(6)	0.02641(5)	0.00857(5)	1.82(3)
RU3	0.24630(6)	0.07121(5)	0.22030(5)	1.91(3)
S1	0.48343(19)	0.18946(16)	0.10111(15)	1.99(8)
N2	0.3353 (6)	0.2553 (5)	0.2559 (5)	2.1 (3)
C15	0.6072 (8)	0.1253 (8)	0.2743 (7)	2.7 (4)
N1	0.4801 (7)	0.4086 (5)	0.2249 (5)	2.5 (3)
C16	0.1892 (8)	0.1144 (7)	-0.0410 (6)	2.5 (4)
O18	0.1421 (6)	-0.1942 (5)	0.1467 (5)	3.7 (4)
C18	0.1817 (8)	-0.0953 (8)	0.1755 (6)	2.4 (4)
O19	0.3645 (7)	0.0893 (6)	0.4262 (5)	4.2 (4)
C1	0.4250 (8)	0.2927 (6)	0.2051 (5)	1.9 (3)
C9	0.7245 (9)	0.4274 (8)	0.1924 (7)	3.3 (5)
C14	0.4864 (8)	-0.1084 (8)	0.1715 (7)	2.9 (4)
O17	0.0726 (6)	-0.2077 (5)	-0.1017 (5)	3.9 (3)
C17	0.1516 (8)	-0.1184 (7)	-0.0592 (6)	2.5 (4)
O15	0.6725 (7)	0.1886 (6)	0.3526 (5)	4.5 (4)
C8	0.5948 (8)	0.4545 (7)	0.1832 (6)	2.6 (4)
O14	0.4852 (7)	-0.1927 (6)	0.1834 (6)	4.9 (4)
O16	0.1370 (6)	0.1678 (6)	-0.0728 (5)	4.2 (4)
C3	0.3520 (9)	0.3813 (7)	0.4346 (6)	2.9 (4)
C2	0.2870 (8)	0.3428 (7)	0.3360 (6)	2.3 (4)
C5	0.1916 (11)	0.5066 (9)	0.4900 (8)	4.4 (5)
C4	0.3038 (10)	0.4647 (9)	0.5127 (7)	4.3 (5)
C6	0.1289 (9)	0.4653 (7)	0.3934 (8)	3.7 (5)
C7	0.1739 (9)	0.3833 (7)	0.3162 (7)	3.0 (4)
C19	0.3235 (8)	0.0845 (7)	0.3487 (7)	2.6 (4)
C13	0.5792 (10)	0.5311 (8)	0.1391 (8)	4.0 (6)
C12	0.6931 (14)	0.5810 (10)	0.1019 (10)	6.1 (8)
O20	-0.0429 (6)	0.1101 (6)	0.2789 (5)	3.8 (4)
O1S	0.5687 (7)	0.3692 (5)	0.6491 (5)	3.8 (3)
C20	0.0639 (9)	0.0990 (7)	0.2578 (6)	2.7 (4)
C1S	0.6548 (9)	0.3219 (7)	0.6698 (7)	3.1 (4)
O4S	-0.0371 (9)	0.0905 (9)	0.6288 (8)	7.8 (7)
C2S	0.6585 (11)	0.2000 (9)	0.6021 (8)	4.7 (6)
C3S	0.7619 (11)	0.3836 (8)	0.7616 (8)	4.4 (5)
C11	0.8210 (13)	0.5502 (10)	0.1078 (11)	6.2 (7)
C4S	0.0727 (14)	0.1418 (11)	0.6158 (9)	5.7 (7)
C10	0.8338 (10)	0.4740 (9)	0.1511 (9)	5.1 (6)
C6S	0.2087 (13)	0.1163 (14)	0.6460 (10)	7.8 (10)
C5S	0.0841 (16)	0.2283 (13)	0.5704 (13)	8.9 (11)
H2R	0.209 (9)	0.048 (8)	0.108 (7)	4.6 (24)
H3R	0.644 (8)	-0.003 (7)	0.081 (6)	3.7 (20)

Biso is the Mean of the Principal Axes of the Thermal Ellipsoid

Symmetry operator a) 1-x, -y, -z.

Table 45: Atomic coordinates and B_{iso} for 17.

	x	y	z	Biso
RU 1	0.80175(4)	0.16152(4)	0.16062(3)	1.688(23)
RU 2	1.09157(4)	0.02965(4)	0.22876(3)	1.892(25)
RU 3	1.03841(4)	-0.21724(4)	0.35289(4)	2.31 (3)
RU 4	0.74019(4)	-0.08075(4)	0.28513(4)	1.870(24)
S 1	0.88600(13)	0.01136(12)	0.37384(10)	2.02 (5)
S 2	0.95272(13)	-0.08302(13)	0.15083(11)	2.17 (5)
N 1	0.6258 (5)	0.3223 (4)	0.3124 (4)	2.79 (19)
N 2	0.6469 (5)	0.4741 (4)	0.1359 (4)	2.81 (20)
C 1	0.6794 (5)	0.3411 (5)	0.2020 (4)	2.18 (20)
C 2	0.5429 (7)	0.4339 (6)	0.3628 (6)	3.9 (3)
C 3	0.6903 (8)	0.5329 (6)	0.0133 (5)	4.1 (3)
C 4	0.9730 (6)	0.2399 (6)	0.1217 (5)	2.95 (24)
O 4	1.0111 (5)	0.3349 (5)	0.0713 (5)	5.6 (3)
C 5	1.2284 (6)	-0.1782 (6)	0.3300 (5)	2.81 (25)
O 5	1.3544 (4)	-0.2311 (4)	0.3531 (4)	4.02 (21)
C 6	0.5995 (5)	0.1048 (5)	0.1959 (4)	2.03 (20)
O 6	0.4765 (4)	0.1608 (4)	0.1710 (4)	3.66 (19)
C11	0.7345 (5)	0.2369 (5)	0.0067 (4)	2.31 (21)
O11	0.6910 (5)	0.2800 (4)	-0.0885 (3)	3.68 (21)
C21	1.1811 (6)	0.1110 (6)	0.3062 (5)	3.05 (25)
O21	1.2336 (6)	0.1629 (6)	0.3517 (4)	4.9 (3)
C22	1.2421 (6)	0.0260 (6)	0.1125 (5)	2.59 (24)
O22	1.3328 (5)	0.0234 (5)	0.0445 (4)	4.19 (23)
C31	1.0636 (7)	-0.3142 (7)	0.5138 (6)	4.0 (3)
O31	1.0853 (6)	-0.3738 (7)	0.6119 (4)	6.5 (3)
C32	1.1107 (6)	-0.3890 (6)	0.3194 (7)	4.0 (3)
O32	1.1549 (7)	-0.4892 (6)	0.2913 (7)	7.7 (4)
C41	0.6148 (6)	-0.1183 (6)	0.4134 (5)	2.65 (24)
O41	0.5361 (5)	-0.1455 (6)	0.4911 (4)	5.0 (3)
C42	0.6749 (6)	-0.1891 (6)	0.2225 (5)	2.87 (24)
O42	0.6347 (7)	-0.2581 (5)	0.1854 (5)	5.3 (3)

Biso is the Mean of the Principal Axes of the Thermal Ellipsoid

Table 46: Atomic coordinates and B_{iso} for **18**.

	x	y	z	Biso
RU1	0.00462(9)	0.14581(7)	0.32699(5)	3.07(5)
RU2	0.08533(9)	0.33067(8)	0.33378(5)	3.41(5)
RU3	-0.18146(9)	0.37614(8)	0.40920(5)	3.28(5)
RU4	-0.09991(9)	0.38949(7)	0.16165(5)	2.87(5)
RU5	-0.22403(10)	0.39102(8)	0.05033(5)	3.62(6)
RU6	-0.39540(9)	0.50114(8)	0.18858(5)	3.50(6)
RU7	-0.20604(9)	0.09739(7)	0.18210(5)	3.06(5)
RU8	-0.15546(10)	-0.08565(8)	0.28101(5)	3.84(6)
RU9	-0.38688(9)	0.12547(8)	0.33167(5)	3.43(5)
S1	-0.0762 (3)	0.33268(23)	0.28072(14)	2.90(14)
S2	-0.2407 (3)	0.29745(22)	0.15996(14)	2.98(15)
S3	-0.1561 (3)	0.09708(23)	0.29465(15)	3.12(16)
C11	0.0618 (13)	0.0160 (12)	0.3869 (7)	4.6 (8)
O11	0.0993 (12)	-0.0593 (9)	0.4217 (6)	8.7 (9)
C12	0.1478 (13)	0.0501 (11)	0.2430 (7)	4.5 (7)
O12	0.2358 (10)	-0.0080 (9)	0.1939 (6)	7.4 (6)
C21	0.2526 (14)	0.2750 (12)	0.2531 (7)	4.6 (8)
O21	0.3514 (10)	0.2387 (10)	0.2035 (6)	7.2 (7)
C22	0.0530 (13)	0.4909 (13)	0.3267 (7)	4.5 (8)
O22	0.0298 (12)	0.5871 (9)	0.3233 (5)	7.2 (8)
C23	0.1491 (13)	0.3234 (11)	0.4176 (8)	4.8 (8)
O23	0.1826 (12)	0.3234 (11)	0.4671 (6)	8.0 (9)
C31	-0.3567 (13)	0.3769 (10)	0.4410 (6)	3.8 (6)
O31	-0.4621 (10)	0.3778 (8)	0.4674 (5)	6.3 (6)
C32	-0.1580 (14)	0.3735 (11)	0.5060 (8)	5.1 (8)
O32	-0.1462 (12)	0.3698 (10)	0.5627 (6)	7.9 (8)
C33	-0.2530 (12)	0.5459 (12)	0.4107 (6)	4.1 (7)
O33	-0.2938 (10)	0.6439 (8)	0.4092 (5)	6.4 (7)
C41	0.0761 (14)	0.2627 (12)	0.1149 (6)	3.9 (7)
O41	0.1795 (10)	0.1898 (8)	0.0861 (5)	6.3 (6)
C42	-0.0278 (12)	0.5000 (11)	0.1608 (6)	3.7 (7)
O42	0.0167 (10)	0.5651 (8)	0.1595 (5)	5.9 (6)
C51	0.0313 (13)	0.2108 (9)	-0.0638 (6)	8.1 (8)
O51	-0.0675 (15)	0.2755 (11)	-0.0218 (7)	4.7 (8)
C52	-0.3485 (16)	0.3622 (12)	0.0156 (7)	5.4 (9)
O52	-0.4236 (13)	0.3462 (11)	-0.0056 (7)	8.4 (9)
C53	-0.2523 (13)	0.5329 (12)	-0.0024 (7)	4.5 (8)
O53	-0.2682 (10)	0.6145 (9)	-0.0305 (6)	6.9 (6)
C61	-0.5489 (16)	0.4921 (12)	0.1732 (8)	5.5 (9)
O61	-0.6402 (12)	0.4855 (10)	0.1655 (7)	8.3 (8)
C62	-0.4765 (12)	0.5491 (11)	0.2939 (8)	4.5 (7)
O62	-0.5286 (11)	0.5897 (9)	0.3530 (6)	6.7 (7)
C63	-0.4485 (13)	0.6591 (11)	0.1587 (8)	5.2 (9)
O63	-0.4762 (12)	0.7491 (10)	0.1401 (7)	8.7 (9)
C71	-0.0300 (14)	0.0376 (11)	0.1126 (7)	4.3 (7)
O71	0.0764 (10)	-0.0044 (8)	0.0697 (6)	6.9 (6)
C72	-0.2865 (14)	0.0854 (11)	0.1099 (8)	4.8 (8)
O72	-0.3395 (12)	0.0807 (10)	0.0682 (6)	7.9 (8)
C81	0.0352 (16)	-0.1906 (12)	0.2324 (8)	5.7 (9)
O81	0.1485 (12)	-0.2497 (10)	0.2049 (8)	9.7 (8)
C82	-0.1498 (15)	-0.1302 (11)	0.3769 (9)	5.7 (9)
O82	-0.1477 (14)	-0.1512 (10)	0.4361 (7)	8.9 (9)
C83	-0.2386 (14)	-0.1841 (11)	0.2675 (7)	4.8 (8)
O83	-0.2868 (12)	-0.2418 (9)	0.2579 (6)	7.9 (8)
C91	0.4991 (14)	0.0551 (12)	0.3283 (8)	5.5 (9)

Table 46: cont.

O91	0.4282 (10)	0.0126 (9)	0.3274 (6)	7.6 (7)
C92	-0.4111 (13)	0.1097 (11)	0.4348 (8)	4.8 (8)
O92	-0.4296 (14)	0.1004 (11)	0.4968 (6)	9.6 (10)
C93	-0.5189 (14)	0.2915 (12)	0.3442 (7)	4.5 (8)
O93	0.3972 (10)	0.3838 (9)	0.3486 (6)	6.3 (6)
H12	0.082	0.175	0.360	3.7 (22)
H31	-0.159	0.256	0.389	6.8 (30)
H45	-0.130	0.423	0.077	7.8 (34)
H46	-0.277	0.514	0.210	3.6 (21)

8iso is the Mean of the Principal Axes of the Thermal Ellipsoid

Table 47: Atomic coordinates and B_{iso} for **22**.

	x	y	z	8iso
RU1	0.03893(5)	0.12091(5)	0.216557(19)	1.980(22)
RU2	-0.11319(5)	0.32035(5)	0.295998(19)	2.013(21)
RU3	-0.35153(6)	0.35158(5)	0.344039(20)	2.331(21)
RU4	-0.33479(5)	0.11515(5)	0.298743(19)	2.144(20)
RU5	-0.18952(5)	-0.05688(5)	0.223995(19)	1.943(21)
RU6	-0.19143(5)	0.11267(5)	0.147010(18)	1.679(20)
P1	-0.15089(17)	0.28228(15)	0.09109 (6)	1.89 (7)
S1	-0.19018(16)	0.17298(14)	0.22983 (5)	1.74 (6)
S2	-0.12546(18)	0.12802(16)	0.34516 (6)	2.34 (7)
N1	-0.1142 (7)	0.1328 (6)	0.44167 (20)	3.7 (3)
N2	-0.2605 (6)	0.2740 (5)	0.40749 (19)	2.73 (24)
C1	-0.1752 (7)	0.1872 (7)	0.40365 (24)	2.7 (3)
O42	-0.0600 (6)	-0.2519 (5)	0.15653 (19)	3.51 (23)
O37	-0.4600 (6)	0.4371 (6)	0.24800 (20)	4.5 (3)
O46	-0.1513 (6)	-0.0859 (5)	0.06590 (19)	4.0 (3)
C46	-0.1659 (7)	-0.0116 (6)	0.09694 (24)	2.4 (3)
O43	-0.4806 (6)	-0.1780 (5)	0.20994 (24)	4.8 (3)
O36	0.0295 (7)	0.4819 (6)	0.37587 (22)	5.5 (3)
O38	-0.3039 (6)	0.6312 (5)	0.38485 (22)	4.4 (3)
O40	-0.5894 (5)	0.1229 (7)	0.23925 (23)	5.1 (3)
O39	-0.6438 (6)	0.3002 (6)	0.38004 (23)	5.1 (3)
C14	-0.2392 (7)	0.4305 (6)	0.09782 (24)	2.3 (3)
O45	-0.4982 (5)	0.0853 (6)	0.13211 (21)	4.5 (3)
O35	-0.1243 (7)	0.5568 (5)	0.23491 (23)	5.4 (3)
C39	-0.5321 (8)	0.3209 (7)	0.3679 (3)	3.3 (3)
C15	-0.3154 (7)	0.4538 (6)	0.14000 (25)	2.6 (3)
O41	-0.4867 (7)	-0.0085 (6)	0.38244 (23)	6.0 (3)
C42	-0.1095 (7)	-0.1795 (6)	0.18172 (24)	2.5 (3)
O44	-0.1247 (8)	-0.2054 (5)	0.31446 (21)	5.8 (4)
O33	0.2220 (6)	-0.0711 (6)	0.17131 (21)	4.7 (3)
O34	0.1767 (6)	0.0587 (7)	0.31137 (20)	5.1 (3)
C25	-0.1240 (7)	0.2120 (7)	-0.0097 (3)	3.0 (3)
C17	-0.3919 (8)	0.6474 (7)	0.1066 (3)	3.4 (3)
C33	0.1540 (7)	0.0007 (8)	0.18781 (25)	3.0 (3)
C22	-0.4009 (8)	0.1499 (7)	-0.0212 (3)	3.2 (3)
C44	-0.1486 (9)	-0.1446 (7)	0.2824 (3)	3.4 (3)
C20	-0.2078 (7)	0.2280 (6)	0.02957 (22)	2.0 (3)
C36	-0.0253 (8)	0.4218 (7)	0.3449 (3)	3.4 (3)
O32	0.2310 (6)	0.3691 (6)	0.2019 (3)	5.6 (3)
C35	-0.1197 (8)	0.4662 (7)	0.2576 (3)	3.3 (3)
C40	-0.4926 (7)	0.1189 (8)	0.2621 (3)	3.3 (3)
C23	-0.3143 (9)	0.1357 (7)	-0.0602 (3)	3.6 (3)

Table 47: cont.

C31	0.1200 (7)	0.2388 (7)	0.0735 (3)	2.8	(3)
C8	-0.3011 (9)	0.3191 (7)	0.4556 (3)	3.5	(3)
C32	0.1558 (8)	0.2806 (8)	0.2077 (3)	3.5	(3)
C26	0.0306 (7)	0.3337 (6)	0.08381 (24)	2.4	(3)
C37	-0.4155 (8)	0.4061 (7)	0.2836 (3)	3.2	(3)
C16	-0.3901 (8)	0.5626 (7)	0.1436 (3)	3.3	(3)
C43	-0.3731 (8)	-0.1320 (6)	0.2159 (3)	2.9	(3)
C24	-0.1749 (9)	0.1658 (8)	-0.0546 (3)	3.9	(4)
C13	-0.4153 (10)	0.2597 (9)	0.4779 (3)	4.6	(4)
C9	-0.2270 (10)	0.4243 (8)	0.4778 (3)	4.4	(4)
C34	0.1183 (7)	0.0840 (8)	0.2786 (3)	3.2	(3)
C41	-0.4319 (8)	0.0396 (7)	0.3488 (3)	3.5	(3)
C27	0.0850 (8)	0.4617 (7)	0.0897 (3)	3.4	(3)
C45	-0.3832 (7)	0.0933 (7)	0.1375 (3)	2.8	(3)
C2	-0.0245 (8)	0.0316 (7)	0.43766 (24)	3.0	(3)
C19	-0.2416 (8)	0.5184 (7)	0.0602 (3)	3.1	(3)
C21	-0.3485 (7)	0.1970 (7)	0.0233 (3)	2.9	(3)
C30	0.2588 (8)	0.2699 (8)	0.0685 (3)	3.6	(4)
C18	-0.3164 (9)	0.6263 (7)	0.0640 (3)	3.6	(4)
C38	-0.3210 (7)	0.5262 (7)	0.3706 (3)	3.0	(3)
C29	0.3105 (8)	0.3968 (9)	0.0748 (3)	4.3	(4)
C10	-0.2734 (12)	0.4720 (9)	0.5231 (3)	5.6	(5)
C7	-0.0765 (10)	-0.0958 (9)	0.4324 (4)	5.2	(5)
C11	-0.3846 (11)	0.4135 (9)	0.5444 (3)	5.7	(5)
C4	0.2025 (10)	-0.0360 (14)	0.4362 (4)	7.6	(7)
C28	0.2241 (9)	0.4928 (8)	0.0853 (4)	4.5	(4)
C3	0.1128 (9)	0.0617 (10)	0.4394 (4)	5.3	(5)
C12	-0.4551 (11)	0.3085 (11)	0.5230 (3)	5.9	(5)
C5	0.1487 (14)	-0.1625 (12)	0.4296 (3)	8.1	(7)
C6	0.0118 (13)	-0.1920 (10)	0.4284 (4)	7.0	(6)
CL 1	0.4068 (6)	0.6890 (6)	0.32602 (17)	14.1	(3)
CL 2	0.1942 (7)	0.6750 (8)	0.2576 (3)	23.1	(6)
C1S	0.2752 (21)	0.7441 (23)	0.2969 (7)	15.7	(17)

Biso is the Mean of the Principal Axes of the Thermal Ellipsoid

Table 48: Atomic coordinates (x 10^4) and U_{eq} (x 10^3) ($Å^2$) for **26**.

	x	y	z	U(eq)
Ru(1)	3813(1)	1665(1)	6929(1)	42(1)
Ru(2)	747(1)	2612(1)	7125(1)	45(1)
Ru(3)	1876(1)	1612(1)	5829(1)	47(1)
Ru(4)	1123(1)	3088(1)	8891(1)	50(1)
Ru(5)	4192(1)	2195(1)	8701(1)	47(1)
Ru(6)	2083(1)	1395(1)	9462(1)	47(1)
S(1)	2198(3)	1813(2)	8127(2)	42(1)
S(2)	2855(4)	3209(2)	6738(2)	47(1)
N(1)	2497(12)	2747(7)	5271(6)	52(3)
N(2)	3356(14)	4010(8)	5346(7)	96(4)
C(1)	2893(15)	3320(9)	5663(7)	50(3)
C(2)	2412(16)	2886(10)	4417(8)	59(4)
C(3)	1300(18)	3489(13)	4154(9)	88(6)
C(4)	1154(25)	3600(15)	3320(13)	118(8)
C(5)	2165(27)	3119(14)	2796(10)	101(7)
C(6)	3275(23)	2469(13)	3058(9)	85(6)
C(7)	3402(20)	2380(11)	3867(9)	79(5)
C(8)	3749(17)	4688(9)	5766(8)	57(4)

Table 48: cont.

C(9)	5007(18)	4510(11)	6118(9)	69(4)
C(10)	5312(22)	5180(16)	6518(11)	99(7)
C(11)	4473(30)	6002(14)	6490(14)	112(8)
C(12)	3276(29)	6129(14)	6096(14)	117(8)
C(13)	2924(19)	5481(12)	5725(12)	91(6)
C(91)	1376(15)	622(10)	6430(8)	55(4)
N(91)	1077(14)	50(9)	6781(7)	68(3)
C(92)	687(23)	-723(11)	7202(10)	90(6)
C(93)	1862(26)	-1538(13)	6932(14)	138(9)
C(94)	589(25)	-549(13)	8088(11)	118(8)
C(95)	-804(25)	-774(17)	6954(15)	155(11)
O(101)	4724(13)	-279(7)	7133(8)	93(4)
C(101)	5245(18)	1637(11)	6086(9)	72(4)
O(102)	6077(13)	1663(9)	5543(8)	108(4)
C(102)	4410(15)	439(11)	7072(8)	60(4)
O(21)	-1091(13)	3884(9)	6056(8)	112(5)
C(21)	-386(16)	3402(11)	6471(9)	69(4)
O(22)	-1631(13)	1652(8)	7511(8)	99(4)
C(22)	-723(17)	2028(11)	7375(9)	66(4)
O(31)	3550(14)	317(8)	4595(7)	98(4)
C(31)	2926(17)	818(10)	5043(8)	58(4)
O(32)	-938(15)	1965(12)	4983(8)	131(6)
C(32)	137(19)	1788(13)	5292(10)	82(5)
O(41)	1020(15)	3636(10)	10521(8)	117(5)
C(41)	1021(19)	3567(12)	9907(12)	91(6)
O(42)	387(18)	4821(8)	8013(8)	125(5)
C(42)	683(19)	4168(11)	8299(9)	77(5)
O(43)	-2053(12)	2944(9)	9122(7)	97(4)
C(43)	-873(17)	2992(10)	9038(9)	65(4)
O(51)	5163(14)	2520(9)	10303(7)	101(4)
C(51)	4837(16)	2439(10)	9700(9)	63(4)
O(52)	6024(12)	3265(8)	7688(7)	88(4)
C(53)	5632(15)	1112(11)	8625(8)	60(4)
C(52)	5306(14)	2869(10)	8027(9)	62(4)
O(53)	6509(11)	502(7)	8572(6)	78(3)
O(61)	2519(16)	1751(9)	11182(7)	112(5)
C(61)	2379(18)	1627(11)	10544(9)	73(4)
O(62)	3932(12)	-460(8)	9455(8)	88(4)
C(62)	3231(16)	229(11)	9484(9)	66(4)
O(63)	-931(13)	987(9)	9828(8)	103(4)
C(63)	181(18)	1127(9)	9694(8)	57(4)
O(99)	3204(36)	5284(20)	9318(24)	151(14)
C(98)	3529(47)	5709(40)	8753(32)	236(73)
C(97)	2358(50)	6564(29)	8566(24)	114(20)
C(96)	5247(45)	5433(32)	8745(25)	260(77)